Scuola Internazionale Superiore di Studi Avanzati - Trieste

Elementary Particle Theory Sector

Thesis submitted in partial fulfillment of the requirements
for the degree of Doctor Philosophiæ

Neutrino mass matrix: reconstruction and implications

CANDIDATE:
Michele Frigerio

SUPERVISOR:
Professor Alexei Yu. Smirnov

EXTERNAL EXAMINER:
Professor Ferruccio Feruglio

ACADEMIC YEAR 2002-2003

SISSA – Via Beirut 2-4 – 34014 TRIESTE – ITALY

SISSA-ISAS

INTERNATIONAL SCHOOL FOR ADVANCED STUDIES

Elementary Particle Theory Sector

Thesis submitted in partial fulfillment of the requirements for the degree of Doctor Philosophiæ

Neutrino mass matrix: reconstruction and implications

CANDIDATE:
Michele Frigerio

SUPERVISOR:
Professor Alexei Yu. Smirnov

EXTERNAL EXAMINER:
Professor Ferruccio Feruglio

ACADEMIC YEAR 2002-2003

Contents

Chapter 1

Introduction

1.1 Historical remarks

Even though the existence of non-zero neutrino masses has received confirmation only in the last years, the question of massiveness of neutrinos appeared at the very beginning of neutrino history. In 1930 Wolfgang Pauli assumed the existence of a spin 1/2 neutral particle, with mass of the order of the electron [1]. He wanted to save the spin-statistic theorem and the energy conservation law, which both seemed violated in β-decays of integer spin nuclei. He called the new particle the "neutron". The existence of spin 1/2 neutrons in nuclei and their emission together with the electron in β-decays allowed Pauli to explain the observed spin of nuclei and, at the same time, the continuous energy spectrum of the emitted electron.

After the discovery of the neutron in 1932, in 1934 Enrico Fermi proposed the first theory of β-decay [2]: a light spin 1/2 neutral particle, the "neutrino", is created together with the electron in the transition from a neutron inside a nucleus into a proton. He wrote the effective Hamiltonian for the β-decay, which was generalized later by Gamow and Teller in 1936 [3]. Fermi and Perrin [4] suggested to search the mass of the neutrino by measuring the shape of the high energy part of β-decay spectra. In the forties, the first experiments using this technique found $m_\nu < 500$ eV.

In the beginning of the fifties F.Reines and C.L.Cowan gave the direct proof of the existence of the electron (anti)neutrino using the reaction $\bar{\nu}_e\ p \rightarrow e^+\ n$ [5]. The source of antineutrinos was the Savannah River nuclear reactor. Raymond Davis in 1955 showed [6] that neutrino and antineutrino are different particles, putting an upper bound on the reaction $\bar{\nu}_e\ ^{37}Cl \rightarrow e^-\ ^{37}Ar$. This suggested the existence of a conserved lepton number, which distinguishes leptons from antileptons.

In 1956 C.S.Wu et al. discovered parity violation in β-decay [7]. A theory with maximal parity violation for neutrinos has been proposed in 1957 by Landau [8], Salam [9], Lee and Yang [10]: they predicted massless neutrinos with left-handed helicity and massless right-handed antineutrinos. The helicity of the neutrino was determined experimentally in 1957 by Goldhaber et al. [11].

However, in 1957-58 Bruno Pontecorvo pointed out that there is no symmetry reason requiring zero neutrino mass (gauge invariance gives such a reason in the case of the photon). He also suggested that neutrino-antineutrino oscillations are a very sensitive method for the measurements of tiny neutrino masses (that is, too small to be detected in β-decay experiments) [12, 13].

At that time a unique flavor of neutrinos was known. Pontecorvo, comparing electron and muon captures by protons came to the conclusion that the weak interaction is universal for $e - \nu$ and $\mu - \nu$ pairs [14, 15]. The neutrinos emitted in the electron and muon captures could be, in principle, different particles. This was proved in 1962 using neutrinos from accelerator at Brookhaven: Lederman, Schwartz, Steinberger et al. [16] observed only muons (not electrons) in the final state of $\nu_\mu - N$ interactions (neutrinos came from pion decays and, therefore, were mainly muonic neutrinos). In this way the existence of conserved flavor lepton numbers was established.

In 1962 Maki, Nakagawa and Sakata suggested that electron and muon neutrinos are linear orthogonal combinations of neutrino mass eigenstates [17]. In fact their paper was unknown to many physicists for many years, till the review on neutrino oscillations by Pontecorvo and Bilenky drew attention on it [18].

In 1967 Pontecorvo [19] introduced the notion of sterile neutrinos (in relation with neutrino-antineutrino oscillations), discussed oscillations between active neutrinos and foresaw the solar neutrino problem. In 1969 Gribov and Pontecorvo [20] obtained the expression of ν_e survival probability in the case of vacuum oscillations. In the seventies in Dubna and other places many experiments for the search of neutrino oscillations were proposed.

At that time the success of the two-component neutrino theory and the affirmation of the Standard Model of particle physics induced the general belief that neutrinos are massless particles (the upper bound on neutrino mass was of the order of 100 eV, coming from β-decay spectra). However, in the seventies theories beyond the Standard Model and in particular Grand Unification Theories were constructed, where neutrinos can be in the same gauge multiplets as other fermions: this provided a theoretical framework for the existence of non-zero neutrino masses.

The first indication of neutrino oscillations came from radiochemical experiments, initiated by R.Davis in 1967 [21]. He used the reaction $\nu_e\ ^{37}Cl \rightarrow e^-\ ^{37}Ar$ and observed a deficit in the flux of electron neutrinos from the Sun with respect to the prediction of the Standard Solar Model (solar neutrino problem). This deficit was confirmed by the water-Cerenkov detectors Kamiokande [22] and Super-Kamiokande [23, 24] in the nineties, where neutrinos were detected through the process $\nu\ e \rightarrow \nu\ e$. Confirmations came also from gallium radiochemical experiments [25, 26, 27]. The SNO experiment [28, 29, 30] obtained in 2002 a model independent evidence of transition of ν_e into ν_μ and ν_τ, measuring in a heavy water Cerenkov detector both charged current and neutral current neutrino reactions. All these results can be interpreted in terms of two neutrino oscillations, taking into account the crucial effect of solar matter along the neutrino propagation (Mikheyev-Smirnov-Wolfenstein (MSW) effect [31, 32, 33]). Combined fits

of solar neutrino data favor the Large Mixing Angle (LMA) MSW solution of the solar neutrino problem. This solution has been confirmed in 2003 in the reactor experiment KamLAND [34], through the detection of the process $\bar{\nu}_e\, p \to e^+\, n$. Global fits of solar and KamLAND data [35, 36, 37, 38, 39, 40, 41, 42, 43] allow to extract the mixing angle θ_{12} and the mass squared difference Δm^2_{12} which control oscillation probabilities.

Even though solar neutrino experiments started before, the first strong evidence that $m_\nu \neq 0$ came from atmospheric neutrinos. An anomaly was observed starting from 1988 [44] by Kamiokande [45] and IMB [46] experiments in the ratio between fluxes of muon and electron atmospheric neutrinos, which was significantly smaller than expected. The evidence for an oscillation explanation of the atmospheric neutrino anomaly was found by the Super-Kamiokande experiment [47] in 1998, through the measurement of the zenith angle dependence of the number of neutrino events. Data are explained by vacuum oscillations of ν_μ into ν_τ as the dominant mode. Confirmation came from other atmospheric experiments [48, 49] as well as from K2K, the first long baseline accelerator experiment [50]. Combined analysis of atmospheric and K2K data [51] allows to extract the corresponding mixing angle θ_{23} and the mass squared difference Δm^2_{23}.

The reactor experiments CHOOZ [52] and Palo Verde [53] used the process $\bar{\nu}_e\, p \to e^+\, n$ for detecting electron antineutrinos. The neutrino disappearance effect has not been observed on a baseline relevant for the atmospheric mass squared difference, thus putting an upper bound on the mixing angle θ_{13}, the one not determined by solar and atmospheric experiments.

1.2 The neutrino mass matrix

Significant amount of information about neutrino masses and mixing has already been obtained from experiments on the atmospheric and solar neutrinos, from laboratory experiments, in particular the reactor experiments and neutrinoless double beta decay searches [54, 55], from astrophysics and cosmology [56, 57, 58, 59, 60, 61, 62]. New substantial results are expected soon.

Neutrino masses and mixing are considered to be the manifestation of physics beyond the Standard Model. The question is: how far beyond? What are implications of experimental results for the fundamental theory, for the mechanism of neutrino mass generation? What is the origin of large lepton mixing? Is there any relation between the quark and the lepton masses?

A first fundamental issue is to establish what kind of fermions neutrinos are. All known spin 1/2 elementary particles but neutrinos possess a non-zero conserved electric and/or color charge. This implies that all these particles are Dirac fermions. If the lepton number L is conserved, also neutrinos should be Dirac fermions. Then, Dirac-type neutrino masses can be generated as other fermion masses. Only violation of lepton flavor numbers occurs. However, also total lepton number could be violated, if neutrinos are truly neutral particles, that is Majorana-type fermions [63]. In this

case a Majorana mass for neutrinos can be written using only left-handed fields [20]. Processes with $\Delta L = 2$ like neutrinoless 2β-decay are then allowed [64]. Even though an experimental confirmation is lacking, many theoretical considerations (see, e.g., [65]) prefer the Majorana nature for neutrinos and we will assume that in the following.

The neutrino masses and mixing appear from diagonalization of the Majorana neutrino mass matrix. In a sense, the mass matrix *unifies* the information which is contained in the masses and mixing angles (which appear as independent physical observables). So, the underlying theory should be interpreted in terms of properties of the mass matrix.

The mass matrix can contain also possible complex phases, which would signal a violation of the CP symmetry. It is known for a long time that CP is indeed violated in the quark sector [66]. It is therefore natural to investigate the effect of CP violating phases also in the lepton sector. In the case of Majorana neutrinos extra physical phases appear in the mass matrix [67, 68]; their effect can be observed, in principle, in $\Delta L = 2$ processes. In particular, for the system of three Majorana neutrinos there are three CP violating phases: the Dirac phase, δ (the unique phase in the mixing matrix relevant for oscillations), and two Majorana phases, which are the relative phases of the three mass eigenstates. The structure of the mass matrix depends strongly on the unknown CP violating phases, especially in the case of degenerate spectrum.

It is expected that the matrix structure can be explained by certain (broken) symmetry realized in certain basis (the *symmetry basis*) at some high mass scale [69]. Thus, to approach the fundamental theory, one should find the mass matrix in the symmetry basis and at the corresponding *symmetry scale*. Both abelian (*e.g.*, [70, 71, 72, 73, 74, 75, 76]) and non abelian (*e.g.*, [77, 78, 79, 80]) symmetries, broken (spontaneously) at the various symmetry scales, have been widely considered (see also the reviews [81, 82]). Also, the possibilities have been studied to identify the flavor symmetry scale with other known scales in the theory like the Grand Unification scale or the string scale.

The first step to the fundamental theory is the reconstruction of the matrix in the *flavor basis* using all available experimental data. The flavor basis, formed by ν_e, ν_μ, ν_τ, is determined as the basis in which the mass matrix of charge leptons is diagonal. There is a number of attempts to reconstruct neutrino mass matrix in the flavor basis using the experimental results [83, 84, 85, 86, 87, 88, 89, 90, 91]. Most of the studies have been performed in the context of three Majorana neutrinos. Apart from the oscillation parameters (mass squared differences and mixing angles), the mass matrix depends on non-oscillation parameters: the absolute mass scale and the CP violating Majorana phases. Furthermore, even not all the oscillation parameters are known. In particular, there is only an upper bound on the mixing angle θ_{13} and there is no information about the value of the Dirac phase δ. Also the type of mass hierarchy (ordering) of the states is unknown.

The studies performed so far were concentrated, mainly, on identification of the dominant structures of the mass matrix and possible zeros of certain matrix ele-

ments. It was realized that in the case of spectrum with normal mass hierarchy, $m_1 \ll m_2 \ll m_3$, the mass matrix has a structure with dominant $\mu\tau$-block, formed by $M_{\mu\mu}, M_{\mu\tau}, M_{\tau\tau}$ elements, and small elements of the $e-$row ($M_{ee}, M_{e\mu}, M_{e\tau}$) [85, 88, 92]. In the case of inverted mass hierarchy, the dominant structure can be formed by elements of the $e-$row: $M_{e\mu}$ and $M_{e\tau}$ [83, 84, 93]. These structures may be related to an underlying $L_e - L_\mu - L_\tau$ symmetry [94]. In the case of degenerate mass spectrum new dominant structures appear depending on the CP-parities of the mass eigenstates (see, *e.g.*, [83, 84, 93, 95]). In particular, it has been found that the diagonal elements, being equal to each other, can form the dominant structure for equal CP-parities of all three neutrinos. Another interesting possibility is the dominant structure formed by the $ee-$, $\mu\tau-$ and $\tau\mu-$elements (moreover, $|M_{ee}| \approx |M_{\mu\tau}|$), which could imply, *e.g.*, $SO(3)$ flavor symmetry or $U(1)$ symmetry, with charge prescription $(0, 1, -1)$ and an additional permutation symmetry. It was shown that experimental data can be explained in models with universal Yukawa couplings [96, 97, 98, 99], which lead to "democratic" mass matrices with all mass matrix elements having the same modulus but different phases.

Completely different approach is based on "Anarchy" of the mass matrix [100, 101, 102]. It has been proposed that the elements of the mass matrix appear as random numbers from certain interval and there is no special structure of the mass matrix dictated by certain symmetry. It was estimated how frequently neutrino oscillation data can be reproduced in this way. Some criticism to this approach can be found in [103, 104]. Random values of the complex phases of the mass matrix elements $M_{\alpha\beta}$ have also been considered [88, 89].

1.3 Neutrinos as probe of physics at the high energy scale

Using the experimental information, it is possible to reconstruct (at least partially) the Majorana mass matrix of neutrinos at the electroweak scale m_Z. However, the origin of the neutrino mass matrix is, most probably, in new physics above a very high scale m_0, where the lepton number is violated. To find the structure of the matrix at m_0, it is necessary to take into account the renormalization effects between m_Z and m_0.

One usually assumes that the mass matrix is generated by an effective five dimensional operator [105, 106]. The Renormalization Group Equation (RGE) for this operator has been extensively studied both in the Standard Model (SM) and Minimal Supersymmetric Standard Model (MSSM) [107, 108, 109, 110]. Also low energy threshold corrections have been computed; their effect can be important in the MSSM case [111, 112, 113]. A non-standard source of neutrino masses (operators in the Kähler potential) has been considered in [114, 115] and the corresponding radiative corrections have been studied. In the context of the see-saw mechanism [116, 117, 118, 119], the RGE effects have been computed between the GUT scale and the seesaw scale [120, 121], considering also the case of non-degenerate heavy right-handed neutrinos [122].

The goal of these analyses was to understand how radiative corrections could affect the mass squared differences Δm^2_{ij} and the mixing angles θ_{ij} observed in neutrino oscillation experiments. A general conclusion is that the effect of running is small for hierarchical mass spectra, while, in the case of quasi-degenerate mass spectrum, the observables can be strongly modified by radiative corrections. In particular, in the degenerate case $\Delta m^2_{\rm sol}$ can have purely radiative origin [123].

Once the radiative corrections to the neutrino mass matrix have been analyzed, a further question arises: what is the origin of the effective operator that generates the mass matrix?

In this connection, the seesaw mechanism [116, 117, 118, 119] provides a very simple and appealing explanation of the smallness of the neutrino mass. The particles exchanged at the high energy scale are right-handed (RH) neutrinos. These heavy neutrinos are connected to the light left-handed ones via Yukawa couplings, which lead to a Dirac mass term at the electroweak (EW) scale. The low-energy neutrino mass matrix M is given in terms of the Majorana mass matrix of RH neutrinos, M_R, and the Dirac mass matrix, m_D, as $M = -m_D M_R^{-1} m_D^T$. While the elements of m_D are expected to be at or below the EW scale, the characteristic mass scale of RH neutrinos is GUT or parity breaking scale, since they are EW singlets.

A very important feature of the seesaw mechanism, which makes it even more attractive, is that it has a simple and elegant built-in mechanism of production of the baryon asymmetry of the Universe: baryogenesis through leptogenesis [124].

The main prediction of the seesaw mechanism is the existence of RH Majorana neutrinos N_i. Being extremely heavy, these neutrinos are not accessible to direct experimental studies, though several indirect ways of probing the properties of the RH sector are known:
- studies of leptogenesis [125, 126, 127, 128, 129, 130, 131];
- searches for signatures of Grand Unification;
- renormalization group running effects induced by RH neutrinos (*e.g.*, on the $b - \tau$ unification [132, 133]).

What can be learned about the heavy RH neutrino sector, using the currently available low-energy neutrino data as an input? The matrix M can to a large extent be reconstructed from the data; then the seesaw formula can be used to study M_R.

Obviously, for such an analysis one would also need to know the Dirac neutrino mass matrix m_D. Unfortunately, at present no information on m_D is available, since there are almost no ways of studying it experimentally (though, in the context of certain SUSY models, some information on m_D can be obtained from the studies of the rare decays like $\mu \to e\gamma$, $\tau \to e\gamma$ [134, 135]). One is, therefore, forced to resort to some theoretical arguments. Such arguments are in general provided by theories with quark-lepton symmetry, in particular by GUTs, in which m_D is typically related at the unification scale to the mass matrices of up-type or down-type quarks or of charged leptons. Since all the quark and charged lepton masses are highly hierarchical, one expects this to be true also for m_D. Moreover, in models in which m_D is related to

the up-type quark mass matrices and the mass matrix of charged leptons m_l, to the down-type quark matrix, one can expect that the left-handed rotations diagonalizing m_l and m_D are nearly the same. Their mismatch should be comparable to the Cabibbo mixing in the quark sector. The large leptonic mixing observed in the low-energy sector is then a consequence of the "seesaw enhancement of lepton mixing" [136, 137, 138, 139, 140, 141]. Such an enhancement requires a strong (quadratic) mass hierarchy of RH neutrinos and/or off-diagonal structure of M_R (there also exist different seesaw models in which the large low-energy leptonic mixing is due to the large left-handed Dirac-type mixing [142, 143, 144, 145]).

In this framework, studies of the structure of RH sector and leptogenesis have been performed in a number of publications [146, 147, 148]. It was realized that, due to a strong hierarchy of neutrino Dirac Yukawa couplings (analogous to that of up-type quarks), the predicted baryon asymmetry is much smaller than the observed one, especially [149, 150] in the case of the LMA MSW solution of the solar neutrino problem. The asymmetry can be much larger if the hierarchy of Yukawa couplings is similar to that of the down quarks or charged leptons and the largest coupling is of order one [151, 152]. In this case the hierarchy between the masses of RH neutrinos becomes weaker and, furthermore, large RH mixing can appear.

In general, it is a nontrivial task to find a scenario in which successful baryogenesis via leptogenesis takes place respecting, at the same time, constraints coming from low-energy neutrino data and cosmology.

Chapter 2

The possible structures of the neutrino mass matrix

We will present in this chapter the main results of Refs. [153, 154]. We perform a systematic and comprehensive study of the neutrino mass matrix structure describing, in particular, the dependence on the CP violating phases. We concentrate on the first step of the "bottom - up" approach to the underlying theory: the reconstruction of the mass matrix in the flavor basis.

In most of previous studies, the CP violating phases were neglected and definite CP-parities [155, 156] have been discussed mainly, which is equivalent to the absence of CP violation (some works discussing phases are Refs. [157] and [158], where the role of phases in the generation of large solar mixing is considered). Moreover, exact bimaximal mixing has been often considered and usual assumptions are either strongly hierarchical or completely degenerate mass spectra. Special attention has been given to the small elements of the mass matrix [87]. In some recent works [157, 159, 160, 161] the matrices with two independent entries exactly equal to zero have been classified.

We will show that the assumptions of definite CP-parities, bimaximal mixing, strictly hierarchical or degenerate spectrum and exactly zero elements exclude a number of interesting matrix structures.

In section 2.1 we describe in detail the experimental input. In section 2.2 we give general parameterizations of the neutrino mass matrix. We introduce useful graphical representations of the matrix element dependence on CP violating phases (section 2.3). In section 2.4 we describe the possible matrix structures for the different mass spectra. In section 2.5 we discuss the possibility to obtain a complete experimental determination of the mass matrix. A discussion of hierarchies among matrix elements, flavor alignment, basis dependence and of other theoretical issues will be presented in section 2.6.

2.1 The experimental data

The three left-handed neutrino fields in flavor basis, ν_e, ν_μ, ν_τ, can be expressed in terms of the three mass eigenstates, ν_1, ν_2, ν_3, as

$$\nu_\alpha = (U_{PMNS})_{\alpha i}\nu_i \ .$$

The unitary matrix U_{PMNS} [12, 13, 17] is the leptonic mixing matrix, for which we use the standard parameterization:

$$U_{PMNS} \equiv U \cdot K_0 \ , \tag{2.1}$$

where

$$U = \begin{pmatrix} c_{12}c_{13} & s_{12}c_{13} & s_{13}e^{-i\delta} \\ -c_{23}s_{12} - s_{23}c_{12}s_{13}e^{i\delta} & c_{23}c_{12} - s_{23}s_{12}s_{13}e^{i\delta} & s_{23}c_{13} \\ s_{23}s_{12} - c_{23}c_{12}s_{13}e^{i\delta} & -s_{23}c_{12} - c_{23}s_{12}s_{13}e^{i\delta} & c_{23}c_{13} \end{pmatrix} \tag{2.2}$$

and

$$K_0 = diag(e^{i\rho}, 1, e^{i\sigma}) \ . \tag{2.3}$$

Here $c_{ij} \equiv \cos\theta_{ij}$, $s_{ij} \equiv \sin\theta_{ij}$, δ is the CP-violating Dirac phase and ρ and σ are the two CP-violating Majorana phases. The mixing angles vary between 0 and $\pi/2$, δ between 0 and 2π, ρ and σ between 0 and π.

2.1.1 The three neutrino masses

The three neutrino masses, m_1, m_2, m_3, are constrained by a number of experiments. Two mass squared differences are known from data on neutrino oscillations. The mass squared difference for the Large Mixing Angle (LMA) MSW solution of the solar neutrino problem, at 90% C.L., is given by [43]:

$$\Delta m^2_{sol} \equiv m_2^2 - m_1^2 = (7^{+10}_{-2}) \cdot 10^{-5}\text{eV}^2 \ . \tag{2.4}$$

From atmospheric neutrino analysis we have, at the 90% C.L. [47, 162],

$$\Delta m^2_{atm} \equiv |m_3^2 - m_2^2| \simeq |m_3^2 - m_1^2| = (2.5^{+1.4}_{-0.9}) \cdot 10^{-3}\text{eV}^2 \ . \tag{2.5}$$

During the completion of this thesis, a recent paper [163], based on a preliminary reanalysis of systematics by SuperKamiokande, gave the following revised estimate: $\Delta m^2_{atm} = (2^{+0.4}_{-0.3}) \cdot 10^{-3}\text{eV}^2$ at 1σ. If confirmed, this shift should be taken into account in all the following discussion.

The absolute mass scale of neutrinos is presently unknown. A solid upper limit is given by the direct kinematic bound on the mass of electron neutrino in tritium β-decay [164, 165]:

$$m_e \equiv \sum_i |U_{ei}|^2 m_i < 2.2 \text{ eV} \qquad (95\% \text{ C.L.}) \ . \tag{2.6}$$

Since mass squared differences are much smaller than $\sim$ eV, this bound is relevant for the case of quasi-degenerate spectrum ($m_1 \approx m_2 \approx m_3$) and, because of the unitarity of the matrix U, it immediately translates into $m_i < 2.2$ eV. However, the cosmological bound on the sum of light neutrino masses (at 95% C.L.) [60, 61],

$$\sum_i m_i < (0.7 \div 2.1) \text{ eV} , \tag{2.7}$$

leads to the strongest limit on individual masses: $m_i < (0.23 \div 0.70)$ eV. There is also a recent analysis [62] suggesting that cosmological data prefers non-zero neutrino masses, thus implying a lower bound on m_i:

$$m_i = (0.19^{+0.10}_{-0.09}) \text{ eV} \tag{2.8}$$

at 1σ C.L., assuming three quasi-degenerate neutrinos.

In addition to the unknown absolute mass scale, there is another ambiguity in the neutrino mass spectrum, since present data do not allow to discriminate between normal ordering of the spectrum:

$$m_1 < m_2 < m_3 ,$$

and inverted ordering:

$$m_3 < m_1 < m_2$$

(notice that in both cases the electron flavor is mainly concentrated in ν_1 and ν_2 mass eigenstates). In general, the spectra with normal and inverted hierarchy have different phenomenology (cosmological consequences, absolute mass scale, neutrinoless beta decay rate, oscillations). In oscillations the difference between the two spectra appears if 1-3 mixing differs from zero. At present, the only observation which could be sensitive to the mass hierarchy is the neutrino burst from the supernova SN1987A. It was shown that the data (especially, energy spectra detected by Kamiokande and IMB) can be better described in the case of normal hierarchy with Earth matter effect to be taken into account [166, 167, 168, 169, 170]. The inverted mass hierarchy is disfavored (see, however, [171, 172]). These statements depend on the original neutrino spectra produced in the star as well on the value of 1-3 mixing. Recent calculations show that the difference of the fluxes of different neutrino types can be rather small [173], thus diminishing possible oscillation effects and therefore difference of predictions for normal and inverted hierarchy.

The present knowledge of the three light neutrino masses is summarized in Figs. 2.1 and 2.2. A very important feature of the mass spectrum is the relative size of mass differences with respect to the absolute mass scale. In the case of normal ordering (Fig. 2.1), all three masses are hierarchical for $m_1 \lesssim 0.01$eV. For $0.01\text{eV} \lesssim m_1 \lesssim 0.1$eV, the neutrinos in the solar pair are quasi-degenerate but much lighter than the third neutrino. For $m_1 \gtrsim 0.1$eV all three neutrinos are quasi-degenerate. The three possibility are called "hierarchy", "partial-degeneracy" and "degeneracy" respectively.

From Fig.2.2 it is clear that, for inverted mass ordering, the solar pair is formed by two quasi-degenerate neutrinos for any value of m_3. For $m_3 \gtrsim 0.1$eV all three neutrinos are close in mass. The two situations $m_1 \approx m_2 \gg m_3$ and $m_1 \approx m_2 \gtrsim m_3$ are called "inverted hierarchy" and "inverted ordering" respectively.

We will see that, if the absolute scale of neutrino masses is close to 0.1 eV or larger, the mass matrix structures with normal or inverted ordering become practically indistinguishable.

The horizontal lines in Figs. 2.1 and 2.2 show the bounds (2.6), (2.7) and (2.8). The possibility of quasi-degenerate spectrum is constrained by upper limits but it is favored by the analysis [62].

2.1.2 The three mixing angles

The information on the mixing angles in the lepton sector is extracted by neutrino oscillation data.

The mixing angle which drives oscillations of solar neutrinos is θ_{12}. The LMA MSW allowed range, at 90% C.L., is [43]

$$\tan^2\theta_{12} = 0.42^{+0.2}_{-0.1} \ . \tag{2.9}$$

From atmospheric neutrino analysis we take, at the 90% C.L. [47, 162],

$$\tan\theta_{23} = 1^{+0.35}_{-0.25} \ . \tag{2.10}$$

We use the CHOOZ and Palo Verde bound on θ_{13} at the 90% C.L. [52, 53]:

$$\sin\theta_{13} \lesssim 0.22 \quad (\Delta m^2_{atm} \gtrsim 2\cdot 10^{-3}\text{eV}^2). \tag{2.11}$$

This bound is correlated with Δm^2_{atm} and should be relaxed if Δm^2_{atm} is smaller, as suggested by a recent global fit, which uses a preliminary reanalysis of SuperKamiokande data [163].

The values of lepton mixing angles are represented graphically in Fig. 2.3, where also quark mixing angles are shown for comparison. The quark mixings are known with much larger precision [174] and all three of them are quite small. On the contrary, two lepton mixing angles are large and one is quite small. Only θ_{23} can be maximal ($\pi/4$), since recent solar neutrino experiments have excluded $\theta_{12} = \pi/4$ at more than 3σ C.L.. Notice, however, that this does not necessarily imply $\theta_{12} < \theta_{23}$: using the 90% C.L. allowed ranges given above one can get, e.g., $\theta_{23} = 37°$ and $\theta_{12} = 38°$! This can be seen in Fig. 2.3.

The theory should of course explain why large mixing angles exist, but it is still unclear if one of these angles is really sticked to the maximal value or not. As far as θ_{13} is concerned, the present upper bound is still too weak to indicate clearly a large hierarchy between its value and the other mixing angles. Of course a stronger bound would require some underlying mechanism keeping θ_{13} tiny.

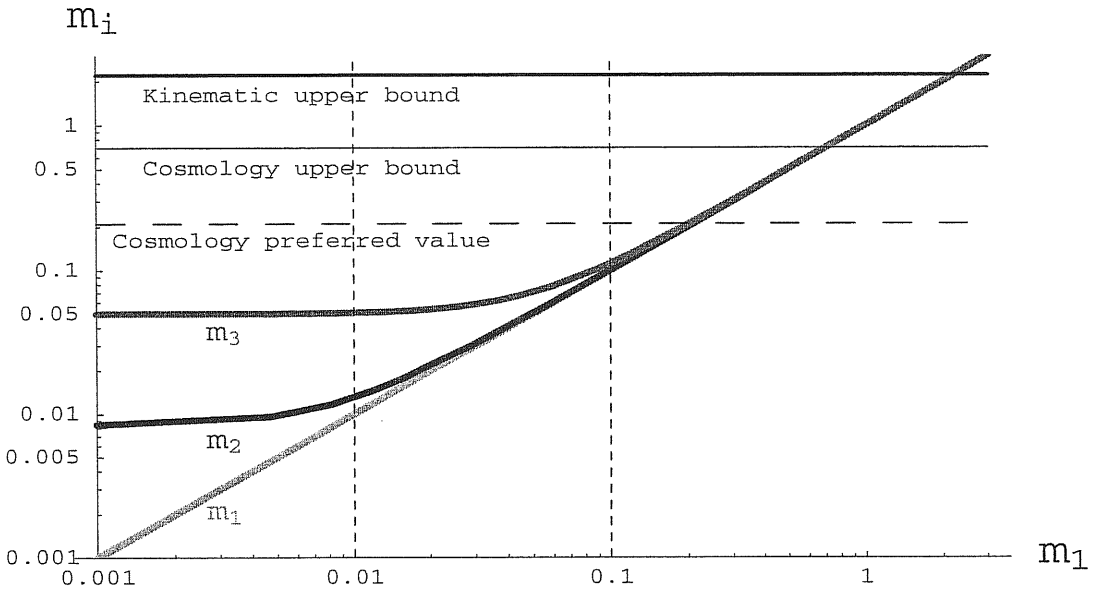

Figure 2.1: The three masses m_i of light neutrinos (in eV) as a function of m_1, in the case of normal ordering of the mass spectrum. We show also the upper bounds from tritium β-decay (Eq.(2.6)) and from WMAP (taking the most conservative higher value in Eq.(2.7)), as well as the preferred cosmological value (2.8).

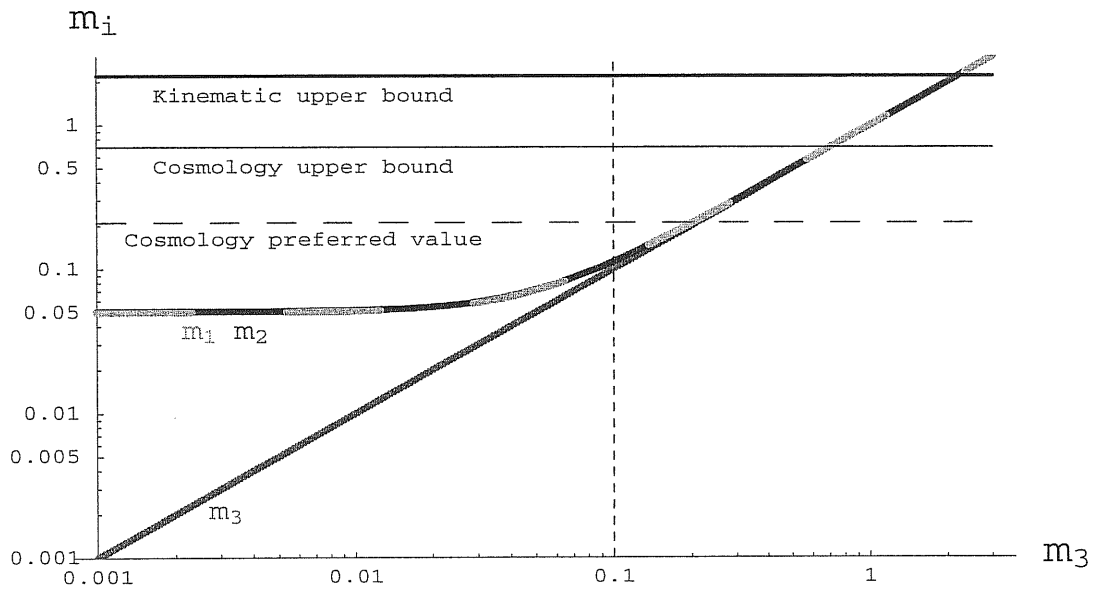

Figure 2.2: The three masses m_i of light neutrinos (in eV) as a function of m_3, in the case of inverted ordering of the mass spectrum. Notice that m_1 and m_2 lines are superimposed. The same bounds as in Fig. 2.1 are shown.

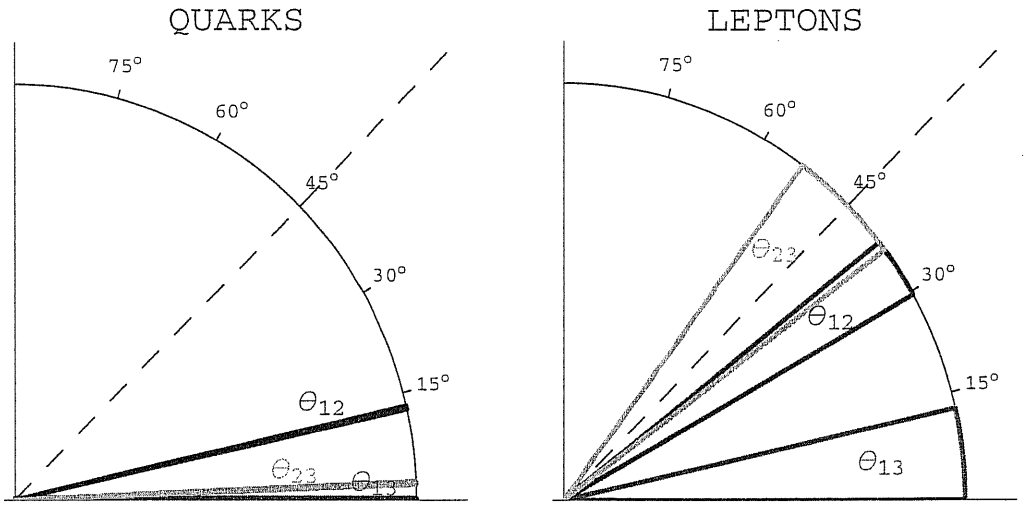

Figure 2.3: The 90% C.L. allowed ranges for the three mixing angles in the quark and in the lepton sector.

2.1.3 The three CP-violating phases

Let us emphasize that the experimental input (2.4) - (2.11) does not depend on the relative phases of neutrino mass eigenstates, ρ and σ, which can be observed only in processes with $\Delta L = 2$, therefore not in usual flavor oscillations.

The input does not depend also on the Dirac phase, δ. This can be explicitly seen from the parameterization (2.2): at the level of present experimental accuracy, the solar and atmospheric neutrino results are determined by U_{e1}, U_{e2} and $U_{\mu 3}, U_{\tau 3}$ respectively. CHOOZ gives the bound on $|U_{e3}|$. All these quantities do not depend on δ.

The phase δ can be measured in future long baseline accelerator experiments [175], as well as in neutrino factories [176], if θ_{13} is not too small. It is well-known that a vanishing mixing angle implies no CP-violation in oscillations.

The unique accessible way to probe Majorana phases is neutrinoless double-beta ($0\nu 2\beta$)-decay (in assumption that the exchange of the light Majorana neutrinos is the only mechanism of the decay). The present upper limit on the effective Majorana neutrino mass probed in ($0\nu 2\beta$)-decay is [54, 55]:

$$m_{ee} \equiv \left| \sum_i (U^*_{PMNS})^2_{ei} m_i \right| < (0.35 \div 1.3) \text{ eV} \qquad (90\% \text{ C.L.}) \,, \tag{2.12}$$

where uncertainties in the nuclear matrix elements are taken into account. A positive result on $0\nu 2\beta$-decay has been recently announced [177], with the following allowed range (95% C.L.):

$$m_{ee} = (0.39^{+0.17}_{-0.28}) \text{ eV} \,.$$

This claim has still a controversial interpretation (see discussion in [95, 178, 179, 180]).

Since the contribution of m_3 to m_{ee} is suppressed by the small factor s^2_{13}, the $(0\nu 2\beta)$-decay is more sensitive to the relative phase ρ between ν_1 and ν_2 than to the phase σ. In the limit $s_{13} \to 0$, Eqs. (2.1) and (2.12) imply

$$m_{ee} = \left| c^2_{12} m_1 e^{-2i\rho} + s^2_{12} \sqrt{m^2_1 + \Delta m^2_{sol}} \right| .$$

If θ_{12}, Δm^2_{sol} and m_1 are measured independently, in principle the value of ρ can be extracted from $(0\nu 2\beta)$-decay.

An independent determination of the phase σ defined in Eq.(2.3) seems out of the reach of near future experiments. We will discuss in detail this problem in section 2.5.

2.2 The mass matrix in flavor basis

2.2.1 Parameterization

The neutrino Majorana mass term in the Lagrangian is given by

$$\Delta\mathcal{L}^{Maj} = -\frac{1}{2}\, \overline{\nu^c_\alpha}\, M_{\alpha\beta}\, \nu_\beta + \text{h.c.} .$$

The neutrino mass matrix in flavor basis, M, can be written as

$$M = U^* M^{diag} U^\dagger , \tag{2.13}$$

where U is defined in Eq.(2.2) and

$$M^{diag} \equiv diag(m_1 e^{-2i\rho},\ m_2,\ m_3 e^{-2i\sigma}) . \tag{2.14}$$

The matrix M is symmetric and, therefore, it is defined by six elements. These are determined by 6 absolute values and 6 phases. Three phases can be eliminated by rephasing of the neutrino flavor eigenstates, so that only 9 quantities have physical meaning. This matches 9 parameters (3 phases, 3 masses and 3 angles) which appear in our parameterization. According to Eqs.(2.13,2.14), the mass matrix elements can be written explicitly as

$$M_{\alpha\beta} = (U^*_{\alpha 1} U^*_{\beta 1})\, m_1 e^{-2i\rho} + (U^*_{\alpha 2} U^*_{\beta 2})\, m_2 + (U^*_{\alpha 3} U^*_{\beta 3})\, m_3 e^{-2i\sigma} , \quad \alpha, \beta = e, \mu, \tau . \tag{2.15}$$

The matrix elements, as functions of the CP violating phases, depend on the parameterization. Our choice of parameterization has the following motivations. We ascribe the Majorana phases to the first and the third mass eigenstates (Eq.(2.14)), so that in the limit of strong normal (inverted) mass hierarchy the dependence on the phase ρ (σ) disappears. Furthermore, in the limit of degeneracy the interplay of the two Majorana phases (due to mixing) is weaker if σ is attached to the third mass

eigenstate. The standard parameterization (Eq.(2.2)) of the mixing matrix U has the advantage that the Dirac phase is associated to s_{13}. So, the influence of δ on the structure of the matrix is suppressed and, moreover, with improvements of the bound on s_{13} the effect of the phase will decrease. In our parameterization the m_{ee} element depends on all three phases. In particular, the phase δ enters in the combination $(\sigma - \delta)$. The dependence of m_{ee} on $(\sigma - \delta)$ is very weak being suppressed by s_{13}^2.

In what follows we will mainly analyze the absolute values of mass matrix elements, $m_{\alpha\beta}$:

$$M_{\alpha\beta} = m_{\alpha\beta} e^{i\phi_{\alpha\beta}} \ , \quad \alpha, \beta = e, \mu, \tau \ . \tag{2.16}$$

The absolute values may give straightforward information on possible underlying symmetry. The phases of the mass matrix elements, $\phi_{\alpha\beta}$, can also be important for the theory and we will discuss their main features in the following.

Using Eq. (2.15) and treating ρ and σ as free parameters, it is easy to see that the maximal value of the individual matrix element is given by

$$m_{\alpha\beta}^{max} = \sum_i m_i |U_{\alpha i} U_{\beta i}| . \tag{2.17}$$

The minimal value is

$$m_{\alpha\beta}^{min} = \max \left\{ 0 \ , \ \left[2 \max_i (m_i |U_{\alpha i} U_{\beta i}|) - \sum\nolimits_i (m_i |U_{\alpha i} U_{\beta i}|) \right] \right\} \ . \tag{2.18}$$

These relations have been given for the element m_{ee} in [181] and generalized to other elements in [182, 183].

Notice that, in flavor basis, $m_{\alpha\beta}$ are physical quantities, that is, they can be *directly* measured in physical processes. In particular, the rate of the neutrinoless 2β-decay is proportional to m_{ee}^2. Other entries are in principle measurable in processes with $\Delta L = 2$, like the decay $K^+ \to \pi^- \mu^+ \mu^+$ or the scattering $e^- p \to \nu_e l^{\pm} l'^{\pm} X$ (for a review see [184]). The rates of these processes are proportional to $m_{\alpha\beta}^2$, where α and β are the flavors of the two produced leptons in the final state or leptons in the initial and final states. The present bounds on the elements $m_{\alpha\beta}$ other than m_{ee} are many orders of magnitude weaker than indirect limits. For instance the bound on $m_{e\mu}^2$ is 16 orders of magnitude above the limit obtained from oscillations [183]. Clearly, the possibility to improve direct limits deserves further studies.

According to Eq. (2.13), the mixing matrix U distributes the masses from M^{diag} to the elements of the flavor mass matrix M:

$$m_1, m_2, m_3 \to m_{\alpha\beta} .$$

The following sum rule is useful for the analysis of the flavor mass matrix:

$$S_0 \equiv \sum_{i=1,2,3} m_i^2 = \sum_{\alpha,\beta=e,\mu,\tau} m_{\alpha\beta}^2 \ . \tag{2.19}$$

That is, the sum of moduli squared of all the elements of the mass matrix is invariant under basis transformation (rotation). The equality (2.19) is the straightforward consequence of the unitarity of the transformation [153].

It is very useful to define the mass ratios

$$k \equiv \frac{m_1}{m_2} , \qquad r \equiv \frac{m_3}{m_2} \tag{2.20}$$

and the quantities

$$\begin{aligned} X &\equiv x e^{i\phi_x} \equiv s_{12}^2 k e^{-2i\rho} + c_{12}^2 , \\ Y &\equiv y e^{i\phi_y} \equiv s_{12} c_{12} (1 - k e^{-2i\rho}) , \\ Z &\equiv z e^{i\phi_z} \equiv c_{12}^2 k e^{-2i\rho} + s_{12}^2 . \end{aligned} \tag{2.21}$$

For $k = 0$ (normal mass hierarchy), X, Y and Z are real and depend only on θ_{12}. For $k = 1$ (limit of degenerate m_1 and m_2), it follows from Eq.(2.21) that

$$x = z = \sqrt{1 - y^2} = \sqrt{1 - \sin^2 2\theta_{12} \sin^2 \rho} \tag{2.22}$$

and, taking into account that $c_{12} > s_{12}$,

$$-\phi_x = \phi_z + 2\rho = \arctan\left(\frac{\sin 2\rho}{\cot^2 \theta_{12} + \cos 2\rho}\right) , \qquad \phi_y = \frac{\pi}{2} - \rho . \tag{2.23}$$

Notice that the phase ϕ_x varies in a rather narrow interval, which decreases with θ_{12}:

$$\sin \phi_x \in [-\tan^2 \theta_{12}, \tan^2 \theta_{12}] .$$

One can write the matrix elements as series of powers of the small parameter s_{13}. Using Eqs.(2.20) and (2.21), we obtain

$$\begin{aligned} M_{ee}/m_2 &= Z - s_{13}^2 Z' , \\ M_{e\mu}/m_2 &= c_{13}(c_{23} Y - s_{13} s_{23} e^{-i\delta} Z') , \\ M_{e\tau}/m_2 &= c_{13}(-s_{23} Y - s_{13} c_{23} e^{-i\delta} Z') , \\ M_{\mu\mu}/m_2 &= c_{23}^2 X + s_{23}^2 r e^{-2i\sigma} - s_{13} \sin 2\theta_{23} e^{-i\delta} Y + s_{13}^2 s_{23}^2 e^{-2i\delta} Z' , \\ M_{\tau\tau}/m_2 &= s_{23}^2 X + c_{23}^2 r e^{-2i\sigma} + s_{13} \sin 2\theta_{23} e^{-i\delta} Y + s_{13}^2 c_{23}^2 e^{-2i\delta} Z' , \\ M_{\mu\tau}/m_2 &= s_{23} c_{23}(-X + r e^{-2i\sigma}) - s_{13} \cos 2\theta_{23} e^{-i\delta} Y - s_{13}^2 s_{23} c_{23} e^{-2i\delta} Z' , \end{aligned} \tag{2.24}$$

where

$$Z' \equiv z' e^{i\phi_{z'}} = Z - r e^{2i(\delta - \sigma)} . \tag{2.25}$$

2.2.2 Zero order mass matrix

The dominant structure of the mass matrix can be defined as the set of contributions to the matrix elements which are not proportional to small parameters. We will call "zero oder" mass matrix a matrix where some small parameters are put to zero.

As far as mixing angles are concerned, two small parameters can be identified:

1) the 1-3 mixing (see (2.11)):

$$s_{13} \lesssim 0.2 \ ;$$

2) the deviation of 2-3 mixing from maximal value (see (2.10)):

$$\xi \equiv \cos 2\theta_{23} \in (-0.3 \div 0.3) \ . \tag{2.26}$$

At present, both s_{13} and ξ are compatible with zero. Future experimental studies could further restrict the upper bounds or, alternatively, measure non-zero values of these parameters.

As far as mass eigenvalues are concerned, the smallness of mass ratios strongly depends on the type of mass spectrum. However, a "universal quantity" relevant for all possible mass spectra is the ratio of masses squared differences:

$$R \equiv \sqrt{\frac{\Delta m^2_{sol}}{\Delta m^2_{atm}}} = 0.17 \ ^{+0.16}_{-0.06} \ , \tag{2.27}$$

where the central value corresponds to the best fit values of mass squared differences and the interval is obtained varying Δm^2_{atm} and Δm^2_{sol} in the 90% C.L. ranges (see (2.4),(2.5)). Notice that this small parameter cannot be zero and, in fact, cannot be very small ($r_\Delta \gtrsim 0.1$). It is much larger than any other mass ratio between quarks or charged leptons of different generations.

To find the zero order mass matrix let us start neglecting $\mathcal{O}(s_{13})$ terms with respect to $\mathcal{O}(1)$ terms. Of course the subdominant structure of the matrix, formed by small ($\mathcal{O}(s_{13})$) elements, cannot be studied in this approximation. Using Eq.(2.24), for $s_{13} = 0$ we get:

$$m(s_{13}=0) = m_2 \begin{pmatrix} z & c_{23}y & s_{23}y \\ \dots & |c^2_{23}x + s^2_{23}re^{-2i\sigma_x}| & s_{23}c_{23}|-x+re^{-2i\sigma_x}| \\ \dots & \dots & |s^2_{23}x + c^2_{23}re^{-2i\sigma_x}| \end{pmatrix} \ , \tag{2.28}$$

where

$$\sigma_x \equiv \sigma + \phi_x/2 \ . \tag{2.29}$$

We have seen in section 2.1.1 that the solar mass split is tiny with respect to absolute neutrino masses apart from the case of normal hierarchy. The solar mass difference do not affect the dominant structure of the mass matrix if k is approximately equal to 1. For $m_1^2 \gg \sqrt{\Delta m^2_{sol}}$ we can write

$$k \equiv 1 - \epsilon \ , \qquad \epsilon \approx \frac{\Delta m^2_{sol}}{2m_1^2} \tag{2.30}$$

For example, $k > 0.95$ for $m_1^2 \gtrsim 9\Delta m_{sol}^2$. In the limit $k = 1$ ($\epsilon = 1, m_1 = m_2$), Eq.(2.22) holds and therefore the mass matrix (2.28) becomes:

$$m^0 \equiv m(s_{13} = \epsilon = 0) = m_2 \begin{pmatrix} x & c_{23}\sqrt{1-x^2} & s_{23}\sqrt{1-x^2} \\ \dots & |c_{23}^2 x + s_{23}^2 r e^{-2i\sigma_x}| & s_{23}c_{23}|-x+re^{-2i\sigma_x}| \\ \dots & \dots & |s_{23}^2 x + c_{23}^2 r e^{-2i\sigma_x}| \end{pmatrix} , \tag{2.31}$$

where ϕ_x is now given by Eq.(2.23).

Let us consider the properties of the matrix (2.31).

1) It depends on four independent parameters: $x = x(\rho, \theta_{12})$, $\sigma_x = \sigma_x(\sigma, \rho, \theta_{12})$, r, θ_{23}. According to the experimental input, we find that parameters are restricted, at 90% C.L., in the following ranges:

$$c_{23}^2 \in [0.35, 0.65] , \quad x \in [\cos 2\theta_{12}, 1] = [0.25, 1] , \quad \sigma_x \in [0, \pi) . \tag{2.32}$$

The value of x in this interval is fixed by ρ. The phase σ_x is unconstrained, because σ is. Therefore, the matrix structure can depend significantly on the values of the two Majorana phases. To put to zero also ξ (Eq.(2.26)) amounts to substitute $c_{23}^2 = s_{23}^2 = 1$.

Different mass spectra are described by Eq.(2.31), depending on the value of r: inverted hierarchy (ordering) for $0 \leq r < 1$, degeneracy for $r = 1$, normal ordering for $1 < r \lesssim 2 \div 3$. For larger values of r (normal hierarchy, $3 \lesssim r \lesssim 10$), the approximation $k = 1$ is no longer valid and one should use Eq.(2.28).

2) Using the bounds (2.32), we get the following maximal and minimal values of the matrix elements:

$$m_{ee} \in m_2[0.25, 1] , \quad m_{e\mu(e\tau)} \in m_2[0, 0.6] , \quad m_{\mu\mu(\mu\tau)(\tau\tau)} \in m_2[0, (1+r)/2] . \tag{2.33}$$

For previous studied of the allowed values of the matrix elements see [183, 185].

3) CP is conserved only for extreme values of x:

$$\begin{aligned} x = x_{min} \equiv \cos 2\theta_{12} : &\quad \rho = \pi/2 ; \\ x = x_{max} \equiv 1 : &\quad \rho = 0 . \end{aligned}$$

4) The best fit value of 1-2 mixing (according to the LMA solution of the solar neutrino problem) implies

$$x_{min}^{bf} \approx 0.41 . \tag{2.34}$$

The upper bound (2.9) on 1-2 mixing gives $x_{min} > 0.25$. These results have important implications for the structure of the mass matrix. In particular, m_{ee} cannot be small:

$$m_{ee} > \cos 2\theta_{12} m_2 > 0.25 m_2 , \tag{2.35}$$

where $m_2 \gg \sqrt{\Delta m_{sol}^2}$ since we are in the case $k \approx 1$.

5) The six elements of matrix (2.31) are functions of only four parameters, so that there are two relations among the elements:

$$m_{ee}^2 + m_{e\mu}^2 + m_{e\tau}^2 = m_2^2 \,, \tag{2.36}$$

$$(m_2^2 - m_{ee}^2)(m_{\mu\mu}^2 - m_{\tau\tau}^2) = (m_{e\mu}^2 - m_{e\tau}^2)(2m_{ee}^2 - \Sigma_{\mu\tau}) \,, \tag{2.37}$$

where

$$\Sigma_{\mu\tau} \equiv m_{\mu\mu}^2 + m_{\tau\tau}^2 + 2m_{\mu\tau}^2 \tag{2.38}$$

is the sum of $\mu\tau$-block elements squared. Moreover, the parameters are restricted to the ranges given in (2.32). Therefore, the zero order matrix structure is constrained and there are correlations among the values of different elements.

There are two other useful relations for the zero order matrix elements:

$$m_{e\mu}^2 + m_{e\tau}^2 = (1 - x^2)m_2^2 \,, \qquad \Sigma_{\mu\tau} = (x^2 + r^2)m_2^2 \,. \tag{2.39}$$

The sum of all matrix elements squared is equal to the sum of mass eigenvalues squared (Eq.(2.19)):

$$\sum_{\alpha,\beta} m_{\alpha\beta}^2 = (2 + r^2)m_2^2 \,. \tag{2.40}$$

This equality holds also when s_{13}-corrections are included.

2.2.3 Small parameter contributions

The zero order mass matrix receives corrections proportional to the small parameters. The case of normal hierarchy is quite singular, since the zero order matrix (2.28) is sensitive to the Δm_{sol}^2. The e-row elements are suppressed by the ratio R (Eq.(2.27)) with respect to $\mu\tau$-block. We will discuss corrections to the matrix (2.28) in the section 2.4.1, dedicated specifically to the case of normal hierarchy.

Let us consider now the case $k \approx 1$ and discuss the $\mathcal{O}(s_{13})$ and $\mathcal{O}(\epsilon)$ corrections to the matrix (2.31). The structure of the leading order (linear in s_{13} and ϵ) corrections to m^0 can be parameterized by the matrices $m^{(s)}$ and m^ϵ:

$$m = \left| m^0 + s_{13} m^s + \epsilon m^\epsilon \right| + \mathcal{O}(s_{13}^2, \epsilon^2, s_{13}\epsilon) \,. \tag{2.41}$$

Defining

$$\varphi_1 \equiv \phi_{z'} - \phi_y - \delta \,, \qquad \varphi_2 \equiv \phi_y - \delta \,, \qquad \varphi_{\alpha\beta} \equiv \arg M_{\alpha\beta}(s_{13} = \epsilon = 0) \,, \tag{2.42}$$

we get, using Eq.(2.24),

$$m^{(s)} = m_2 \begin{pmatrix} 0 & -s_{23} z' \cos\varphi_1 & c_{23} z' \cos\varphi_1 \\ \dots & -\sin 2\theta_{23}\sqrt{1-x^2}\cos(\varphi_2 - \varphi_{\mu\mu}) & -\cos 2\theta_{23}\sqrt{1-x^2}\cos(\varphi_2 - \varphi_{\mu\tau}) \\ \dots & \dots & \sin 2\theta_{23}\sqrt{1-x^2}\cos(\varphi_2 - \varphi_{\tau\tau}) \end{pmatrix} . \tag{2.43}$$

The maximal values of these corrections can be easily computed: using Eqs.(2.25,2.22), one finds

$$z'^2 = x^2 + r^2 + 2rx\cos(2\delta - 2\sigma - \phi_z) \quad \in \quad [(x-r)^2, (x+r)^2]\,.$$

The main features of the matrix $m^{(s)}$ are the following:

- $m^s_{ee} = 0$, m_{ee} receives corrections only at the order s^2_{13}.
- In the case of maximal atmospheric mixing ($\theta_{23} = \pi/4$), also $m^s_{\mu\tau} = 0$. Moreover, corrections to $m_{e\mu}$ and $m_{e\tau}$ are equal and have opposite sign ($m^s_{e\mu} = -m^s_{e\tau}$). The same is true for $m_{\mu\mu}$ and $m_{\tau\tau}$: $m^s_{\mu\mu} = -m^s_{\tau\tau}$.
- The elements $m^s_{\alpha\beta}$ can be zero or take their maximal value depending on the value of the Dirac phase δ (see Eqs.(2.42),(2.43)).

Thus, the $\mathcal{O}(s_{13})$ corrections change the splitting between $m_{e\mu}$ and $m_{e\tau}$ as well as between $m_{\mu\mu}$ and $m_{\tau\tau}$ elements. Moreover, this splitting depends strongly on δ. For maximal possible value of s_{13}, the terms $s_{13}m^s_{\alpha\beta}$ can be as large as $(0.1 \div 0.2)m_2$. Future experiments may strengthen the upper bound on s_{13}, making the s_{13} corrections even smaller.

The smallness of s_{13} could be a signal of an underlying symmetry. The pattern of s_{13} corrections to the mass matrix in flavor basis could suggest how this symmetry is related to the flavor of neutrinos.

Finally, we give the explicit expression of the matrix $m^{(\epsilon)}$, introduced in Eq.(2.41):

$$m^{(\epsilon)} = m_2 \begin{pmatrix} -c^2_{12}\cos(2\rho + \phi_z) & c_{23}c_{12}s_{12}\cos(2\rho + \phi_y) & s_{23}c_{12}s_{12}\cos(2\rho + \phi_y) \\ \cdots & -c^2_{23}s^2_{12}\cos(2\rho + \varphi_{\mu\mu}) & c_{23}s_{23}s^2_{12}\cos(2\rho + \varphi_{\mu\tau}) \\ \cdots & \cdots & -s^2_{23}s^2_{12}\cos(2\rho + \varphi_{\tau\tau}) \end{pmatrix}. \tag{2.44}$$

The cosines in Eq.(2.44) take always the values ± 1 for $\rho, \sigma = 0, \pi/2$. This is important since we will see that very small matrix elements usually appear in m^0 for $\rho, \sigma \approx 0, \pi/2$ (see section 2.6.1).

Let us describe some general features of the ϵ-corrections.

- All matrix elements receive corrections proportional to Δm^2_{sol}; $m^{(\epsilon)}_{\alpha\beta} = 0$ for particular values of the phases ρ and σ only.
- In the case of maximal atmospheric mixing ($\theta_{23} = \pi/4$), corrections to $m_{e\mu}$ and $m_{e\tau}$ are equal to each other: $m^\epsilon_{e\mu} = m^\epsilon_{e\tau}$. The same is true for the corrections to $m_{\mu\mu}$ and $m_{\tau\tau}$: $m^\epsilon_{\mu\mu} = m^\epsilon_{\tau\tau}$.

From Eq.(2.30), in the case of inverted ordering we get, for the best fit values of Δm^2, $\epsilon \lesssim \frac{\Delta m^2_{sol}}{2\Delta m^2_{atm}} \approx 10^{-2}$, therefore the corrections $m^{\epsilon}_{\alpha\beta}$ are about 1% (using for Δm^2 the ranges in Eqs.(2.4) and (2.5) we get $\epsilon \lesssim 0.05$). In the case of normal ordering, the corrections become larger as long as m_1 decreases going to the case of normal hierarchy.

In all cases these corrections have crucial phenomenological consequence: they break the degeneracy between m_1 and m_2 and thus explain the solar neutrino conversion. The smallness of corrections means that the value of the solar mass difference emerges from minor details of the mass matrix (this is not the case for normal hierarchy). The pattern of $\mathcal{O}(\epsilon)$ corrections could give some information about the origin of the small parameter $\Delta m^2_{sol}/\Delta m^2_{atm}$.

2.3 Matrix elements and CP-violating phases

The CP violating phases are presently unknown. This leads to large uncertainties in the mass matrix structure, since the value of matrix elements strongly depends on these phases. We have seen that the Dirac-type phase can be always associated with s_{13}. Therefore it does not enter in the dominant structure of the mass matrix. Vice versa, the Majorana-type CP phases play a crucial role, as one can see in Eqs. (2.28) and (2.31).

CP is conserved if ρ and σ are equal to 0 or $\pi/2$ (definite CP parities of the three neutrino mass eigenstates). To our knowledge, there is not a theoretical principle which privileges CP conserving values of the Majorana phases ρ and σ over CP violating ones. Therefore, it is important to consider both the structures which correspond to definite CP parity assignments and the others. In particular, certain "symmetric" features of the mass matrix imply CP violation. For example, the elements $m_{\mu\mu}$, $m_{\mu\tau}$ and $m_{\tau\tau}$, in Eq.(2.31), are equal for $\theta_{23} = \pi/4$ and $\sigma_x = \pi/4, 3\pi/4$. The elements m_{ee}, $m_{e\mu}$ and $m_{e\tau}$ are equal only for $\theta_{23} = \pi/4$ and $x = 1/\sqrt{3}$, that corresponds to $\rho \approx \pi/3, 2\pi/3$.

In this section we will describe the dependence of mass matrix elements on the CP-violating phases using several graphical representations:
1) phase diagrams;
2) m_1-plots;
3) $\rho - \sigma$ plots of the matrix element moduli;
4) $\rho - \sigma$ plots of the matrix element arguments.

2.3.1 The phase diagrams and the m_1-plots

The matrix elements are the sums of 3 contributions corresponding to the 3 different mass eigenvalues (Eq.(2.15)). So, in the complex plane the masses $M_{\alpha\beta}$ can be represented as sums of 3 vectors (corresponding to the 3 contributions). The lengths of these vectors are determined by the mass eigenvalues (equivalently, by the ratios k and r in Eq.(2.20)) and by the moduli of $U_{\alpha i}$. The angles between vectors are given by

combinations of the phases ρ, σ and the arguments of $U_{\alpha i}$. In first approximation, one can consider, for each of the 3 contributions, only the leading order term in $U_{\alpha i}U_{\beta i}$, that is the one with the smallest power of s_{13}.

We will call this graphic representation, introduced for m_{ee} in [186] and used in [187, 182], the *phase diagram*. The phase diagrams allow one easily to find minimal and maximal values (Eqs. (2.17) and (2.18)) as well as phases of the matrix elements, and possible correlations between them. In Fig.2.4 we show phase diagrams for the case of normal ordering with partial degeneracy: $k \approx 1$, $r \approx 2$.

From the phase diagrams it is evident that the mass matrix elements are periodic functions of the CP violating phases. In section 2.4 we will analyze these dependences by quantifying for each phase the amplitude of variations, the period and the average value of the elements. We define the latter as the average between maximal and minimal possible values of the element. We will also consider the relative phases of variations of different elements and the correlations between them.

The relative weight of the 3 vectors change considerably with the absolute mass scale of neutrinos, let us say m_1. Therefore phase diagrams are useful only for a definite mass spectrum. In fact, for fixed value of the phases, the different elements vary with m_1 in strongly different ways. This can be seen in m_1-*plots* (Fig.2.5), where we show the dependence of $m_{\alpha\beta}$ on m_1 for different values of the Majorana phases σ and ρ. We assume here normal ordering.

For $m_1/\sqrt{\Delta m^2_{atm}} \lesssim 0.1$ ($m_1 \lesssim 0.005$ eV), $\mu\tau$-block elements are significantly larger than e-row elements, independently on phases. This interval of m_1 corresponds to hierarchical spectrum. The structure with dominant $\mu\tau-$block disappears for $m_1/\sqrt{\Delta m^2_{atm}} \sim 0.3 \div 0.5$ ($m_1 \sim (0.02 \div 0.03)$ eV), that is for partially degenerate spectrum. For $m_1 \gtrsim \sqrt{\Delta m^2_{atm}} \approx 0.05$ eV, the spectrum converges to the degenerate one. In this last case, the structure of the mass matrix depends substantially on the Majorana phases. Notice that, in general, the pairs of elements $m_{\mu\mu}$ and $m_{\tau\tau}$, as well as $m_{e\mu}$ and $m_{e\tau}$, have similar dependences on m_1.

For large part of the phase parameter space, all elements of the mass matrix increase with m_1, as expected. However there are cases (Fig. 2.5 a,f) where some elements goes to zero for increasing mass scale. Equalities among certain elements appear for some values of m_1. Particular structures are realized for the specific values of phases $(\rho, \sigma \approx 0, \pi/4, \pi/2)$ shown in Fig.2.5.

The drawback of this second kind of diagrams is that they are useful only for fixed values of the CP phases. We will overcome this problem in the next subsection.

2.3.2 The $\rho - \sigma$ plots

Once θ_{12} and θ_{23} are fixed (measured), the zero order mass matrix (2.28) is determined by k, r, ρ and σ. Taking also the limit $k \to 1$ (Eq.(2.31)), the matrix depends only on r, $x = x(\rho)$ and $\sigma_x = \sigma_x(\rho, \sigma)$. The dependences of various matrix elements on the

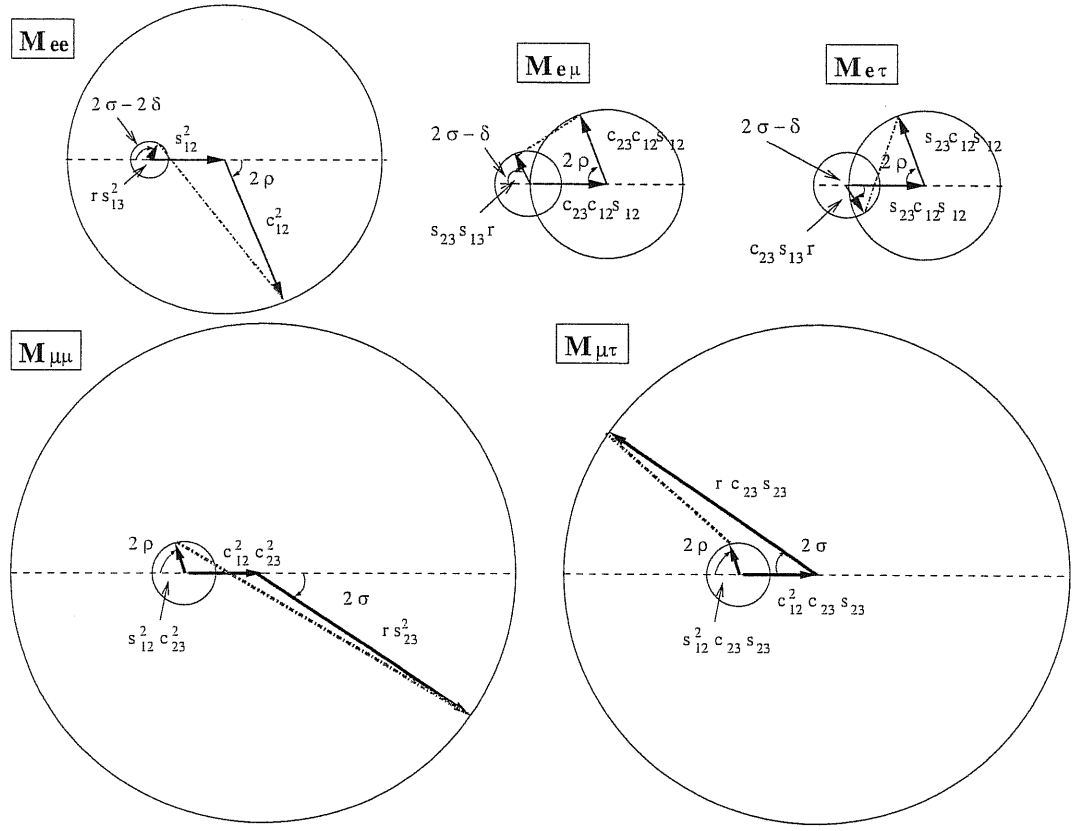

Figure 2.4: Phase diagrams of the mass matrix elements $M_{\alpha\beta}$ in the complex plane. Thick arrows represent the contributions of the three terms in Eq.(2.15), in leading order in s_{13}. The diagram for $M_{\tau\tau}$ is obtained from the $M_{\mu\mu}$-diagram with the substitution $s_{23} \leftrightarrow c_{23}$. The length of the red dash-dotted line gives the value of the matrix element modulus. The diagrams correspond to the normal ordering spectrum with partial degeneracy ($k \approx 1$, $r \approx 2$). The corresponding $\rho - \sigma$ plots are shown in Fig. 2.7.

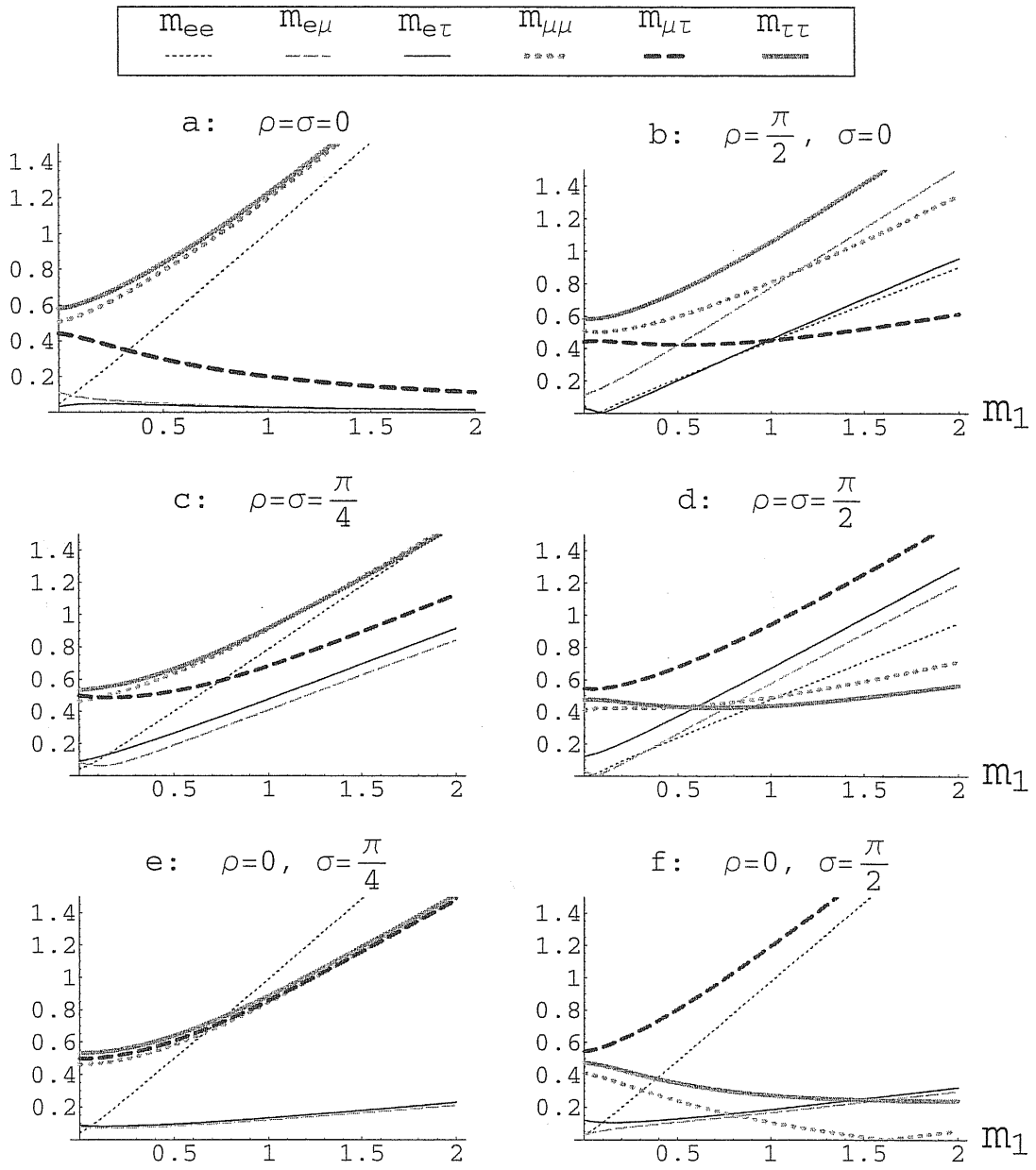

Figure 2.5: Dependence of the absolute value of neutrino mass matrix elements (in units $\sqrt{\Delta m^2_{atm}}$) on m_1. We show dependences for different values of the phases ρ and σ. We take $\Delta m^2_{sol} = 5 \cdot 10^{-5}\text{eV}^2$, $\Delta m^2_{atm} = 2.5 \cdot 10^{-3}\text{eV}^2$ and $\tan^2\theta_{12} = 0.36$, $\tan\theta_{23} = 0.93$, $s_{13} = 0.1$, $\delta = 0$.

Majorana phases are correlated.

Therefore, in order to perform a complete scanning of possible structures of the matrix, it is convenient to plot the matrix element moduli, $m_{\alpha\beta}$, as a function of ρ and σ, for different values of r. Let us introduce, therefore, the $\rho - \sigma$ plots, which show lines of constant masses $m_{\alpha\beta}$ in the plane of the Majorana phases ρ and σ [153, 154]. For m_{ee}, the Majorana phase plots (using a different parameterization) have been considered in [188, 189].

In the Figs. 2.6-2.10, we show the $\rho - \sigma$ plots for different values of the hierarchy parameter r. We have fixed solar and atmospheric parameters to their best fit values and we have taken $s_{13} = 0.1$, $\delta = 0$.

The $\rho - \sigma$ plots allow one immediately to see (i) the mass range in which a given matrix element can change, (ii) ranges of phases in which a given element can be zero (small), (iii) correlations among values of different elements.

The periodicity in ρ and σ implies that the opposite sides of the plots must be identified. For example, the case of equal CP parities of ν_1, ν_2 and ν_3 corresponds to any of the four corners of the plots. In general, any pair of values (ρ, σ) in the range $[0, \pi) \times [0, \pi)$ represents a physically independent mass matrix (obviously, the same point should be taken for all the elements). However, if $\delta = 0$ or π, it follows from (2.15) that

$$m_{\alpha\beta}(\sigma, \rho) = m_{\alpha\beta}(\pi - \sigma, \pi - \rho) \; .$$

This reflection symmetry is present in all the Figs. 2.6-2.10, but not in Fig.2.11, where $\delta = \pi/2$.

The phase ρ is associated with the mass m_1, therefore, in the case of strong normal hierarchy ($m_1 \to 0$), the dependence of $m_{\alpha\beta}$ on ρ disappears and the iso-mass contours become parallel to the axis ρ. Similarly, the dependence on σ disappears (contours parallel to the axis σ) for strong inverted hierarchy ($m_3 \to 0$). The contours for m_{ee} are nearly parallel to σ axis for any mass spectrum, since m_{ee} depends on σ via $O(s_{13}^2)$ terms. Also σ-dependence of $m_{e\mu}$ and $m_{e\tau}$ is suppressed by s_{13}. The pattern for $m_{\mu\tau}$ is approximatively complementary to that for $m_{\mu\mu}$ and $m_{\tau\tau}$, in the sense that regions of large $m_{\mu\tau}$ correspond to regions of small $m_{\mu\mu}$ and $m_{\tau\tau}$ and *vice versa*.

One can identify in the diagrams the effects of non-zero values of Δm^2_{sol} and s_{13}, as deformations of the zero order form (2.31) of the mass matrix. For example, $\theta_{23} = \pi/4$ implies $m^0_{e\mu} = m^0_{e\tau}$ and $m^0_{\mu\mu} = m^0_{\tau\tau}$. Also the $\mathcal{O}(\epsilon)$ corrections (Eq.(2.44)) do not break the degeneracy. The differences between the plots of these pairs of elements are due to s_{13} different from zero (Eq.(2.43)). The split between $m_{e\mu}$ and $m_{e\tau}$ is given by the following s_{13} terms (see (2.24)):

$$\pm s_{13} e^{-i\delta} Z'/\sqrt{2} \; ; \tag{2.45}$$

the split between $m_{\mu\mu}$ and $m_{\tau\tau}$ is given by

$$\pm s_{13} e^{-i\delta} Y \; . \tag{2.46}$$

A further split between these pairs of elements can be observed in the case of non maximal 2-3 mixing (Fig. 2.13).

According to Figs. 2.6-2.10, a large class of structures is allowed by the present data. Using $\rho - \sigma$ plots, one can identify the regions of parameters for which the matrix has:
- hierarchical structure: in which some elements are very small (light regions) and others are large (dark regions);
- non-hierarchical structure: where all matrix elements are of the same order - have gray color; one can find structures with certain ordering of elements;
- democratic structure: where all elements take the same or nearly the same value.
We will discuss these structures in detail in section 2.6.

Let us comment on specific features of Figs. 2.6 -2.10.

In Fig. 2.6 we show the plots for spectrum with normal ordering: $r = 5$ and $k \approx 0.6$. There is a sharp separation of the e-row and dominant $\mu\tau$-block elements. The structuring within these two groups is rather weak.

In Fig. 2.7 we show the plots for normal ordering spectrum with partial degeneracy: $r = 2$ and $k \approx 1$. The dependence of elements on ρ becomes stronger with increase of m_1. The $\mu\tau$-block elements have more profound structure. The elements $m_{e\mu}$ and $m_{e\tau}$ are small in the regions near the corners of the plots.

The plots for spectrum with strong degeneracy ($r \approx k \approx 1$) is shown in Fig. 2.8. Now the e-row elements depend strongly on ρ, whereas the dependence on σ is rather weak. With increase of m_1 the ρ-dependence becomes stronger also for the $\mu\tau$-block elements. The contribution of the term (2.46) for $m_{\mu\mu}$ adds constructively with the other ρ-dependent term (see Eq.(2.24)). For $m_{\tau\tau}$, instead, the contribution has an opposite sign, therefore ρ-dependence remains weak.

In Fig. 2.9 we consider the case of inverted ordering: $r = 0.5$ and $k \approx 1$. The heaviest element is m_{ee} for almost any choice of ρ and σ. All other elements cannot be very large. The dependence on σ decreases for decreasing r.

In Fig. 2.10 we move toward inverted hierarchy, taking $r = 0.1$. Now σ-dependence of elements is much weaker. The $\mu\tau$-block elements are smaller for $\rho \sim \pi/2$ while $m_{e\mu}$ and $m_{e\tau}$ are smaller for $\rho \approx 0, \pi$.

Let us consider now the modifications in the $\rho - \sigma$ plots due to variations of parameters in the allowed experimental ranges. The same mass spectrum as in Fig.2.8 (quasi-degeneracy) but with some parameters modified is considered in Figs. 2.11-2.14, to illustrate the role of different degrees of freedom for the determination of the matrix structure.

In Fig. 2.11 we show the plots for $\delta = \pi/2$. The difference between the plots for $m_{\mu\mu}$ and $m_{\tau\tau}$ becomes smaller in comparison with the case $\delta = 0$. For $\delta = \pi$, the $\rho - \sigma$ plots for $m_{\mu\mu}$ and $m_{\tau\tau}$ would interchange as compared with those in Fig.2.8 (see Eq.(2.46)). The pattern for $m_{\mu\tau}$ is almost unchanged. In the first approximation, the effect of $\delta = \pi/2$ on the e-row elements (instead of $\delta = 0$) is reduced to a shift of σ by $\pi/4$ for $m_{e\mu}$ and $m_{e\tau}$ and by $\pi/2$ for m_{ee} (see Eqs. (2.60) and (2.61)).

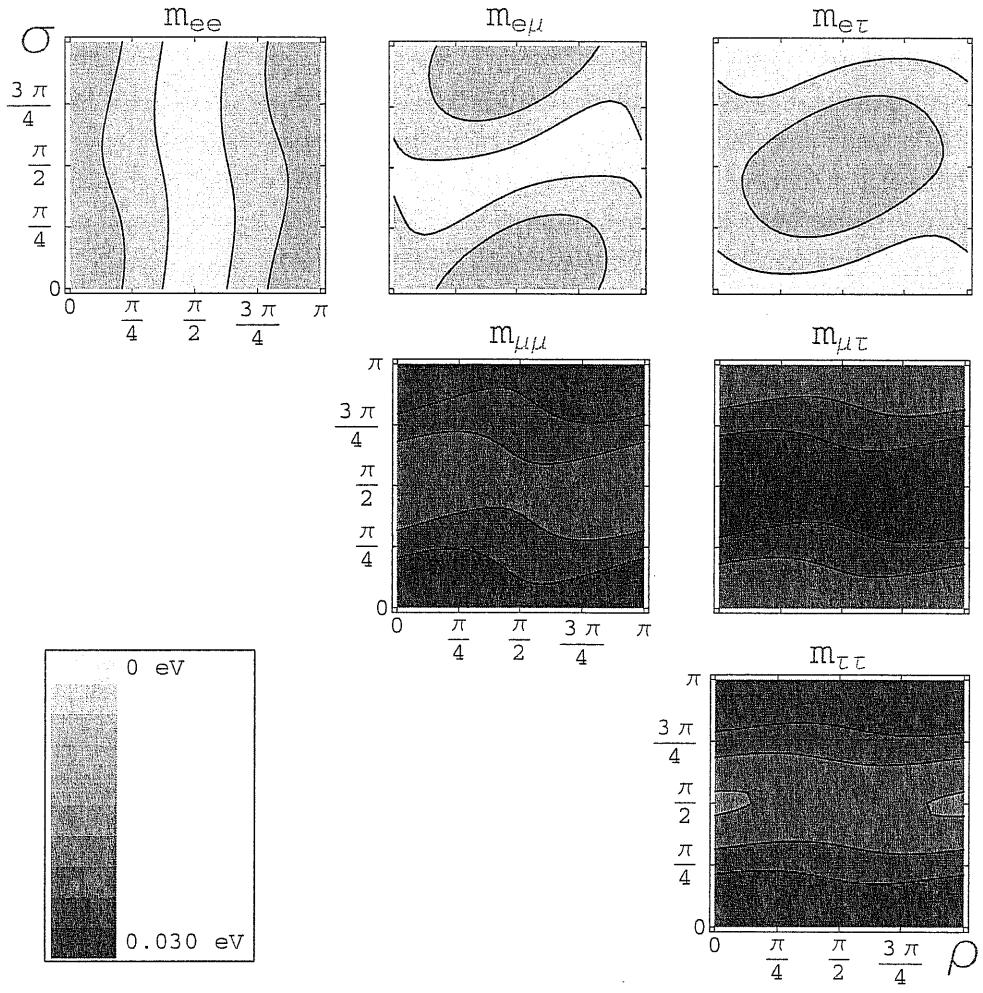

Figure 2.6: The $\rho - \sigma$ plots for $r \equiv m_3/m_2 = 5$, corresponding to normal ordering with $m_1 \approx 0.006$ eV. We show contours of constant mass (iso-mass) $m = (0.1, 0.2, \ldots, 0.9)m^{max}$, where $m^{max} = 0.03$ eV is the maximal value that the matrix elements can have, so that the lightest regions correspond to the mass interval $(0 - 0.003)$ eV and the darkest ones to $(0.027 - 0.030)$ eV. We take $\Delta m^2_{sol} = 7 \cdot 10^{-5}\text{eV}^2$, $\Delta m^2_{atm} = 2.5 \cdot 10^{-3}\text{eV}^2$ and $\tan^2\theta_{12} = 0.42$, $\tan\theta_{23} = 1$, $s_{13} = 0.1$, $\delta = 0$.

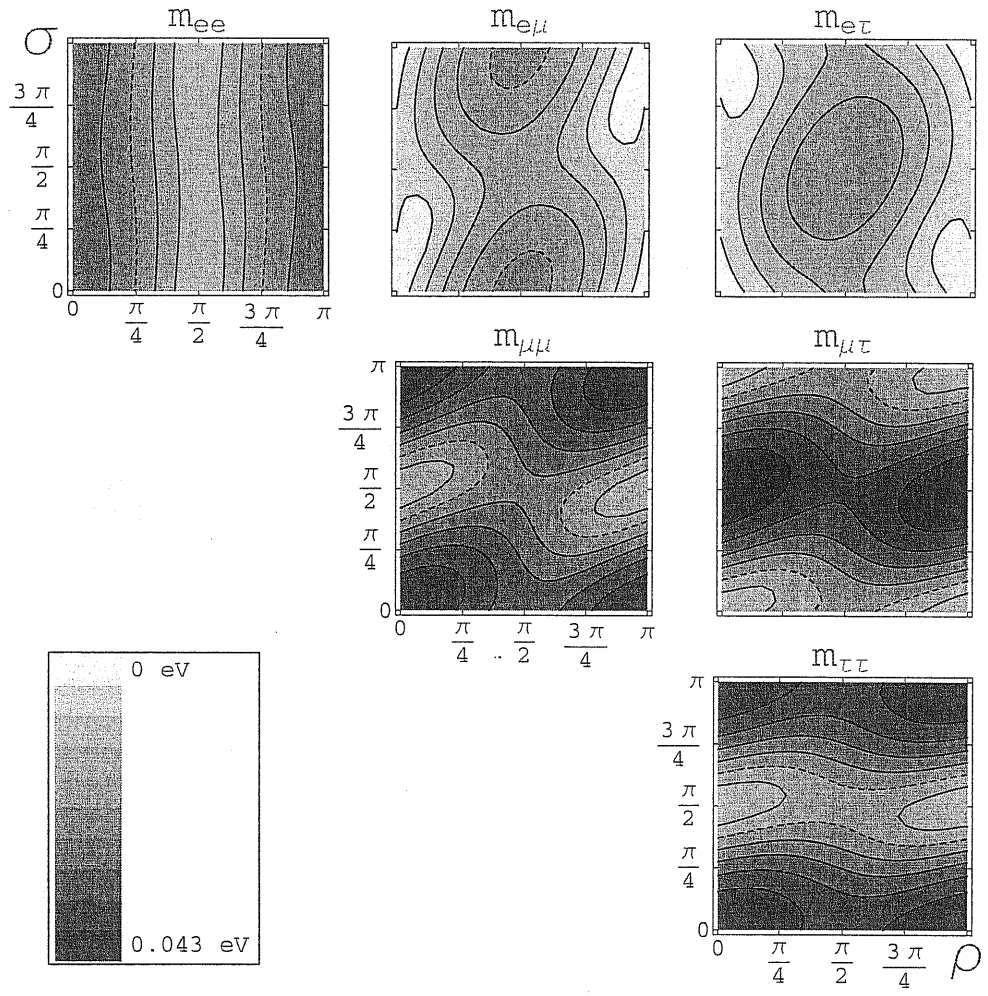

Figure 2.7: The $\rho - \sigma$ plots for $r = 2$, corresponding to normal ordering with $m_1 \approx 0.027$ eV. The other parameters are the same as in Fig.2.6. In this case $m^{max} = 0.043$ eV. The contour $m = 0.5\ m^{max}$ is dashed.

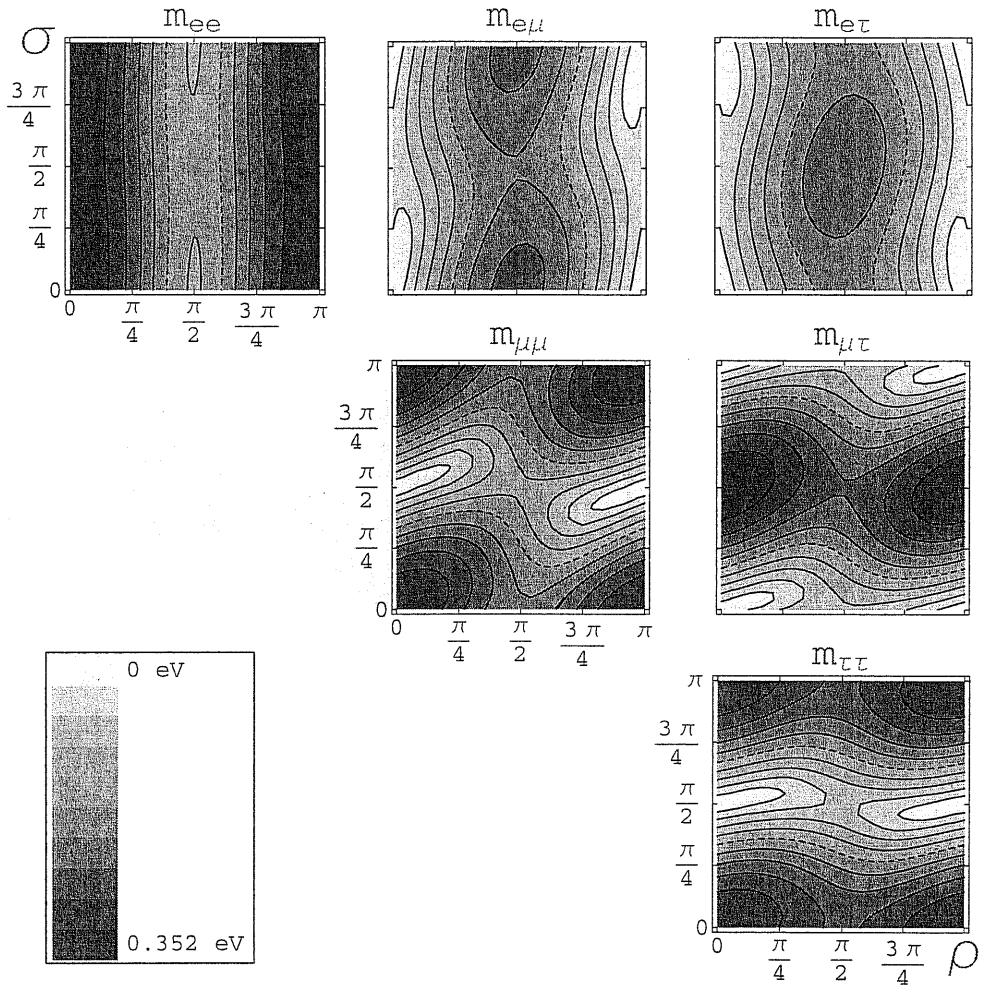

Figure 2.8: The $\rho - \sigma$ plots for $r = 1.01$, corresponding to normal ordering with $m_1 \approx 0.35$ eV (quasi-degeneracy). The other parameters are the same as in Fig.2.6. In this case $m^{max} = 0.352$ eV. The contour $m = 0.5\ m^{max}$ is dashed.

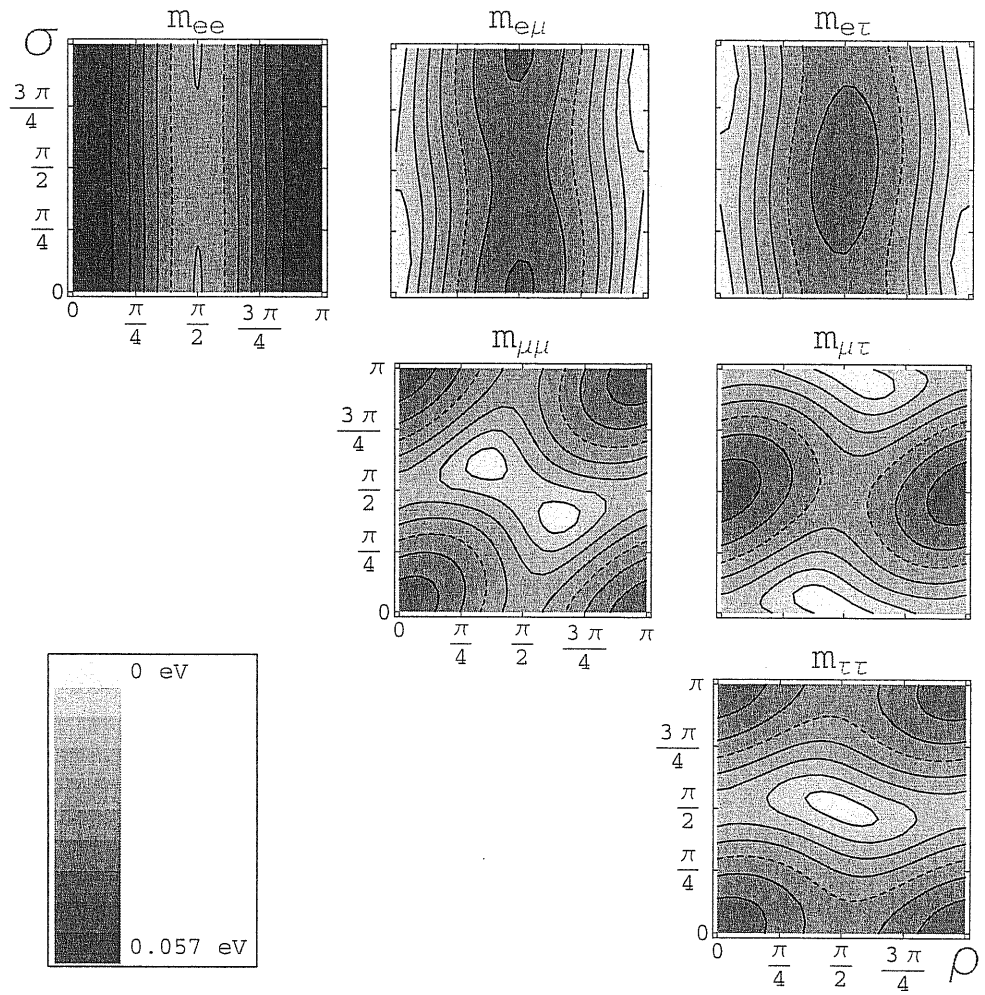

Figure 2.9: The $\rho - \sigma$ plots for $r = 0.5$, corresponding to inverted ordering with $m_3 \approx 0.029$ eV. The other parameters are the same as in Fig.2.6. In this case $m^{max} = 0.057$ eV. The contour $m = 0.5\ m^{max}$ is dashed.

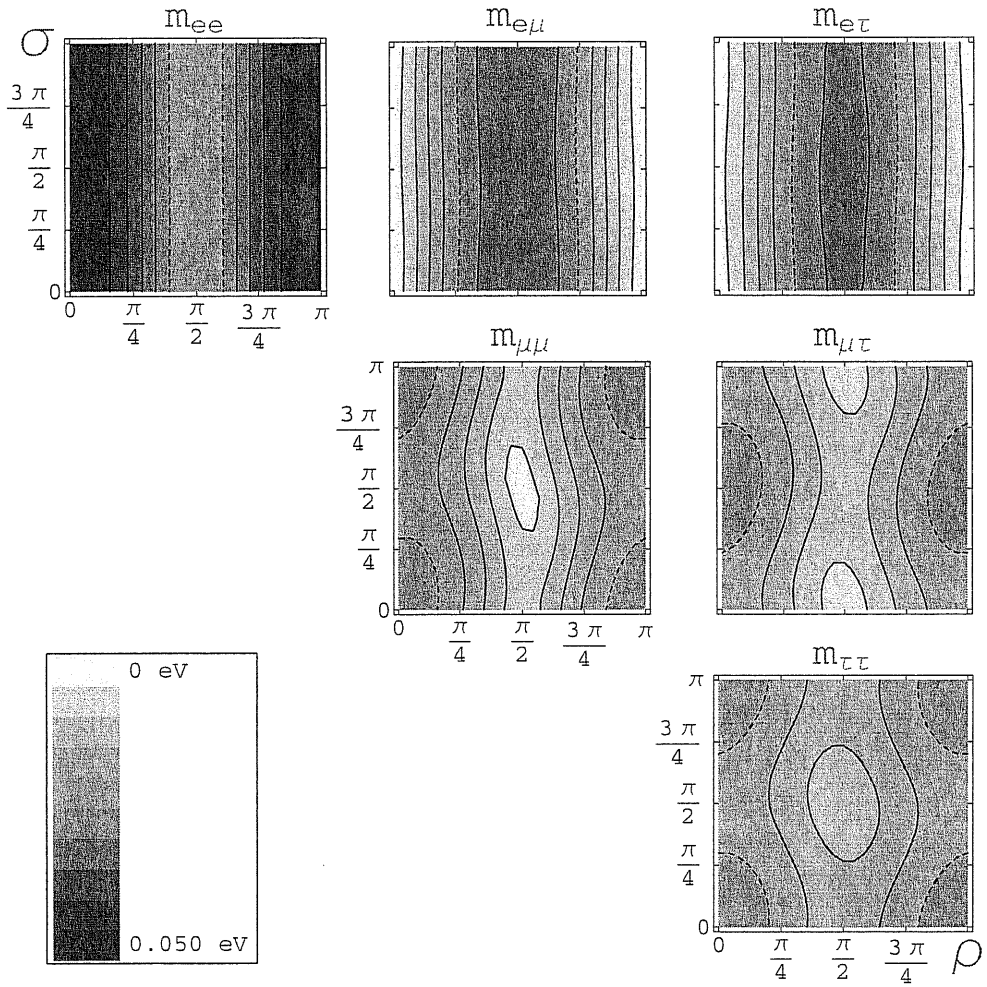

Figure 2.10: The $\rho - \sigma$ plots for $r = 0.1$, corresponding to inverted ordering with $m_3 \approx 0.005$ eV. The other parameters are the same as in Fig.2.6. In this case $m^{max} = 0.05$ eV. The contour $m = 0.5\ m^{max}$ is dashed.

In Fig. 2.12 we show the plots for $s_{13} = 0.2$. With increase of s_{13}, the dependence of e-row elements on σ becomes stronger, patterns for $m_{\mu\mu}$ and $m_{\tau\tau}$ become much more different, as well as $m_{e\mu}$ and $m_{e\tau}$.

In Fig. 2.13 we show the plots for non-maximal 2-3 mixing ($\tan\theta_{23} = 0.75$). The pattern for m_{ee} is unchanged and the one for $m_{\mu\tau}$ changes weakly. In contrast, the difference between the patterns for $m_{e\mu}$ and $m_{e\tau}$ increases. In particular, $m_{e\mu}$ can be large for $\rho \approx \pi/2$ and $\sigma \approx 0, \pi$. Also the difference between the patterns for $m_{\mu\mu}$ and $m_{\tau\tau}$ increases. Dependence of $m_{\tau\tau}$ on phases becomes weaker and regions with very small values of $m_{\tau\tau}$ disappear. In contrast, for $m_{\mu\mu}$ the region of small values appears near the center of the plot: $\rho \sim \sigma \sim \pi/2$. For $\tan\theta_{23} > 1$ (not shown) the situation is opposite: a region of small values at $\rho \sim \sigma \sim \pi/2$ appears for $m_{\tau\tau}$. Also $m_{e\tau}$ becomes, in general, larger than $m_{e\mu}$.

In Fig. 2.14 we show the plots for the 90% C.L. upper bound value of 1-2 mixing: $\tan^2\theta_{12} = 0.62$. The ρ dependence becomes strong for all the elements and especially for m_{ee}. This element can be quite small at $\rho \approx \pi/2$.

2.3.3 The phases of matrix element

Let us consider the complex phases of matrix elements. They are, in general, functions of all the unknown physical parameters: $\phi_{\alpha\beta} = \phi_{\alpha\beta}(m_1, \rho, \sigma, \delta, s_{13})$. In the limits of strong mass hierarchy or/and small s_{13}, the expressions are simplified and for some elements the phases are zero. In certain situations the phases of some elements depend only on ρ or on σ.

The values of the phases correlate (or anti-correlate) with the absolute values of the corresponding elements. Strong change of phase occurs typically in the regions of the parameter space where the modulus of the element is small. There are also correlations between phases of different elements.

These features are illustrated in Fig. 2.15, which correspond to degenerate mass spectrum with the same choice of parameters as in Fig. 2.8. The phase ϕ_{ee} depends mainly on ρ. The magnitude of the phase anti-correlates with the absolute value of the element: maximal m_{ee} corresponds to $\phi_{ee} \approx 0$. The phases $\phi_{e\mu}$ and $\phi_{e\tau}$ change with ρ and (weaker) with σ. The patterns are complementary: at $\rho \sim \pi/2$, $\phi_{e\mu}$ has minimum whereas $\phi_{e\tau}$ has maximum. Phases of the $\mu\tau$-block depend mainly on σ. The patterns for $\phi_{\mu\mu}$ and $\phi_{\tau\tau}$ are rather similar. Maximal (π) values of these phases are achieved at $\sigma \sim \pi/2$ and minimal (zero) values are at $\sigma \sim 0, \pi$.

One should worry about which phases are physical here, since we know that only three independent physical phases are contained in the 3×3 Majorana mass matrix of neutrinos. In fact, the phases of flavor eigenstates $\nu_{e,\,\mu,\,\tau}$ are not observable, that is one can arbitrarily redefine $\nu_\alpha \to e^{i\phi_\alpha}\nu_\alpha$. The matrix elements phases plotted in Fig. 2.15 depend on these redefinitions and, therefore, their values have no direct physical meaning. However, Fig. 2.15 allows to see correlations among the phases of different elements and between the phase and the modulus of a given element by comparison

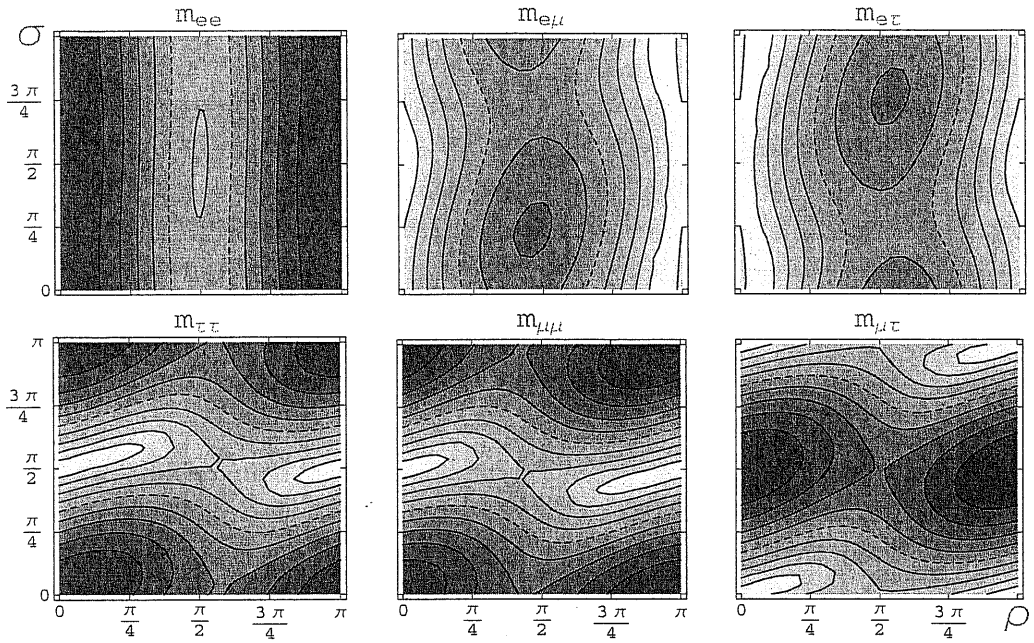

Figure 2.11: The same as in Fig.2.8, but for non-zero Dirac phase: $\delta = \pi/2$.

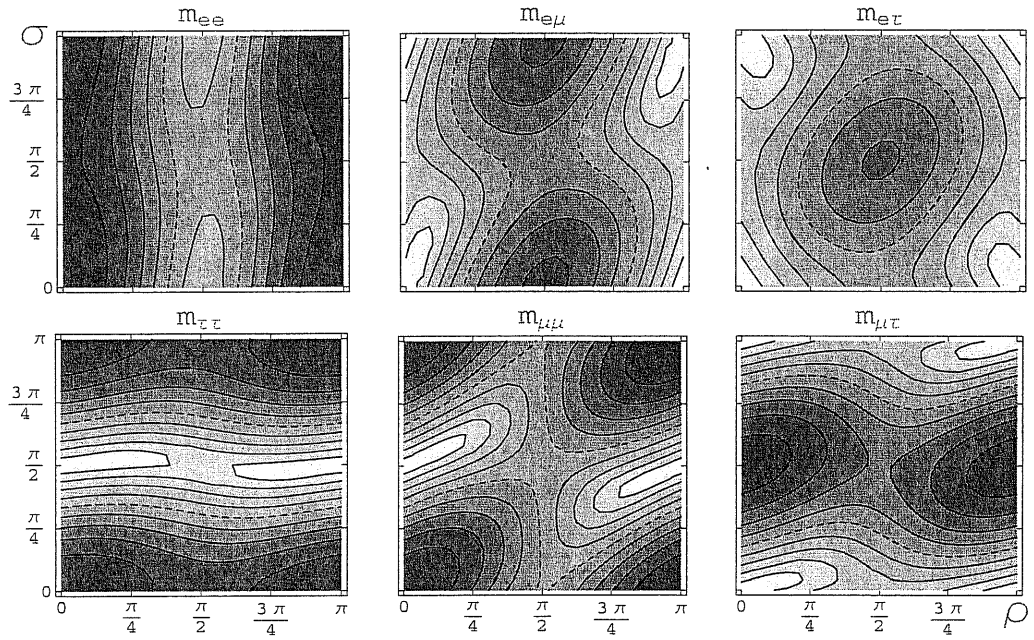

Figure 2.12: The same as in Fig.2.8, but for relatively large 1-3 mixing: $s_{13} = 0.2$.

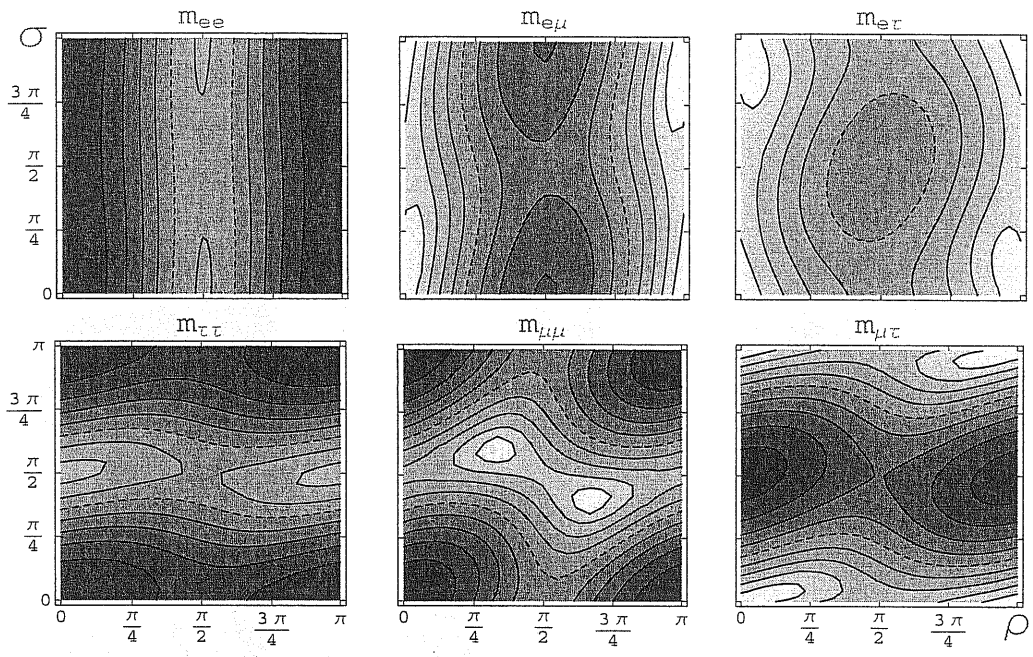

Figure 2.13: The same as in Fig.2.8, but for non-maximal 2-3 mixing: $\tan\theta_{23} = 0.75$.

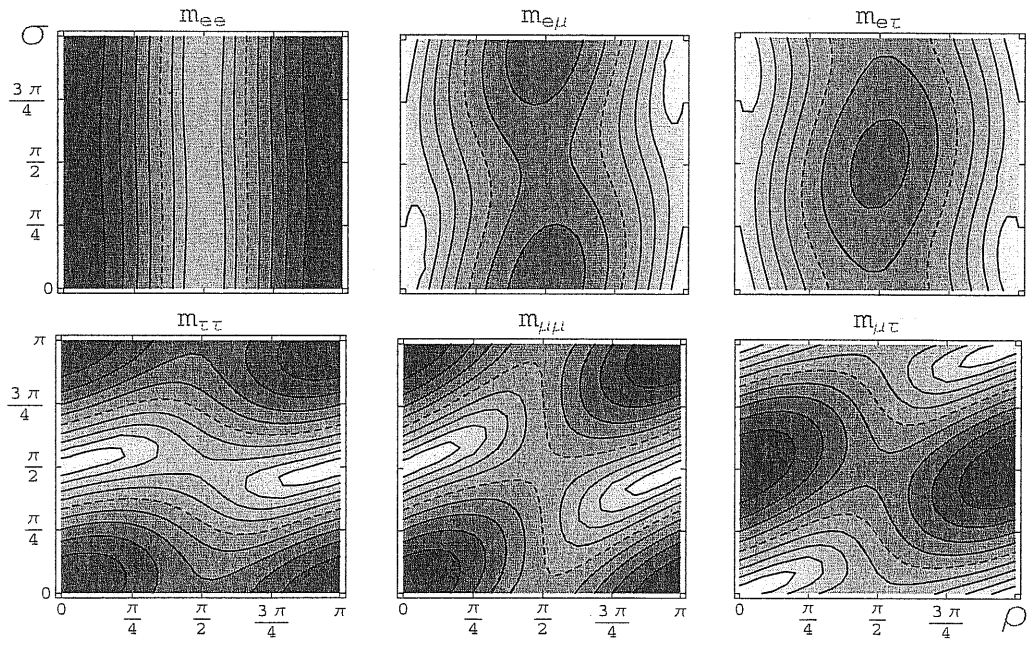

Figure 2.14: The same as in Fig.2.8, but for larger 1-2 mixing: $\tan^2\theta_{12} = 0.62$.

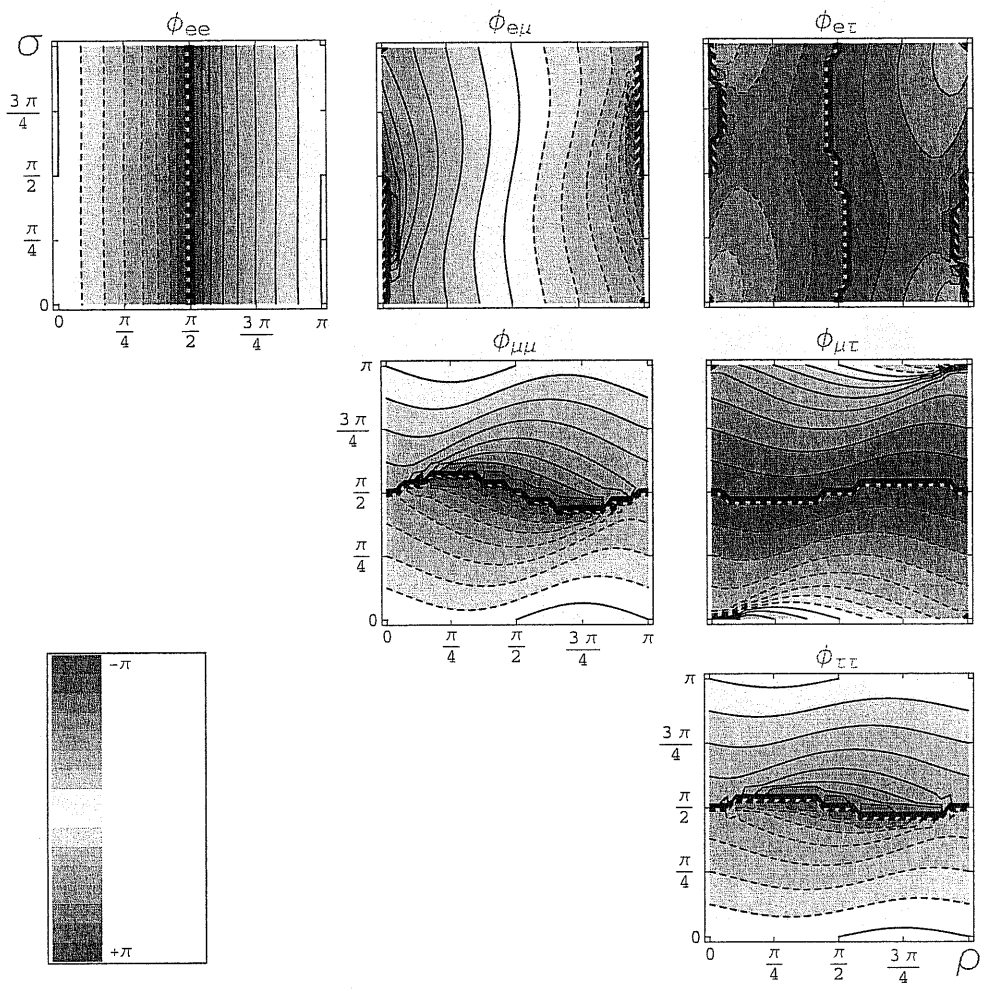

Figure 2.15: The $\rho-\sigma$ plots of the phases of mass matrix elements for the same set of parameters as in Fig.2.8. Shown are the contours of constant phase (iso-phase) $\phi_{\alpha\beta} = -\pi + n\pi/8$ for $n = 0, ..., 7$ (dashed contours) and for $n = 8, ..., 15$ (continuous contours).

with Fig. 2.8.

One can define three combinations of matrix element phases that are invariant under flavor eigenstate rephasing:

$$\Delta_{\alpha\beta} \equiv \phi_{\alpha\alpha} + \phi_{\beta\beta} - 2\phi_{\alpha\beta} = \arg\left(\frac{M_{\alpha\alpha}M_{\beta\beta}}{M_{\alpha\beta}^2}\right) , \qquad \alpha\beta = e\mu,\ e\tau,\ \mu\tau\ . \tag{2.47}$$

In general $\Delta_{\alpha\beta}$ are complicated functions of neutrino masses, mixing angles and of δ, ρ and σ. In Fig. 2.16 we show the $\rho - \sigma$ plots of these three phases for the same sets of parameters used in Figs. 2.8 and 2.15.

The values of $\Delta_{\alpha\beta}$ are physical and should be directly connected with the underlying physics that generates the neutrino mass matrix. Notice, for example, that $\Delta_{\mu\tau}$ is the unique phase invariant related with the $\mu\tau$-block of the matrix. In chapter 4 we will find that the value of $\Delta_{e\mu}$ is crucial to get successful leptogenesis.

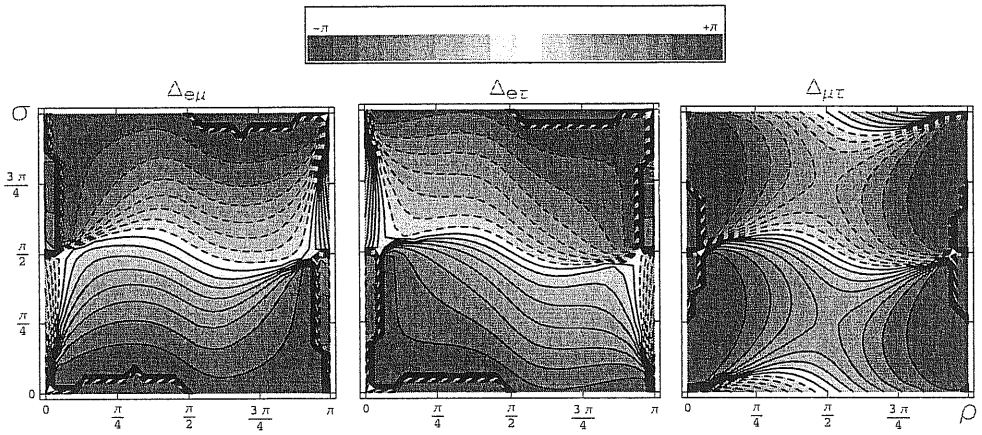

Figure 2.16: The $\rho - \sigma$ plots of the physical combinations $\Delta_{\alpha\beta}$ of matrix element phases (see Eq.(2.47)). We use the same set of parameters as in Fig.2.8. Shown are the contours of constant phase (iso-phase) $\Delta_{\alpha\beta} = -\pi + n\pi/8$ for $n = 0, ..., 7$ (dashed contours) and for $n = 8, ..., 15$ (continuous contours).

2.4 The matrix structure for the different mass spectra

In this section we will describe the detailed features of the neutrino mass matrix structure, discussing in turn all possible mass spectra.

2.4.1 Normal hierarchy

Let us consider the limit of strong mass hierarchy, when $m_1 \approx 0$, $m_2^2 \approx \Delta m_{sol}^2$ and $m_3^2 \approx \Delta m_{atm}^2$. Then $r \approx 6$ and the dependence on the Majorana phase ρ disappears.

Moreover, since $k \approx 0$, Eq.(2.21) implies $X \approx c_{12}^2$, $Y \approx s_{12}c_{12}$ and $Z \approx s_{12}^2$. Using Eq.(2.28), the matrix of the moduli for $s_{13} \to 0$ is:

$$m(m_1 = s_{13} = 0) = m_2 \begin{pmatrix} s_{12}^2 & c_{23}s_{12}c_{12} & s_{23}s_{12}c_{12} \\ \dots & \left|c_{12}^2 c_{23}^2 + s_{23}^2 r e^{-2i\sigma}\right| & s_{23}c_{23}\left|-c_{12}^2 + r e^{-2i\sigma}\right| \\ \dots & \dots & \left|c_{12}^2 s_{23}^2 + c_{23}^2 r e^{-2i\sigma}\right| \end{pmatrix} . \tag{2.48}$$

As far as matrix element phases are concerned, in this limit the e-row elements are real, $\phi_{e\alpha} = 0$, whereas the phases of $\mu\tau$-block elements are $\approx -2\sigma$; the corrections are proportional to $1/r$.

In Figs. 2.17, 2.18 we show the six mass matrix elements, $m_{\alpha\beta}$, $\alpha, \beta = e, \mu, \tau$, as functions of the phase σ, for different values of the mixing angles θ_{23} and θ_{13}, from the allowed regions given in (2.10) and (2.11).

The dependence of $\mu\tau$-block elements on θ_{23} can be described in terms of deviations from maximal mixing using the parameter $\xi \equiv \cos 2\theta_{23}$ (Eq.(2.26)). According to (2.48) and keeping only leading terms in r, we have:

$$m_{\mu\mu} = \frac{m_3}{2}(1 - \xi) , \qquad m_{\tau\tau} = \frac{m_3}{2}(1 + \xi) , \qquad m_{\mu\tau} = \frac{m_3}{2}\sqrt{1 - \xi^2} . \tag{2.49}$$

The element $m_{\mu\tau}$ is almost unchanged with respect to maximal θ_{23}, while $m_{\mu\mu}$ and $m_{\tau\tau}$ vary with ξ significantly and in opposite directions. In this approximation the determinant of the $\mu\tau$-block is zero and there is no dependence on CP violating phases.

The dependence of $\mu\tau$-block elements on σ is a result of the interplay of the main, $\mathcal{O}(r)$, terms and of the $\mathcal{O}(1)$ terms in Eq.(2.48); $m_{\mu\tau}$ has an opposite phase with respect to the two other elements. The relative amplitudes of variations equal

$$\frac{\Delta m^\sigma}{\bar{m}} \approx \frac{c_{12}^2}{r} \times \begin{cases} \cot^2\theta_{23}, & m_{\mu\mu} \\ \tan^2\theta_{23}, & m_{\tau\tau} \\ 1, & m_{\mu\tau} \end{cases} , \tag{2.50}$$

where $\bar{m}$ is the average value of the element. For the best fit values of the parameters the amplitudes are of order 10%. In the case of non-maximal 2-3 mixing, the amplitudes can reach $\sim 25\%$. The $\mu\tau$-block elements depend on s_{13} very weakly (see Figs.2.17,2.18). The corrections $\sim s_{13}$ (see Eq.(2.24)) lead to small phase shift and small change of the amplitude of variations.

When s_{13} is not negligibly small, the e-row elements are strongly modified, since the s_{13}-terms are enhanced by r and therefore can be comparable with the contributions in Eq.(2.48). Neglecting terms of the order $s_{13}s_{12}^2$, we get from Eq.(2.24) the expressions for $m_{e\mu}$ and $m_{e\tau}$:

$$m_{e\mu} \approx m_2 \left|s_{12}c_{12}c_{23} + r\ s_{13}s_{23}e^{i(\delta - 2\sigma)}\right| , \tag{2.51}$$

$$m_{e\tau} \approx m_2 \left|s_{12}c_{12}s_{23} - r\ s_{13}c_{23}e^{i(\delta - 2\sigma)}\right| . \tag{2.52}$$

So, the elements $m_{e\mu}$ and $m_{e\tau}$ depend on phases in the combination $(\delta - 2\sigma)$, they change with $(\delta - 2\sigma)$ in opposite phase, their values are determined by the interplay of the order 1 and order rs_{13} terms, which can have comparable sizes. Maximal values of $m_{e\mu}$ and $m_{e\tau}$ increase with s_{13}. The relative amplitude of variations of $m_{e\mu}$ with $(\delta - 2\sigma)$ is maximal when the two terms in (2.51) have the same modulus:

$$s_{13} = s_{13}^0 \equiv \frac{1}{2r} \sin 2\theta_{12} \cot \theta_{23} \approx 0.08 \ . \tag{2.53}$$

If $s_{13} = s_{13}^0$,

$$m_{e\mu} = 0 \qquad \text{for} \qquad \delta - 2\sigma = \pi \tag{2.54}$$

and the maximal value of $m_{e\mu}$ is $m_{e\mu}^{max} = 2\bar{m}_{e\mu} = m_2 \sin 2\theta_{12} c_{23}$. For $s_{13} < s_{13}^0$ (Fig. 2.17 panels a,c,e), the average value of $m_{e\mu}$ is determined by the first term in (2.51), whereas the amplitude of variations is given by s_{13}/s_{13}^0. For $s_{13} > s_{13}^0$, the second term in (2.51) dominates. It determines the average value of $m_{e\mu}$, around which variations occur. The relative amplitude of variations is given by the factor s_{13}^0/s_{13} (Fig. 2.17 b,d,f). The behavior of the element $m_{e\tau}$ is similar: the two terms in (2.52) are equal and can cancel each other if

$$s_{13} = \bar{s}_{13}^0 \equiv \frac{1}{2r} \sin 2\theta_{12} \tan \theta_{23} \tag{2.55}$$

($\bar{s}_{13}^0 = s_{13}^0$ for maximal 2-3 mixing), so

$$m_{e\tau} = 0 \qquad \text{for} \qquad \delta - 2\sigma = 0 \ . \tag{2.56}$$

Corrections of order $s_{13}s_{12}^2$, neglected in (2.51) and (2.52), produce a small relative shift of the phases of $m_{e\mu}$ and $m_{e\tau}$ (see Fig.2.17).

For the ee-element we have:

$$m_{ee} \approx m_2 \left| c_{13}^2 s_{12}^2 + r \ s_{13}^2 e^{2i(\delta - \sigma)} \right| \ . \tag{2.57}$$

It depends on the combination of phases $2(\delta - \sigma)$. Both contributions in (2.57) can be comparable in spite of the s_{13}^2-order of the second term. The two terms are equal at

$$\tan \theta_{13} = s_{12}/\sqrt{r} \approx 0.22 \ ,$$

that is, near the upper limit for s_{13}. In this case the amplitude of variation can be maximal and

$$m_{ee} = 0 \qquad \text{for} \qquad \delta - \sigma = \pi/2, \ 3\pi/2 \ . \tag{2.58}$$

Such a situation is approximately realized in Fig. 2.17 b,d,f. For small values of s_{13} ($s_{13} \ll 0.2$), the dependence of m_{ee} on phases is negligible (Fig.2.17 a,c,e). The relative amplitude of variations is determined by the ratio $\tan^2 \theta_{13} r/s_{12}^2$ and the average value equals $\overline{m}_{ee} \approx m_2 s_{12}^2$.

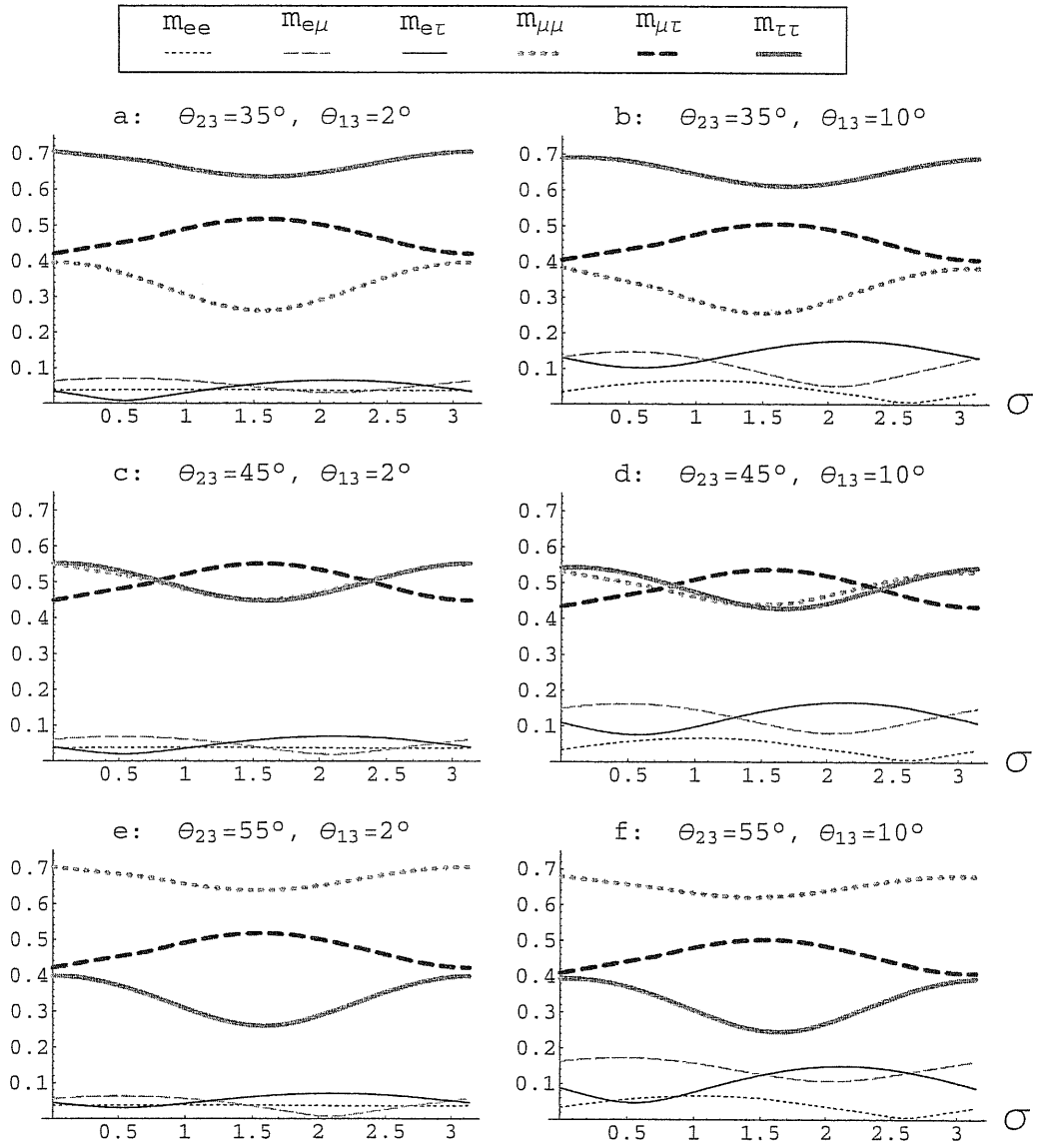

Figure 2.17: Dependence of the absolute value of neutrino mass matrix elements (in units $\sqrt{\Delta m^2_{atm}} = 0.05$ eV) on σ, for different values of θ_{23} and θ_{13}. We take $\tan^2\theta_{12} = 0.36$, $\delta = \pi/3$, $m_2 = 0.14\, m_3$, $m_1 = 0$.

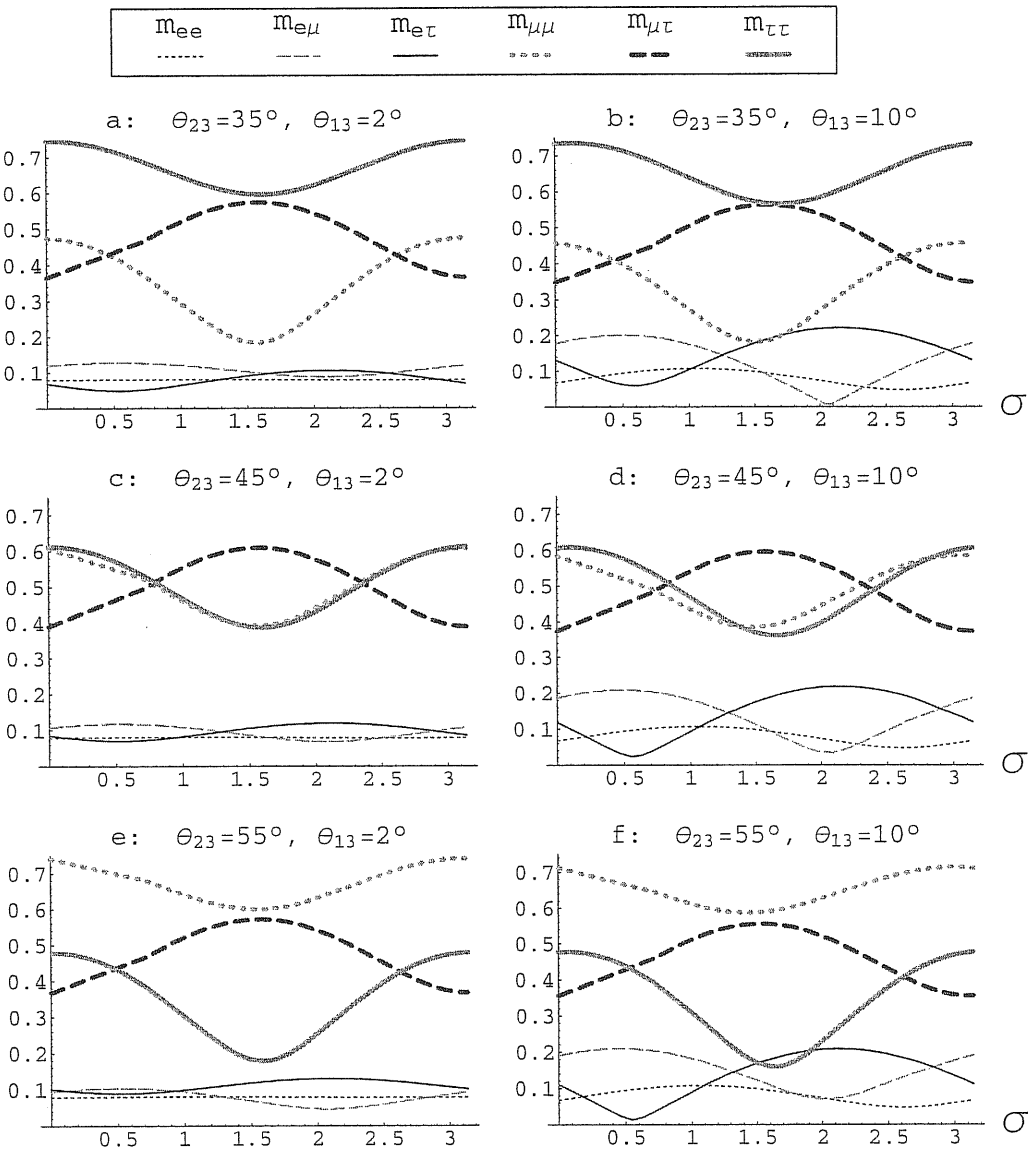

Figure 2.18: The same as in Fig.2.17, but for $m_2 = 0.3\ m_3$.

Let us analyze the dependence of matrix elements on the Dirac phase δ. The elements of $\mu\tau$-block depend on δ very weakly, via order s_{13} corrections. E.g., for $s_{13} \approx 0.14$ (Fig.2.17 b,d,f), we find $\Delta m^{\delta}_{\mu\mu}/\bar{m}_{\mu\mu} \approx \Delta m^{\delta}_{\tau\tau}/\bar{m}_{\tau\tau} \sim 0.02$. The dependence of $m_{\mu\tau}$ on δ is further suppressed by the factor $\xi \equiv \cos 2\theta_{23}$.

The elements of e-row have much stronger relative dependence on δ. As we pointed out, the elements $m_{e\mu}$ and $m_{e\tau}$ depend on phases in the combination $(\delta - 2\sigma)$ (this feature is weakly violated by corrections $\sim s_{13}$, which depend on the phase δ only). So, up to corrections of order s_{13}, one can extract the information on the δ dependence of the elements from the Fig.2.17 (or Fig.2.18 for larger $R \equiv m_2/m_3$) immediately. In fact, the change of δ by amount $\Delta\delta$ is equivalent to horizontally shift the lines which correspond to $m_{e\mu}$ and $m_{e\tau}$ along with σ-axis by $\Delta\delta/2$ and the m_{ee} line by $\Delta\delta$, with respect to the lines of $\mu\tau$-block, which are almost unchanged. The phase δ can be selected in such a way that certain features of the m_{ee} line and other e-row lines will occur at the same value of σ. For instance, according to Fig.2.17b, one can get $m_{ee} \ll m_{e\mu} \ll m_{e\tau}$.

All the elements have the same period of variation with σ, although the phases of variations are different. There is a phase shift by π within different groups:

$$\phi(m_{\mu\mu}) = \phi(m_{\tau\tau}) = \phi(m_{\mu\tau}) + \pi = -2\sigma \; ; \tag{2.59}$$

$$\phi(m_{e\mu}) = \phi(m_{e\tau}) + \pi = -2\sigma + \delta \; . \tag{2.60}$$

There is a relative shift of phase between $\mu\tau$-block and e-row elements which is determined by δ:

$$\phi(m_{e\mu}) - \phi(m_{\mu\mu}) = \delta \; , \qquad \phi(m_{ee}) - \phi(m_{e\mu}) = \delta. \tag{2.61}$$

These relations are weakly broken by corrections of order s_{13}.

Variations of θ_{12} within the allowed LMA region, given in (2.9), do not produce substantial changes of results shown in Fig.2.17. With increase of θ_{12}, the amplitudes of variations of $\mu\tau$-block elements with σ (see (2.50)) decrease as c^2_{12}. In contrast, the amplitude of variations of these elements with δ increases as $\sin 2\theta_{12}$. For the e-row elements, the critical value s^0_{13} is proportional to $\sin 2\theta_{12}$ (see Eq.(2.53)). The ee-element m_{ee} could be two times larger for almost maximal solar mixing angle than for the best fit value (see Eq.(2.57)).

Changes of Δm^2_{sol} and Δm^2_{atm} within the allowed regions, (2.4) and (2.5), produce strong effect on the structure of the mass matrix. In Fig.2.18 we show the dependence of mass matrix elements on σ for $R = 0.3$ (see Eq.(2.27)), corresponding, *e.g.*, to $\Delta m^2_{sol} \approx 1.5 \cdot 10^{-4}\text{eV}^2$ and $\Delta m^2_{atm} \approx 1.7 \cdot 10^{-3}\text{eV}^2$. For the $\mu\tau$-block elements, the amplitudes increase linearly with $R \equiv 1/r$ (Eq.(2.50)) and for $R \approx 0.3$ they can be larger than 30%. For the e-row elements the critical value s^0_{13} (Eq.(2.53)) also increases linearly with R; for $R \approx 0.3$, we get $s^0_{13} \approx 0.13$. For $s_{13} < s^0_{13}$, the average values of elements increase as $m_{e\mu} \sim m_{e\tau} \sim \sqrt{\Delta m^2_{sol}}$, but the amplitude of variations with

$(\delta - 2\sigma)$ does not change (compare Fig.2.18, panels a,c,e, with corresponding panels in Fig.2.17). For $s_{13} \gtrsim s^0_{13}$, the average values of $m_{e\mu}$ and $m_{e\tau}$ increases with $\sqrt{\Delta m^2_{atm}}$, while their amplitudes can be maximal (Fig.2.18, panels b,d,f). The average value of ee-element increases with $\sqrt{\Delta m^2_{sol}}$; the amplitude of variations with $2(\delta - \sigma)$ does not change.

Till now, we have considered the case $m_1 = 0$. A strong normal hierarchy among mass eigenvalues, $m_1 \ll m_2 \ll m_3$, holds for m_1 up to approximately 0.002 eV ($k < 0.3$). Notice that, for $m_1 \neq 0$, both Majorana phases become relevant. We have checked that varying m_1 between 0 and 0.002eV, the dependence of $m_{\alpha\beta}$ on angles and CP phases, showed in Figs.2.17,2.18, is qualitatively the same as for $m_1 = 0$, except for the dependence of m_{ee}. The ee-element can be about two times larger. Indeed, neglecting terms of order s^2_{13}, we get:

$$m_{ee} \approx m_2 s^2_{12} \left(1 + k \cot^2\theta_{12} \cos 2\rho\right) \ .$$

The second term in the brackets is of order one for, *e.g.*, $m_1 = 0.002$ eV, $m_2 = 0.006$ eV, $\tan^2\theta_{12} = 0.35$ and $\rho = 0, \pi$. Depending on ρ, the ratio of m_{ee} and the other e-row elements can significantly change. For increasing m_1, the dependence of all matrix elements on ρ increases and it's worthwhile to use $\rho - \sigma$ plots (see Fig.2.6 for the case $m_1 = 0.006$eV, that is $k \approx 0.6$). We will discuss this case in the next subsection.

Let us now analyze the overall structure of the mass matrix:

1. As follows from Figs.2.17,2.18, the sharp structure with the dominant $\mu\tau$-block and subdominant e-row appears for small s_{13}, best fit value of Δm^2_{sol} and near maximal 2-3 mixing. In this case

$$m_{ee} \sim m_{e\mu} \sim m_{e\tau} \ll m_{\mu\mu} \sim m_{\mu\tau} \sim m_{\tau\tau},$$

$$\frac{m(e - \text{row})}{m(\mu\tau - \text{block})} \sim [s_{13}, 1/r] \sim (0.1 \div 0.2) \ , \qquad (2.62)$$

where $m(e - \text{row})$ and $m(\mu\tau - \text{block})$ refer to typical masses of the $e-$row and $\mu\tau$-block elements. Improvements of the upper bound on s_{13} and on ξ, as well as establishing Δm^2_{sol} near its present best fit value, will confirm this structure in assumption of mass hierarchy. In the limit of sharp structure [$\mu\tau$-block]-[e-row], the elements of dominant block depend very weakly on δ and have about 10% variations (determined by $1/r$) due to the phase σ. The elements $m_{e\mu}$ and $m_{e\tau}$ depend significantly on the combination $(\delta - 2\sigma)$, unless very strong upper bound on s_{13} will be established. The $ee-$element varies with $2(\delta - \sigma)$, with amplitude $\sim r s^2_{13}$. Thus, uncertainties in the structure of the mass matrix due to unknown CP violating phases can be substantially reduced by further measurements of mixing angles and mass squared differences.

According to Figs. 2.17,2.18, for a large part of the parameter space (θ_{23}, θ_{13}, r, δ, σ), the structure [$\mu\tau$-block]-[e-row] is less profound or even disappears. Indeed, in the case of large ξ or/and small r, the split between masses within the $\mu\tau$-block can be larger than the gap between $m(e-\text{row})$ and $m(\mu\tau-\text{block})$, depending on σ. The separation of the elements in two groups loses any sense. For the extreme case of small values of r, the elements $m_{e\mu}$ and $m_{e\tau}$ can be even larger than $m_{\mu\mu}$ or $m_{\tau\tau}$.

2. Dependence of the gap between $\mu\tau$-block and e-row elements on s_{13} and r can be seen comparing left and right panels in Figs.2.17,2.18 and Fig.2.17 with Fig.2.18, respectively. The deviation of θ_{23} from 45°, leading to a spread among the $\mu\tau$-block elements (see (2.49)), can strongly decrease the gap.

   Let us quantify the size of gap. Taking only leading terms in ξ, $1/r$ and s_{13}, one has for the $\mu\tau$-block elements:

$$m(\mu\tau-\text{block}) \geq m(\mu\tau-\text{block})^{min} \equiv \frac{m_3}{2}(1-|\xi|-c_{12}^2/r)\ ,$$

   where $m(\mu\tau-\text{block})^{min}$ is the value of $m_{\mu\mu}$ (or $m_{\tau\tau}$) for $\sigma=\pi/2$. The upper bound on the e-row elements is given by

$$m(e-\text{row}) \leq m(e-\text{row})^{max} \equiv \frac{m_2}{\sqrt{2}}(r\ s_{13}+c_{12}s_{12})\ ,$$

   where $m(e-\text{row})^{max}$ is the value of $m_{e\mu}$ (or $m_{e\tau}$) for $\delta-2\sigma=0$ or π, respectively. Therefore, minimal value of the gap equals

$$m(\mu\tau-\text{block})^{min}-m(e-\text{row})^{max}=\frac{m_3}{2}\left[1-|\xi|-\frac{1}{r}(c_{12}^2+\sqrt{2}c_{12}s_{12})-\sqrt{2}s_{13}\right]\ . \tag{2.63}$$

   One can also characterize the split of the elements by the ratio of mean values of the e-row and $\mu\tau$-block elements. Up to terms quadratic in ξ, $1/r$ and s_{13}, $\overline{m}(\mu\tau-\text{block})\approx m_3/2$, while for the e-row we can take

$$\overline{m}(e-\text{row})\equiv\sqrt{\frac{m_{e\mu}^2+m_{e\tau}^2}{2}}\approx\frac{m_2}{\sqrt{2}}(r^2s_{13}^2+c_{12}^2s_{12}^2)^{1/2}\ .$$

   Then

$$\frac{\bar{m}(e-\text{row})}{\bar{m}(\mu\tau-\text{block})}\approx\sqrt{2(s_{13}^2+c_{12}^2s_{12}^2/r^2)}\ , \tag{2.64}$$

   in accordance with (2.62). The ratio (2.64) does not depend on CP phases and on θ_{23}.

3. Apart from special choice of phases, the ee-element is typically of the order of the other e-row elements. The CP violating phases can change significantly the structure of the e-row. As follows from Figs. 2.17,2.18, one can get, *e.g.*,

$$\begin{array}{ll} m_{ee} \ll m_{e\mu} \ll m_{e\tau} & \text{(large } r\text{, large } s_{13}) \ ; \\ m_{ee} \ll m_{e\mu} \approx m_{e\tau} & \text{(large } r\text{, large } s_{13}) \ ; \\ m_{ee} \approx m_{e\mu} \approx m_{e\tau} & \text{(small } r\text{, small } s_{13}) \ ; \\ m_{e\mu} \ll m_{ee} \ll m_{e\tau} & \text{(small } r\text{, large } s_{13}) \ . \end{array} \tag{2.65}$$

   Any element of the e-row can be the smallest one. All possible orderings of e-row elements can be realized by appropriate choice of the phases.

4. Depending on phases, one can find a configuration with almost uniform splits among the six mass matrix elements and then the structure with the dominant $\mu\tau$-block disappears. Still the average value of the e-row elements is smaller than the average value of the $\mu\tau$-block elements (see (2.64)). Thus one can get flavor alignment (correlation of the neutrino masses and masses of charge leptons): see section 2.6.3.

2.4.2 From normal hierarchy to quasi-degeneracy

If one abandons the limit $m_1 \to 0$, the structure of the mass matrix depends on two additional parameters: the mass ratio k and the phase ρ. These parameters enter the mass matrix elements in the combinations X, Y, Z (Eq.(2.24)). In the limit of very small s_{13} the mass matrix of moduli is given by Eq.(2.28). Now the elements of the e-row have non-zero phases which depend on ρ. The phases of $\mu\tau$-block elements depend mainly on σ, with corrections which are functions of ρ.

For $m_1 \lesssim \sqrt{\Delta m^2_{sol}}$, we have $k \lesssim 1$, and $r \gg 1$. The corresponding $\rho - \sigma$ plots are given in Fig. 2.6. The largest mass is given by $m_3 \approx \sqrt{\Delta m^2_{atm}}$. The contributions of m_1 to the $\mu\tau$-block elements appear as small corrections, but they can be of order 1 for the e-row elements.

Neglecting terms of order s_{13}, we can use for the $\mu\tau$-block elements the expressions from Eq.(2.28). Comparing with the hierarchical case (Eq.(2.48)), we find that the effect of m_1 is reduced to renormalization of the mass ratio r and shift of the phase σ:

$$r \to r_x \equiv r\frac{c_{12}^2}{x}, \qquad \sigma \to \sigma_x \equiv \sigma + \frac{1}{2}\phi_x \ . \tag{2.66}$$

That is, dependence of the elements on phases can be found from Figs.2.17,2.18, by appropriate change of r and σ. Depending on the phase ρ, the contribution related to m_1 can suppress or enhance the amplitude of variations of $\mu\tau$-block elements with σ (Eq.(2.50)). The extreme modifications are determined by

$$r_x = \begin{cases} r/(1 + k\tan^2\theta_{12}) \ , & \text{for} \quad \rho = 0 \\ r/(1 - k\tan^2\theta_{12}) \ , & \text{for} \quad \rho = \pi/2 \end{cases} \ .$$

For $k \lesssim 1$ and $\tan^2\theta_{12} \lesssim 0.5$, the relative effect of m_1 is below 50%. For $\rho = 0, \pi/2$, we have $\phi_x = 0$ and no phase shift occurs. In general, the phase ϕ_x is in the interval $(-\phi_x^{max} \div \phi_x^{max})$, where $\sin\phi_x^{max} = k\tan^2\theta_{12}$. This maximal phase corresponds to $r_x = r/\sqrt{1-k^2\tan^4\theta_{12}}$.

For the elements of e-row, the s_{13} corrections should be taken into account (Eq.(2.24)):

$$\begin{array}{l} m_{e\mu} \approx m_2 \left| c_{23}y + rs_{13}s_{23}e^{i(\delta-2\sigma_y)} \right| , \\ m_{e\tau} \approx m_2 \left| s_{23}y - rs_{13}c_{23}e^{i(\delta-2\sigma_y)} \right| . \end{array} \qquad (2.67)$$

Again, the effect of m_1 is reduced to a renormalization of r and a shift of phase (compare with Eqs.(2.51,2.52)):

$$r \to r_y \equiv r\frac{s_{12}c_{12}}{y}, \qquad \sigma \to \sigma_y \equiv \sigma + \frac{1}{2}\phi_y \, . \qquad (2.68)$$

Minimal and maximal values of r_y are given by:

$$r_y = \left\{ \begin{array}{ll} r/(1-k) \, , & \text{for} \quad \rho = 0 \\ r/(1+k) \, , & \text{for} \quad \rho = \pi/2 \end{array} \right. .$$

In these extreme cases there is no phase shift. In general, for arbitrary values of ρ, ϕ_y is in the interval $(-\phi_y^{max} \div \phi_y^{max})$, where $\sin\phi_y^{max} = k$ and this maximal value corresponds to $r_y = r/\sqrt{1-k^2}$.

Notice that, for $m_{e\mu}$ and $m_{e\tau}$, modifications of r can be larger than for the elements of $\mu\tau$-block; moreover, r_y and r_x are changing with ρ in opposite phases. The phases of variations of $\mu\tau$-block elements are correlated as in the hierarchical case. No phase shift among these elements is induced by m_1 contribution: in (2.59) one should substitute $\sigma \to \sigma_x$. A similar conclusion is valid for the e-row elements: in (2.60) σ should be substituted by σ_y.

For the ee-element, similarly to the previous cases, we get (including s_{13} corrections):

$$m_{ee} = \frac{m_2 z}{s_{12}^2}\left| c_{13}^2 s_{12}^2 + r_z s_{13}^2 e^{2i(\delta-\sigma_z)} \right| , \qquad (2.69)$$

where

$$r_z \equiv r\frac{s_{12}^2}{z}, \qquad \sigma_z \equiv \sigma + \frac{1}{2}\phi_z . \qquad (2.70)$$

Now the difference between r and r_z can be substantially larger:

$$r_z = \left\{ \begin{array}{ll} r/(1+k\cot^2\theta_{12}) \, , & \text{for} \quad \rho = 0 \\ r/|1-k\cot^2\theta_{12}| \, , & \text{for} \quad \rho = \pi/2 \end{array} \right. ,$$

and r_z changes with ρ in phase with r_x. Notice that, for $k < \tan^2\theta_{12}$, the shift ϕ_z is restricted to the interval $(-\phi_z^{max} \div \phi_z^{max})$, where $\sin\phi_z^{max} = k\cot^2\theta_{12}$. For $k > \tan^2\theta_{12}$, the shift is unrestricted. The $ee-$element is zero for

$$\tan\theta_{13} = \sqrt{z/r} = s_{12}/\sqrt{r_z}, \qquad (\delta - \sigma_z) = \frac{\pi}{2}, \frac{3\pi}{2} \, .$$

Since r_z can be larger than r, or even diverging, the equality $m_{ee} = 0$ can be realized for smaller values of s_{13} than in the hierarchical case. Now the strongly hierarchical structure of the e-row,

$$m_{ee} \ll m_{e\mu} \ll m_{e\tau} \ ,$$

can be easily achieved. Maximal value of m_{ee} equals approximately $m_{ee}^{max} \approx m_2(s_{12}^2 + kc_{12}^2)$.

The dependences of the mass matrix elements on phases can be deduced from Fig.2.17 and Fig.2.18. Since, now, the "effective" value of r is different for the $\mu\tau-$block elements (r_x) and the e-row elements (r_y, r_z), one should take, *e.g.*, lines which correspond to the $\mu\tau$-block from Fig.2.17 and lines which correspond to the e-row from Fig.2.18 or *vice versa*.

Let us analyze the dependence of the elements on the phase ρ. The relative amplitudes of variations of the $\mu\tau-$block elements are suppressed by a factor $s_{12}^2 k/r$:

$$\frac{\Delta m^{\rho}}{\bar{m}} \approx \frac{s_{12}^2 k}{r} \times \begin{cases} \cot^2\theta_{23}, & m_{\mu\mu} \\ \tan^2\theta_{23}, & m_{\tau\tau} \\ 1, & m_{\mu\tau} \end{cases} . \qquad (2.71)$$

The influence of ρ on the $e-$row elements is much stronger. If $s_{13} \approx 0$, we have

$$m_{e\mu} \approx m_2 c_{23} s_{12} c_{12} |1 - ke^{-2i\rho}|$$

(for $m_{e\tau}$ one should substitute $c_{23} \to s_{23}$) and the relative amplitude of variations is given by k. The amplitude of ee-element can be maximal if $k \geq \tan^2\theta_{12}$.

For $\sqrt{\Delta m_{sol}^2} \ll m_1 \lesssim \sqrt{\Delta m_{atm}^2}$, we get the spectrum with partial degeneracy $m_1 \approx m_2 \lesssim m_3$ ($k \approx 1$, $r \gtrsim 1$). The corresponding $\rho - \sigma$ plots are given in Fig. 2.7. The scale of masses is determined by $m_3 \approx \sqrt{m_1^2 + \Delta m_{atm}^2} \sim (1 \div 2)\sqrt{\Delta m_{atm}^2}$. Now the zero order mass matrix is given by Eq.(2.31).

Let us consider first the dependence of the masses on phase σ (see Fig.2.19 panels a,c,e and phase diagrams in Fig.2.4). In the limit of small s_{13}, we get

$$\begin{aligned} m_{\mu\mu} &\approx m_2 \left| r s_{23}^2 e^{-2i\sigma} + c_{23}^2 X_{k=1} \right| , \\ m_{\tau\tau} &\approx m_2 \left| r c_{23}^2 e^{-2i\sigma} + s_{23}^2 X_{k=1} \right| , \\ m_{\mu\tau} &\approx m_2 s_{23} c_{23} \left| r e^{-2i\sigma} - X_{k=1} \right| . \end{aligned} \qquad (2.72)$$

The mass $m_{\mu\mu}$ oscillates with σ around $m_3 s_{23}^2$; the amplitude of variations depends on the phase ρ. Maximal amplitude is for $\rho = 0$, which corresponds to $X_{k=1} = 1$. The mass $m_{\tau\tau}$ oscillates in phase with $m_{\mu\mu}$ around the average value $m_3 c_{23}^2$; the mass $m_{\mu\tau}$ varies in opposite phase. The amplitudes of variations of all $\mu\tau$-block elements decrease with increase of the phase ρ and it is minimal for $\rho = \pi/2$.

The corrections of order s_{13} change the amplitudes of variations and produce a phase shift. The largest influence of these corrections is for $\rho = \pi/2$ (see Eq.(2.43)).

For $\delta = 0$, the corrections suppress the amplitude of variations of $m_{\mu\mu}$ and enhance the amplitude of $m_{\tau\tau}$ and $m_{\mu\tau}$ variations (see Fig.2.19e). For $\delta = \pi/2$ the situation is opposite: variations of $m_{\mu\mu}$ are enhanced. In the approximation (2.72), all the elements of $\mu\tau$-block depend on the phase ρ in the same way. So, there is no relative shift and the relative phases are determined as in (2.59). The phase shift seen in Fig.2.19c is due to the interplay of the s_{13} corrections and the phase ρ.

The dependence of elements of the e-row on σ (as well as δ) appears due to terms of the order rs_{13} (see Fig.2.19 panels a,c,e). Neglecting corrections $\sim s_{13}$, we get (for ρ being not to close to 0):

$$m_{e\mu} \approx m_2 \left| c_{23} Y_{k=1} + r\ s_{13} s_{23} e^{i(\delta - 2\sigma)} \right|, \quad m_{e\tau} \approx m_2 \left| s_{23} Y_{k=1} - r\ s_{13} c_{23} e^{i(\delta - 2\sigma)} \right| . \tag{2.73}$$

The masses $m_{e\mu}$ and $m_{e\tau}$ vary with $(\delta - 2\sigma)$ in opposite phase (small phase shift may appear due to the interplay of order s_{13} corrections and the phase ρ). The amplitude of variations is proportional to s_{13}. The average values of the elements increase with ρ, and they reach maxima, $m_{e\mu}^{max} = m_2 \sin 2\theta_{12} c_{23}$ and $m_{e\tau}^{max} = m_2 \sin 2\theta_{12} s_{23}$, at $\rho = \pi/2$. The configuration with $\rho = 0$ or $\rho \approx 0$ is special (see Fig.2.19a). In this case $Y_{k=1}$ vanishes and only terms proportional to s_{13} are present. The elements $m_{e\mu}$ and $m_{e\tau}$ vary in phase; both the average value and the amplitude are proportional to s_{13}.

Changing the phase δ by $\Delta\delta$ one shifts lines which correspond to $m_{e\mu}$ and $m_{e\tau}$, with respect to the lines of $\mu\tau$-block elements by $\Delta\sigma = \Delta\delta/2$. For instance, according to Fig.2.19c, one can get the equalities $m_{\mu\mu} = m_{\tau\tau} = m_{\mu\tau}$ and $m_{e\mu} = m_{e\tau}$ simultaneously.

Variations of the ee-element with σ as well as with δ are strongly suppressed by the factor s_{13}^2, so that

$$m_{ee} \approx m_2 \left| Z_{k=1} \right| . \tag{2.74}$$

The average value decreases with increase of the phase ρ. It varies from $m_{ee}^{max} \approx m_2$ for $\rho \approx 0, \pi$ down to $m_{ee}^{min} \approx m_2 \cos 2\theta_{12}$ for $\rho \approx \pi/2$. Variations of m_{ee} with ρ are in opposite phase with respect to $m_{e\mu}$ and $m_{e\tau}$.

Let us analyze the dependence of masses on the phase ρ (Fig.2.20 panels a,c,e). The amplitudes of variations of the $\mu\tau$-block elements with ρ, $\Delta m^{\rho} \propto s_{12}^2/r$, are smaller (for non-maximal solar mixing) than the amplitudes of σ variations. The average values of $m_{\mu\mu}$ and $m_{\tau\tau}$ decrease whereas the average of $m_{\mu\tau}$ increases with increase of σ from 0 to $\pi/2$. Strong split of masses in the $\mu\tau$-block (see Fig.2.20a,2.20e) is due to cancellation of contributions related to m_3 (first term in (2.72)) and to m_1 and m_2 (second term). For large s_{13}, the terms of order s_{13} can enhance the variations with ρ. According to (2.73), variations of the e-row elements with ρ are strong: the amplitude can be close to maximal one. For large values of s_{13}, the phase $(2\sigma - \delta)$ changes significantly the average values of the elements $m_{e\mu}$ and $m_{e\tau}$ and also modifies the amplitudes of variations with ρ.

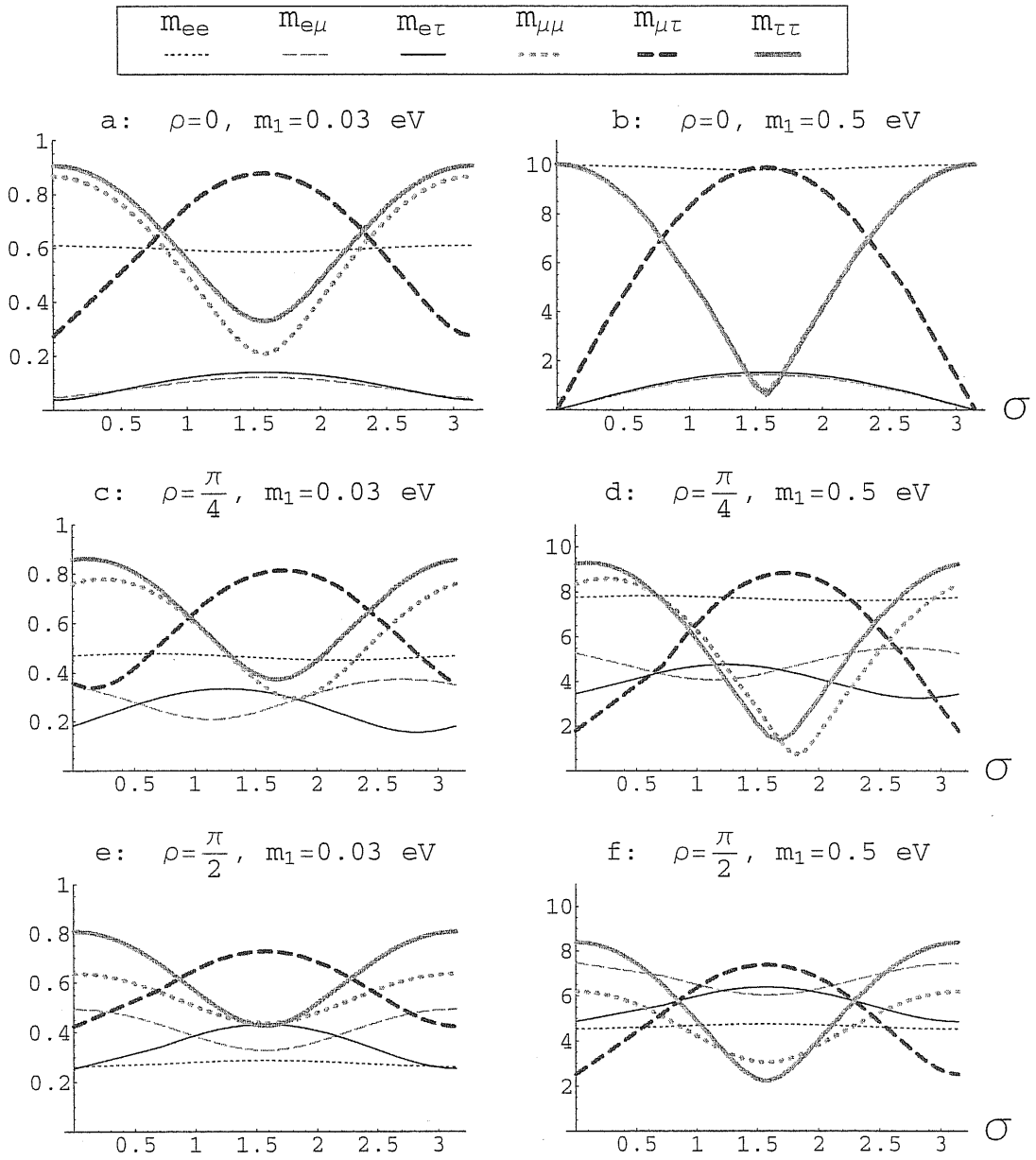

Figure 2.19: Dependence of the absolute value of mass matrix elements (in units $\sqrt{\Delta m^2_{atm}}$) on σ, for partially degenerate spectrum (panels a,c,e) and completely degenerate spectrum (panels b,d,f). We show dependences for different values of the phase ρ. We take $\Delta m^2_{sol} = 5 \cdot 10^{-5}\text{eV}^2$, $\Delta m^2_{atm} = 2.5 \cdot 10^{-3}\text{eV}^2$ and $\tan^2\theta_{12} = 0.36$, $\tan\theta_{23} = 0.93$, $s_{13} = 0.1$, $\delta = 0$.

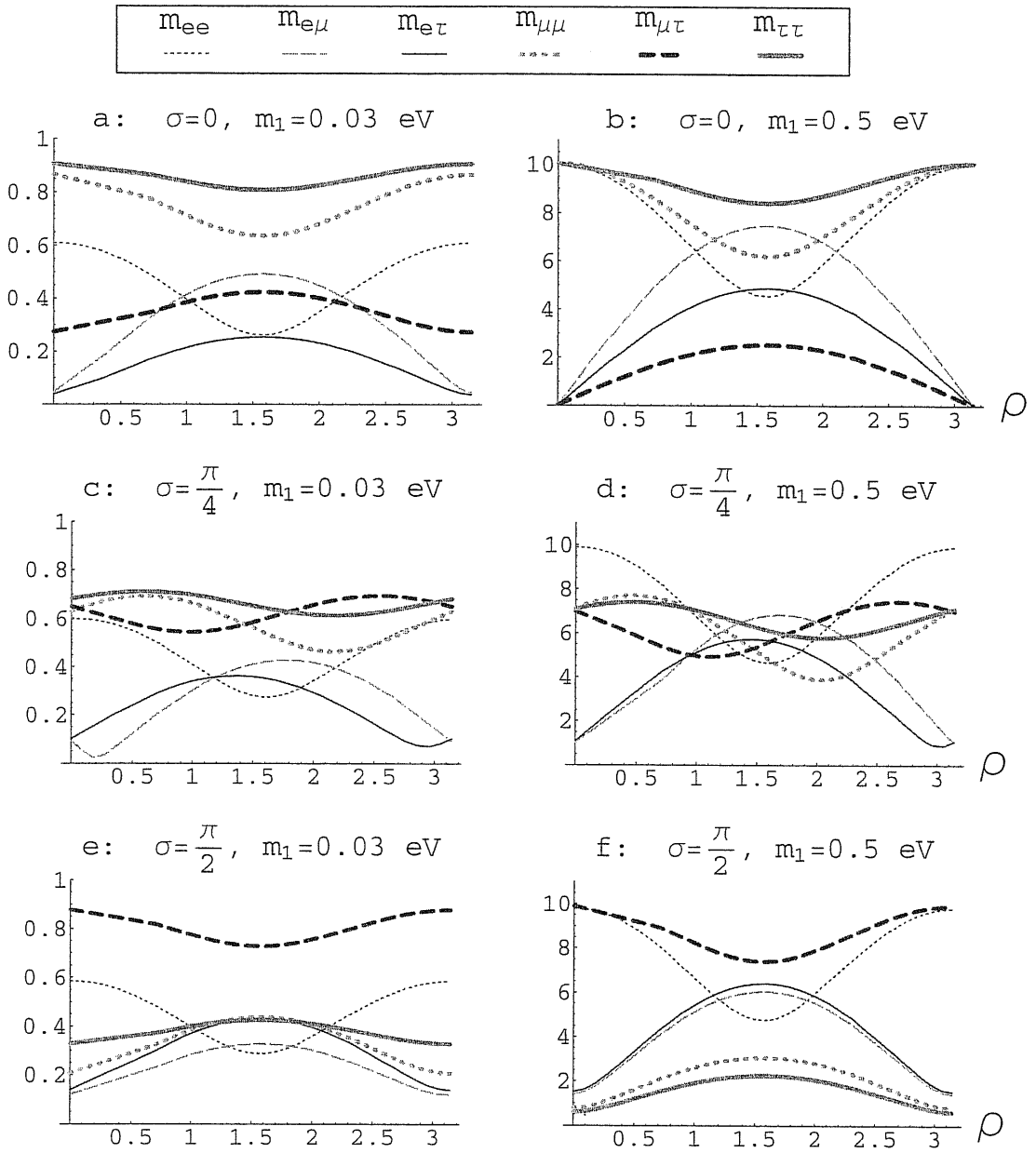

Figure 2.20: Dependence of the absolute value of mass matrix elements (in units $\sqrt{\Delta m^2_{atm}}$) on ρ, for partially degenerate spectrum (panels a,c,e) and completely degenerate spectrum (panels b,d,f). We show dependences for different values of the phase σ. We take $\Delta m^2_{sol} = 5 \cdot 10^{-5}\text{eV}^2$, $\Delta m^2_{atm} = 2.5 \cdot 10^{-3}\text{eV}^2$ and $\tan^2\theta_{12} = 0.36$, $\tan\theta_{23} = 0.93$, $s_{13} = 0.1$, $\delta = 0$.

The matrix elements are all correlated. This can be seen in the limit of very small s_{13}, when the matrix is given by Eq.(2.31). The relations (2.36)-(2.40) among the elements hold. It is also interesting that

$$\frac{m_{e\mu}}{m_{e\tau}} = \tan\theta_{23} \ , \qquad m^2_{\tau\tau} - m^2_{\mu\mu} = m^2_2(r^2 - x^2)\cos 2\theta_{23} \ . \tag{2.75}$$

Notice that $m_{\tau\tau} = m_{\mu\mu}$ either for $\theta_{23} = 45°$ or for $r = x$. Since for normal ordering $r > 1$, the latter corresponds to completely degenerate spectrum and $\rho = 0$. In this case

$$m_{\tau\tau} = m_{\mu\mu} = m_3\sqrt{1 - \sin^2 2\theta_{23}\sin^2\sigma} \ , \qquad m_{\mu\tau} = m_3 \sin 2\theta_{23}\sin\sigma \ .$$

Using the second equality in Eq.(2.39), we get

$$m^2_{\mu\mu} + m^2_{\tau\tau} + 2m^2_{\mu\tau} - m^2_{ee} = m^2_3 \ ,$$

which quantifies the difference between the mass of the $\mu\tau$-block and that of the ee-element.

2.4.3 Quasi-degeneracy

For $m_1 \gg \sqrt{\Delta m^2_{atm}}$, we have $m_1 \approx m_2 \approx m_3$ and the ratio of masses is given by

$$r \approx 1 \pm \frac{\Delta m^2_{atm}}{2m^2_1} \ ,$$

where the $+(-)$ sign corresponds to normal (inverted) ordering. The corresponding $\rho - \sigma$ plots are shown in Fig. 2.8. For $m_1 = 0.5$ eV, the deviation of r from 1 is smaller than 1% and we can neglect it in comparison with other small parameters, like s_{13} and ξ. Notice that, in the approximation $r \approx 1$, the structure of the mass matrix for normal and inverted hierarchy is the same. The information about the type of mass ordering is imprinted in small, $O(\Delta m^2_{atm}/m^2_1)$, deviation of r from 1.

In the normal ordering case, the transition from partial degeneracy to complete degeneracy does not produce qualitative changes in the dependences of the matrix elements on phases (see Fig.2.19 b,d,f and Fig.2.20 b,d,f). Amplitudes of variations of the $\mu\tau$-block elements increase and can reach maximal size for specific values of phases. This leads to zero (small) values of certain matrix elements and therefore to the appearance of a hierarchical structure of the mass matrix. For example, for $r = 1$ and in the case of maximal 2-3 mixing and $\rho = 0$, we find from (2.31):

$$m \approx m_2 \begin{pmatrix} 1 & 0 & 0 \\ \dots & \frac{1}{2}|1 + e^{-2i\sigma}| & \frac{1}{2}|-1 + e^{-2i\sigma}| \\ \dots & \dots & \frac{1}{2}|1 + e^{-2i\sigma}| \end{pmatrix} \ . \tag{2.76}$$

Therefore, $m_{\mu\mu} = m_{\tau\tau} = 0$ for $\sigma = \pi/2$, while $m_{\mu\tau} = 0$ for $\sigma = 0$ (Fig.2.19b). Moreover, s_{13} corrections to $\mu\tau$-block elements cancel in Eq.(2.43) when $k = 1$ and

$\rho = 0$. For non-maximal 2-3 mixing, using (2.72) we find that $m_{\mu\mu} = 0$ for

$$\sin^2\rho = \frac{\cos 2\theta_{23}}{c_{23}^4 \sin^2 2\theta_{12}}, \qquad \cos 2\sigma = -\frac{c_{23}^4 \cos 2\theta_{12} + s_{23}^4}{2c_{12}^2 s_{23}^2 c_{23}^2}.$$

In this case, however, $m_{\tau\tau}$ differs from zero. Such a configuration is realized approximately in Fig.2.19d.

The amplitudes of variations with ρ (Fig.2.20 b,d,f) increase and, for $\rho \approx 0, \pi$, hierarchical structure of the mass matrix appears (Fig.2.20b,2.20f). For some values of phases all the elements become approximately equal to each other (see, *e.g.*, Fig.2.20d at $\rho = 1.3\pi$).

2.4.4 From quasi-degeneracy to inverted hierarchy

In this section we will examine the transformation of the matrix structure (2.31) when r goes from 1 (quasi-degeneracy) to 0 (inverted hierarchy). The mass scale m_2 decreases with r as

$$m_2 = \sqrt{\frac{\Delta m_{atm}^2}{1 - r^2}}\ . \tag{2.77}$$

The e-row elements in the zero order mass matrix (2.31) decrease proportionally to m_2. Their dependence on ρ is independent from r, as one can see comparing Figs. 2.8, 2.9, 2.10. Their dependence on σ, related with terms of order rs_{13}, becomes smaller and smaller.

The zero order form of $\mu\tau$-block elements (Eq.(2.31)) depends on r, therefore they are strongly modified for decreasing r. Their maximum value decreases from $(1+x)/2$ to $x/2$ (assuming maximal $2-3$ mixing). They become lighter than m_{ee} for almost any value of ρ and σ.

The $\mu\tau$-block elements can be very small only for $x \approx r$. One can get $m_{\mu\mu}$ or $m_{\tau\tau}$ equal to zero for values of r as small as $\sim x_{min}/2$, because of non-maximal 2-3 mixing. Instead, the equalities $m_{\mu\tau} = 0$ or $m_{\mu\mu} = m_{\tau\tau} = 0$ can be realized only for r as large as $\sim x_{min} \gtrsim 0.4$. If one requires that $m_{e\mu}$ and $m_{e\tau}$ are small together with some $\mu\tau$-block elements, the condition $x \approx 1$ enforces the minimal value of r to be larger: $r_{min} \sim 1/2$ for small $m_{\mu\mu}$ or $m_{\tau\tau}$; $r_{min} \sim 1$ for small $m_{\mu\tau}$ or both $m_{\mu\mu}$ and $m_{\tau\tau}$. For a small value of r, the $\mu\tau$-block elements cannot be very small and their dependence on σ is weak, as one can see in Fig.2.10 ($r = 0.1$).

2.4.5 Inverted hierarchy

Let us consider the case $m_3 \ll m_1 \lesssim m_2$. Taking $r = 0$ ($m_3 = 0$) in (2.31), we get the zero order matrix

$$m^0 = \sqrt{\Delta m_{atm}^2}\, x \begin{pmatrix} 1 & c_{23}\sqrt{1/x^2 - 1} & s_{23}\sqrt{1/x^2 - 1} \\ \cdots & c_{23}^2 & s_{23}c_{23} \\ \cdots & \cdots & s_{23}^2 \end{pmatrix} \tag{2.78}$$

which depends on two parameters only, x and θ_{23}. The dependence of m^0 on the Majorana phase σ, associated with m_3, disappears. Furthermore, once θ_{12} and θ_{23} are fixed, the matrix (2.78) depends only on $x = x(\rho)$. In Fig.2.21, we show the absolute values of the matrix elements as functions of ρ. The only freedom (associated to variations of ρ (x)) is reduced to change the relative size of two groups of elements: m_{ee} plus $\mu\tau$-block elements on one side and $m_{e\mu}, m_{e\tau}$ on the other.

We have (see Eq.(2.40))

$$\sum_{\alpha,\beta} m^2_{\alpha\beta} = 2m_2^2 = 2\Delta m^2_{atm} \ . \tag{2.79}$$

The sums of $e-$row and $\mu\tau-$block elements are (see Eq.(2.39))

$$m^2_{ee} + 2(m^2_{e\mu} + m^2_{e\tau}) = m_2^2(2 - x^2) \ , \qquad \Sigma_{\mu\tau} = m_2^2 x^2 = m^2_{ee} \ . \tag{2.80}$$

So, the e-row elements dominate over the $\mu\tau-$block elements. They are comparable for $x = 1$, which corresponds to $m_{ee} = m_2$. The second equality in (2.80) quantifies the dominance of the $ee-$element.

In the matrix (2.78) $m_{ee} = \sqrt{\Delta m^2_{atm}}x$ is non-zero. Furthermore, the $\mu\tau$-block elements vary in restricted ranges:

$$m^0_{\mu\mu,\tau\tau} \in m_2[0.1, 0.65] \ , \qquad m^0_{\mu\tau} \in m_2[0.1, 0.5] \ ,$$

so that they cannot be zero either. Therefore, the only hierarchical structure which appears in the case of inverted hierarchy corresponds to $m_{e\mu} \approx m_{e\tau} \approx 0$. These masses are small, simultaneously, for $x \approx 1$ $(\rho \approx 0, \pi)$. Substituting $x = 1$ in Eq.(2.78), we get

$$m^0 = \Delta m^2_{atm} \begin{pmatrix} 1 & 0 & 0 \\ \dots & c^2_{23} & s_{23}c_{23} \\ \dots & \dots & s^2_{23} \end{pmatrix} \ . \tag{2.81}$$

In this limit ($s_{13} = m_3 = 0$ and $x = 1$) CP violation is absent (δ and σ are irrelevant and $\rho = 0$).

The hierarchical structure with $m_{ee} \approx m(\mu\tau - block) \approx 0$, widely discussed in literature [93, 190, 191, 192, 193] in connection to $L_e - L_\mu - L_\tau$ symmetry, is strongly disfavored now. For the allowed values of x, the symmetry has to be strongly broken, or realized in a basis which differs from the flavor one [194].

For maximal atmospheric mixing, the mass matrix (2.78) takes the form:

$$m^0 = \sqrt{\Delta m^2_{atm}}x \begin{pmatrix} 1 & \sqrt{\frac{1-x^2}{2x^2}} & \sqrt{\frac{1-x^2}{2x^2}} \\ \dots & 1/2 & 1/2 \\ \dots & \dots & 1/2 \end{pmatrix} \ . \tag{2.82}$$

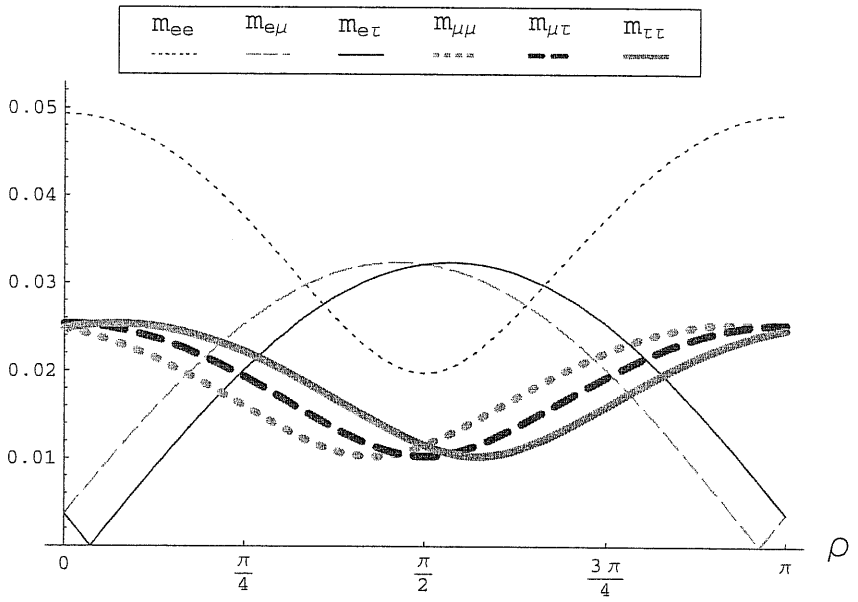

Figure 2.21: Dependence of the absolute value of mass matrix elements (in eV) on ρ, in the case of mass spectrum with strong inverted hierarchy ($r = 0$). We take $\Delta m^2_{sol} = 7 \cdot 10^{-5}\text{eV}^2$, $\Delta m^2_{atm} = 2.5 \cdot 10^{-3}\text{eV}^2$ and $\tan^2\theta_{12} = 0.42$, $\tan\theta_{23} = 1$, $s_{13} = 0.1$, $\delta = \pi/2$.

Depending on x, the ratio between $m_{e\mu}$ ($m_{e\tau}$) and the other matrix elements can strongly change, as shown in Fig.2.21. Three interesting cases,

$$\begin{pmatrix} 1 & 0 & 0 \\ \dots & 1/2 & 1/2 \\ \dots & \dots & 1/2 \end{pmatrix}, \quad \sqrt{\frac{2}{3}}\begin{pmatrix} 1 & 1/2 & 1/2 \\ \dots & 1/2 & 1/2 \\ \dots & \dots & 1/2 \end{pmatrix}, \quad \sqrt{\frac{1}{3}}\begin{pmatrix} 1 & 1 & 1 \\ \dots & 1/2 & 1/2 \\ \dots & \dots & 1/2 \end{pmatrix}, \tag{2.83}$$

are realized for $x = 1$, $x = \sqrt{2/3}$ and $x = \sqrt{1/3}$, respectively. Only the first of these three structures, which corresponds to CP conservation ($\rho = 0$), has been considered before [93]. It is a particular case of the matrix (2.81).

As follows from Eq.(2.43), for $r = 0$ and $\theta_{23} = \pi/4$, the $\mathcal{O}(s_{13})$ corrections to the elements of the matrix (2.82) have very simple form:

$$\begin{aligned} m^s_{ee} &= m^s_{\mu\tau} = 0\,, \\ m^s_{e\tau} &= -m^s_{e\mu} = m_2 x \cos\varphi_1/\sqrt{2}\,, \\ m^s_{\tau\tau} &= -m^s_{\mu\mu} = m_2\sqrt{1-x^2}\cos(\varphi_2 - \phi_x)\,, \end{aligned}$$

where φ_1 and φ_2 are defined in Eq.(2.42). Taking into account these corrections, one can explain the details of Fig.2.21. In particular, for $\rho = 0$ ($x = 1$, first matrix in Eq.(2.83)), the corrections to the $\mu\tau$-block elements disappear ($m^s_{\tau\tau} = 0$), and s_{13}−terms give dominant contributions to the e-row elements ($m^s_{e\tau} = m_2\cos\delta/\sqrt{2}$).

When $m^0_{e\mu} \approx m^0_{e\tau} \approx 0$ ($x \approx 1$), $\mathcal{O}(s_{13})$ corrections can be used to get the inequality $m_{e\mu} \gg m_{e\tau}$ (or *vice versa*). Indeed, introducing the small parameter $\gamma \equiv \sqrt{1-x^2}$, we find:

$$m_{e\mu} \approx \frac{m_2}{\sqrt{2}} \left| \gamma - s_{13}\sqrt{1-\gamma^2}\cos\varphi_1 \right| , \qquad m_{e\tau} \approx \frac{m_2}{\sqrt{2}} \left| \gamma + s_{13}\sqrt{1-\gamma^2}\cos\varphi_1 \right| .$$

Choosing δ such that $\cos\varphi_1 = -1$, one gets $m_{e\mu} \gg m_{e\tau}$ for $\gamma \approx s_{13}\sqrt{1-\gamma^2}$.

2.5 Experimental perspectives

Let us discuss the impact of future experimental data on the determination of the neutrino mass matrix structure.

The following results from forthcoming oscillation experiments will put severe constraints on the structure of the mass matrix:

- more stringent bound on (or determination of) the deviation $\xi \equiv \cos 2\theta_{23}$ from maximal 2-3 mixing;
- narrower upper bound on θ_{12};
- improvement of the upper bound on (or determination of) s_{13};
- determination of the mass ordering (normal or inverted) through 3ν effects (for example using supernova neutrinos).

In the case of normal hierarchy, also a better accuracy on the parameter $\Delta m^2_{sol}/\Delta m^2_{atm}$ is important for fixing the matrix structure.

Let us assume that all oscillation parameters are precisely determined. Than, given an absolute mass scale m_1 and some fixed values of the phases ρ and σ, a unique matrix structure is identified.

As far as the measurement of the absolute mass scale is concerned, the future direct kinematic measurements have a planned sensitivity of 0.25 eV [195]. This can constrain the quasi-degenerate scenario but probably not exclude it. Stronger sensitivity is expected in indirect cosmological measurements, at the order of $(0.03 - 0.1)$ eV [56, 57, 58, 196, 59, 197]. This could distinguish between normal and inverted hierarchy. As discussed in section 2.1.1, there are even indications of non-zero (~ 0.2 eV) neutrino masses, coming from present cosmological data [62].

Another quantity sensitive to both absolute mass scale and Majorana phases is the effective Majorana mass m_{ee}, which deserves a detailed discussion.

2.5.1 The role of neutrinoless 2β-decay

The ee-element, m_{ee}, is the only matrix element for which we have immediate experimental access, through $0\nu2\beta$-decay searches (under the assumption that the exchange of the light Majorana neutrinos is the only mechanism of the decay).

Suppose that experimental searches give the upper bound $m_{ee} < m_{ee}^{up}$. Since $m_{ee}^{up} \gtrsim 0.3$ eV at present (see Eq.(2.12)), the bound is relevant only for quasi-degenerate spectrum ($m_1 \approx m_2 \approx m_3$). In this case we obtain from Eq.(2.18)

$$m_{ee}^{min} \approx m_i(c_{13}^2 \cos 2\theta_{12} - s_{13}^2) = m_i(0.17 \div 0.52) \ ,$$

where we have used the allowed ranges for θ_{12} and θ_{13} (Eqs. (2.9) and (2.11)). This means that the upper bound on m_{ee} translates into an upper bound on the absolute mass scale: $m_i \lesssim m_{ee}^{up}/0.17 \approx 6m_{ee}^{up}$. The bound becomes stronger if upper limits on θ_{12} and θ_{13} are strengthened.

Let us assume now that the mass scale is known by some other experiments and let us investigate the role of neutrinoless 2β-decay to constrain the Majorana phases and therefore the mass matrix structure. The $\rho - \sigma$ plots allow one to find immediately the implications of the results from $0\nu2\beta$-decay searches for the structure of the matrix. The iso-mass contours of m_{ee} are nearly parallel to the axis σ. Weak dependence of m_{ee} on σ appears due to the term of the order s_{13}^2. For very small s_{13} and (partially) degenerate spectrum ($k \approx 1$), the iso-mass contours are determined by

$$m_{ee} \approx m_2\sqrt{1 - \sin^2 2\theta_{12} \sin^2 \rho} \ . \tag{2.84}$$

According to Figs. 2.6-2.10, there are two iso-mass contours in the $\rho - \sigma$ plots, which correspond to a given value m_{ee}^{up} ($m_{ee}(\rho, \sigma) = m_{ee}^{up}$) for a given set of the other parameters (r, s_{13}, δ, etc.): $\rho_1 = \rho_1(\sigma)$ ($\rho_1 < \pi/2$) and $\rho_2 = \rho_2(\sigma)$ ($\rho_2 > \pi/2$). The upper experimental limit $m_{ee} < m_{ee}^{up}$ excludes the following regions in the $\rho - \sigma$ plots (obviously for all the matrix elements):

$$\rho \in [0, \rho_1(\sigma)] \ , \qquad \rho \in [\rho_2(\sigma), \pi] \ . \tag{2.85}$$

The position and the shape of the contours $\rho_i(\sigma)$ (i = 1,2) depend on m_2, θ_{12} and s_{13}. Taking, *e.g.*, $m_2 \approx 0.35$ eV, $s_{13} = 0.1$, $\tan^2\theta_{12} = 0.42$ and a bound $m_{ee}^{up} = 0.25$ eV, we find from Fig.2.8 that the regions covered by the three darkest strips are excluded. They correspond approximately to $\rho < \pi/4$ and $\rho > 3\pi/4$. These regions are excluded for all the elements. In this particular case, all corners of the plots and sides with $\rho \approx 0, \pi$, which correspond to some very small matrix elements, are excluded. Clearly no constraint on the structure appears for weaker bound, $m_{ee}^{up} > 0.35$ eV (which is allowed by the uncertainty in the nuclear matrix elements, see Eq.(2.12)). More in general, $m_{ee}^{up} > m_2$ does not lead to any constraint on the phase ρ.

For $s_{13} \to 0$ and $k \to 1$, the mass matrix can be written immediately in terms of m_{ee}, using Eq.(2.31):

$$m = \begin{pmatrix} m_{ee} & c_{23}\sqrt{m_2^2 - m_{ee}^2} & s_{23}\sqrt{m_2^2 - m_{ee}^2} \\ \cdots & |c_{23}^2 m_{ee} + s_{23}^2 m_2 r e^{-2i\sigma_x}| & s_{23}c_{23}|-m_{ee} + m_2 r e^{-2i\sigma_x}| \\ \cdots & \cdots & |s_{23}^2 m_{ee} + c_{23}^2 m_2 r e^{-2i\sigma_x}| \end{pmatrix} \ . \tag{2.86}$$

Here $m_{ee} = m_2 x \leq m_2$. This form shows how strongly the determination of m_{ee} can influence the structure of the mass matrix.

If not only an upper bound but a positive result of $0\nu 2\beta$-decay is found, then the observed allowed range will correspond to two strips in the $\rho - \sigma$ plot, one for $\rho < \pi/2$ and one for $\rho > \pi/2$ (or to one strip if $\rho \approx \pi/2$).

2.5.2 Toward a unique matrix structure?

Is it possible to determine uniquely the mass matrix, at least in principle? Let us take the most optimistic set of forthcoming experimental data: suppose that the neutrinoless 2β decay is discovered with $m_{ee} > 0.1$ eV and the direct measurements of neutrino mass give $m > 0.3$ eV with high precision. Let us assume also that mixing angles are measured with high accuracy. In this case, the spectrum is strongly degenerate and one can use $0\nu 2\beta$ decay data to determine the CP violating phases. The problem is that m_{ee} depends both on ρ and on σ and the dependence on σ is very weak being suppressed by s^2_{13}. This means that ρ can be measured with rather good accuracy, whereas no bound on σ can be obtained: small variations of ρ can imitate the effect of σ in the whole possible range. The only exception is if the measured m_{ee} is at the maximal (or minimal) possible value predicted for a given (measured) absolute scale of the masses. That would correspond to certain CP-parity of ν_1 and $\delta - \sigma = 0$ or $\pi/2$. Then, measuring δ (in neutrino oscillation experiments) one can determine σ.

Clearly this program looks very challenging. Other experimental situations are even more difficult. The determination of σ looks practically impossible, unless methods of direct measurement or independent reconstruction of at least one other matrix element (apart from m_{ee}) will be found.

The $\rho - \sigma$ plots give a clear description of the uncertainty in the structure of the mass matrix if σ is unknown. As discussed in the previous section, knowing the absolute mass scale and ρ, we will be able to select a narrow vertical strip in the $\rho - \sigma$ diagram. This will constrain the value of all the elements, but significant uncertainty will be left due to their dependence on the phase σ along the strip. In particular the structure of the $\mu\tau$-block will be largely unfixed.

Let us analyze the main uncertainties in the matrix structure, for the different mass spectra:

- Normal Hierarchy. To identify this mass spectrum, very sensitive measurements of neutrino masses are needed ($\lesssim \Delta m^2_{atm}$). The phase ρ cannot be determined, but it is not relevant for the matrix structure when $m_1 \to 0$. The dependence on the unknown phase σ, described in detail in section 2.4.1, decreases for decreasing s_{13} and/or decreasing R (Eq.(2.27)). If these parameters are close to their minimal allowed values, the structure with dominant $\mu\tau$-block is well-determined. Vice versa, if s_{13} and R are relatively large, the matrix can have quite different structures depending on σ.

- Normal partial degeneracy. The dependence on ρ is quite strong for e-row elements. Since the element m_{ee} is smaller than the heaviest mass m_3, quite high sensitivity in $0\nu2\beta$ decay searches is needed to measure ρ. The dependence on σ of $\mu\tau$-block elements increase with the mass scale. Therefore the structure of the $\mu\tau$-block becomes strongly uncertain.

- Quasi-degeneracy. In the limit $r \to 1$, the zero order mass matrix (2.31) depends on two unknown parameters: x and $\sigma_x \equiv \sigma + \phi_x/2$. The first one (as well as ϕ_x) can be determined from measurements of the absolute mass scale and detection of the neutrinoless 2β decay ($x \approx m_{ee}/m_2$). Sensitivities close to the present ones can be enough. The only free parameter to which we have no access is the phase σ. The variations of the $\mu\tau$-block elements with σ have the maximal possible amplitude when $r \to 1$. One will not be able to distinguish between structures with zero or large $\mu\tau$-block elements.

- Inverted ordering. Measuring m_2 and m_{ee} requires larger sensitivities as far as the mass scale decreases. The unknown phase σ can change the structure of the $\mu\tau$-block, even though the dependence on σ weakens with the mass scale.

- Inverted hierarchy. The mass matrix could be determined completely if measurements of neutrino masses were sensitive to $m \approx \sqrt{\Delta m^2_{atm}}$. This can be obtained by future cosmological measurements, which will be sensitive to sum of neutrino masses of the order of 0.1 eV. Then ρ can be fixed if m_{ee} is measured in the $0\nu2\beta$ decay. There is no dependence on σ.

2.6 Theoretical perspectives

To gain further insight into the origin of the neutrino mass matrix, it is useful to classify the possible structures in the following way:

- Hierarchical matrices, with certain dominant elements much larger than others.

- Matrices with certain equalities among the magnitude of different elements. A particular case is the democratic matrix, with equal moduli of all the elements: $m_{\alpha\beta} \approx \bar{m}$ for any choice of α and β.

- Matrices with can be described in terms of an expansion parameter. One can identify flavor alignment or flavor disorder (flavor "anarchy").

Each of these structures can have some underlying symmetry origin. In what follows, we will study these possibilities in order. Finally we will comment on the implications of a given choice of basis and on the differences between flavor and symmetry basis.

2.6.1 Zero matrix elements: hierarchical structures

We will refer to the mass matrix structure as to a hierarchical one if some elements are smaller than others by a factor $\lesssim 0.1$. Large elements (that is, of the order of the heaviest neutrino mass) belong to the dominant block, other elements to the sub-dominant block. Also further structuring is possible within the dominant and sub-dominant blocks. The hierarchical structures of the mass matrix may testify for the existence of certain symmetries.

The hierarchical matrices can be found by searching for zeroes (small values) of some elements. They can be identified as light regions in the $\rho - \sigma$ plots. Notice that the "light" zones are often at the corners or in the center of the plot, which corresponds to definite CP-parities or small CP-violating phases. So, the most of hierarchical structures can be identified by considering certain CP-parities (no CP violation).

Let us start with the case of normal hierarchical spectrum. We have seen in section 2.4.1 that the dominant block of the mass matrix is formed by the $\mu\tau$-elements. However, we have also shown that the smallness of e-row elements with respect to $\mu\tau$-block ones cannot exceed one order of magnitude in average (Eq.(2.64)). This means that all e-row elements cannot be close to zero at the same time and the reason is that $\Delta m^2_{sol}/\Delta m^2_{atm} \gtrsim 0.1$.

A strong hierarchy is still allowed between $\mu\tau$-block and some e-row elements or even within the e-row (see Eq.(2.65)). The conditions for the zero value of one e-row elements are discussed in Eqs. (2.53)-(2.58). It is not possible to realize an extreme smallness of both $m_{e\mu}$ and $m_{e\tau}$ at the same time, as can be deduced from Eqs. (2.51) and (2.52). This is easily understood: $m_{e\mu} = m_{e\tau} = 0$ implies that ν_1 is completely unmixed with ν_2 and ν_3. In contrast, it is possible to get, at the same time, $m_{ee} \to 0$ and $m_{e\mu(e\tau)} \to 0$. This can be seen in Fig. 2.6.

Summarizing, five different combinations of very small matrix elements can be realized and, correspondingly, five hierarchical matrix structures are allowed in the case of normal hierarchy:

$$\begin{pmatrix} 0 & * & * \\ * & * & * \\ * & * & * \end{pmatrix}, \quad \begin{pmatrix} * & 0 & * \\ 0 & * & * \\ * & * & * \end{pmatrix}, \quad \begin{pmatrix} * & * & 0 \\ * & * & * \\ 0 & * & * \end{pmatrix}, \quad \begin{pmatrix} 0 & 0 & * \\ 0 & * & * \\ * & * & * \end{pmatrix}, \quad \begin{pmatrix} 0 & * & 0 \\ * & * & * \\ 0 & * & * \end{pmatrix},$$

where "$*$" denotes elements of the same order of magnitude (within a factor ~ 5). Notice that the realization of zeros in the e-row requires specific (non-zero) values of s_{13} and also specific choices of the CP violating phases.

For mass spectra other than normal hierarchy, let us use the zero order matrix (2.31) to look for hierarchical structures.

1) The element m_{ee} cannot be zero (see Eq.(2.35)). It belongs to the dominant structure of the matrix. The hierarchical structures with $m_{ee} \approx 0$, widely discussed in the literature [93, 190, 191, 192, 193], are strongly disfavored now.

2) The elements $m_{e\mu}$ and $m_{e\tau}$ are simultaneously zero (small) when $x = 1$. This corresponds to $\rho = 0$ and, consequently, $\phi_x = 0$ and $\sigma_x = \sigma$. For $x = 1$, the zero order matrix (2.31) becomes:

$$m^0 = m_2 \begin{pmatrix} 1 & 0 & 0 \\ \dots & |c_{23}^2 + s_{23}^2 r e^{-2i\sigma}| & s_{23}c_{23}|-1+re^{-2i\sigma}| \\ \dots & \dots & |s_{23}^2 + c_{23}^2 r e^{-2i\sigma}| \end{pmatrix} . \qquad (2.87)$$

The s_{13} and ϵ terms (section 2.2.3) can give the main contributions to the elements $m_{e\mu}$ and $m_{e\tau}$. Notice that the zero order matrix (2.31) can take the form (2.87) for any value of r, that is for any mass spectrum (apart from normal hierarchy, of course).

3) Using Eq.(2.31), we find the conditions at which one of the elements of the $\mu\tau$-block is zero:

$$\begin{aligned} m_{\mu\mu} = 0: &\quad \cos 2\sigma_x = -1, \quad x = r\tan^2\theta_{23}\ ; \\ m_{\tau\tau} = 0: &\quad \cos 2\sigma_x = -1, \quad r = x\tan^2\theta_{23}\ ; \\ m_{\mu\tau} = 0: &\quad \cos 2\sigma_x = 1, \quad r = x\ . \end{aligned} \qquad (2.88)$$

These analytic expressions describe the position of light regions in the $\rho - \sigma$ plots, in first approximation. Some additional shift of these regions is due to s_{13} corrections (that is, zeros can be realized for changed values of ρ and σ); ϵ corrections are negligible.

As follows from (2.88), almost maximal atmospheric mixing implies that the $\mu\tau$-block elements can be zero only for $r \sim x$, that is for *non-hierarchical* mass spectrum. The exact equality $x = r$ implies

$$\sin^2\rho = \frac{1-r^2}{\sin^2 2\theta_{12}}\ , \qquad \cos 2\theta_{12} \leq r \leq 1\ . \qquad (2.89)$$

The Eq. (2.89) shows that, for increasing r, the regions of small $\mu\tau$-block elements move from $\rho \approx \pi/2$ to $\rho \approx 0, \pi$, as one can see comparing Figs. 2.10, 2.9 and 2.8.

In the case of inverted ordering and taking $\delta = 0$ (π), one can check that a light region appears in the plot of $m_{\mu\mu}$ ($m_{\tau\tau}$) for r as small as ≈ 0.1. This is a case in which s_{13} corrections are important: deviation of θ_{23} from maximal value and relatively large s_{13} can add coherently, increasing the difference between $m_{\mu\mu}$ and $m_{\tau\tau}$.

Substituting the conditions (2.88) for $m_{\mu\mu} = 0$ into Eq. (2.31), the matrix takes the form

$$m^0 = m_2 \begin{pmatrix} x & \sqrt{\frac{r(1-x^2)}{r+x}} & \sqrt{\frac{x(1-x^2)}{r+x}} \\ \dots & 0 & \sqrt{rx} \\ \dots & \dots & |x-r| \end{pmatrix} , \qquad (2.90)$$

where $r = x\cot^2\theta_{23}$. Since $x - r = r(\tan^2\theta_{23} - 1)$, the element $m_{\tau\tau}$ is proportional to the deviation of the atmospheric mixing from maximal one. In the case $m_{\tau\tau} = 0$, the matrix has an analogous form, but with the interchanges $m_{e\mu} \leftrightarrow m_{e\tau}$ and $m_{\mu\mu} \leftrightarrow m_{\tau\tau}$. The structure (2.90) is realized in Figs. 2.13 and 2.10, for $\rho \approx \sigma \approx \pi/2$.

Both diagonal elements of the $\mu\tau$-block can be zero at maximal 2-3 mixing and $x = r$, so that

$$m^0 = m_2 \begin{pmatrix} r & \sqrt{\frac{1-r^2}{2}} & \sqrt{\frac{1-r^2}{2}} \\ \dots & 0 & r \\ \dots & \dots & 0 \end{pmatrix} . \tag{2.91}$$

This structure is realized in Fig.2.9, in the regions $\rho \approx \sigma \approx \pi/2$.

In the case $m_{\mu\tau} = 0$, the matrix (2.31) has the form:

$$m^0 = m_2 \begin{pmatrix} r & c_{23}\sqrt{1-r^2} & s_{23}\sqrt{1-r^2} \\ \dots & r & 0 \\ \dots & \dots & r \end{pmatrix} . \tag{2.92}$$

Notice that the three diagonal elements are necessarily equal. This structure is shown in Fig.2.9, for $\sigma \approx 0, \pi$ and $\rho \approx \pi/2$.

4) The conditions for zero values of the e-row elements ($x = 1$) and $\mu\tau$-block elements are consistent with each other, so that one may have any combination of zeros in both blocks. In particular, taking $x = 1$ in Eq.(2.90), we get

$$m^0 = m_2 \begin{pmatrix} 1 & 0 & 0 \\ \dots & 0 & \sqrt{r} \\ \dots & \dots & |1-r| \end{pmatrix} , \tag{2.93}$$

or the same with $m_{\mu\mu} \leftrightarrow m_{\tau\tau}$, if $m_{\tau\tau} = 0$.

If $x = r = 1$ (degenerate spectrum), in (2.91) only m_{ee} and $m_{\mu\tau}$ differ from zero (and equal to m_2). This hierarchical structure is shown in Fig.2.8, for $\sigma \approx \pi/2$ and $\rho \approx 0, \pi$.

For $x = r = 1$, in (2.92) also $m_{e\mu} = m_{e\tau} = 0$ and the matrix becomes the identity. This structure appears in Figs. 2.8 and 2.11-2.14, for $\rho \approx \sigma \approx 0, \pi$. Notice that when the matrix approaches the identity, all the mixings angles are generated by small corrections to the dominant structure.

The discussed mass matrices with zero elements are shown in Table 2.1. In the Table we give also the intervals of r and $\tan\theta_{23}$ for which the structures can be realized. These intervals are computed requiring non-zero elements to be quite large ($> 0.3m_2$), in order to clearly distinguish between dominant and sub-dominant blocks. So, the matrices we have found have hierarchical structure.

One can check, using analytic relations given in Eqs. (2.31) and (2.22), (2.23), that all matrices with zeros can be obtained using $\rho, \sigma = 0, \pi/2$, that is definite CP-parities.

The "zero" elements are zeroes up to $\mathcal{O}(s_{13}, \epsilon)$ corrections. In general, corrections are small ($\sim 10\%$) and could be very small ($\sim 1\%$), if the upper bound on s_{13} becomes more stringent and $m_1 \gg \Delta m^2_{sol}$. Moreover, in all the hierarchical structures with $m_{e\mu} = m_{e\tau} = 0$ ($x = 1$), the $\mu\tau$-block elements have no $\mathcal{O}(s_{13})$ corrections (see

	$\mathcal{O}(s_{13},\epsilon)$ entries	Range for r	Range for $\tan\theta_{23}$	$\frac{m^0}{m_2}$
I	$m_{e\mu}, m_{e\tau}$	$0 \leq r \lesssim 3$	$0.75 \div 1.35$	$\begin{pmatrix} 1 & 0 & 0 \\ 0 & * & * \\ 0 & * & * \end{pmatrix}$
II	$m_{\mu\mu}, m_{\tau\tau}$	$0.4 \lesssim r \lesssim 0.8$	$0.95 \div 1.05$	$\begin{pmatrix} * & * & * \\ * & 0 & * \\ * & * & 0 \end{pmatrix}$
III	$m_{\mu\tau}$	$0.4 \lesssim r \lesssim 0.8$	$0.75 \div 1.35$	$\begin{pmatrix} * & * & * \\ * & * & 0 \\ * & 0 & * \end{pmatrix}$
IV	$m_{e\mu}, m_{e\tau}, m_{\mu\mu}, m_{\tau\tau}$	$r \approx 1$	$0.95 \div 1.05$	$\begin{pmatrix} 1 & 0 & 0 \\ 0 & 0 & 1 \\ 0 & 1 & 0 \end{pmatrix}$
V	$m_{e\mu}, m_{e\tau}, m_{\mu\tau}$	$r \approx 1$	$0.75 \div 1.35$	$\begin{pmatrix} 1 & 0 & 0 \\ 0 & 1 & 0 \\ 0 & 0 & 1 \end{pmatrix}$
II'	$m_{\mu\mu}$	$0.2 \lesssim r \lesssim 1.8$	$0.75 \div 0.85$ $1.15 \div 1.35$	$\begin{pmatrix} * & * & * \\ * & 0 & * \\ * & * & * \end{pmatrix}$
II"	$m_{\tau\tau}$	$0.2 \lesssim r \lesssim 1.8$	$0.75 \div 0.85$ $1.15 \div 1.35$	$\begin{pmatrix} * & * & * \\ * & * & * \\ * & * & 0 \end{pmatrix}$
IV'	$m_{e\mu}, m_{e\tau}, m_{\mu\mu}$	$0.6 \lesssim r \lesssim 0.8$ $1.3 \lesssim r \lesssim 2$	$1.15 \div 1.35$	$\begin{pmatrix} 1 & 0 & 0 \\ 0 & 0 & * \\ 0 & * & * \end{pmatrix}$
IV"	$m_{e\mu}, m_{e\tau}, m_{\tau\tau}$	$0.6 \lesssim r \lesssim 0.8$ $1.3 \lesssim r \lesssim 2$	$0.75 \div 0.85$	$\begin{pmatrix} 1 & 0 & 0 \\ 0 & * & * \\ 0 & * & 0 \end{pmatrix}$

Table 2.1: Hierarchical structures of the mass matrix for all the mass spectra except normal hierarchy. The classification is based on the very small ($\mathcal{O}(s_{13},\epsilon)$) entries of the matrix, which are listed in the second column. In the third and fourth columns the corresponding allowed ranges for r and $\tan\theta_{23}$ are given. When $r \approx 1$, zero elements in m^0 receive also $\mathcal{O}(\eta)$ corrections (see Eq.(2.94)). The matrices m^0, shown in the last column, are simplified forms of the structures given in Eqs.(2.87, 2.90-2.93). Parameters can be chosen in such a way that the elements denoted with "$*$" belong to the range $0.3 - 2$. The $\mathcal{O}(s_{13})$ corrections can be as large as 0.2 for the elements $e\mu$, $e\tau$, $\mu\mu$ and $\tau\tau$ (see Eq.(2.43)).

Eq.(2.43)). Notice that, when one takes the limit $r = 1$, terms of order η are neglected, where

$$\eta \equiv 1 - r \approx \pm \frac{\Delta m^2_{atm}}{2m_2^2} \,. \tag{2.94}$$

Therefore, in the case $r \to 1$, "zero" elements are zeroes up to $\mathcal{O}(s_{13}, \eta)$ corrections. For $m_2 \gtrsim 0.2$ eV, one gets $\eta \lesssim 3 \cdot 10^{-2}$.

Instead of looking for small matrix elements, neglecting s_{13} and ϵ terms, one can find the conditions for exact zeros in the matrix. There are seven possible combinations of two (and only two) exact zero elements [157]:

- The two cases $m_{ee} = m_{e\mu(e\tau)} = 0$. We have shown above that they correspond to normal hierarchy and require $s_{13} \neq 0$.

- The four cases $m_{e\tau} = m_{\mu\mu(\tau\tau)} = 0$ or $m_{e\mu} = m_{\mu\mu(\tau\tau)} = 0$. The elements $m_{e\mu}$ and $m_{e\tau}$ cannot be both zero exactly, otherwise there is no solar mixing. However, our analysis shows that, if one is small, also the other is, because they cannot be zero separately in the limit $s_{13} = \epsilon = 0$.

- The case $m_{\mu\mu} = m_{\tau\tau} = 0$. This possibility is present also in the limit $s_{13} = \epsilon = 0$ (Eq.(2.91)).

As far as study of possible matrix structures is concerned, the requirement of exact zero values of some elements can be misleading. Indeed, some elements can be small or very small but non-zero. The smallness of an element could be explained by some flavor symmetry. However, the flavor symmetry is broken anyway: it is difficult to expect exact zeros. Moreover, zeros which exist at tree level can be unstable under radiative corrections, as we will show in chapter 3.

2.6.2 Equal matrix elements

Equalities of some matrix elements can be considered as the signature of certain symmetry or certain origin of the neutrino masses. In the case of normal hierarchy ($k \ll 1$), equalities are possible within the e-row or within the $\mu\tau$-block. The conditions for such equalities can be easily obtained from the analysis made in section 2.4.1. Increasing the mass scale (k going from 0 to 1) also equalities among certain e-row and $\mu\tau$-block elements become possible, as described in section 2.4.2. Here we focus our attention on the case $k \to 1$ ($m_1 \gg \sqrt{\Delta m^2_{sol}}$), when the zero order mass matrix of moduli is given by Eq.(2.31).

1) **"Democratic" matrix** of moduli. The matrix (2.31) can have all six equal

elements,

$$m^0 = \frac{m_2}{\sqrt{3}} \begin{pmatrix} 1 & 1 & 1 \\ \dots & 1 & 1 \\ \dots & \dots & 1 \end{pmatrix} , \tag{2.95}$$

if and only if

$$\theta_{23} = \frac{\pi}{4} , \quad x = \sqrt{\frac{1}{3}} , \quad r = 1 , \quad \cos 2\sigma_x = 0 . \tag{2.96}$$

That is, the "democratic" matrix of moduli corresponds to degenerate mass spectrum, maximal 2-3 mixing and large CP-violating phases. According to Eq.(2.22), the condition $x = \sqrt{1/3}$ gives

$$\sin^2 \rho = \frac{2}{3 \sin^2 2\theta_{12}} . \tag{2.97}$$

For the best fit value of 1-2 mixing we have $\sin \rho \approx 0.9$. Then, the condition $\cos 2\sigma_x = 0$ implies (see Eqs. (2.29) and (2.23)) $\sin \sigma \approx 0.56$ or ≈ 0.83. The present solar neutrino data admit $\rho = \pi/2$ ($\sigma = \pi/4, 3\pi/4$). Non-zero ρ and σ lead to non-zero phases $\phi_{\alpha\beta}$ of the matrix elements.

The absolute value m_{dem} of democratic matrix elements in Eq.(2.95) is consistent with the mass squared conservation (2.19). Indeed, in the degeneracy case we have $\sum_i m_i^2 = 3m_2^2$. For the democratic matrix the sum of all elements equals $\sum_{\alpha,\beta} m_{\alpha\beta}^2 = 9m_{dem}^2$. According to the mass conservation, we have $9m_{dem}^2 = 3m_2^2$, or $m_{dem}^2 = m_2^2/3$.

Notice that the values of parameters (2.96) correspond to the structure (2.95) only for $s_{13} = 0$. Substituting (2.96) in Eq.(2.43) and taking $s_{13} \approx 0.2$, we find that $m_{e\mu}$ and $m_{e\tau}$ can receive corrections (with opposite sign) as large as 35% of their zero order value. Also $m_{\mu\mu}$ and $m_{\tau\tau}$ can be shifted by 30% in opposite directions. The magnitude of corrections depends strongly on δ. In principle, for $s_{13} \neq 0$, parameters can be readjusted in order to recover the structure (2.95). In particular, this requires a deviation from maximal 2-3 mixing. If quite large s_{13} and exactly maximal 2-3 mixing were found in future experiments, the democratic structure of moduli would be excluded.

2) **Equal e-row elements.** All the e-row elements in Eq.(2.31) are equal, $m_{ee} = m_{e\mu} = m_{e\tau}$, if and only if

$$\theta_{23} = \frac{\pi}{4}, \quad x = \sqrt{\frac{1}{3}} . \tag{2.98}$$

In this case, one has also $m_{\mu\mu} = m_{\tau\tau}$. Under the condition (2.98), we get

$$m^0 = \frac{m_2}{\sqrt{3}} \begin{pmatrix} 1 & 1 & 1 \\ \dots & \frac{1}{2}\left|1 + \sqrt{3} r e^{-2i\sigma_x}\right| & \frac{1}{2}\left|1 - \sqrt{3} r e^{-2i\sigma_x}\right| \\ \dots & \dots & \frac{1}{2}\left|1 + \sqrt{3} r e^{-2i\sigma_x}\right| \end{pmatrix} . \tag{2.99}$$

The ratio r is not restricted, so that equality of the e-row elements can be realized for any type of mass spectrum.

Using the free parameters r and σ_x, one can produce further structures or reach equalities in the $\mu\tau-$block. If

$$\cos 2\sigma_x = \pm\frac{\sqrt{3}(1-r^2)}{2r},$$

the diagonal elements (sign plus) or off-diagonal elements (sign minus) of the $\mu\tau$-block are equal to e-row elements and we arrive at the zero order matrices:

$$\frac{m_2}{\sqrt{3}}\begin{pmatrix} 1 & 1 & 1 \\ \dots & 1 & a(r) \\ \dots & \dots & 1 \end{pmatrix}, \qquad \frac{m_2}{\sqrt{3}}\begin{pmatrix} 1 & 1 & 1 \\ \dots & a(r) & 1 \\ \dots & \dots & a(r) \end{pmatrix}, \tag{2.100}$$

where

$$a(r) \equiv \sqrt{\frac{3r^2-1}{2}}.$$

The elements $m_{\mu\mu} = m_{\tau\tau} \propto a(r)$ in the first case and $m_{\mu\tau} \propto a(r)$ in the second one are zero if $r^2 = 1/3$, are equal to the other elements if $r = 1$, as in (2.95), and for $r = 2$ they are ~ 2.5 times larger than the others. Notice that for larger r the approximation $k \approx 1$ does not apply ($r \gtrsim 2 \Rightarrow k \lesssim 0.95$).

All elements of the $\mu\tau-$block in Eq.(2.99) are equal to each other if $r \cdot \cos 2\sigma_x = 0$. This condition can be realized for $r = 0$ (and arbitrary σ_x), which corresponds to strong inverted hierarchy, or for $\sigma_x = \pi/4, 3\pi/4$ and arbitrary spectrum. In the first case one gets the third matrix in Eq.(2.83). In the second case the matrix has the form

$$\frac{m_2}{\sqrt{3}}\begin{pmatrix} 1 & 1 & 1 \\ \dots & b(r) & b(r) \\ \dots & \dots & b(r) \end{pmatrix}, \tag{2.101}$$

where

$$b(r) = \frac{m(\mu\tau - \text{block})}{m(e - \text{row})} \equiv \frac{1}{2}\sqrt{3r^2+1}.$$

The ratio $b(r)$ changes from $1/2$, for inverted hierarchy, to 1, for degenerate spectrum, up to ≈ 2 for normal ordering. The structure (2.101) suggests that the magnitude of matrix element can be connected to the electron flavor.

3) **Equal $\mu\tau$-block elements.** The $\mu\tau$-block elements can be equal, $m_{\mu\mu} = m_{\mu\tau} = m_{\tau\tau}$, in three cases:

(a) $\theta_{23} = \frac{\pi}{4}, \quad \cos 2\sigma_x = 0.$

The matrix has the following form:

$$m^0 = m_2\begin{pmatrix} x & \sqrt{\frac{1-x^2}{2}} & \sqrt{\frac{1-x^2}{2}} \\ \dots & \frac{1}{2}\sqrt{x^2+r^2} & \frac{1}{2}\sqrt{x^2+r^2} \\ \dots & \dots & \frac{1}{2}\sqrt{x^2+r^2} \end{pmatrix}. \tag{2.102}$$

There are several interesting particular cases. The $\mu\tau$-block elements are equal to m_{ee} if $r^2 = 3x^2$:

$$m^0 = \frac{m_2}{\sqrt{3}} \begin{pmatrix} r & \sqrt{\frac{3-r^2}{2}} & \sqrt{\frac{3-r^2}{2}} \\ \dots & r & r \\ \dots & \dots & r \end{pmatrix} . \tag{2.103}$$

The elements $m_{e\mu}$ and $m_{e\tau}$ are larger than the other elements for inverted ordering (notice that $\sqrt{3}x_{min} < r$), are equal to them for $r = 1$ and decrease to zero for r growing up to $\sqrt{3}$. The case $r = 0$, discussed in the literature [93], requires $x = 0$ and therefore maximal solar mixing, which is now excluded by data.

If $r^2 = 2 - 3x^2$, the matrix (2.102) becomes:

$$m^0 = m_2\sqrt{\frac{1+r^2}{6}} \begin{pmatrix} \sqrt{\frac{2(2-r^2)}{1+r^2}} & 1 & 1 \\ \dots & 1 & 1 \\ \dots & \dots & 1 \end{pmatrix} . \tag{2.104}$$

All elements but m_{ee} are equal. For $r = 0$, m_{ee} is two times larger than the other elements (second matrix in Eq.(2.83)); for $r = 1$, all the elements are equal. Since the maximal allowed value of r^2 is $2 - 3x^2_{min}$, m_{ee} is always larger than about one half of the other elements (see Eq.(2.32)).

(b) $\theta_{23} = \frac{\pi}{4}$, $\quad r = 0$.

This case corresponds to strong inverted hierarchy. The zero order mass matrix is given in Eq.(2.82) and its properties have been discussed in detail in section 2.4.5.

(c) $x = r$, $\quad 2\sin^2\sigma_x \sin^2 2\theta_{23} = 1$.

The matrix takes the form

$$m^0 = \frac{m_3}{\sqrt{2}} \begin{pmatrix} \sqrt{2} & c_{23}c(r) & s_{23}c(r) \\ \dots & 1 & 1 \\ \dots & \dots & 1 \end{pmatrix} , \tag{2.105}$$

where

$$c(r) \equiv \frac{\sqrt{2-2r^2}}{r} .$$

The function $c(r)$ varies between 0 and ~ 5 (for $r = x_{min}$). If $\theta_{23} = \pi/4$, this is just the particular case $x = r$ of (a). The element $m_{e\mu}$ ($m_{e\tau}$) is equal to $\mu\tau$-block elements if $c(r) = 1/c_{23}$ ($= 1/s_{23}$). According to Eq.(2.32), this implies $0.45 \lesssim r \lesssim 0.65$. Then the mass matrix takes the form:

$$m^0 = \frac{m_3}{\sqrt{2}} \begin{pmatrix} \sqrt{2} & 1 & \frac{1}{r}\sqrt{2-3r^2} \\ \dots & 1 & 1 \\ \dots & \dots & 1 \end{pmatrix} \tag{2.106}$$

(or the same with $m_{e\mu} \leftrightarrow m_{e\tau}$).

The equality of $\mu\tau$-block elements can be an indication of a flavor symmetry with the same charge assigned to ν_μ and ν_τ, such as $L_e - L_\mu - L_\tau$. This symmetry would imply also $m_{e\mu} = m_{e\tau}$. Notice that this equality holds in the cases (a) and (b).

4) **Equal diagonal elements.** There are two possibilities for $m_{ee} = m_{\mu\mu} = m_{\tau\tau}$:

(a) $\theta_{23} = \frac{\pi}{4}$, $\quad \cos 2\sigma_x = \frac{3x^2 - r^2}{2xr}$.

In this case, $x \leq r \leq 3x$. The mass matrix has the form

$$m = m_2 \begin{pmatrix} x & \sqrt{\frac{1-x^2}{2}} & \sqrt{\frac{1-x^2}{2}} \\ \dots & x & \sqrt{\frac{r^2-x^2}{2}} \\ \dots & \dots & x \end{pmatrix} . \tag{2.107}$$

Imposing equalities of diagonal elements also with $m_{e\mu}$ (with $m_{\mu\tau}$) we reproduce the first matrix in Eq.(2.100) (Eq.(2.103)). Notice that the diagonal elements can be much larger than off-diagonal elements only in the limit $x \to 1$, $r \to 1$, which corresponds to degenerate spectrum.

(b) $x = r$, $\quad \cos 2\sigma_x = 1$.

The matrix is given by Eq.(2.92). If $r = c_{23}/\sqrt{1 + c_{23}^2}$ ($0.35 \lesssim r \lesssim 0.65$), also $m_{e\mu}$ is equal to the diagonal elements and the matrix becomes

$$m = m_3 \begin{pmatrix} 1 & 1 & \frac{1}{r}\sqrt{1 - 2r^2} \\ \dots & 1 & 0 \\ \dots & \dots & 1 \end{pmatrix} . \tag{2.108}$$

The matrix with $m_{e\tau}$ equal to the diagonal elements can be found by substituting $c_{23} \leftrightarrow s_{23}$ and $m_{e\mu} \leftrightarrow m_{e\tau}$ in (2.108).

Notice that it is not possible to have all diagonal elements close to zero, as predicted, e.g., by the Zee model [198].

5) **Equal off-diagonal elements.** The conditions for the equality $m_{e\mu} = m_{e\tau} = m_{\mu\tau}$ can be found from Eq.(2.31):

$$\theta_{23} = \frac{\pi}{4}, \qquad \cos 2\sigma_x = \frac{3x^2 + r^2 - 2}{2xr} .$$

In this case the mass matrix has the following form:

$$m^0 = \frac{m_2}{\sqrt{2}} \begin{pmatrix} \sqrt{2}x & \sqrt{1 - x^2} & \sqrt{1 - x^2} \\ \dots & \sqrt{2x^2 + r^2 - 1} & \sqrt{1 - x^2} \\ \dots & \dots & \sqrt{2x^2 + r^2 - 1} \end{pmatrix} . \tag{2.109}$$

Imposing equalities also with m_{ee} ($m_{\mu\mu}$), we get the second matrix in Eq.(2.100) (Eq.(2.104)).

For $r = 1$, we get, at the same time, equal diagonal and off-diagonal elements. In this case the parameter x can vary between 1/3 and 1, so that the ratio between off-diagonal and diagonal elements, $\sqrt{\frac{1-x^2}{2x}}$, can vary between 2 and 0. This kind of equality suggests a permutation symmetry S_3 of the flavor neutrinos [78].

6) **Another equality**. The equality of the four elements $m_{e\mu} = m_{e\tau} = m_{\mu\mu} = m_{\tau\tau}$ can be achieved if and only if

$$\theta_{23} = \frac{\pi}{4}, \qquad 2 = 3x^2 + r^2 + 2rx\cos 2\sigma_x \; . \tag{2.110}$$

In this case, the matrix is the same as in Eq.(2.109), with $m_{\mu\tau}$ and $m_{\mu\mu} = m_{\tau\tau}$ interchanged. This is the unique case in which the request to have four equal elements leaves two parameters free in Eq.(2.31). In the other cases only one free parameter is left. This is the reason why in the first matrix of Eq.(2.100) and in Eq.(2.104) one can get the equality of five (and not six) elements. The other four equalities of five elements require also the equality of the sixth element.

2.6.3 Ordering structures, flavor alignment, expansion parameter

As one can see in the $\rho - \sigma$ plane, there are regions where all the matrix elements are of the same order (intermediate gray in the $\rho - \sigma$ plots). In these regions the matrix may have certain "ordering" structures.

Do masses correlate with flavors? That is, are there any correlations between charged lepton and neutrino masses? We will call such a correlation the *flavor alignment*. To some extent, the lepton mixing matrix itself is the measure of the flavor alignment, so that small mixing would imply strong alignment. The observed large lepton mixing means weak ordering or absence of the flavor ordering.

The question of flavor ordering can be studied in terms of the mass matrix in flavor basis. A *normal flavor alignment* is present if masses decrease with transition from the τ-flavor to the e-flavor, that is,

$$m_{\tau\tau} \gtrsim m_{\mu\tau} \gtrsim m_{\mu\mu} \sim m_{e\tau} \gtrsim m_{e\mu} \gtrsim m_{ee} \; . \tag{2.111}$$

The ordering between $m_{e\tau}$ and $m_{\mu\mu}$ is not fixed in the absence of more quantitative arguments.

One criterion of alignment (motivated by possible horizontal symmetry) can be introduced prescribing different lepton charges, q_α, for different flavor neutrino states, $\alpha = e, \mu, \tau$. Suppose the that neutrino masses equal

$$m_{\alpha\beta} = m\lambda^{q_\alpha + q_\beta}, \qquad \lambda < 1 \; . \tag{2.112}$$

Then the normal alignment exists if $q_e > q_\mu > q_\tau$. The smaller λ or/and the larger the difference of charges q_α, the stronger is the alignment. In the case $q_\mu = q_\tau$ (which

might be indicated by maximal $\mu - \tau$ mixing), one can speak of "partial" alignment, associated to the lepton number L_e. In this case all $\mu\tau$-block elements are equal.

Let us consider first the possibility of "partial" alignment. In the limit $k \to 1$, the most general form of zero order mass matrix with equal $\mu\tau$-block elements and $m_{e\mu} = m_{e\tau}$ (as required by $q_\mu = q_\tau$) is Eq.(2.102). In this matrix we have $m_{ee} < m_{e\mu}$ provided that $x^2 < 1/3$ (which is consistent with Eq.(2.34)). Then, the inequality $m_{e\mu} < m_{\tau\tau}$ requires $r > 1$, which implies normal ordering. Under these conditions "partial" alignment is realized. The alignment respects the factorization relation (2.112) if

$$m_{ee}/m_{e\mu} = m_{e\mu}/m_{\tau\tau} \quad \Rightarrow \quad r = \sqrt{1 - 2x^2}/x \ . \tag{2.113}$$

In this case one obtains the factorized matrix

$$m^0 = N \begin{pmatrix} \lambda^2 & \lambda & \lambda \\ \dots & 1 & 1 \\ \dots & \dots & 1 \end{pmatrix} , \tag{2.114}$$

where $\lambda^2 = 2x^2/(1 - x^2)$ and $N = m_2(1 - x^2)/(2x)$. If all three lepton charges are equal, the matrix acquires a "democratic" structure, $m_{ee} = m_{e\mu} = m_{\tau\tau}$, corresponding to $x^2 = 1/3$ and $r = 1$.

In the case of normal hierarchy, the structure (2.114) can be realized with $\lambda \sim s_{13}$, but other structuring of the $e-$row elements is also possible. For example, another structure with partial flavor ordering is

$$m \propto \begin{pmatrix} \lambda & \lambda & \lambda \\ \lambda & 1 & 1 \\ \lambda & 1 & 1 \end{pmatrix} , \tag{2.115}$$

where $\lambda \approx \sqrt{2(s_{13}^2 + r^2 c_{12}^2 s_{12}^2)}$ (Eq.(2.64)).

If 2-3 mixing deviates from maximal, a split appears between $m_{e\mu}$ and $m_{e\tau}$ as well as $\mu\tau$-block elements in Eq.(2.31), thus opening the possibility of complete alignment. The same consideration as above holds for averaged values of the e-row and $\mu\tau$-block elements: $m_{ee}^2 < (m_{e\mu}^2 + m_{e\tau}^2)/2 < \Sigma_{\mu\tau}/4$ if and only if $x^2 < 1/3$ and $r > 1$ (see Eq.(2.39)).

However, it is easy to check that $m_{e\mu} < m_{e\tau}$ implies $\theta_{23} > \pi/4$, while, for $r > 1$, $m_{\mu\mu} < m_{\tau\tau}$ implies $\theta_{23} < \pi/4$, so that complete alignment cannot be realized in m^0. If s_{13} corrections (Eq.(2.43)) are sizable, they can contribute to improve the alignment, since they have opposite signs for the pairs $m_{e\mu}$, $m_{e\tau}$ and $m_{\mu\mu}$, $m_{\tau\tau}$. These corrections can produce flavor ordering, as can be seen, *e.g.*, in Fig.2.18b, for the case of normal hierarchy, $m_1 = 0$, and in Fig.2.19e (shifting e-row lines using the freedom in the choice of δ), for the case $r \sim 1$.

In general structures with complete alignment have an expansion parameter quite large, like $\lambda \approx \tan\theta_{23} \approx 0.8$. This is the case in the following structures (see

Figs.2.17,2.18):

$$m \propto \begin{pmatrix} \lambda^4 & \lambda^3 & \lambda^2 \\ \lambda^3 & \lambda^2 & \lambda \\ \lambda^2 & \lambda & 1 \end{pmatrix}, \qquad m \propto \begin{pmatrix} \lambda^6 & \lambda^4 & \lambda^3 \\ \lambda^4 & \lambda^2 & \lambda \\ \lambda^3 & \lambda & 1 \end{pmatrix}. \tag{2.116}$$

An incomplete alignment can be realized with smaller value of λ: according to Fig. 2.18 a,b, we may have

$$m \propto \begin{pmatrix} \lambda^2 & \lambda^2 & \lambda \\ \lambda^2 & \lambda & 1 \\ \lambda & 1 & 1 \end{pmatrix}, \tag{2.117}$$

with $\lambda \approx 0.3$.

Let us discuss the possibility of "partial" inverted alignment, $q_e < q_\mu = q_\tau$. Using Eq.(2.102), the inequality $m_{ee} > m_{e\mu} > m_{\tau\tau}$ is satisfied for $x^2 > 1/3$ and $r < 1$. If the condition (2.113) is also satisfied (this is possible for $1/3 \leq x^2 \leq 1/2$), one gets the factorized matrix

$$m^0 = N \begin{pmatrix} 1 & \lambda & \lambda \\ \dots & \lambda^2 & \lambda^2 \\ \dots & \dots & \lambda^2 \end{pmatrix}, \tag{2.118}$$

where $\lambda^2 = (1 - x^2)/(2x^2)$ and $N = m_2 x$. Notice that $1/2 \leq \lambda^2 \leq 1$.

A complete *inverted flavor alignment* ($q_e < q_\mu < q_\tau$) can be achieved for non-maximal 2-3 mixing. For example, inserting $r = 0$, $x^2 = 1/2$ and $c_{23}^2 = s_{23}$ into (2.31), we get

$$m^0 = \frac{m_2}{\sqrt{2}} \begin{pmatrix} 1 & \lambda & \lambda^2 \\ \dots & \lambda^2 & \lambda^3 \\ \dots & \dots & \lambda^4 \end{pmatrix}, \tag{2.119}$$

with $\lambda = \tan\theta_{23} \approx 0.79$. The role of μ and τ flavors are interchanged if $c_{23} = s_{23}^2$. In this case a structure analogous to (2.119) is realized, with $\lambda = \cot\theta_{23} \approx 0.79$.

In general, structures in which μ and τ flavors are associated with substantially different mass scales are excluded. Indeed, the difference $m_{\mu\mu}^2 - m_{\tau\tau}^2$ is proportional to the small parameter $\cos 2\theta_{23}$. Moreover, if there is a strong ordering between $m_{\mu\mu}$ and $m_{\tau\tau}$, the element $m_{\mu\tau}$ is larger than both of them (see Eqs.(2.90),(2.93)), while flavor alignment would require an intermediate value.

Notice that free parameters r, ρ, σ, etc. can be found for which no correlation of the masses and lepton charges of the matrix elements exist at all. This possibility can be called *flavor disorder*. Nevertheless, there are possibilities different from flavor ordering to parameterize the mass matrix by powers of a unique expansion parameter $\lambda \ll 1$:

$$m_{\alpha\beta} = m c_{\alpha\beta} \lambda^{n_{\alpha\beta}}, \tag{2.120}$$

where $c_{\alpha\beta}$ are numbers of order 1.

For example, in the case of normal hierarchy the e-row can have a structure without flavor ordering, like $(\lambda^2, \lambda^2, \lambda)$ or $(\lambda^2, \lambda, \lambda^2)$, with $\lambda \approx 0.3$ (see Fig.2.18). In the case of partial or complete degeneracy, (see Fig.2.5e and Eq.(2.103) with $r = \sqrt{3}$), the mass matrix can have the following form:

$$m \propto \begin{pmatrix} 1 & \lambda & \lambda \\ \lambda & 1 & 1 \\ \lambda & 1 & 1 \end{pmatrix} , \tag{2.121}$$

with

$$\lambda \approx \frac{s_{13}}{r\sqrt{2}} . \tag{2.122}$$

Two other possibilities are (see Figs. 2.5f and 2.20f):

$$m \propto \begin{pmatrix} 1 & \lambda & \lambda \\ \lambda & \lambda & 1 \\ \lambda & 1 & \lambda \end{pmatrix} , \qquad m \propto \begin{pmatrix} 1 & \lambda & \lambda \\ \lambda & \lambda^2 & 1 \\ \lambda & 1 & \lambda^2 \end{pmatrix} , \tag{2.123}$$

with $\lambda \approx s_{13}/\sqrt{2}$, which should be taken of order 0.1 for the left matrix and 0.2 for the right matrix.

Notice that value of λ which appears in all the matrices of this section and which is, therefore, consistent with present data, can not be too small. We find

$$\lambda \gtrsim 0.1 - 0.2 . \tag{2.124}$$

Values $\sim 0.3 - 0.4$ are also allowed. The value of the parameter (2.124) can be equal to $\sin\theta_c$, where θ_c is the Cabibbo angle, used as an expansion parameter for quark mass matrices. In the flavor basis the structure of the charge lepton mass matrix is characterized by the two ratios: $m_\mu/m_\tau = 0.059$ and $m_e/m_\mu = 0.0049$. These ratios can also be reproduced as powers of λ:

$$m_e : m_\mu : m_\tau \approx \lambda^6 : \lambda^2 : 1 ,$$

with $\lambda \approx 0.24$.

In the case when all elements are very close to each other with small spread (e.g., Fig.2.19f at $\sigma \approx 0.7$), one can describe the mass matrix as the democratic one plus small deviations:

$$m = m^{dem} + \Delta m ,$$

where $m^{dem}_{\alpha\beta} = m_{dem}$, $\Delta m \sim \mathcal{O}(\lambda)$ and λ is a small parameter. Here λ can be taken of order s_{13} or ξ or $(1 - r)$ (deviation from degeneracy). An interesting possibility could be to take for λ the deviation of ρ or σ from the values $0, \pi/2$, which correspond to definite CP parities.

2.6.4 Symmetry basis and deviation from bimaximal mixing

As we have outlined in the introduction, to obtain further theoretical inference, one needs to find the matrix in the symmetry basis and at the symmetry energy scale. As far as the dependence on the scale is concerned, we will discuss it at length in chapter 3. Here we give some remarks on the choice of basis for the three neutrinos.

In general, the symmetry basis differs from the flavor basis. The mass matrices in symmetry basis of charged leptons, M_l, and of neutrinos, M_ν, are in general non-diagonal:

$$M_l = U_l diag(m_e, m_\mu, m_\tau) U_r^\dagger \ , \qquad M_\nu = U_\nu^* M^{diag} U_\nu^\dagger \ .$$

Then the neutrino mass matrices in symmetry and flavor bases are related by

$$M_\nu = U_l^* M U_l^\dagger \ .$$

The lepton mixing matrix is given by $U_{PMNS} = U_l^\dagger U_\nu$.

The matrix U_l is unknown and some additional assumptions are needed to fix its structure. Clearly this introduces a further ambiguity in the analysis. Here we mention two possibilities (two assumptions) which allow one to immediately relate the matrices in flavor basis and symmetry basis.

1) It may happen that due to strong hierarchy of the masses of the charged leptons, the charged lepton mixing is rather small and $U_l \approx \mathbb{1}$. This is true, e.g., in Grand Unification Theories like minimal $SO(10)$, where charged lepton and up-type quark mass matrices are equal at GUT scale. In this case, the structures of the mass matrix M, discussed in this chapter, are not modified significantly under transition to the symmetry basis.

2) Being related to the ratio of masses of the μ and τ lepton, the 2-3 angle, $\theta_{23}^l \sim \sqrt{m_\mu/m_\tau} \approx 0.24$, can be the only large angle in U_l (1-2 and 1-3 mixing angles are very small, if they are connected with the tiny electron mass). In this case, the effect of charged lepton mixing on the neutrino mass matrix is reduced to a change of the 2-3 angle between symmetry and flavor bases:

$$\theta_{23} = \theta_{23}^{sym} - \theta_{23}^l \ .$$

Taking into account this shift of the angle, the neutrino mass matrices in flavor and symmetry bases can be immediately related: for example, if the reconstructed matrix structure shows significant deviation from maximal $2-3$ mixing, this can be interpreted as a measure of θ_{23}^l, under the assumption that some symmetry reason enforces maximal mixing in symmetry basis.

There exist different models in which charged lepton mass matrix is strongly off-diagonal in symmetry basis, more precisely large left-handed rotation U_l is required to diagonalize the matrix; see, e.g., [82, 84, 192]. The discrepancy with the quark sector can be explained, e.g., relating charged lepton mass matrix with the transposed down quark mass matrix (like in minimal SU(5)). In this way left-handed lepton mixing is

related to right-handed quark mixing, which is unobservable and, therefore, can be large. In this kind of models the structure of the mass matrix appears very different in flavor and symmetry bases. Nevertheless, a given model should give predictions for both M_ν and U_l, so that M can be computed and compared with the allowed by data structures discussed in this chapter.

In section 2.6.1 and 2.6.2 we have looked for zero (small) matrix elements and for equalities among elements in flavor basis. Exactly zero (equal) elements in symmetry basis will receive contributions from the diagonalization of charged lepton mass matrix and of possible non-canonical kinetic terms [199]. Still small (equal) elements which appear in flavor basis can have physical meaning: first, they can indicate that symmetry basis is indeed close to the flavor basis, like in the cases 1) and 2) discussed above; second, they can testify for a correlation between U_l and U_ν (that is, between M_l and M_ν).

Let us consider, finally, the possibility of bimaximal mixing ($\theta_{12} = \theta_{23} = 45^\circ$, $\theta_{13} = 0$). We know that this possibility is strongly disfavored by recent data, since solar mixing angle seems significantly smaller than maximal. Nevertheless, bimaximal mixing could be realized in symmetry basis. In this case the observable non-maximal 1-2 mixing is the result of the rotation U_l.

A number of different matrix structures can lead to bimaximal mixing. In some cases the dominant matrix structure is the same in flavor basis and in "bimaximal basis". For example, for $\rho = 0$ ($x = 1$), the zero order mass matrix (2.31) does not depend on θ_{12} and therefore has the same form in the two basis. However, this is not always the case: when $\theta_{12} = \pi/4$, the parameter x in Eq.(2.31) can be zero (using Eq.(2.22), one has $x = \cos\rho$). Correspondingly, a large variety of mass matrix structures appear which are not allowed in flavor basis. In particular, for $\rho = \pi/2$, independently from the value of σ we obtain the matrix

$$m = \frac{m_2}{2} \begin{pmatrix} 0 & \sqrt{2} & \sqrt{2} \\ \sqrt{2} & r & r \\ \sqrt{2} & r & r \end{pmatrix} , \qquad (2.125)$$

discussed in the literature [93]. For r equal to zero (inverted hierarchy), this matrix has exact $L_e - L_\mu - L_\tau$ symmetry.

It is interesting that the rotation U_l connecting a "bimaximal basis" with the flavor basis can be quite small. In fact, it has been shown in [200, 201] that the choice $U_l \approx U_{CKM}$ is viable. In this case the $1-2$ rotation in U_l is the largest one ($\theta_c \approx 0.2$), in contrast with the case 2) discussed above.

Chapter 3

From electroweak to GUT scale: radiative corrections

In this chapter we will analyze in detail renormalization effects on the neutrino mass matrix structure, presenting the main results of Ref. [202]. Previous studies, discussed in the introduction, focused their attention on the running of the observables between the electroweak scale and some high energy scale. However, mass squared differences and mixing angles are the outcome of the diagonalization of the mass matrix and it is this matrix the object more closely related to the underlying theory. Our goal is to analyze the stability of the matrix structure under the effect of radiative corrections.

In section 3.1 we discuss the generation of the neutrino mass matrix at the high scale m_0. We study first the radiative corrections in SM and MSSM (section 3.2). Then, we consider other extensions of the SM at some intermediate scale m_X, with $m_Z < m_X < m_0$ (section 3.3). In section 3.4 we identify the conditions under which the observables (masses, mixings and phases) can be generated by radiative corrections. Finally (section 3.5), we consider four specific matrix structures at m_0: (i) the matrix proportional to the unit; (ii) the matrix with only ee and $\mu\tau$ elements different from zero; (iii) the matrix with non-zero M_{ee} and $\mu\tau$-block elements; (iv) the matrix with non-zero $\mu\tau$-block. We will study the predictions for the low energy parameters in the case of standard and non-standard radiative corrections.

3.1 A unique effective operator and the scale m_0

With the SM fields, one can construct a unique Lorentz and gauge invariant effective five dimensional operator (see Fig.3.1) that gives Majorana masses to neutrinos [105, 106]:

$$\frac{C_{\alpha\beta}}{m_0}(\overline{L^c}_\alpha \; i\sigma_2 \; \phi)(\phi \; i\sigma_2 \; L_\beta) + \text{h.c.} \; . \tag{3.1}$$

Here $C_{\alpha\beta}$ are dimensionless couplings, m_0 is the mass scale at which this effective interaction is generated, α and β are flavor indexes, ϕ and L are the SM Higgs and

lepton doublets. An analogue operator appears in the case of MSSM (without R-parity violation). After the electroweak symmetry breaking, the operator (3.1) generates the neutrino mass matrix:

$$M_{\alpha\beta} = \frac{2C_{\alpha\beta}\langle\phi^0\rangle^2}{m_0}.$$

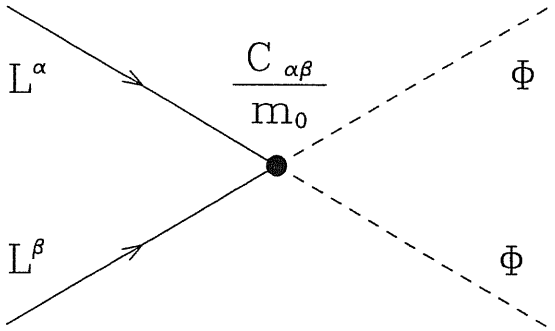

Figure 3.1: The unique five dimensional operator contributing to neutrino masses.

Different possible mechanisms can lead to the effective operator (3.1). One possibility is the exchange of heavy right-handed neutrinos (type-I seesaw [116, 117, 118, 119], Fig.3.2a). In this case m_0 should be identified with the mass m_R of the lightest right-handed neutrino N_R and one gets

$$C_{\alpha\beta} = -\frac{m_0}{2}(Y_\nu M_R^{-1} Y_\nu^T)_{\alpha\beta}\,, \tag{3.2}$$

where Y_ν is the matrix of neutrino Yukawa couplings and M_R is the Majorana mass matrix of right-handed neutrinos, both evaluated at the scale $m_0 = m_R$. Notice that the fermion exchanged in the diagram of Fig.3.2a can be an isosinglet (the usual right-handed neutrino) but also an isotriplet [203].

Another possibility is to introduce a scalar isotriplet Δ with hypercharge 1 and renormalizable coupling to the SM lepton doublets:

$$Y_{\alpha\beta}\overline{L^c}_\alpha \sigma^i L_\beta \Delta_i + \text{h.c.}\,. \tag{3.3}$$

A heavy triplet ($m_\Delta \gg m_Z$) can get a small induced VEV due to the coupling $M_{\Delta\phi}\Delta^*\phi\phi + \text{h.c.}$ (type-II seesaw [204, 205, 206, 207, 208], Fig.3.2b):

$$\langle\Delta^0\rangle = \frac{M_{\Delta\phi}\langle\phi^0\rangle^2}{m_\Delta^2}.$$

If the exchange of the triplet is the dominant contribution to the neutrino mass matrix, m_0 should be identified with m_Δ and

$$C_{\alpha\beta} = Y_{\alpha\beta}\frac{M_{\Delta\phi}}{m_0}. \tag{3.4}$$

The following remarks are in order:

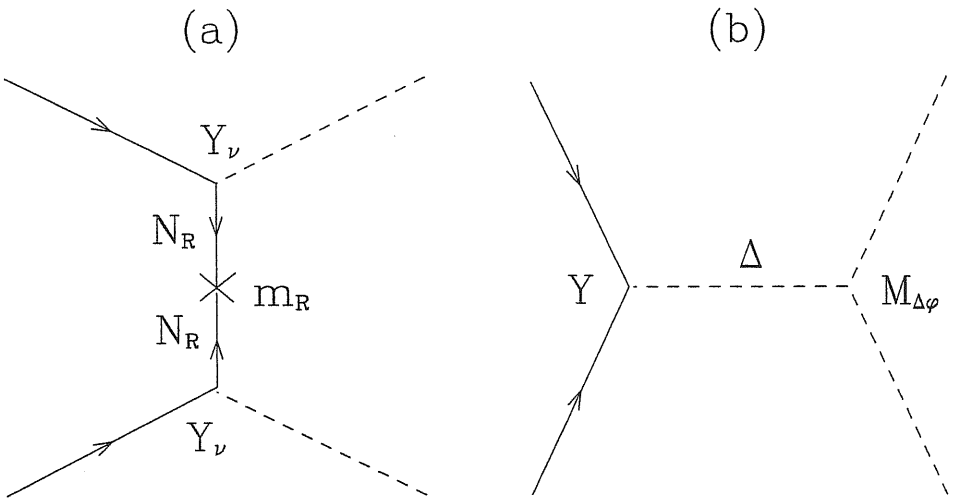

Figure 3.2: The two possible seesaw contributions to the five dimensional operator in Fig. 3.1.

1. The neutrino mass matrix can receive both contributions of the form (3.2) and (3.4). In this case $m_0 = \min\{m_R, m_\Delta\}$.

2. The running between $m_0 = \min\{m_R, m_\Delta\}$ and $\tilde{m}_0 = \max\{m_R, m_\Delta\}$ can be important for the neutrino mass matrix structure, if N_R and Δ contributions are comparable.

3. There can be a hierarchy among the masses of right-handed neutrinos, so that the operator (3.1) is formed in a large energy interval. Corrections in this interval can be important [122, 209, 210].

The relative size and the structure of the various (N_R, Δ, maybe some other [203]) contributions to the neutrino mass matrix are model-dependent. We will elaborate on the seesaw mechanism in chapter 4. Here we will limit ourselves to study the running below m_0.

3.2 Renormalization of the mass matrix in the SM (MSSM)

Let us consider, first, the renormalization of the mass matrix when the only particles with mass below m_0 are the SM (MSSM) particles. Then the β-function of the operator (3.1), $\beta_M \equiv \mu\frac{\mathrm{d}}{\mathrm{d}\mu}M$, can be written as [107, 108, 109]:

$$\begin{aligned} 16\pi^2\beta_M^{SM} &= -\frac{3}{2}\left[M(Y_l^\dagger Y_l) + (Y_l^\dagger Y_l)^T M\right] + K_{SM}M\,, \\ 16\pi^2\beta_M^{MSSM} &= \left[M(Y_l^\dagger Y_l) + (Y_l^\dagger Y_l)^T M\right] + K_{MSSM}M\,, \end{aligned} \tag{3.5}$$

where Y_l is the 3×3 matrix of charged lepton Yukawa couplings and $K_{SM(MSSM)}$ is a real parameter describing flavor universal radiative corrections.

The flavor non-universal corrections (terms in square brackets in Eq. (3.5)) come from two types of diagrams only (figure 3.3), generated by charged lepton Yukawa couplings: renormalization of the wavefunction of lepton doublets (a) and vertex correction (b). In the SM, the coefficient $-3/2$ in Eq. (3.5) is the sum of a contribution $1/2$ from (a) and -2 from (b). In the MSSM, only (a) contributes, due to SUSY non-renormalization, and the coefficient is $1/2 \times 2 = 1$, where the factor 2 corresponds to the double number of particles with respect to SM.

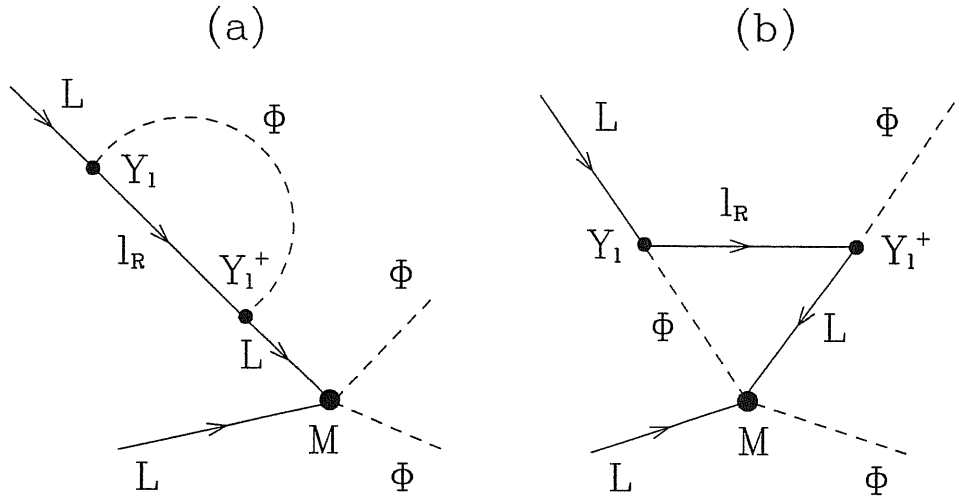

Figure 3.3: The flavor non-universal diagrams in the case of SM (MSSM).

In flavor basis, the matrix Y_l is diagonal and it can be made real by absorbing the phases in the fields:

$$Y_l^\dagger Y_l = diag(y_e^2, y_\mu^2, y_\tau^2)\,.$$

Furthermore, y_α, taken real at a certain scale, will remain real during the running [211]. In this basis, the RGE equation for $M_{\alpha\beta}$ can be easily integrated, giving [212]:

$$M_{\alpha\beta}(m_Z) = I_K \exp\left[-k\int_0^{t_Z}(y_\alpha^2(t)+y_\beta^2(t))dt\right] M_{\alpha\beta}(m_0)\,, \tag{3.6}$$

where

$$t_Z \equiv \frac{\log(m_0/m_Z)}{16\pi^2}\,, \qquad k=-\frac{3}{2}\quad (\mathrm{SM})\,, \qquad k=1\quad (\mathrm{MSSM})\,.$$

The flavor universal corrections are contained in the prefactor

$$I_K = \exp\left(-\int_0^{t_Z} K(t)dt\right).$$

I_K does not change the structure of the mass matrix and, moreover, the overall renormalization effect is small: $I_K \approx 1$. We will consider only 1-loop radiative corrections and therefore neglect the evolution of y_α in Eq. (3.6), taking the values of charged lepton Yukawa couplings at the electroweak scale: $y_\alpha(t) \approx y_\alpha(0)$.

Several important conclusions follow immediately from Eq. (3.6):

- In flavor basis, each element of the mass matrix evolves independently from the values of other elements. The value of the element at m_Z is proportional to its value at m_0:

$$M_{\alpha\beta}(m_Z) \propto M_{\alpha\beta}(m_0)\,. \tag{3.7}$$

  In particular, elements which are zero at some scale, remain zero at any scale.

- The phases of $M_{\alpha\beta}$ do not evolve, because the r.h.s. in Eq. (3.6) is real. In contrast, the three CP-violating phases δ, ρ and σ depend on the moduli of $M_{\alpha\beta}$ and therefore can be strongly renormalized. However, if there is no CP violation at some scale (M is real), no CP violation can be induced by radiative corrections at any scale.

- The corrections to matrix elements have opposite sign in SM and MSSM, due to the different sign of k. The same matrix at m_Z will develop different features at the scale m_0 depending on whether low energy supersymmetry is present or not.

Notice that, in principle, SM and MSSM could be discriminated by the ordering of mass eigenvalues: exactly degenerate neutrinos at the scale m_0 could be split into a normal mass spectrum in SM and into an inverted spectrum in MSSM or vice versa, depending on mixings and phases. However, using only SM (MSSM) radiative corrections, it is hard to reproduce data starting with exactly degenerate neutrinos [213]. Also the scenario with only two degenerate neutrinos at high energy has been recently studied [214, 215] and the difference of predictions between SM and MSSM has been analyzed.

The largest flavor dependent contribution to the running in Eq. (3.6) is due to the τ Yukawa coupling:

$$y_\tau(m_Z) = \begin{cases} \dfrac{m_\tau}{v} \approx 10^{-2} & \text{(SM)} \\ \dfrac{m_\tau}{v\cos\beta} \approx \tan\beta \cdot 10^{-2} & \text{(MSSM)} \end{cases}, \tag{3.8}$$

where $v \approx 174\,\text{GeV}$ is the VEV of the SM Higgs and $\tan\beta$ is the ratio of VEV's of the two MSSM Higgs doublets. The other Yukawa couplings are much smaller, therefore the largest corrections are for elements which have the τ-flavor. Neglecting y_e and y_μ corrections, Eq. (3.6) gives:

$$\begin{aligned} M_{\tau\tau}(m_Z) &\approx I_K M_{\tau\tau}(m_0)(1-2k\epsilon_\tau)\,, \\ M_{e\tau}(m_Z) &\approx I_K M_{e\tau}(m_0)(1-k\epsilon_\tau)\,, \\ M_{\mu\tau}(m_Z) &\approx I_K M_{\mu\tau}(m_0)(1-k\epsilon_\tau)\,, \end{aligned}$$

where, taking $m_0 = 10^n$ GeV,

$$\epsilon_\tau \equiv \frac{y_\tau^2(m_Z)}{16\pi^2}\log\frac{m_0}{m_Z} \begin{cases} \approx 1.5(n-2)10^{-6} & \text{(SM)} \\ \approx 3.5(n-2)10^{-3}\left(\dfrac{\tan\beta}{50}\right)^2 & \text{(MSSM)} \end{cases}. \tag{3.9}$$

The effect of running is apparently very small even for $M_{\tau\tau}$.

We conclude that radiative corrections (in SM and MSSM) practically do not change the structure of neutrino mass matrix up to the scale m_0. Zero elements remain zero and non-zero elements acquire very small relative corrections, which are at most few percents. Symmetry properties of the matrix at m_0 are almost unchanged by running to low energy, where the matrix structure can be reconstructed using experimental input for mixing angles and mass eigenvalues, as well as CP violating phases (see chapter 2). In other words, the structure of the mass matrix is stable with respect to radiative corrections in SM and MSSM, independently of type of mass ordering (normal or inverted), level of degeneracy, values of mixing angles and CP violating phases.

3.3 Renormalization of the mass matrix due to new particles

It may happen that new physics exists at some intermediate scale m_X in the range $m_Z - m_0$, which does not contribute to neutrino masses at tree-level but leads to renormalization effects.

3.3.1 Non-standard Yukawa interactions

Let us consider new fermions and scalar bosons, with mass $\sim m_X$. We assume that new scalars have zero VEV's, otherwise they would generate neutrino masses at the scale $m_X < m_0$. We analyze radiative corrections to the operator (3.1) induced by the couplings of these scalars and fermions to the lepton doublets L_α:

- An extra scalar doublet, ϕ', with the coupling

$$Y^{\phi'}_{\alpha\beta}\overline{L}_\alpha \phi' l_{R\beta} + \text{h.c.}\,, \tag{3.10}$$

  contributes to the wavefunction renormalization (diagram analogue to figure 3.3*a*). There is no vertex diagram with ϕ' in the loop (analogue to figure 3.3*b*), because only ϕ enters the operator (3.1).

- An extra scalar singlet ρ or triplet χ can couple with two lepton doublets:

$$Y^{\rho}_{\alpha\beta}\overline{L}_\alpha i\sigma_2 L^c_\beta \rho + \text{h.c.}\,, \tag{3.11}$$

$$Y^{\chi}_{\alpha\beta}\overline{L}_\alpha i\sigma_2 \sigma^i L^c_\beta \chi_i + \text{h.c.}\,. \tag{3.12}$$

  The renormalization of the operator (3.1) is induced by the two diagrams in figure 3.4. In the singlet case, the matrix Y is antisymmetric, because $\overline{L}_\alpha i\sigma_2 L^c_\beta = -\overline{L}_\beta i\sigma_2 L^c_\alpha$ (in the triplet case, Y is symmetric).

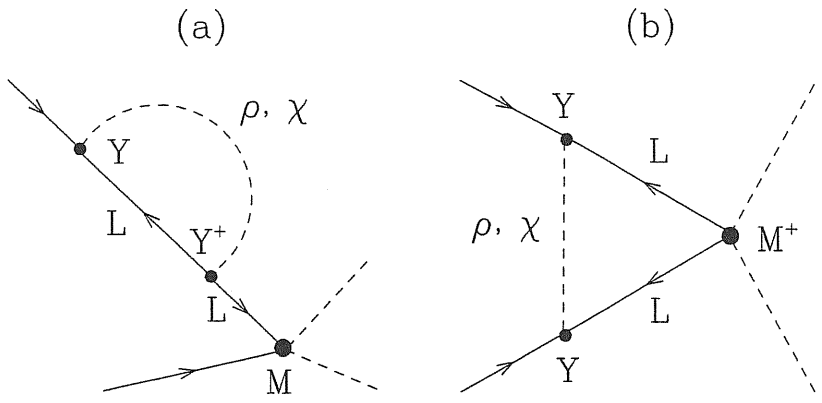

Figure 3.4: The diagrams generated by a new scalar singlet ρ or triplet χ (Eqs. (3.11), (3.12)).

- If a new right-handed doublet fermion D_R exists at the scale m_X, ρ and χ can have the following interactions:

$$Y_\alpha^{D\rho}\overline{L}_\alpha D_R \rho + \text{h.c.}\,, \tag{3.13}$$

$$Y_\alpha^{D\chi}\overline{L}_\alpha \sigma^i D_R \chi_i + \text{h.c.}\ . \tag{3.14}$$

  In this case there are no vertex corrections, because D_R and ρ (χ) do not enter in the operator (3.1). Only the diagram shown in figure 3.5 contributes.

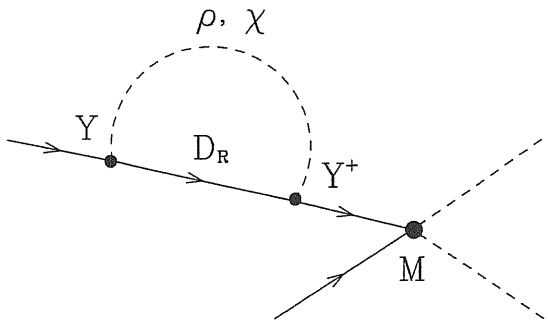

Figure 3.5: The diagram generated by a new scalar singlet ρ (triplet χ) and a new fermion doublet D_R (Eqs. (3.13), (3.14)).

- A right-handed fermion singlet S_R, with the Yukawa interaction

$$Y_\alpha^S \overline{L}_\alpha \phi S_R + \text{h.c.}\,. \tag{3.15}$$

  contributes both to wavefunction and vertex renormalization, as shown in figure 3.6. The scalar doublet in the diagram 3.6(a) can be the SM one, ϕ, or some new doublet ϕ'.

The new chiral fermions (D_R, S_R) can lead to anomalies, however one can consider them as part of new vector-like fermions. The vertex diagrams in figures 3.4*b* and 3.6*b*

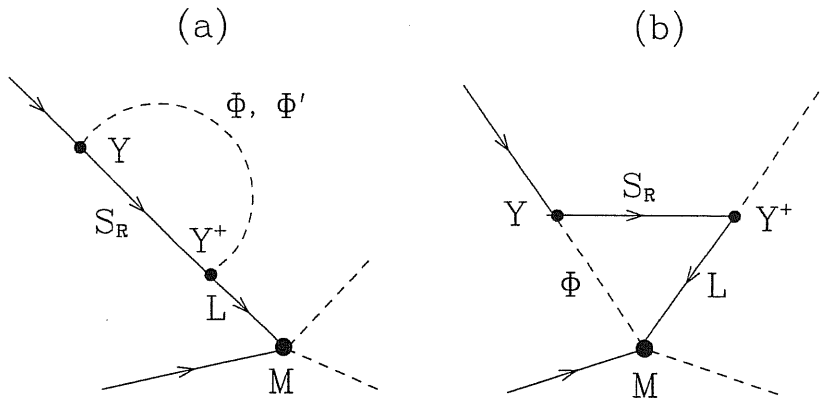

Figure 3.6: The diagrams generated by a new fermion singlet S_R (Eq. (3.15)).

give no contributions in the supersymmetric case, because of non-renormalization theorem.

For any of the interactions in Eqs. (3.10)–(3.15), the contribution to the β-function of neutrino mass matrix elements can be written as

$$16\pi^2(\beta_M^Y)_{\alpha\beta} = k_Y^{(1)}\left[M(Y^\dagger Y) + (Y^\dagger Y)^T M\right]_{\alpha\beta} + k_Y^{(2)}\left[YM^\dagger Y^T\right]_{\alpha\beta}. \qquad (3.16)$$

where Y are the new particle Yukawa couplings and the prefactors $k_Y^{(i)}$ depend on the type of particles and interactions considered. The first term in square brackets of Eq. (3.16) (analogue to those in Eq. (3.5)) corresponds to all diagrams discussed above (analogue to those in figure 3.3), except the diagram in figure 3.4*b*. This diagram generates the second term in square brackets of Eq. (3.16). Therefore, $k_Y^{(2)} \neq 0$ only for the interactions in Eqs. (3.11), (3.12).

Let us emphasize the main differences in the running with respect to SM (MSSM):

- If the matrix $Y^\dagger Y$ (or, in the case of Eqs. (3.11), (3.12), the matrix Y) is not diagonal in flavor basis, the RGE's for different matrix elements are coupled. A given matrix element receives corrections proportional to other matrix elements; in this way small elements can be modified significantly.

- The size of corrections depends on the size of Yukawa couplings Y. It can be much larger than in SM. In the perturbative regime, $Y \lesssim 1$, the effect can be of the order of few percents, as in MSSM.

- The corrections can be further enhanced if several non-standard multiplets are present. E.g., one can introduce three generations of new particles. In this case corrections can be as large as $\sim 10\%$ of the large matrix elements.

- The size of corrections is proportional to $\log(m_0/m_X)$. Corrections are suppressed for $m_X \sim m_0$.

- In all diagrams but figure 3.4*b*, only one external lepton leg is involved in flavor changing interactions. As a consequence, a given element $M_{\alpha\beta}$ receives contributions proportional to matrix elements in the rows (columns) α and β only. In contrast, if the diagram in figure 3.4*b* is present, all matrix elements can contribute to the renormalization of a given element $M_{\alpha\beta}$.

Since radiative effects are small, with a good approximation we can consider only lowest order corrections to matrix elements. Using Eq. (3.16), we get:

$$\Delta M^Y_{\alpha\beta} \approx -\frac{\log(m_0/m_X)}{16\pi^2}\left(k_Y^{(1)}\left[M(Y^\dagger Y)+(Y^\dagger Y)^T M\right]_{\alpha\beta}+k_Y^{(2)}\left[YM^\dagger Y^T\right]_{\alpha\beta}\right). \tag{3.17}$$

3.3.2 Non-universal $U(1)$ gauge interaction

Let us consider the effect of extra heavy vector bosons X_μ, which have flavor non-universal interactions. These bosons can be related to the existence of horizontal (flavor) gauge symmetries [69].

We restrict ourselves to the case of an extra $U(1)_X$ gauge group. In the flavor basis, the interaction of lepton doublets with the new gauge bosons X_μ has the form

$$g_X Q_{\alpha\beta}\overline{L}_\alpha\gamma^\mu X_\mu L_\beta\,, \tag{3.18}$$

where g_X is the gauge coupling and Q is the hermitian matrix of "charges", which can be non-diagonal in flavor basis. The possible anomalies of the extra $U(1)_X$ gauge group can be canceled using the Green-Schwarz mechanism [216].

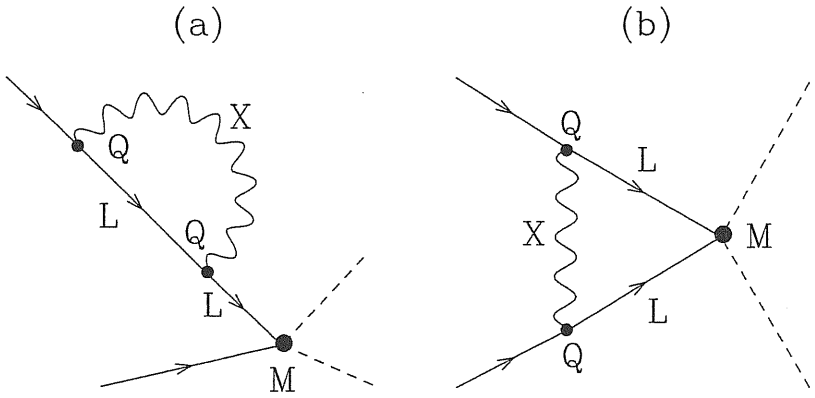

Figure 3.7: The diagrams generated by a new gauge boson X_μ (Eq. (3.18)).

In figure 3.7 we show the two 1-loop gauge diagrams that give non-universal radiative corrections to the operator (3.1). Their contribution to the β-function of matrix elements takes the following form:

$$16\pi^2(\beta_M^X)_{\alpha\beta} = g_X^2 k_X^{(a)}[M\ Q^2+(Q^2)^T M]_{\alpha\beta}+g_X^2 k_X^{(b)}[Q^T M\ Q]_{\alpha\beta}\,. \tag{3.19}$$

The first and the second square brackets of Eq. (3.19) are the contribution of the diagrams in figure 3.7*a* and 3.7*b*, respectively. The β-function (3.19) has analogous features to the one in Eq. (3.16): the RGE's of different elements are coupled because of the off-diagonal entries in the matrix Q; the corrections are proportional to the gauge coupling g_X^2 and cannot be larger than few percents of the largest element in M. Like in figure 3.4*b*, in figure 3.7*b* both lepton external legs enter in the loop. As a consequence, a given element $M_{\alpha\beta}$ can receive contributions proportional to all matrix elements. In lowest order, corrections can be written as:

$$\Delta M^X_{\alpha\beta} \approx -\frac{g_X^2 \log(m_0/m_X)}{16\pi^2}\left(k_X^{(a)}[M\ Q^2 + (Q^2)^T M]_{\alpha\beta} + k_X^{(b)}[Q^T M\ Q]_{\alpha\beta}\right). \quad (3.20)$$

3.4 Radiative origin of low energy observables

Even though the matrix structure is stable, observables, i.e. the values of the mass differences and the form of the mixing matrix, can be strongly affected by the radiative corrections. There is a number of studies [217, 212, 218, 121, 219, 110, 220, 221, 222, 211, 223, 224, 225, 226] in which the RGE's for mixing angles and Δm^2_{ij} have been analyzed and conditions for strong renormalization effects have been identified.

In contrast with these studies, we discuss the effect of renormalization on observables in terms of the mass matrix structure. The matrix of Standard Model (MSSM) corrections can be written as:

$$\Delta M \approx -\epsilon_K M^0 - k \begin{pmatrix} 2\epsilon_e M^0_{ee} & (\epsilon_e+\epsilon_\mu) M^0_{e\mu} & (\epsilon_e+\epsilon_\tau) M^0_{e\tau} \\ \dots & 2\epsilon_\mu M^0_{\mu\mu} & (\epsilon_\mu+\epsilon_\tau) M^0_{\mu\tau} \\ \dots & \dots & 2\epsilon_\tau M^0_{\tau\tau} \end{pmatrix}, \quad (3.21)$$

where M^0 is the matrix at the scale m_0 and $\epsilon_{K,e,\mu}$ can be obtained from the expression (3.9), by substituting y_τ^2 with K, y_e^2, y_μ^2 respectively. If new particles are present between m_0 and m_Z, one should add to Eq. (3.21) the contributions of Eqs. (3.17) and (3.20).

The effect on a given observable depends on how strong is the influence ("imprint") of this observable on the structure of the matrix. When two eigenstates are almost degenerate in mass, the matrix structure depends very weakly on their mass squared difference Δm^2_{ij} and on the mixing angle θ_{ij} (see chapter 2). In other words, Δm^2_{ij} and θ_{ij} are not "imprinted" in the matrix structure. In this case the small radiative corrections (3.21) can strongly modify these observables. Let us give a rough estimation: θ_{ij} and Δm^2_{ij} can receive large radiative corrections if the absolute neutrino mass scale m is large enough to satisfy $\Delta m^2_{ij} \sim \epsilon_\tau\ m^2$. Because of the smallness of ϵ_τ, this condition requires quasi-degenerate neutrino masses.

If some observable is zero in M^0 and acquires a non-zero value in $M(m_Z)$, we can say that this observable has radiative origin. Since the corrections (3.21) are small, only observables which are not connected with the dominant structure of the matrix

can have radiative origin. Following our analysis of the matrix dominant structure (chapter 2), we conclude that possible radiatively generated observables are

- Δm^2_{atm}, only in the case of quasi-degenerate spectrum.
- Δm^2_{sol}, for all mass spectra but normal hierarchy.
- θ_{13} and δ, always.
- θ_{12}, when $\rho \approx 0, \pi$ $(x \approx 1)$.
- θ_{23}, only when M is close to the unit matrix.
- ρ, in the case of normal hierarchy.
- σ, in the case of inverted hierarchy.

Of course one can consider also non-zero initial values of some observables, like $\theta_{12} = \pi/4$ or $\theta_{23} = \pi/4$ or $\rho, \sigma = \pi/2$, and analyze the radiative origin of deviations from such values.

In the next section we will use Eq. (3.21) (and also (3.17), (3.20)) to discuss the effect of radiative corrections for some particular structures of M^0. We will give some explicit realizations of radiative origin of observables.

3.5 Radiative generation of the sub-dominant matrix elements

We have seen in section 2.6.1 that, in agreement with experimental data, the neutrino mass matrix in flavor basis can have a hierarchical structure, with some elements much smaller than the others. Small elements are suppressed by factors s_{13}, $\Delta m^2_{\rm sol}/\Delta m^2_{\rm atm}$ or, in the case of degenerate spectrum ($m_1 \approx m_2 \approx m_3$), by $\Delta m^2_{\rm atm}/m^2_1$. All possible hierarchical structures allowed by the data have been identified in section 2.6.1.

Non-standard radiative effects can generate non-zero matrix elements even if they are zero at the scale m_0. These elements can receive a radiative contribution up to $\sim 10\%$ of the largest matrix element. In what follows we will consider mass matrices with various hierarchical structures and study the possibility to generate all small elements of these matrices radiatively. It has been found that matrices with three or more exactly zero elements at the scale m_Z cannot reproduce the experimental data [157]. We will show that these matrices, realized at m_0, agree with phenomenology if non-standard radiative corrections are taken into account.

Let us write the neutrino mass matrix with hierarchical structure as

$$M = M_D + M_S\,,$$

where M_D is the matrix of dominant elements and M_S is the matrix of sub-dominant elements. In general, large matrix elements are the sum of a dominant contribution

from M_D and a small correction from M_S. Small matrix elements are contained in M_S only. We assume that, at the high scale m_0,

$$M(m_0) = M_D(m_0)\,, \qquad M_S(m_0) = 0 \tag{3.22}$$

and, at the low scale m_Z,

$$M(m_Z) = M_D(m_0) + M_S(m_Z)\,, \qquad M_S(m_Z) = M_{\rm rad}\,, \tag{3.23}$$

where $M_{\rm rad}$ is the matrix of radiative corrections. In general, $M_{\rm rad}$ can be written as

$$M_{\rm rad} = M_{SM(MSSM)} + M_{NS}\,,$$

where M_{NS} is the contribution of non-standard corrections. In particular, we will analyze the corrections given by Eq. (3.17), assuming $k_Y^{(2)} = 0$. In this case, $M_{\rm rad}$ can be written as

$$M_{\rm rad} = \lambda_{rad}(XM_D + M_D X^T)\,, \tag{3.24}$$

where

$$X \equiv (Y^\dagger Y)^T\,, \qquad \lambda_{rad} \equiv -\frac{k_Y^{(1)}}{16\pi^2}\log\frac{m_0}{m_X}\,. \tag{3.25}$$

The non-standard (flavor changing) couplings Y affect also the evolution of the charged lepton Yukawa coupling matrix Y_l, inducing non-zero off-diagonal entries. As a consequence, flavor basis should be redefined at the scale m_Z through a rotation U_l of charged leptons. Due to the strong hierarchy of charged lepton masses, the mixing angles generated in the charged lepton sector are small, being of the order of radiative corrections themselves: $U_l = \mathbb{1} + U_{\rm rad}$. Therefore, the neutrino mass matrix in flavor basis is given by:

$$M^{fl} = U_l(M_D + M_{\rm rad})U_l^T \approx M_D + M_{\rm rad} + U_{\rm rad}M_D + M_D U_{\rm rad}^T\,, \tag{3.26}$$

where we have neglected terms quadratic in radiative corrections. While the neutrino masses at m_Z can be extracted from $M = M_D + M_{\rm rad}$, the mixing angles are influenced by U_l rotation and all the terms in Eq. (3.26) should be considered.

The term $(U_{\rm rad}M_D + M_D U_{\rm rad}^T)$ in Eq. (3.26), describing the effect of charged leptons, has the same structure as $M_{\rm rad}$ in Eq. (3.24). Therefore, the effect of rotation to flavor basis amounts to a redefinition:

$$X \to X + \frac{U_{\rm rad}}{\lambda_{rad}}\,, \tag{3.27}$$

where X and λ_{rad} are defined in Eq. (3.25). In the following, we will extract some results independent from the form of X.

Let us comment on our assumption of exact zeros at m_0 (see Eq. (3.22)). Zero values of matrix elements can be a consequence of certain symmetry at m_0. The

radiative contributions to these elements are generated by interactions which break this symmetry. In general, the symmetry breaking leads to finite contributions already at m_0. On the other hand, if some particles producing radiative corrections are light ($m_X \ll m_0$), the largest contribution to zero elements is given by the leading logarithms and can be computed by RGE methods in the context of the effective theory. We are considering here these logarithmic contributions.

In what follows we will discuss corrections to different dominant structures M_D.

3.5.1 Unit matrix

Let us consider the matrix with dominant structure proportional to the unit matrix:

$$M_D = m\ diag(1,1,1) \equiv m\mathbb{1}\,. \tag{3.28}$$

At m_Z, the approximate degeneracy of neutrino masses ($m_1 \approx m_2 \approx m_3$) is broken by $\Delta m^2_{\rm atm}$ and $\Delta m^2_{\rm sol}$. Let us remind the definitions (2.94) and (2.30):

$$\eta \equiv 1 - \frac{m_3}{m_2} \approx \pm\frac{\Delta m^2_{\rm atm}}{2\ m_1^2}\,, \qquad \epsilon \equiv 1 - \frac{m_1}{m_2} \approx \frac{\Delta m^2_{\rm sol}}{2m_1^2}\,,$$

where the sign of η is $+$ for inverted ordering ($m_3 < m_2$) and $-$ for normal ordering ($m_3 > m_2$). Taking $m_i \approx 0.3$eV (a value allowed by all existing upper bounds [54, 164, 61, 227]), one finds $\epsilon \ll \eta \lesssim 5 \cdot 10^{-3}$. This means that deviations from $M(m_Z) = m\mathbb{1}$ can be smaller than 1%.

For simplicity, at m_Z we assume zero Majorana phases, $\sin\theta_{13} = 0$ and maximal atmospheric mixing ($\theta_{23} = \pi/4$). Then, the phenomenological mass matrix can be written as (see Eq.(2.24)):

$$M^{ph}(m_Z) = m_2 \begin{pmatrix} 1-\epsilon c_{12}^2 & \epsilon c_{12}s_{12}/\sqrt{2} & -\epsilon c_{12}s_{12}/\sqrt{2} \\ \dots & 1-(\eta+\epsilon s_{12}^2)/2 & (-\eta+\epsilon s_{12}^2)/2 \\ \dots & \dots & 1-(\eta+\epsilon s_{12}^2)/2 \end{pmatrix}\,. \tag{3.29}$$

Let us consider, first, radiative corrections in the case of SM (MSSM). Substituting the matrix (3.28) in Eq. (3.21), it is evident that off-diagonal elements remain zero and, therefore, no mixing is produced. Standard corrections lead to a split among diagonal elements. Using Eq. (3.21), one finds that mass squared differences in the range required by phenomenology can be obtained at m_Z in the case of MSSM with large $\tan\beta$, however one gets the following prediction:

$$\frac{\Delta m^2_{\rm sol}}{\Delta m^2_{\rm atm}} \approx \frac{\epsilon_\mu - \epsilon_e}{\epsilon_\tau - \epsilon_\mu} \approx \frac{m_\mu^2}{m_\tau^2} \approx 3.5 \cdot 10^{-3}\,.$$

This ratio is about ten times smaller than the best fit value $\approx 3 \cdot 10^{-2}$.

Let us consider now radiative corrections which originate from new scalars and fermions (section 3.3.1). Substituting the matrix (3.28) in Eq. (3.24), we get corrections

to matrix elements of the following form:

$$M_{\rm rad} \approx 2\ m\ \lambda_{rad} \begin{pmatrix} X_{ee} & {\rm Re}X_{e\mu} & {\rm Re}X_{e\tau} \\ \dots & X_{\mu\mu} & {\rm Re}X_{\mu\tau} \\ \dots & \dots & X_{\tau\tau} \end{pmatrix}, \tag{3.30}$$

where X and λ_{rad} are defined in Eq. (3.25). Since the matrix X is hermitian, the corrections to all matrix elements are real, so that no CP violation is induced in this case.

The corrections to the different elements are related if a specific form of the matrix X is given. We consider an interaction like those in Eqs. (3.13)–(3.15). Then, $X_{\alpha\beta} = Y_\alpha Y_\beta^*$ and, defining

$$\lambda_\alpha \equiv 2\lambda_{rad}|Y_\alpha|^2\,, \qquad c_{\alpha\beta} \equiv \cos(\arg Y_\alpha - \arg Y_\beta)\,, \qquad \alpha = e,\mu,\tau\,, \tag{3.31}$$

we get

$$M(m_Z) \equiv M_D + M_{\rm rad} = m \begin{pmatrix} 1+\lambda_e & \sqrt{\lambda_e\lambda_\mu}c_{e\mu} & \sqrt{\lambda_e\lambda_\tau}c_{e\tau} \\ \dots & 1+\lambda_\mu & \sqrt{\lambda_\mu\lambda_\tau}c_{\mu\tau} \\ \dots & \dots & 1+\lambda_\tau \end{pmatrix}. \tag{3.32}$$

The small parameters λ_α are real and have all the same sign, which is opposite to the sign of $k_Y^{(1)}$ (see Eq. (3.25)). The parameters $c_{\alpha\beta}$ can vary between -1 and 1, but only two of them are independent.

Before comparing the matrix (3.32) with the phenomenological mass matrix (3.29), one needs to perform an additional rotation U_l. If U_l is real, substituting $M_D \propto \mathbb{1}$ in Eq. (3.26) we get

$$M^{fl} = M_D + M_{\rm rad} + \mathcal{O}(U_{\rm rad}M_{\rm rad})\,.$$

In this case, we can neglect the rotation U_l.

Let us show that the matrix (3.32) can reproduce the matrix (3.29). For simplicity, we take $m = m_2$. Then, from the condition $M_D + M_{\rm rad} = M^{ph}(M_Z)$, we find:

$$\begin{aligned} \lambda_e &= -\epsilon c_{12}^2\,, \\ \lambda_\mu &= \lambda_\tau = -\frac{1}{2}(\eta + \epsilon s_{12}^2) \approx -\frac{\eta}{2}\,, \\ c_{\mu\tau} &= \frac{\eta - \epsilon s_{12}^2}{\eta + \epsilon s_{12}^2} \approx 1\,, \\ c_{e\mu} &= -c_{e\tau} = \frac{\sqrt{\epsilon}\ s_{12}}{\sqrt{\eta + \epsilon s_{12}^2}} \approx \sqrt{\frac{\epsilon}{\eta}}\ s_{12}\,. \end{aligned} \tag{3.33}$$

Since λ_e is negative, also λ_μ and λ_τ are negative. This corresponds to inverted mass spectrum ($\eta > 0$) and requires a positive $k_Y^{(1)}$ (see Eqs. (3.31) and (3.25)). The Eq. (3.33) shows that, to reproduce the correct phenomenology, the new Yukawa couplings Y_μ and Y_τ should be equal (also in phase), while Y_e should be much smaller and with a relative phase $\pi/2$ with respect to $Y_{\mu,\tau}$.

If m is not equal to m_2, other solutions are possible. It turns out that the matrices (3.29) and (3.32) can be equal only if m is one of the three eigenvalues. Requiring $m = m_1 \equiv (1-\epsilon)m_2$, one gets

$$\lambda_e \approx \epsilon s_{12}^2\,, \qquad \lambda_\mu = \lambda_\tau \approx -\frac{\eta}{2}\,, \qquad c_{\mu\tau} \approx 1\,, \qquad c_{e\mu} = -c_{e\tau} \approx \sqrt{-\frac{\epsilon}{\eta}}\, c_{12}\,. \tag{3.34}$$

This corresponds to normal mass spectrum. Requiring $m = m_3 \equiv (1-\eta)m_2$, one gets

$$\lambda_e \approx \eta\,, \qquad \lambda_\mu = \lambda_\tau \approx \frac{\eta}{2}\,, \qquad c_{\mu\tau} = -1\,, \qquad c_{e\mu} = -c_{e\tau} \approx \frac{\epsilon c_{12} s_{12}}{|\eta|}\,. \tag{3.35}$$

This can correspond to both normal and inverted mass spectrum.

3.5.2 Dominant M_{ee} and $M_{\mu\tau}$

Let us consider the hierarchical matrix with dominant block given by

$$M_D = m \begin{pmatrix} 1 & 0 & 0 \\ 0 & 0 & -1 \\ 0 & -1 & 0 \end{pmatrix}. \tag{3.36}$$

For this matrix $\theta_{23} = \pi/4$, $\theta_{13} = 0$ and the eigenvalues equal $(m, m, -m)$. Substituting the matrix (3.36) in Eq. (3.21), one sees that SM (MSSM) radiative corrections generate a solar mass squared difference: $\Delta m^2_{\rm sol} \approx 2m^2\epsilon_\tau|k|$. However, atmospheric mass squared difference and solar mixing angle remain zero.

We assume that the relative phases among eigenvalues at m_Z are the same as at m_0, that is $(1, 1, -1)$ and also the values of θ_{23} and θ_{13} remain $\pi/4$ and 0, respectively. Then, the phenomenological mass matrix is real and can be written as (see Eq.(2.24)):

$$M^{ph}(m_Z) = m_2 \begin{pmatrix} 1-\epsilon c_{12}^2 & \epsilon c_{12}s_{12}/\sqrt{2} & -\epsilon c_{12}s_{12}/\sqrt{2} \\ \dots & (\eta - \epsilon s_{12}^2)/2 & -1 + (\eta + \epsilon s_{12}^2)/2 \\ \dots & \dots & (\eta - \epsilon s_{12}^2)/2 \end{pmatrix}. \tag{3.37}$$

Let us study non-standard radiative corrections. Substituting the matrix (3.36) in Eq. (3.24), we get

$$M(m_Z) \equiv M_D + M_{\rm rad} = m \begin{pmatrix} 1+\lambda_1 & \lambda_2 & -\lambda_2^* \\ \dots & \lambda_3 & -1+\lambda_4 \\ \dots & \dots & \lambda_3^* \end{pmatrix}, \tag{3.38}$$

where, using the definitions in Eq. (3.25),

$$\lambda_1 = 2\lambda_{rad}X_{ee}\,, \quad \lambda_2 = \lambda_{rad}(X_{\mu e} - X_{e\tau})\,, \quad \lambda_3 = -2\lambda_{rad}X_{\mu\tau}\,, \quad \lambda_4 = -\lambda_{rad}(X_{\mu\mu} + X_{\tau\tau})\,.$$

To reproduce the phenomenological matrix (3.37) with the matrix (3.38), one needs to take λ_2 and λ_3 real (λ_1 and λ_4 are real by definition, since X is hermitian). Then, assuming for simplicity $m = m_2$, the equation $M(m_Z) = M^{ph}(m_Z)$ leads to the following

relations:

$$\tan 2\theta_{12} = \frac{2\sqrt{2}\lambda_2}{\lambda_3 - \lambda_1 - \lambda_4}, \qquad \eta = \lambda_3 + \lambda_4, \qquad \epsilon = \lambda_4 - \lambda_1 - \lambda_3. \tag{3.39}$$

Let us consider the specific form $X_{\alpha\beta} = Y_\alpha Y_\beta^*$, where Y_α are non-standard Yukawa couplings. In general, before a comparison with Eq. (3.37), this form of X should be modified as in Eq. (3.27). Assuming that the effect of this redefinition is very small or can be absorbed in a redefinition of Y_α, one can express the equality $M(m_Z) = M^{ph}(m_Z)$ in terms of the parameters defined in Eq. (3.31). In particular, the equality of matrices is realized for $m = m_3$ and the same values of parameters as in Eq. (3.35).

Non-standard radiative corrections to the matrix (3.36) has been discussed also in [228, 229], in connection with a non-abelian discrete symmetry that leads to the matrix (3.36) at high energy.

3.5.3 Dominant M_{ee} and $\mu\tau$-block

Let us assume that the matrix with dominant block at the scale m_0 is given by

$$M_D = m \begin{pmatrix} 1 & 0 & 0 \\ 0 & 1/2 & -1/2 \\ 0 & -1/2 & 1/2 \end{pmatrix}. \tag{3.40}$$

This matrix leads to $\theta_{23} = \pi/4$, $\theta_{13} = 0$ and the eigenvalues equal $(m, m, 0)$. It corresponds to inverted mass spectrum. The SM (MSSM) radiative corrections do not generate $1-2$ mixing because the zero elements $M_{e\mu}$ and $M_{e\tau}$ are not modified by these corrections.

Let us consider the phenomenological mass matrix with the dominant block structure (3.40). We assume, for simplicity, $m_3 = \arg(m_1/m_2) = \theta_{13} = 0$ and $\theta_{23} = \pi/4$. Then, the matrix can be written as (Eq.(2.24)):

$$M^{ph}(m_Z) = m_2 \begin{pmatrix} 1 - \epsilon c_{12}^2 & \epsilon c_{12}s_{12}/\sqrt{2} & -\epsilon c_{12}s_{12}/\sqrt{2} \\ \dots & (1 - \epsilon s_{12}^2)/2 & -(1 - \epsilon s_{12}^2)/2 \\ \dots & \dots & (1 - \epsilon s_{12}^2)/2 \end{pmatrix}, \tag{3.41}$$

where $m_2 = \sqrt{\Delta m^2_{\rm atm}} \approx 0.05$eV and $\epsilon \approx \Delta m^2_{\rm sol}/(2\Delta m^2_{\rm atm}) \approx 0.01$.

Let us study non-standard radiative corrections. Substituting the matrix (3.40) in Eq. (3.24) and requiring $M_{e\mu} = -M_{e\tau}$ and $M_{\mu\mu} = M_{\tau\tau}$ (necessary to reproduce the matrix (3.41)), we get

$$M(m_Z) \equiv M_D + M_{\rm rad} = m \begin{pmatrix} 1 + \lambda_1 & \lambda_2 & -\lambda_2 \\ \dots & 1/2 + \lambda_3 & -1/2 - \lambda_3 \\ \dots & \dots & 1/2 + \lambda_3 \end{pmatrix}, \tag{3.42}$$

where, using the definitions in Eq. (3.25),

$$\lambda_1 = 2\lambda_{rad} X_{ee}, \qquad \lambda_2 = 2\lambda_{rad} {\rm Re} X_{e\mu}, \qquad \lambda_3 = \lambda_{rad}(X_{\mu\mu} - X_{\mu\tau}).$$

Then, assuming for simplicity $m = m_2$, the equation $M(m_Z) = M^{ph}(m_Z)$ leads to the following relations:

$$\lambda_2 = \sqrt{\lambda_1 \lambda_3}\,, \qquad \tan^2\theta_{12} = \frac{2\lambda_3}{\lambda_1}\,, \qquad \epsilon = -\lambda_1 - 2\lambda_3\,. \tag{3.43}$$

If the matrix X has the specific form $X_{\alpha\beta} = Y_\alpha Y_\beta^*$, one can express the equality $M(m_Z) = M^{ph}(m_Z)$ in terms of the parameters defined in Eq. (3.31). For $m = m_2$, we get:

$$\lambda_e = -\epsilon c_{12}^2\,, \qquad \lambda_\mu = \lambda_\tau = -\frac{\epsilon s_{12}^2}{2}\,, \qquad c_{\mu\tau} = -1\,, \qquad c_{e\mu} = -c_{e\tau} = 1\,.$$

These relations fix the size and phase of the new Yukawa couplings required to reproduce phenomenology (see Eq. (3.31)).

3.5.4 Dominant $\mu\tau$-block

Let us take, at the scale m_0, the matrix with dominant $\mu\tau$-block [85, 92, 88]:

$$M_D = m \begin{pmatrix} 0 & 0 & 0 \\ 0 & 1 & 1 \\ 0 & 1 & 1 \end{pmatrix}. \tag{3.44}$$

It corresponds to the case of normal hierarchical mass spectrum ($m_3 \gg m_2 \gg m_1$).

The mass matrix required by phenomenology can be written as an expansion over the small parameters $\cos 2\theta_{23}$, $\sin\theta_{13}$ and $R \equiv \sqrt{\Delta m^2_{\rm sol}/\Delta m^2_{\rm atm}}$ (see Eq.(2.24)):

$$M^{ph}(m_Z) \approx \frac{m_3}{2}\left[\begin{pmatrix} 0 & 0 & 0 \\ \dots & 1 & 1 \\ \dots & \dots & 1 \end{pmatrix} + \cos 2\theta_{23}\begin{pmatrix} 0 & 0 & 0 \\ \dots & -1 & 0 \\ \dots & \dots & 1 \end{pmatrix} + \right.$$
$$\left. + \sin\theta_{13} e^{i\delta}\begin{pmatrix} 0 & \sqrt{2} & \sqrt{2} \\ \dots & 0 & 0 \\ \dots & \dots & 0 \end{pmatrix} + Re^{2i\sigma}\begin{pmatrix} 2s_{12}^2 & \sqrt{2}s_{12}c_{12} & -\sqrt{2}s_{12}c_{12} \\ \dots & c_{12}^2 & -c_{12}^2 \\ \dots & \dots & c_{12}^2 \end{pmatrix}\right]. \tag{3.45}$$

Let us discuss, first, the effect of SM (MSSM) radiative corrections to the matrix (3.44). Using Eq. (3.21), one sees that e-row elements remain zero along the RGE running. It is a consequence of Eq. (3.7). In contrast, SM (MSSM) corrections to $\mu\tau$-block elements are present. These corrections induce a small deviation from $\theta_{23} = \pi/4$, which can be easily computed comparing Eq. (3.21) with Eq. (3.45):

$$\cos 2\theta_{23} = (\epsilon_\mu - \epsilon_\tau)k + \mathcal{O}(\epsilon^2)\,.$$

The first neutrino remains massless and unmixed. Also m_2 remains zero because the determinant of the $\mu\tau$-block is zero even after the inclusion of radiative corrections. Therefore, the solar mass difference and mixing angle are not generated radiatively.

Let us consider, now, the effect of non-standard radiative corrections. Using the dominant matrix (3.44), the matrix of corrections, given by Eq. (3.24), is:

$$M_{\rm rad} = m \begin{pmatrix} 0 & \lambda_1 & \lambda_1 \\ \dots & 2\lambda_2 & \lambda_2 + \lambda_3 \\ \dots & \dots & 2\lambda_3 \end{pmatrix} . \tag{3.46}$$

where, using the definitions in Eq. (3.25),

$$\lambda_1 = \lambda_{rad}(X_{e\mu} + X_{e\tau}) , \qquad \lambda_2 = \lambda_{rad}(X_{\mu\mu} + X_{\mu\tau}) , \qquad \lambda_3 = \lambda_{rad}(X_{\tau\mu} + X_{\tau\tau}) .$$

The Eq. (3.24) implies that a given element $M_{\alpha\beta}$ receives corrections proportional only to elements in the α and β rows of M_D. Since the first row and column in Eq. (3.44) are zero, the element M_{ee} remains zero. Corrections to $M_{e\mu}$ and $M_{e\tau}$ are equal. The matrix $M = M_D + M_{\rm rad}$ has a zero eigenvalue, so that strong normal hierarchy is preserved by radiative corrections.

Comparing the matrix of radiative corrections (3.46) with the phenomenological matrix (3.45), we find that the atmospheric angle gets a deviation from $\pi/4$ and the angle θ_{13} becomes non-zero:

$$\cos 2\theta_{23} \approx \lambda_3 - \lambda_2 , \qquad \sin\theta_{13} \approx \lambda_1 \frac{e^{-i\delta}}{\sqrt{2}} . \tag{3.47}$$

A problem appears with the generation of solar parameters, because the structure of the term proportional to R in Eq. (3.45) (let us call it $M^{\rm sol}$) differs from the structure (3.46) of radiative corrections:

$$M^{\rm sol}_{ee} \neq 0 , \qquad M^{\rm sol}_{e\mu} = -M^{\rm sol}_{e\tau} , \qquad M^{\rm sol}_{\mu\tau} = -M^{\rm sol}_{\mu\mu} = -M^{\rm sol}_{\tau\tau} ,$$

whereas

$$M^{\rm rad}_{ee} = 0 , \qquad M^{\rm rad}_{e\mu} = M^{\rm rad}_{e\tau} , \qquad M^{\rm rad}_{\mu\tau} = \frac{1}{2}(M^{\rm rad}_{\mu\mu} + M^{\rm rad}_{\tau\tau}) .$$

In fact, computing the eigenvalues of $M = M_D + M_{\rm rad}$, one finds that R is of order λ_i^2:

$$R \equiv \frac{m_2}{m_3} \equiv \sqrt{\frac{\Delta m^2_{\rm sol}}{\Delta m^2_{\rm atm}}} \approx \frac{\lambda_1^2 + (\lambda_2 - \lambda_3)^2/2}{2} . \tag{3.48}$$

To satisfy the lower bound (99% C.L.) on R, which is ~ 0.1 (LMA), one needs $\lambda_i \gtrsim 0.2 \div 0.3$. In other words, LMA solar mass difference can be generated only if radiative corrections are ~ 10 times larger than in the MSSM with large $\tan\beta$.

The equalities $M_{ee} = 0$ and $M_{e\mu} = M_{e\tau} (= m\lambda_1)$ in Eq. (3.46) lead to the following general relations between observables (see section 2.4.1):

$$c^2_{12} = \frac{1+R}{2R}(1 - \sin 2\theta_{23}) , \qquad \tan\theta_{13} = s_{12}\sqrt{R} , \qquad \sin\delta = 0 , \qquad \sigma = \frac{\pi}{2} . \tag{3.49}$$

The first equality in (3.49) shows that the LMA solar mixing angle can be obtained only if atmospheric mixing deviates significantly from maximal value and if R is substantially smaller than the present best fit value. The equality can be satisfied taking 99% C.L. allowed intervals for θ_{12}, θ_{23} and R. The other equalities in (3.49) show that the radiative corrections (3.46) give s_{13} close to the present upper bound ~ 0.2 and lead to CP conservation in oscillations and to opposite CP parity between m_2 and m_3.

We have shown that, using the form (3.46) of corrections, the predictions for $\Delta m^2_{\rm sol}$ and θ_{12} are too small with respect to phenomenological values. However, the corrections related to the second term in square brackets of Eqs. (3.17), (3.20) have qualitatively different features and can give better predictions for the solar parameters. In particular, a non-zero M_{ee} can be generated by these corrections.

For example, let us consider the interaction in Eq. (3.11). The β-function coefficients are, in this case, $k_Y^{(1)} = 1/2$ and $k_Y^{(2)} = 1$. The matrix of couplings Y is antisymmetric, therefore the matrix of corrections ΔM^Y (see Eq. (3.17)) depends on three independent couplings only: $Y_{e\mu}$, $Y_{e\tau}$ and $Y_{\mu\tau}$. We want to compare $M(m_Z) \equiv M_D + \Delta M^Y$ with the phenomenological mass matrix (3.45) (we neglect, for simplicity, the charged lepton rotation U_l). The equality of the two matrices can be realized for $\sin\theta_{13} = \cos 2\theta_{23} = 0$ and

$$m = \frac{m_3}{2} + \frac{m_2}{2}\,, \qquad \lambda_{rad} Y^2_{e\mu} = \lambda_{rad} Y^2_{e\tau} = \frac{R s^2_{12} e^{2i\sigma}}{4(1-R)}\,, \qquad \lambda_{rad} Y^2_{\mu\tau} = \frac{R c^2_{12} e^{2i\sigma}}{2(1-R)}\,, \tag{3.50}$$

where λ_{rad} is defined in Eq. (3.25).

Notice that, while the form (3.46) of corrections predicts R of order λ_i^2, here R is of order λ_i. Therefore, $\sim 10\%$ radiative corrections are enough to generate radiatively $\Delta m^2_{\rm sol}$. Such corrections can be produced if three generations of new particles (e.g., three scalar singlets) are introduced. As follows from Eq. (3.50), also the solar mixing angle θ_{12} can be easily generated radiatively (in the LMA allowed range).

Chapter 4

Seesaw mechanism and leptogenesis

In this chapter, we consider the type-I seesaw mechanism for the generation of small neutrino masses. The low-energy neutrino mass matrix M is given in terms of the Majorana mass matrix of the right-handed (RH) neutrinos, M_R, and the Dirac mass matrix, m_D, as

$$M = -m_D M_R^{-1} m_D^T \ . \tag{4.1}$$

We will reconstruct the masses and mixings of heavy neutrinos and discuss the implications for the underlying theory, presenting the results of Ref. [230].

Under the assumption of hierarchical Dirac masses, we perform a systematic study of all possible structures of the RH neutrino mass matrix consistent with the low energy neutrino data. Although our general formalism is valid for an arbitrary left-handed Dirac-type mixing, in most of our quantitative analysis we assume this mixing to be small; we comment on the opposite situation in the last section. The properties of heavy neutrinos determine the amount of lepton asymmetry that is generated in their decays in the Early Universe. This asymmetry can explain the Baryon Asymmetry of the Universe. We constrain the parameter space of seesaw imposing the constraint of successful Baryogenesis via Leptogenesis. We study the dependence of the produced lepton asymmetry on the structure of M_R, calculating explicitly the RH mixing matrix U_R and the relevant CP-violating phases. In the generic case, too small an asymmetry is produced. We identify and study in detail the special cases in which the observed baryon asymmetry can be generated.

In section 4.1 we formulate our framework. In section 4.2 we discuss the generic case when the three RH neutrinos have strongly hierarchical masses. We give simple analytic expressions for the masses and the mixings of the RH neutrinos. In section 4.3 we describe the conditions under which the special cases are realized. They correspond to partial or complete degeneracy of the RH neutrinos. In section 4.4 we describe the mechanism of Baryogenesis via Leptogenesis. In section 4.5 we compute

the produced asymmetry in the generic case and in the special cases and we identify a unique successful scenario. Section 4.6 contains some discussion on the stability of the result.

4.1 Reconstruction of the heavy neutrino sector

4.1.1 Light neutrino mass matrix

We have seen in chapter 2 that, using the experimental information, one can to a large extent reconstruct the mass matrix M. A significant freedom still exists due to the unknown absolute mass scale m_1 and the CP-violating phases ρ and σ. The dependence of the structure of M on the unknown s_{13} and δ is weaker because of the smallness of s_{13}.

In spite of the above-mentioned freedom, a generic feature of the mass matrix M emerges: all its elements are of the same order (within a factor of 10 or so of each other), except in some special cases. The reason for this is twofold:

- the two large mixing angles θ_{12} and θ_{23};
- a relatively weak hierarchy between the mass eigenvalues:

$$\frac{m_2}{m_3} \geq \sqrt{\frac{\Delta m^2_{sol}}{\Delta m^2_{atm}}} > 0.1 \div 0.15 \ . \tag{4.2}$$

We will refer to the situation when all the matrix elements of M are of the same order and there are no special cancellations as the *generic case*. The "quasi-democratic" structure of the mass matrix M has important implications for the seesaw mechanism and leptogenesis, as we will see in sections 4.2 and 4.5.1.

A strong hierarchy between certain matrix elements of M can be realized only for specific values of the absolute mass scale and CP-violating phases (see section 2.6.1). Some of these strong hierarchies lead to *special cases* for the structure of the right-handed (RH) neutrino sector (sections 4.3.1-4.3.3) and for leptogenesis (sections 4.5.2-4.5.4).

4.1.2 Dirac mass matrix

In the basis where the mass matrix of RH Majorana neutrinos is diagonal, the Dirac mass matrix can be written as

$$m_D = U_L^\dagger m_D^{diag} U_R \ . \tag{4.3}$$

Here U_L and U_R are unitary matrices and $m_D^{diag} \equiv diag(m_u, m_c, m_t)$, with the mass eigenvalues $m_{u,c,t}$ being real and positive. We have denoted the eigenvalues of m_D in analogy with up-type quark masses, but we do not require the exact coincidence of

the quark and leptonic masses. Our main assumption in this chapter is that there is a strong hierarchy of the eigenvalues of m_D:

$$m_u \ll m_c \ll m_t \ , \tag{4.4}$$

similar to the hierarchy of the quark or charged lepton masses. For numerical estimates, we will use the reference values

$$m_u = 1 \text{ MeV} \ , \qquad m_c = 400 \text{ MeV} \ , \qquad m_t = 100 \text{ GeV} \ , \tag{4.5}$$

which approximately coincide with the up-type quark masses at the mass scale $\sim 10^9$ GeV [231].

The matrix U_L defined in Eq. (4.3) describes the mismatch between the left-handed rotations diagonalizing the charged lepton and neutrino Dirac mass matrices and, therefore, is the leptonic analogue of the quark CKM mixing matrix. It differs from the leptonic mixing matrix U_{PMNS}, defined in Eq. (2.1), which is probed in the low-energy neutrino experiments. The difference between U_L and U_{PMNS} is a consequence of the seesaw mechanism. By analogy with the CKM matrix where the mixing is small, one expects that the matrix U_L is close to the unit matrix.

4.1.3 Mass matrix of RH neutrinos

Using the representation (4.3) for m_D, the matrix of light neutrinos can be written as

$$M = -U_L^\dagger m_D^{diag} U_R (M_R^{diag})^{-1} U_R^T m_D^{diag} U_L^* \ .$$

We define $M_R^{diag} \equiv diag(M_1, M_2, M_3)$ with the ordering $M_1 \leq M_2 \leq M_3$. Then, in the basis where

$$m_D = U_L^\dagger m_D^{diag} \ , \tag{4.6}$$

the inverse mass matrix of the RH neutrinos equals

$$W \equiv M_R^{-1} = U_R (M_R^{diag})^{-1} U_R^T \tag{4.7}$$

and, correspondingly, the matrix M_R itself is given by

$$M_R = U_R^* M_R^{diag} U_R^\dagger \ . \tag{4.8}$$

The unitary matrix U_R is defined in such a way that it relates the basis where m_D is diagonal to the basis where M_R is diagonal with real and positive non-zero elements. We parameterize U_R in a way analogous to U_{PMNS} (Eq.(2.1)):

$$U_R \equiv U' \cdot K \ ,$$

where U' is a CKM-like matrix depending on three angles and one phase and

$$K \equiv diag(e^{-i\phi_1/2}, e^{-i\phi_2/2}, e^{-i\phi_3/2}) \tag{4.9}$$

is the diagonal matrix of RH neutrino Majorana phases.

From the seesaw formula one obtains, in the basis (4.6),

$$W = -m_D^{-1} M (m_D^{-1})^T = -(m_D^{diag})^{-1} \hat{M} (m_D^{diag})^{-1} \,, \tag{4.10}$$

where

$$\hat{M} \equiv U_L M U_L^T \,. \tag{4.11}$$

When $U_L = \mathbb{1}$, that is, the Dirac left-handed rotation is absent, one has $\hat{M} = M$. When U_L slightly deviates from $\mathbb{1}$ (*e.g.*, $U_L \approx U_{CKM}$), the difference between $\hat{M}$ and M is within the present experimental uncertainty, apart from some particular cases. In most of our analysis we shall be assuming $U_L = \mathbb{1}$ and neglect the difference between $\hat{M}$ and M. All the analytic expressions that we derive for $U_L = \mathbb{1}$ are also valid for an arbitrary U_L, if one substitutes the matrix elements of M by the corresponding elements of $\hat{M}$.

In supersymmetric scenarios, U_L can be probed in lepton flavor violating decays like $\mu \to e\gamma$ or $\tau \to \mu\gamma$. If $U_L = \mathbb{1}$, these decays are strongly suppressed, whereas for $U_L \approx U_{CKM}$ one finds the predicted branching ratios to be close to the experimental upper bounds, provided that the slepton masses are of the order of $(100 \div 200)$ GeV and the neutrino Dirac masses take the values given in Eq. (4.5). Therefore, if future experiments find a signal close to the present upper bounds, this will not require large left-handed rotations and so will not invalidate our results.

Using $m_D^{diag} \equiv diag(m_u, m_c, m_t)$ in Eq. (4.10) and taking $\hat{M} = M$, we obtain the following symmetric matrix W:

$$W = -\begin{pmatrix} \dfrac{M_{ee}}{m_u^2} & \dfrac{M_{e\mu}}{m_u m_c} & \dfrac{M_{e\tau}}{m_u m_t} \\ \cdots & \dfrac{M_{\mu\mu}}{m_c^2} & \dfrac{M_{\mu\tau}}{m_c m_t} \\ \cdots & \cdots & \dfrac{M_{\tau\tau}}{m_t^2} \end{pmatrix} . \tag{4.12}$$

In what follows we will find the eigenvalues of W and the mixing matrix U_R that diagonalizes W according to Eq. (4.7).

4.2 The generic case

As discussed in section 4.1.1, in general the matrix elements $M_{\alpha\beta}$ are all of the same order of magnitude. We have defined this situation as the generic case. It follows then from (4.12) that the elements of W are highly hierarchical, with W_{11} being by far the largest one. Introducing for illustration the small expansion parameter

$$\lambda \sim \frac{m_u}{m_c} \sim \frac{m_c}{m_t} \sim 10^{-2} \,, \tag{4.13}$$

we obtain

$$W \sim -\frac{M_{ee}}{m_u^2}\begin{pmatrix} 1 & \lambda & \lambda^2 \\ \cdots & \lambda^2 & \lambda^3 \\ \cdots & \cdots & \lambda^4 \end{pmatrix} ,$$

where in each element factors of order 1 are understood.

The largest eigenvalue of W is given, to a very good approximation, by the dominant (11)-element:

$$M_1 e^{i\phi_1} \approx \frac{1}{W_{11}} = -\frac{m_u^2}{M_{ee}} . \tag{4.14}$$

The second largest eigenvalue of W can be obtained from the dominant (12)-block of the matrix (4.12), just by dividing its determinant by W_{11}. The mass M_2 is then the inverse of this eigenvalue:

$$M_2 e^{i\phi_2} \approx \frac{W_{11}}{W_{11}W_{22} - W_{12}^2} = \frac{m_c^2 M_{ee}}{M_{e\mu}^2 - M_{ee}M_{\mu\mu}} . \tag{4.15}$$

The smallest eigenvalue of W can be found from the condition

$$(m_u m_c m_t)^2 = -m_1 m_2 m_3 e^{-2i(\rho+\sigma)} M_1 M_2 M_3 e^{i(\phi_1+\phi_2+\phi_3)} , \tag{4.16}$$

which is obtained by taking the determinants of both sides of Eq. (4.1). This yields

$$M_3 e^{i\phi_3} \approx \frac{m_t^2 (M_{e\mu}^2 - M_{ee}M_{\mu\mu})}{m_1 m_2 m_3 e^{-2i(\rho+\sigma)}} . \tag{4.17}$$

Thus, in the generic case the RH neutrinos have a very strong mass hierarchy: $M_1 \propto m_u^2$, $M_2 \propto m_c^2$, $M_3 \propto m_t^2$, in agreement with the "seesaw enhancement" condition [136].

The matrix W is diagonalized, to a high accuracy, by

$$U_R \approx \begin{pmatrix} 1 & -\left(\frac{M_{e\mu}}{M_{ee}}\right)^* \frac{m_u}{m_c} & \left(\frac{d_{23}}{d_{12}}\right)^* \frac{m_u}{m_t} \\ \left(\frac{M_{e\mu}}{M_{ee}}\right) \frac{m_u}{m_c} & 1 & -\left(\frac{d_{13}}{d_{12}}\right)^* \frac{m_c}{m_t} \\ \left(\frac{M_{e\tau}}{M_{ee}}\right) \frac{m_u}{m_t} & \left(\frac{d_{13}}{d_{12}}\right) \frac{m_c}{m_t} & 1 \end{pmatrix} \cdot K , \tag{4.18}$$

where

$$d_{23} \equiv M_{e\mu}M_{\mu\tau} - M_{\mu\mu}M_{e\tau} , \qquad d_{13} \equiv M_{ee}M_{\mu\tau} - M_{e\mu}M_{e\tau} , \qquad d_{12} \equiv M_{ee}M_{\mu\mu} - M_{e\mu}^2$$

and K is defined in Eq.(4.9).

As can be seen from Eq. (4.18), the RH mixing is very small in the generic case. We therefore encounter an apparently paradoxical situation, when both the left-handed

and RH mixing angles are small and yet one arrives at a strong mixing in the low-energy sector. This is an example of the so-called "seesaw enhancement" of the leptonic mixing [136, 137, 138, 139, 140, 141]. The reason for this enhancement can be readily understood. Indeed, small mixing in m_D and W is related to the hierarchical structures of these matrices; however, in the seesaw formula (4.1) these hierarchies act in the opposite directions and largely compensate each other, leading to a "quasi-democratic" M and thus to large mixing in the low-energy sector.

The masses of the heavy neutrinos (Eqs. (4.14),(4.15) and (4.17)) can be rewritten as functions of the low-energy observables using the expressions of $M_{\alpha\beta}$ in terms of the masses and mixing of light neutrinos. In the limit $\theta_{13} = 0$ and $\theta_{23} = \pi/4$, we find from Eq. (2.13)

$$\begin{aligned} M_1 e^{i\phi_1} &= -\frac{m_u^2}{m_1 e^{-2i\rho} c_{12}^2 + m_2 s_{12}^2} , \\ M_2 e^{i\phi_2} &= -\frac{2m_c^2 (m_1 e^{-2i\rho} c_{12}^2 + m_2 s_{12}^2)}{m_3 e^{-2i\sigma} (m_1 e^{-2i\rho} c_{12}^2 + m_2 s_{12}^2) + m_1 e^{-2i\rho} m_2} , \\ M_3 e^{i\phi_3} &= -\frac{m_t^2 [m_3 e^{-2i\sigma} (m_1 e^{-2i\rho} c_{12}^2 + m_2 s_{12}^2) + m_1 e^{-2i\rho} m_2]}{2 m_1 m_2 m_3 e^{-2i(\rho+\sigma)}} . \end{aligned} \tag{4.19}$$

The dependence of M_i on m_1 is shown in Fig. 4.1. In the case of the normal hierarchy ($m_1 \ll m_{2,3}$), these equalities take a particularly simple form (found previously in [150]):

$$M_1 e^{i\phi_1} \approx -\frac{m_u^2}{m_2 s_{12}^2} , \qquad M_2 e^{i\phi_2} \approx -\frac{2m_c^2}{m_3 e^{-2i\sigma}} , \qquad M_3 e^{i\phi_3} \approx -\frac{m_t^2 s_{12}^2}{2 m_1 e^{-2i\rho}} . \tag{4.20}$$

Notice that the lightest RH neutrino mass M_1 is related to the solar mass squared difference ($m_2^2 \approx \Delta m_{sol}^2$), M_2 to the atmospheric one ($m_3^2 \approx \Delta m_{atm}^2$), and M_3 is inversely proportional to m_1, for which we can use the upper bound $m_1 < \sqrt{\Delta m_{sol}^2}$. It is illuminating to rewrite Eq. (4.20) in the "standard" seesaw form, expressing the light neutrino masses through the heavy neutrino ones:

$$m_1 \approx \frac{m_t^2 s_{12}^2}{2M_3} , \qquad m_2 \approx \frac{m_u^2}{s_{12}^2 M_1} , \qquad m_3 \approx \frac{2m_c^2}{M_2} . \tag{4.21}$$

Comparing this with the naive seesaw expectations, we see that the expected correspondence between the masses of the light neutrinos and the Dirac masses ($m_1 \propto m_u^2$, $m_2 \propto m_c^2$, $m_3 \propto m_t^2$) is completely broken; this is due to the large neutrino mixing angles (in particular, to the fact that the solution of the solar neutrino problem is the LMA MSW one).

Numerically, from Eq. (4.20) we find

$$M_1 \simeq \frac{m_u^2}{s_{12}^2\sqrt{\Delta m_{sol}^2}} \simeq 4.4\cdot 10^5 \text{ GeV}\left(\frac{m_u}{1 \text{ MeV}}\right)^2, \tag{4.22}$$

$$M_2 \simeq \frac{2m_c^2}{\sqrt{\Delta m_{atm}^2}} \simeq 6.4\cdot 10^9 \text{ GeV}\left(\frac{m_c}{400 \text{ MeV}}\right)^2, \tag{4.23}$$

$$M_3 \simeq \frac{m_t^2 s_{12}^2}{2m_1} > 1.8\cdot 10^{14} \text{ GeV}\left(\frac{m_t}{100 \text{ GeV}}\right)^2. \tag{4.24}$$

These values of M_i are illustrated by the leftmost regions (corresponding to $m_1 \to 0$) of the plots in Fig. 4.1. For the inverted mass hierarchy ($m_3 \ll m_1 \simeq m_2$), from Eq. (4.19) one finds

$$M_1 \simeq (2-5)\cdot 10^4 \text{ GeV}\left(\frac{m_u}{1 \text{ MeV}}\right)^2, \tag{4.25}$$

$$M_2 \simeq (3-6)\cdot 10^9 \text{ GeV}\left(\frac{m_c}{400 \text{ MeV}}\right)^2, \tag{4.26}$$

$$M_3 > 10^{14} \text{ GeV}\left(\frac{m_t}{100 \text{ GeV}}\right)^2. \tag{4.27}$$

Similar estimates hold true also in the quasi-degenerate case ($m_1 \simeq m_2 \simeq m_3 \simeq m$), except that the inequality sign in Eq. (4.27) has to be replaced by the approximate equality one and the right-hand sides of Eqs. (4.25) - (4.27) have to be divided by $m/\sqrt{\Delta m_{atm}^2} \approx 20m/\text{eV}$. In particular, for the lightest of the RH neutrinos we obtain

$$M_1 \simeq (1-2.5) \text{ TeV}\left(\frac{m_u}{1 \text{ MeV}}\right)^2\left(\frac{1 \text{ eV}}{m}\right). \tag{4.28}$$

For the highest allowed by cosmological observations value, $m = 0.7$ eV, Eq. (4.28) gives $M_1 \simeq (1.4-3.5)$ TeV. The values of M_i in the quasi-degenerate case are shown on the right-hand side (corresponding to $m_1 \approx m \sim 1$ eV) of panels a, b, d in Fig. 4.1.

4.3 Special cases and level crossing

The results of the previous section were essentially based on two assumptions: (1) $M_{ee} \neq 0$ and is of the order of other elements of M, so that the evaluations (4.14) and (4.15) of $M_{1,2}$ are valid, and (2) $M_{ee}M_{\mu\mu} - M_{e\mu}^2 \neq 0$, so that the evaluations (4.15) and (4.17) of $M_{2,3}$ hold. Let us analyze the situations when one of these conditions or both of them are not satisfied.

Special case I:

$$M_{ee} \to 0$$

or, equivalently, $W_{11} \to 0$. Formally, Eqs. (4.14) and (4.15) imply that $M_1 \to \infty$ and $M_2 \to 0$ when $M_{ee} \to 0$. At some point (the "level crossing" point) they will become equal to each other. The approximate formulas in Eqs. (4.14) and (4.15) do not work

when M_{ee} becomes very small. In exact calculations one gets a significant decrease of the level splitting and, therefore, strong mass degeneracy. This behavior can be seen in Fig. 4.1, where we show the dependence of the RH neutrino masses and of m_{ee} on the lightest mass m_1, for different values of the Majorana phases of the light neutrinos ρ and σ. Small value of m_{ee} appears as a result of a cancellation of different contributions, which can be realized only for $\rho = \pi/2$ (Fig. 4.1, panels b and d). At the crossing points the mixing between the levels becomes maximal (the level crossing of RH neutrinos has been previously discussed in [149]).

Special case II:

$$d_{12} \equiv M_{ee}M_{\mu\mu} - M_{e\mu}^2 \to 0 \ ,$$

or, equivalently, $(W_{11}W_{22} - W_{12}^2) \to 0$. In this limit, according to Eqs. (4.15) and (4.17), M_2 increases and M_3 decreases, so that a crossing occurs between the N_2 and N_3 levels. At the crossing point the mixing becomes maximal. In Fig. 4.1 we show the dependence of $|d_{12}|$ on m_1. The crossing points coincide with zeros of the (12)-subdeterminant. As we will see in section 4.3.2, $|d_{12}|$ is a non-monotonous function of m_1, so that, depending on the phases ρ and σ, there can be zero (Fig. 4.1a), one (Fig. 4.1b) or two (Fig. 4.1d) crossings of this type. For $\rho = 0$, $\sigma = \pi/2$ and quasi-degenerate spectrum of light neutrinos (right-hand part of Fig. 4.1c), $|d_{12}|$ is much smaller than the squares of the light neutrino masses. This leads to a quasi-degeneracy of N_2 and N_3 without level crossing.

Special case III:

$$M_{ee} \to 0 \quad \text{and} \quad d_{12} \to 0 \ .$$

This is equivalent to the requirement that the elements M_{ee} and $M_{e\mu}$ be both very small. In this case all three RH neutrino masses are of the same order. The $1-2$ and $2-3$ crossing regions merge.

In Fig. 4.2 we show the dependence of M_i, m_{ee} and $|d_{12}|$ on m_1 for non-zero s_{13} and different values of the Dirac phase δ. Comparing Fig. 4.1b and Fig. 4.2, which correspond to the same Majorana phases, we find that the effect of s_{13} for zero δ (Fig. 4.2a) is reduced to a small shift of the crossing points. A different choice of the phase δ has more substantial effect: it can remove all crossings (Fig. 4.2b), remove only the $2-3$ crossing (Fig. 4.2c) or change the relative positions of the crossing points leading to quasi-degeneracy of all three RH neutrinos (Fig. 4.2d).

As one can see in Figs. 4.1 and 4.2, the generic case with a strong hierarchy and small mass of the lightest RH neutrino is realized practically in the whole parameter space, excluding the regions of the crossings. In general, with the increase of the overall scale of the light neutrino mass m_1, the masses of the RH neutrinos decrease.

In the following sections we will consider the special cases in detail.

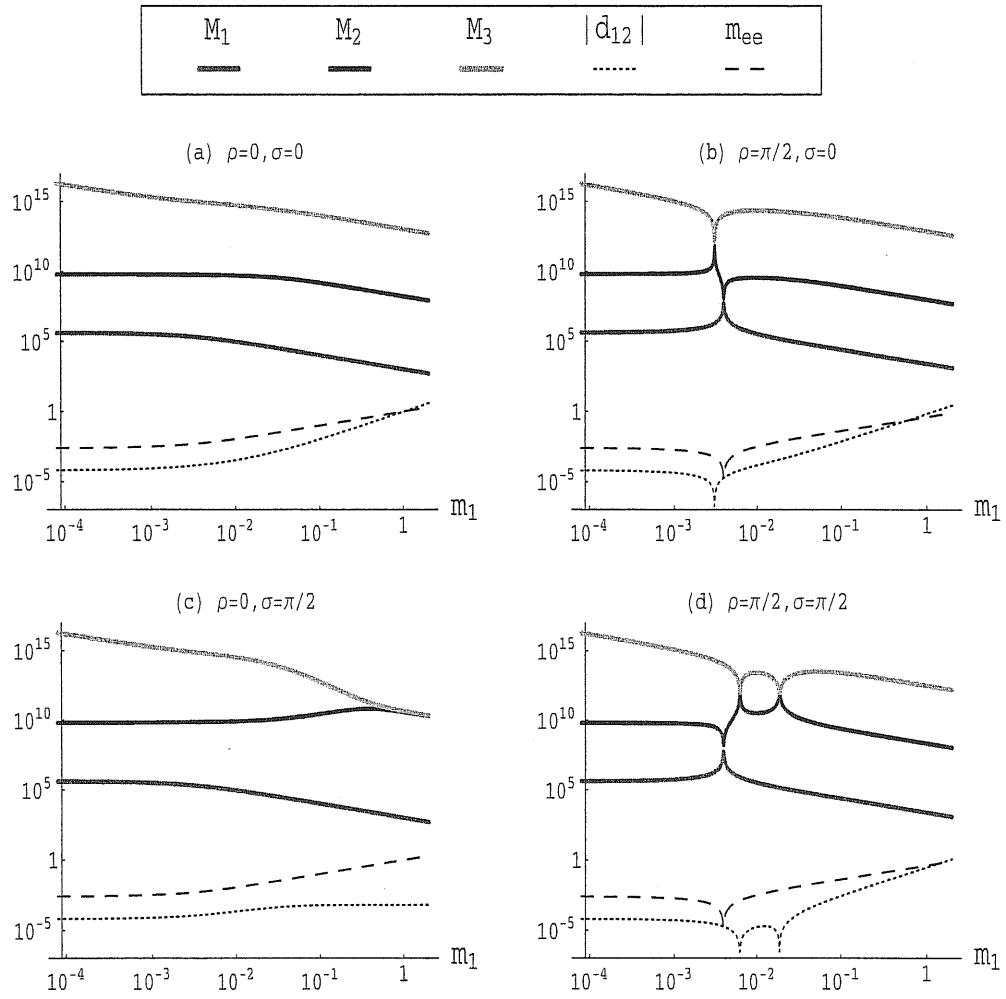

Figure 4.1: The masses of RH neutrinos M_i in GeV as functions of the light neutrino mass m_1 in eV (solid thick lines), for different values of the Majorana phases of light neutrinos, ρ and σ. We have assumed normal mass ordering; $s_{13} = 0$; the best fit values of solar and atmospheric mixing angles and mass squared differences (Eqs. (2.4-2.5) and (2.9-2.10)); the values of Dirac-type neutrino masses $m_{u,c,t}$ given in Eq. (4.5). Also shown are $|d_{12}| \equiv |M_{ee}M_{\mu\mu} - M_{e\mu}^2|$ in eV^2 (dotted thin line) and m_{ee} in eV (dashed thin line) as functions of m_1.

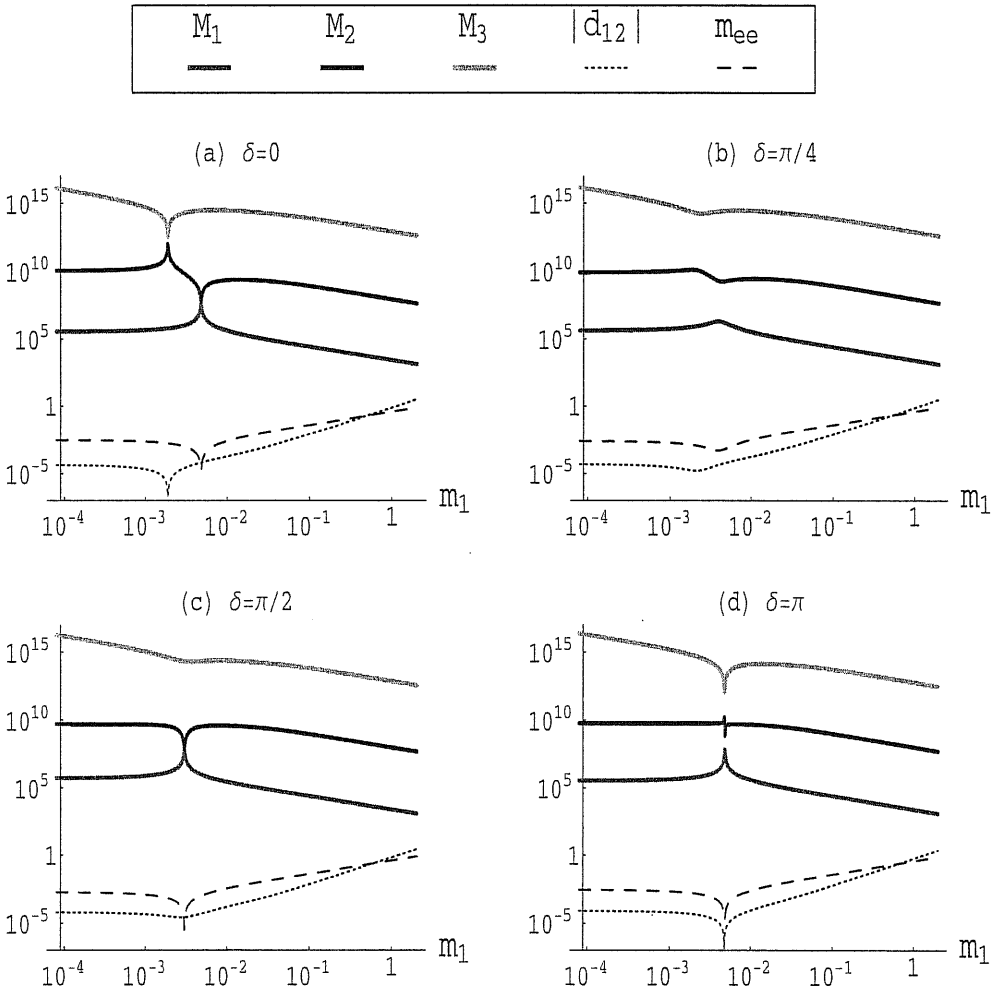

Figure 4.2: Same as in Fig. 4.1, but for $\rho = \pi/2$, $\sigma = 0$, $s_{13} = 0.1$ and different values of the Dirac-type CP-violating phase δ.

4.3.1 Special case I: small m_{ee}

Consider the case

$$m_{ee} \ll \frac{m_u}{m_c} m_{e\mu} \tag{4.29}$$

which corresponds to $|W_{11}| \ll |W_{12}|$ (see Eq. (4.12)). In this case the (12)-block of W is dominated by the off-diagonal entries and, to a good approximation, the RH neutrino masses are

$$M_1 e^{i\phi_1} \approx -M_2 e^{i\phi_2} \approx \frac{1}{W_{12}} \approx -\frac{m_u m_c}{M_{e\mu}} , \qquad M_3 e^{i\phi_3} \approx \frac{m_t^2 M_{e\mu}^2}{m_1 m_2 m_3 e^{-2i(\rho+\sigma)}} . \tag{4.30}$$

Notice that M_1 is increased by a factor $\sim m_c/m_u$ with respect to the generic case (Eq. (4.14)). Moreover, the RH (12)-mixing is nearly maximal while the other mixing angles are very small:

$$U_R \approx \begin{pmatrix} \frac{1}{\sqrt{2}} & \frac{1}{\sqrt{2}} & \left(\frac{M_{\mu\mu}M_{e\tau} - M_{e\mu}M_{\mu\tau}}{M_{e\mu}^2}\right)^* \frac{m_u}{m_t} \\ -\frac{1}{\sqrt{2}} & \frac{1}{\sqrt{2}} & -\left(\frac{M_{e\tau}}{M_{e\mu}}\right)^* \frac{m_c}{m_t} \\ -\frac{M_{e\tau}}{\sqrt{2}M_{e\mu}}\frac{m_c}{m_t} & \frac{M_{e\tau}}{\sqrt{2}M_{e\mu}}\frac{m_c}{m_t} & 1 \end{pmatrix} \cdot K . \tag{4.31}$$

The matrix of phases K is given in Eq. (4.9). Thus, the RH neutrinos N_1 and N_2 are quasi-degenerate, have nearly opposite CP parities and almost maximal mixing ($1-2$ level crossing). The third RH neutrino N_3 is much heavier and weakly mixed with the first two.

Notice that, for $U_L = \mathbb{1}$, M_{ee} is the effective mass directly measurable in the neutrinoless 2β decay experiments. In our parameterization, it is given by

$$M_{ee} = c_{13}^2(m_1 e^{-2i\rho} c_{12}^2 + m_2 s_{12}^2) + s_{13}^2 e^{2i(\delta-\sigma)} m_3 ,$$

so that $M_{ee} \approx 0$ implies

$$\tan^2\theta_{13} \approx -\frac{m_1 e^{-2i\rho} c_{12}^2 + m_2 s_{12}^2}{e^{2i(\delta-\sigma)} m_3} . \tag{4.32}$$

For $s_{13} = 0$ the level crossing ($m_{ee} \to 0$) occurs for

$$m_1 \approx \frac{\tan^2\theta_{12}\sqrt{\Delta m_{sol}^2}}{\sqrt{1-\tan^4\theta_{12}}} \approx (3-4)\cdot 10^{-3}\text{eV} \tag{4.33}$$

(see Fig. 4.1, panels b and d). For substantial deviations of the $1-2$ mixing from the maximal one ($\tan^2\theta_{12} < 1$), Eq. (4.33) can hold only in the case of the normal

mass hierarchy. For the inverted hierarchy or quasi-degenerate spectrum one has $m_1 \gtrsim \sqrt{\Delta m^2_{atm}} \approx 0.05$ eV, so that Eq. (4.33) is not satisfied. Non-zero s_{13} shifts the position of the level crossing. Taking into account the present upper bound on s_{13}, we find that relation (4.32) can be satisfied for $m_1 \lesssim 0.02$ eV. Moreover, the crossing takes place only for specific values of the phase δ (see Fig. 4.2). If a stronger upper bound on θ_{13} is established, Eq. (4.32) will provide a more stringent upper bound on m_1 and also a lower bound on m_1.

Notice that inequality (4.29) implies

$$m_{ee} < 10^{-5}\text{eV}\left(\frac{400 m_u}{m_c}\right) ,$$

where we have taken $m^2_{e\mu} \lesssim \Delta m^2_{sol}$ (the normal hierarchy case). If a positive signal is found in neutrinoless 2β-decay experiments with the near future sensitivity ($m_{ee} \gtrsim 0.01$ eV [232]), this special case will be excluded for $U_L = \mathbb{1}$.

Let us consider the effect of possible left-handed Dirac rotations assuming $U_L \sim U_{CKM}$. Taking for simplicity only a 1-2 rotation with $\theta_L \sim \theta_c = 0.22$, we find from Eq. (4.11)

$$\hat{M}_{ee} = \cos^2\theta_L M_{ee} + 2\sin\theta_L \cos\theta_L M_{e\mu} + \sin^2\theta_L M_{\mu\mu}.$$

Then the $1-2$ crossing condition, $\hat{M}_{ee} \to 0$, leads to the following restriction on the possible values of M_{ee}:

$$M_{ee} \approx -2\tan\theta_L M_{e\mu} - \tan^2\theta_L M_{\mu\mu} , \tag{4.34}$$

which can be considered as the level crossing condition in the flavor basis. For the case of the normal mass hierarchy $m_{e\mu} \sim 0.5\sqrt{\Delta m^2_{sol}}$ and $m_{\mu\mu} \sim 0.5\sqrt{\Delta m^2_{atm}}$ and from (4.34) we find $m_{ee} \leq (3-4)\cdot 10^{-3}$ eV.

The level crossing condition (4.34) can be satisfied also for the inverted mass hierarchy of light neutrinos as well as for the degenerate spectrum, if ν_1 and ν_2 have opposite CP parities. In the case of the inverted hierarchy one has $m_{e\mu} \sim 0.5\sqrt{\Delta m^2_{atm}} > m_{\mu\mu}$ (section 2.4.5), so that Eq. (4.34) implies $m_{ee} \leq (1-2)\cdot 10^{-2}$ eV. For the degenerate spectrum (taking into account the cosmological bound (2.7)) one finds $m_{e\mu} \sim m_{\mu\mu} \sim 0.2 - 0.4$ eV, and consequently $m_{ee} \leq 0.2$ eV.

In the limit $\theta_{13} = 0$, we find from Eqs. (4.30) and (4.32)

$$M_{1,2} \approx \frac{2\sqrt{\cos 2\theta_{12}}}{c_{23}\sin 2\theta_{12}}\frac{m_u m_c}{\sqrt{\Delta m^2_{sol}}} \approx 9\cdot 10^7 \text{ GeV}\left(\frac{m_u}{1 \text{ MeV}}\right)\left(\frac{m_c}{400 \text{ MeV}}\right) , \tag{4.35}$$

$$M_3 \approx \frac{c^2_{23} m^2_t}{\sqrt{\Delta m^2_{atm}}} \approx 10^{14} \text{ GeV}\left(\frac{m_t}{100 \text{ GeV}}\right)^2 \tag{4.36}$$

(see panels b and d of Fig. 4.1).

4.3.2 Special case II: small 12-subdeterminant of M

Let us consider the case in which the (11)-element of the matrix W in Eq. (4.12) is still the dominant one (as in the generic case), but the (12)-subdeterminant of W is very small. Then $(M_R)_{33}$, which is proportional to this subdeterminant, is suppressed. The condition $(M_R)_{33} \ll (M_R)_{23}$ can be written as

$$|d_{12}| \equiv |M_{ee}M_{\mu\mu} - M_{e\mu}^2| \ll \frac{m_c}{m_t}|M_{e\tau}M_{e\mu} - M_{ee}M_{\mu\tau}| \; . \tag{4.37}$$

In this case M_1 is still given by Eq. (4.14), but M_2 cannot be found from the determinant of the (12)-block of W as in Eq. (4.15). One has to consider, instead, the (23)-block of M_R, which is dominated by its off-diagonal entry. This yields

$$M_2 e^{i\phi_2} \approx -M_3 e^{i\phi_3} \approx (M_R)_{23} = \frac{m_c m_t}{m_1 m_2 m_3 e^{-2i(\rho+\sigma)}}(M_{ee}M_{\mu\tau} - M_{e\tau}M_{e\mu}) \; . \tag{4.38}$$

The mixing matrix of RH neutrinos equals

$$U_R \approx \begin{pmatrix} 1 & -\frac{1}{\sqrt{2}}\left(\frac{M_{e\mu}}{M_{ee}}\right)^* \frac{m_u}{m_c} & -\frac{1}{\sqrt{2}}\left(\frac{M_{e\mu}}{M_{ee}}\right)^* \frac{m_u}{m_c} \\ \left(\frac{M_{e\mu}}{M_{ee}}\right)\frac{m_u}{m_c} & \frac{1}{\sqrt{2}} & \frac{1}{\sqrt{2}} \\ \left(\frac{M_{e\tau}}{M_{ee}}\right)\frac{m_u}{m_t} & -\frac{1}{\sqrt{2}} & \frac{1}{\sqrt{2}} \end{pmatrix} \cdot K \; , \tag{4.39}$$

where K is given in Eq. (4.9). From Eq. (4.38) it follows that the phases ϕ_2 and ϕ_3 differ by $\approx \pi$. Therefore in this special case the lightest RH neutrino is weakly mixed with N_2 and N_3, which are much heavier, quasi-degenerate, almost maximally mixed and have nearly opposite CP parities.

Let us consider condition (4.37). In terms of low-energy neutrino parameters, we obtain from Eq. (2.13)

$$d_{12} = c_{23}^2 m_1 e^{-2i\rho} m_2 + s_{23}^2 m_3 e^{-2i\sigma}(c_{12}^2 m_1 e^{-2i\rho} + s_{12}^2 m_2) + \mathcal{O}(s_{13}) \; .$$

Neglecting $\mathcal{O}(s_{13})$ corrections, we find that d_{12} vanishes for

$$m_3 = -\frac{\cot^2\theta_{23} m_1 m_2 e^{2i(\sigma-\rho)}}{c_{12}^2 m_1 e^{-2i\rho} + s_{12}^2 m_2} \; . \tag{4.40}$$

Since $\cot^2\theta_{23} \approx 1$, this relation cannot be satisfied for $m_3 < m_{1,2}$. Therefore this special case is not realized for the inverted ordering of the light neutrino masses, unless U_L deviates significantly from $\mathbb{1}$. For the normal mass ordering, condition (4.40) requires $m_1 \gtrsim 2 \cdot 10^{-3}$ eV (see Fig. 4.1, panels b and d). For the quasi-degenerate mass spectrum, Eq. (4.40) can be satisfied if the CP parity of ν_3 is opposite to the CP parities of ν_1 and ν_2, up to deviations of θ_{23} from $\pi/4$ (see the right-hand side of Fig. 4.1c). Notice that

$$\begin{aligned} M_{e\tau}M_{e\mu} - M_{ee}M_{\mu\tau} &= s_{23}c_{23}[m_1 e^{-2i\rho} m_2 - m_3 e^{-2i\sigma}(c_{12}^2 m_1 e^{-2i\rho} + s_{12}^2 m_2)] + \mathcal{O}(s_{13}) = \\ &= \cot\theta_{23} m_1 e^{-2i\rho} m_2 + \mathcal{O}(s_{13}) \; , \end{aligned}$$

where we have used the condition (4.40) of zero (12)-subdeterminant. Therefore Eq. (4.38) simplifies to

$$M_2 e^{i\phi_2} \approx -M_3 e^{i\phi_3} \approx -\frac{m_c m_t}{m_3 e^{-2i\sigma}} \ . \tag{4.41}$$

Numerically, one finds (see Fig. 4.1, panels b, c, d)

$$M_2 \approx M_3 \approx \frac{m_c m_t}{(0.05-0.7)\text{eV}} \approx (0.6-8)\cdot 10^{11}\ \text{GeV}\left(\frac{m_c}{400\ \text{MeV}}\right)\left(\frac{m_t}{100\ \text{GeV}}\right) \ , \tag{4.42}$$

while M_1 is still given by Eqs. (4.22) and (4.28) for the normal hierarchy and quasi-degenerate case, respectively.

4.3.3 Special case III: small m_{ee} and $m_{e\mu}$

Consider now the case when

$$m_{ee} \ll \frac{m_u}{m_t} m_{e\tau} \ , \qquad m_{e\mu} \ll \frac{m_c}{m_t} m_{e\tau}, \quad \frac{m_u}{m_c} m_{\mu\mu} \ , \tag{4.43}$$

so that the (13)- and (22)-elements of $W \equiv M_R^{-1}$ are the dominant ones (see Eq. (4.12)). In this case, two RH neutrinos form a quasi-degenerate pair (doublet) with almost maximal mixing, opposite CP-parities and masses

$$\pm M_d e^{i\phi_d} \approx \pm W_{13}^{-1} \approx \mp \frac{m_u m_t}{M_{e\tau}} \ . \tag{4.44}$$

The third (singlet) neutrino has small mixing with the other two (of order m_u/m_c or m_c/m_t) and a mass

$$M_s e^{i\phi_s} \approx W_{22}^{-1} \approx -\frac{m_c^2}{M_{\mu\mu}} \ . \tag{4.45}$$

Since $m_u m_t \sim m_c^2$, all the three masses are of the same order. Seesaw mass matrices which correspond to the degeneracy of all three RH neutrinos have been recently considered in [233, 234].

Let us consider conditions (4.43). We have shown in section 4.3.1 that, assuming $U_L \approx \mathbb{1}$, m_{ee} can be very small only in the case of the normal hierarchy, when Eq. (4.32) can be satisfied. At the same time, for certain values of m_1 and s_{13} and of the phases, the value of $m_{e\mu}$ can also be very small. For this to occur, the low-energy parameters should satisfy (see Fig. 4.2d)

$$m_1 \approx m_2 \tan^2\theta_{12} \approx 0.0035\ \text{eV} \ , \qquad s_{13} \approx \frac{m_2}{m_3}\tan\theta_{12} \approx 0.11 \ ,$$

where we used $m_2 \approx \sqrt{\Delta m^2_{sol}}$ and $m_3 \approx \sqrt{\Delta m^2_{atm}}$. The other matrix elements of M are also approximately determined by the conditions $m_{ee} \approx 0$, $m_{e\mu} \approx 0$:

$$m_{e\tau} \approx \sqrt{2}\tan\theta_{12} m_2 \approx 0.008\ \text{eV} \ , \qquad m_{\mu\mu} \approx m_{\mu\tau} \approx m_{\tau\tau} \approx \frac{m_3}{2} \approx 0.025\ \text{eV} \ .$$

For the masses of the RH neutrinos one then finds

$$M_d \simeq 1.2 \times 10^{10}\ \text{GeV} \left(\frac{m_u}{1\ \text{MeV}}\right)\left(\frac{m_t}{100\ \text{GeV}}\right) , \tag{4.46}$$

$$M_s \simeq 6.4 \cdot 10^{9}\ \text{GeV} \left(\frac{m_c}{400\ \text{MeV}}\right)^2 . \tag{4.47}$$

According to Eqs. (4.44) and (4.45), the mass spectrum of RH neutrinos is characterized by the ratio

$$r_{ds} \equiv \frac{M_d}{M_s} = \frac{m_u m_t}{m_c^2}\frac{m_{\mu\mu}}{m_{e\tau}} = 1.9 \left(\frac{m_u}{1\ \text{MeV}}\right)\left(\frac{m_t}{100\ \text{GeV}}\right)\left(\frac{400\ \text{MeV}}{m_c}\right)^2 \frac{m_{\mu\mu}}{3m_{e\tau}} . \tag{4.48}$$

We shall distinguish two subcases, depending on whether the quasi-degenerate pair is lighter or heavier than the singlet state:

(a) $r_{ds} < 1 \Rightarrow M_1 \approx M_2 \lesssim M_3$.

(b) $r_{ds} > 1 \Rightarrow M_1 \lesssim M_2 \approx M_3$.

In the case (a), up to $\mathcal{O}(\lambda^2)$ terms (see Eq.(4.13)), the RH mixing matrix is given by

$$U_R \approx \begin{pmatrix} 1/\sqrt{2} & 1/\sqrt{2} & \delta_1^* \\ \frac{1}{\sqrt{2}}(\delta_2^* - \delta_1) & -\frac{1}{\sqrt{2}}(\delta_2^* + \delta_1) & 1 \\ -1/\sqrt{2} & 1/\sqrt{2} & \delta_2 \end{pmatrix} \cdot K' . \tag{4.49}$$

Here

$$\delta_1 \equiv \frac{m_u}{m_c}\frac{M_{\mu\tau}}{M_{e\tau}}\frac{1}{r_{ds}^2 - 1} , \qquad \delta_2 \equiv \frac{m_u}{m_c}\left(\frac{M_{\mu\tau}}{M_{e\tau}}\right)^* \frac{r_{ds}}{r_{ds}^2 - 1} , \tag{4.50}$$

and $K' = diag(e^{-i\phi_1'/2},\ e^{-i\phi_2'/2},\ e^{-i\phi_3'/2})$, where

$$\phi_1' - \phi_2' \approx \pi , \qquad \phi_3' - \phi_2' \approx 2\arg\left(\frac{M_{e\tau}}{M_{\mu\tau}}\right) . \tag{4.51}$$

Notice that in the parameterization (4.49) the phases ϕ_i' are different from the Majorana phases ϕ_i of RH neutrinos.

In the case (b), the RH mixing matrix is obtained from that in Eq. (4.49) by the cyclic permutation of its columns $3 \to 1$, $1 \to 2$, $2 \to 3$:

$$U_R \approx \begin{pmatrix} \delta_1^* & 1/\sqrt{2} & 1/\sqrt{2} \\ 1 & \frac{1}{\sqrt{2}}(\delta_2^* - \delta_1) & -\frac{1}{\sqrt{2}}(\delta_2^* + \delta_1) \\ \delta_2 & -1/\sqrt{2} & 1/\sqrt{2} \end{pmatrix} \cdot K' . \tag{4.52}$$

Also Eq.(4.51) should be replaced by

$$\phi_2' - \phi_3' \approx \pi , \qquad \phi_1' - \phi_3' \approx 2\arg\left(\frac{M_{e\tau}}{M_{\mu\tau}}\right) . \tag{4.53}$$

For certain values of the parameters, the splitting between the doublet of quasi-degenerate neutrinos can become larger than the difference between the masses of one of them and of the third neutrino. This case can be considered as the limit in which (a) and (b) merge. Notice that, in this limit, the structure of U_R is very unstable, and all three RH mixing angles can be large.

4.4 Baryogenesis via leptogenesis

We are going to consider the constraints on the seesaw parameters coming from the requirement of a successful thermal leptogenesis. We assume that a lepton asymmetry is generated by the CP-violating out-of-equilibrium decays of RH neutrinos [124]. The lepton asymmetry is then converted to a baryon asymmetry through the sphaleron processes [235], thus explaining the baryon asymmetry of the Universe. We will use the recent experimental value of the baryon-to-photon ratio [60],

$$\eta_B = (6.5 \pm^{0.4}_{0.3}) \cdot 10^{-10} \ . \tag{4.54}$$

The lepton number asymmetry, ϵ_i, produced in the decay of a RH neutrino with the mass M_i can be written as [236, 237, 238, 239, 240]:

$$\epsilon_i = \frac{1}{8\pi} \sum_{k \neq i} f\left(\frac{M_k^2}{M_i^2}\right) \frac{\mathrm{Im}(h^\dagger h)^2_{ik}}{(h^\dagger h)_{ii}} \ . \tag{4.55}$$

Here $h \equiv m_D/v$ (where $v = 174$ GeV is the electroweak VEV) is the matrix of neutrino Yukawa couplings in the basis where M_R is diagonal with real and positive eigenvalues. In this basis Eq. (4.3) holds and we can write

$$h^\dagger h = \frac{1}{v^2} U_R^\dagger (m_D^{diag})^2 U_R \ . \tag{4.56}$$

In SUSY models v should be replaced with $v \sin\beta$. For $\tan\beta \gtrsim 3$, this corresponds to a very small rescaling of Yukawa couplings with respect to the non supersymmetric case.

In the standard electroweak model the function f in Eq. (4.55) is given by

$$f(x) = \sqrt{x}\left[\frac{2-x}{1-x} - (1+x)\log\left(\frac{1+x}{x}\right)\right] \ . \tag{4.57}$$

This expression is valid for $|M_i - M_j| \gg \Gamma_i + \Gamma_j$, where Γ_i is the decay width of the RH neutrino N_i, given at tree level by

$$\Gamma_i = \frac{(h^\dagger h)_{ii}}{8\pi} M_i \ .$$

In the limit of the quasi-degenerate neutrinos ($x = M_j^2/M_i^2 \to 1$), one formally obtains from (4.57)

$$f(x) \approx \frac{1}{1-x} \approx \frac{M_i}{2(M_i - M_j)} \to \infty \ . \tag{4.58}$$

However, in reality the enhancement of the asymmetry is limited by the decay widths Γ_i and is maximized when $|M_i - M_j| \sim \Gamma_i + \Gamma_j$ [241].

The left-handed rotation U_L does not enter the expression for the lepton number asymmetry. Furthermore, $h^\dagger h$ is invariant under the transformation

$$U_R \to D U_R \ , \tag{4.59}$$

where

$$D = diag(e^{i\alpha}, e^{i\beta}, e^{i\gamma}) \tag{4.60}$$

and α, β, γ are arbitrary phases. Consequently, all the phases that can be removed from U_R by the transformation (4.59) have no impact on leptogenesis.

The baryon-to-photon ratio can be written as [242]

$$\eta_B \simeq 0.01 \sum_i \epsilon_i \cdot \kappa_i \ ,$$

where the factors κ_i describe the washout of the produced lepton asymmetry ϵ_i due to various lepton number violating processes. The numerical prefactor contains, in particular, the lepton to baryon asymmetry conversion rate due to sphalerons [243]. In the domain of the parameter space which is of interest to us, the factors κ_i depend mainly on the effective mass parameters

$$\tilde{m}_i \equiv \frac{v^2 (h^\dagger h)_{ii}}{M_i} = \frac{[U_R^\dagger (m_D^{diag})^2 U_R]_{ii}}{M_i} \ . \tag{4.61}$$

For 10^{-2} eV $< \tilde{m}_1 < 10^3$ eV, the washout factor κ_1 can be well approximated by [244, 245]

$$\kappa_1(\tilde{m}_1) \simeq 0.3 \left(\frac{10^{-3} \text{ eV}}{\tilde{m}_1} \right) \left(\log \frac{\tilde{m}_1}{10^{-3} \text{ eV}} \right)^{-0.6} \ . \tag{4.62}$$

When $M_1 \ll M_{2,3}$, only the decays of the lightest RH neutrino N_1 are relevant for producing the baryon asymmetry η_B, since the lepton asymmetry generated in the decays of the heavier RH neutrinos is washed out by the L-violating processes involving N_1's, which are very abundant at high temperatures $T \sim M_{2,3}$. At the same time, at $T \sim M_1$ the heavier neutrinos N_2 and N_3 have already decayed and so cannot wash out the asymmetry produced in the decays of N_1.

In Refs. [246, 242], under the assumption $M_1 \ll M_{2,3}$, the following absolute lower bound on the mass of the lightest RH neutrino was found from the condition of the successful leptogenesis:

$$M_1 \gtrsim 4 \cdot 10^8 \text{ GeV} \ . \tag{4.63}$$

The bound (4.63) corresponds to $\tilde{m}_1 \to 0$ and maximal ϵ_1; for other values of $\tilde{m}_1$ and ϵ_1 it is even stronger [242, 247]. Inequality (4.63) has been derived before the latest WMAP data became available [60]. These data (see Eq. (4.54)) strengthen the bound by a factor ~ 1.5: $M_1 \gtrsim 6 \cdot 10^8$ GeV.

4.5 A unique structure for successful leptogenesis

4.5.1 Leptogenesis in the generic case

We now turn to the discussion of leptogenesis in the generic case analyzed in section 4.2. Since the RH neutrino masses are highly hierarchical, the main contribution to the lepton asymmetry comes from the decays of the lightest RH neutrino N_1. From Eq. (4.22) we find that, for $m_u \lesssim 10$ MeV, its mass is at least one order of magnitude smaller than the absolute lower bound (4.63). The normal hierarchy case is the most favorable one: for the other cases m_{ee} is larger, leading to even smaller values of M_1.

Let us compute the value of η_B in the generic case. From Eqs. (4.61), (4.14) and (4.18) we get

$$\tilde{m}_1 \approx \frac{m_{ee}^2 + m_{e\mu}^2 + m_{e\tau}^2}{m_{ee}} = \frac{m_2^2 s_{12}^2 + m_1^2 c_{12}^2}{|m_2 s_{12}^2 + m_1 e^{-2i\rho} c_{12}^2|} + \mathcal{O}(s_{13}) \ . \tag{4.64}$$

In the case of the hierarchical spectra of light neutrinos, this gives

$$\begin{aligned} &\tilde{m}_1 \approx m_2 \approx \sqrt{\Delta m_{sol}^2} \ , && \kappa_1(\tilde{m}_1) \approx 0.02 && \text{(NH)} \ , \\ &\tilde{m}_1 \approx \frac{m_2}{|s_{12}^2 + e^{-2i\rho} c_{12}^2|} \approx \frac{\sqrt{\Delta m_{atm}^2}}{\cos 2\theta_{12} \div 1} \ , && \kappa_1(\tilde{m}_1) \approx 0.001 \div 0.003 && \text{(IH)} \ , \end{aligned} \tag{4.65}$$

where κ_1 has been estimated using Eq. (4.62). For $M_1 \ll M_{2,3}$, the lepton asymmetry ϵ_1, given by Eq. (4.55), can be written as

$$\epsilon_1 \approx -\frac{3}{16\pi} \left[\frac{M_1}{M_2} \frac{\mathrm{Im}(h^\dagger h)_{12}^2}{(h^\dagger h)_{11}} + \frac{M_1}{M_3} \frac{\mathrm{Im}(h^\dagger h)_{13}^2}{(h^\dagger h)_{11}} \right] \ . \tag{4.66}$$

From Eqs. (4.56) and (4.18) we get

$$v^2 (h^\dagger h)_{11} \approx m_u^2 I_{11} \ , \qquad v^2 (h^\dagger h)_{12} \approx m_u m_c I_{12} \ , \qquad v^2 (h^\dagger h)_{13} \approx m_u m_t I_{13} \ ,$$

where $I_{ij} = I_{ij}(m_{\alpha\beta})$ are order 1 coefficients. Using these relations and the expressions (4.14), (4.15) and (4.17) for M_i in Eq. (4.66) we find

$$\epsilon_1 = \frac{3}{16\pi} \frac{m_u^2}{v^2} \cdot I(m_{\alpha\beta}) \ , \qquad I(m_{\alpha\beta}) \sim 1 \ .$$

Then the produced baryon-to-photon ratio is given, up to a factor of order one, by

$$\eta_B \simeq 0.01 \cdot \epsilon_1 \cdot \kappa_1(\tilde{m}_1) \simeq 4 \cdot 10^{-16} \cdot \left(\frac{m_u}{1 \text{ MeV}} \right)^2 \left(\frac{\kappa_1(\tilde{m}_1)}{0.02} \right) \ .$$

To reproduce the observed value of η_B, one would need $m_u \sim 1$ GeV. Thus, a successful leptogenesis requires $m_u \sim m_c$, which contradicts our assumption of a strong hierarchy between the eigenvalues of m_D and goes contrary to the simple GUT expectations.

Our conclusions concerning the mass spectrum of RH neutrinos and the generated baryon asymmetry in the generic case are in accord with those reached in the previous studies [149, 147, 150, 151, 148, 152].

4.5.2 Leptogenesis in the special case I

Let us now turn our attention to the special case $m_{ee} \to 0$ (section 4.3.1). Since N_1 and N_2 are quasi-degenerate and almost maximally mixed, one expects nearly equal contributions to η_B from their decays. Using Eqs. (4.30) and (4.31), we find from (4.61)

$$\tilde{m}_1 \approx \tilde{m}_2 \approx \frac{m_c}{m_u}\frac{m_{e\mu}^2 + m_{e\tau}^2}{2m_{e\mu}} = \frac{m_c}{m_u}\left(\frac{s_{12}c_{12}}{2c_{23}}|m_2 - m_1 e^{-2i\rho}| + \mathcal{O}(s_{13})\right) .$$

Therefore, the maximal RH mixing in the (12)-sector leads to an increase of $\tilde{m}_1$ by a factor $\sim m_c/m_u$ with respect to the generic case (Eq. (4.64)) and, as a consequence, to a strong enhancement of the washout effects. Taking into account Eq. (4.32), we obtain for $s_{13} \approx 0$

$$\tilde{m}_1 \approx \frac{m_c}{m_u}\frac{\sin 2\theta_{12}\sqrt{\Delta m_{sol}^2}}{4c_{23}\sqrt{\cos 2\theta_{12}}} \approx 1.5 \text{ eV}\left(\frac{m_c}{400 m_u}\right) , \tag{4.67}$$

and then, according to Eq. (4.62),

$$\kappa_1(1.5 \text{ eV}) \approx 6 \cdot 10^{-5} . \tag{4.68}$$

The washout effects for lepton asymmetries produced in the decays of N_1 and N_2 are nearly the same: $\kappa_1(\tilde{m}_1) \approx \kappa_2(\tilde{m}_2)$.

Substituting the mixing parameters given by Eq. (4.31) into Eq. (4.56), we find the relevant entries of $(h^\dagger h)$:

$$\begin{aligned}
(h^\dagger h)_{12} &\approx (h^\dagger h)_{21}^* \approx -\frac{1}{2}\frac{m_c^2}{v^2}\left(1 + \frac{m_{e\tau}^2}{m_{e\mu}^2}\right) e^{i(\phi_1 - \phi_2)/2} , \\
(h^\dagger h)_{11} &\approx (h^\dagger h)_{22} \approx \frac{1}{2}\frac{m_c^2}{v^2}\left(1 + \frac{m_{e\tau}^2}{m_{e\mu}^2}\right) , \\
(h^\dagger h)_{13} &\approx e^{i(\phi_1 - \phi_2)/2}(h^\dagger h)_{23} \approx -\frac{1}{\sqrt{2}}\frac{m_c m_t}{v^2}\left(\frac{M_{e\tau}}{M_{e\mu}}\right)^* e^{i(\phi_1 - \phi_3)/2} .
\end{aligned} \tag{4.69}$$

Then the contribution to $\epsilon_{1,2}$ coming from the diagrams with the heaviest RH neutrino N_3 in the loop (terms with $k = 3$ in Eq. (4.55)) can be estimated as follows:

$$\epsilon_{1,2}^{(N_3)} \sim \pm\frac{3}{16\pi}\frac{m_u m_c}{v^2}\sqrt{\frac{\Delta m_{atm}^2}{\Delta m_{sol}^2}} \approx \pm 5 \cdot 10^{-9} .$$

These asymmetries are tiny compared to the values required for a successful leptogenesis and, moreover, have opposite signs for ϵ_1 and ϵ_2. Therefore the dominant contribution should come from the diagrams with N_2 (N_1) in the loop for the decay of N_1 (N_2). The corresponding asymmetries $\epsilon_{1,2}$ can be written as

$$\epsilon_1 \approx \epsilon_2 \approx \frac{1}{16\pi}\frac{M_1}{M_1 - M_2}\frac{\text{Im}[(h^\dagger h)_{12}^2]}{(h^\dagger h)_{11}} \approx \frac{1}{32\pi}\frac{m_c^2}{v^2}\left(1 + \frac{m_{e\tau}^2}{m_{e\mu}^2}\right)\xi , \tag{4.70}$$

where

$$\xi = \frac{M_1}{M_1 - M_2} \sin(\phi_1 - \phi_2) \ . \tag{4.71}$$

The enhancement due to the quasi-degeneracy of N_1 and N_2 competes with the suppression due to their almost opposite CP parities. Indeed, in the limit of exactly vanishing W_{11} and W_{22}, one has $\sin(\phi_1 - \phi_2) = \sin\pi = 0$: in this case the complex phases can be removed by the transformation (4.59). Taking into account terms of order W_{11} and W_{22}, we find

$$\xi \approx \frac{4d \tan\Delta}{(1+d)^2 + (1-d)^2 \tan^2\Delta} \ , \tag{4.72}$$

where

$$d \equiv \frac{|W_{22}|}{|W_{11}|} = \frac{m_u^2 m_{\mu\mu}}{m_c^2 m_{ee}} \ , \qquad \Delta \equiv \frac{1}{2} \arg \frac{W_{12}^2}{W_{11} W_{22}} = \frac{1}{2} \arg \frac{M_{e\mu}^2}{M_{ee} M_{\mu\mu}} \equiv -\frac{1}{2} \Delta_{e\mu} \ . \tag{4.73}$$

Notice that the phase Δ is invariant under the transformation (4.59). In fact, as discussed in section 2.3.3, the phase $\Delta_{e\mu}$ is physical.

For $|1-d| \ll 1/\tan\Delta$, Eq. (4.72) gives

$$\xi \approx \tan\Delta \ ,$$

and for $\Delta \simeq \pi/2$ a significant enhancement of the asymmetries $\epsilon_{1,2}$ can be achieved. The enhancement factor depends on the degree of near-equality of $|W_{22}|$ and $|W_{11}|$.

For $d \to 1$, the level splitting can be written as

$$\frac{M_2 - M_1}{M_1} \approx 2 \frac{|W_{22}|}{|W_{12}|} \cos\Delta = 2 \frac{m_{\mu\mu}}{m_{e\mu}} \frac{m_u}{m_c} \cos\Delta \ , \tag{4.74}$$

so that for $\Delta \approx \pi/2$ the splitting is substantially reduced. As we discussed in section 4.4, the enhancement due to the degeneracy is restricted by the condition

$$\frac{M_2 - M_1}{M_1} \gtrsim \frac{\Gamma_1}{M_1} \ , \tag{4.75}$$

where in the case under the consideration

$$\frac{\Gamma_1}{M_1} \approx \frac{1}{8\pi} \frac{m_c^2}{2v^2} \left(1 + \frac{m_{e\tau}^2}{m_{e\mu}^2}\right) \ . \tag{4.76}$$

Estimating $m_{e\mu} \approx m_{e\tau} \approx m_{\mu\mu}\sqrt{\Delta m_{sol}^2 / \Delta m_{atm}^2}$, from Eqs. (4.74), (4.75) and (4.76) we find the maximal possible enhancement:

$$\xi^{max} \approx \tan\Delta \approx \frac{1}{\cos\Delta} \approx \frac{16\pi v^2 m_u}{m_c^3} \sqrt{\frac{\Delta m_{atm}^2}{\Delta m_{sol}^2}} \approx 1.4 \cdot 10^5 \ . \tag{4.77}$$

In the numerical estimate we have taken the values in Eq. (4.5). Using Eqs. (4.74), (4.76) and (4.70), we can write the maximal asymmetry as

$$\epsilon^{max} = \frac{1}{2}\frac{\Gamma_1}{M_1}\xi^{max} \approx \frac{|W_{22}|}{|W_{12}|} \approx \frac{m_u}{m_c}\sqrt{\frac{\Delta m^2_{atm}}{\Delta m^2_{sol}}} \,,$$

which shows that $\epsilon^{max} \sim 10^{-2}$ is reachable in this scenario.

Combining Eqs. (4.62), (4.70) and (4.77), we find

$$\eta_B \approx 0.01{\cdot}2\epsilon_1\kappa_1 \approx 1.9{\cdot}10^{-8}\left(\frac{400m_u}{m_c}\right)^2\left[1+0.14\log\left(\frac{m_c}{400m_u}\right)\right]^{-0.6}\left[\frac{\xi}{\xi^{max}(m_u,m_c)}\right] .$$

Therefore the value (4.54) of η_B can be obtained for $m_u/m_c \gtrsim 2\cdot 10^{-3}$. For $m_c = 400m_u$, the observed baryon asymmetry is reproduced for $\xi \approx \tan\Delta \approx 5\cdot 10^3$, which corresponds to the relative splitting (see Eq. (4.74))

$$\frac{M_2 - M_1}{M_1} \approx 6\cdot 10^{-6} \,.$$

Thus, in spite of strong washout effects, a sufficiently large baryon asymmetry can be generated in this case, due to the enhancement related to the strong degeneracy of the RH neutrinos. For this to occur, not only the level crossing condition ($m_{ee} \to 0$) has to be satisfied, but also a special phase condition leading to $\Delta \approx \pi/2$ ($\Delta_{e\mu} \approx \pi$) should be fulfilled. This value of $\Delta_{e\mu}$ is consistent with the low energy neutrino data. We have checked the analytic results presented in this section by precise numerical calculations.

4.5.3 Leptogenesis in the special case II

For this special case (section 4.3.2), the predictions for the lepton asymmetry are analogous to those in the generic case. The production of the asymmetry is dominated by the decays of the lightest RH neutrino. Due to the larger RH mixing, the asymmetry ϵ_1 gets an enhancement factor $\sim (m_t/m_c)$ with respect to the generic case, but the leading terms in $\mathrm{Im}(h^\dagger h)^2_{12}$ and $\mathrm{Im}(h^\dagger h)^2_{13}$ cancel because of the nearly opposite CP parities of N_2 and N_3. Indeed, the sum of the two terms is proportional to $\sin(\phi_2 - \phi_3) \approx 0$, where ϕ_i are defined in Eq. (4.9). Thus, the produced lepton asymmetry is insufficient for a successful baryogenesis through leptogenesis. This is in agreement with the fact that in this special case the value of M_1 is still below the absolute lower bound (4.63).

4.5.4 Leptogenesis in the special case III

Let us consider now the predictions for leptogenesis when both $m_{ee} \to 0$ and $m_{e\mu} \to 0$ (section 4.3.3). To compute the produced lepton asymmetry one has to take into account the interplay among all three quasi-degenerate RH neutrinos. The effects related

to mass degeneracy and large RH mixing angles, discussed in section 4.5.2, are present also here. Notice that the maximal RH mixing is now related with the Dirac masses m_u and m_t rather than with m_u and m_c, as in section 4.5.2. Let us discuss separately the two subcases defined at the end of section 4.3.3.

(a) $r_{ds} < 1$, light quasi-degenerate pair.

From Eqs. (4.44), (4.49) and (4.61) we find the effective mass parameter

$$\tilde{m}_1 \approx \tilde{m}_2 \approx \frac{m_t}{2m_u} m_{e\tau} \approx 500 \text{ eV} ,$$

which leads, according to Eq. (4.62), to a very small washout factor

$$\kappa_{1,2}(500 \text{ eV}) \approx 10^{-7} . \tag{4.78}$$

To survive such strong a washout, lepton asymmetries ϵ_i of order unity are required.

The contribution to $\epsilon_{1,2}$ of diagrams with N_3 in the loop can be estimated as

$$\epsilon_{1,2}^{(N_3)} \sim \pm \frac{3}{16\pi} \frac{m_c^2}{v^2} \approx \pm 3 \cdot 10^{-7} ,$$

where we assumed $M_3/M_{1,2} \gtrsim 1.5$, so that the effects of the three-neutrino degeneracy can be disregarded. Let us estimate the contribution to $\epsilon_{1,2}$ of diagrams with $N_{2,1}$ in the loop. The maximal asymmetry is obtained when

$$\frac{M_2 - M_1}{M_1} \approx \frac{\Gamma_{1,2}}{M_1} \approx \frac{m_t^2}{16\pi v^2} . \tag{4.79}$$

In this case the function f in Eq. (4.55) should be replaced by $M_1/(2\Gamma_1)$ [241], and one finds

$$\epsilon_1 \approx \epsilon_2 \approx \frac{1}{16\pi} \frac{M_1}{\Gamma_1} \frac{\text{Im}(h^\dagger h)_{12}^2}{(h^\dagger h)_{11}} \approx \frac{1}{2} \sin(\phi_1' - \phi_2') . \tag{4.80}$$

As in the special case I, the factor $\sin(\phi_1' - \phi_2')$ is suppressed because of the approximately opposite CP parities of N_1 and N_2 (see Eq. (4.51)). Computing also $\mathcal{O}(\lambda^2)$ terms in U_R, we find

$$\sin(\phi_1' - \phi_2') \sim \frac{m_u}{m_t} \approx 10^{-5} . \tag{4.81}$$

As far as ϵ_3 is concerned, the two contributions proportional to $\text{Im}(h^\dagger h)_{31}^2$ and $\text{Im}(h^\dagger h)_{32}^2$ are of order $m_t^2/(16\pi v^2)$, but have opposite sign because of the opposite CP parities of N_1 and N_2. Moreover, ϵ_3 is washed out efficiently by the strong L-violating interactions of N_1 and N_2. Therefore its contribution to η_B can be neglected and we finally obtain

$$\eta_B \approx 0.01 \cdot 2\epsilon_1 \kappa_1 \sim 10^{-14} \left(\frac{10^5 m_u}{m_t} \right) \left(\frac{\kappa_1(m_u/m_t)}{10^{-7}} \right) .$$

Thus, the leptogenesis is not successful in this special case.

Reducing the ratio m_t/m_u, one gets both smaller washout and enhanced asymmetries $\epsilon_{1,2}$ (see Eqs. (4.78), (4.80) and (4.81)). However, to obtain η_B in the correct range, one would have to violate the assumption in Eq. (4.4). Even a strong degeneracy between all three RH neutrinos cannot lead to a sufficient increase of the final baryon asymmetry, because the enhancement due to the degeneracy is limited by the large values of $\Gamma_{1,2}$ given in Eq. (4.79) (see also the discussion at the end of this section). Moreover, the analytic approximation (4.62) most probably underestimates the washout effects in this case, because of the very large values of $\tilde{m}_1$ and $\tilde{m}_2$ (~ 500 eV). To the best of our knowledge, no numerical solutions of the relevant Boltzmann equations in this regime are available in the literature, since it is usually assumed that $\tilde{m}_1$ does not exceed the mass of the heaviest left-handed neutrino m_3. The present special case shows that this is not always true.

(b) $r_{ds} > 1$, heavy quasi-degenerate pair.

In this case ϵ_1 gives the dominant contribution to the final baryon asymmetry. Now U_R is given by Eq. (4.52). Using the approximation (see Eqs. (4.48) and (4.50))

$$\delta_2 \approx \frac{m_c}{m_t}\frac{r_{ds}^2}{r_{ds}^2-1}e^{-i\phi/2} ,$$

we obtain from Eq. (4.56)

$$\begin{aligned}(h^\dagger h)_{11} &\approx \frac{m_c^2}{v^2}\frac{1-2r_{ds}^2+2r_{ds}^4}{1-2r_{ds}^2+r_{ds}^4} ,\\ (h^\dagger h)_{12} &\approx -e^{i(\phi_3'-\phi_2')/2}(h^\dagger h)_{13} \approx \frac{m_t m_c}{\sqrt{2}v^2}\frac{r_{ds}^2}{1-r_{ds}^2}e^{i(\phi+\phi_1'-\phi_2')/2} .\end{aligned}$$

Then for $\tilde{m}_1$ and κ_1 we find

$$\tilde{m}_1 \gtrsim 2m_{\mu\mu} \approx 0.05 \text{ eV} , \qquad \kappa_1(\tilde{m}_1) \lesssim 3\cdot 10^{-3} .$$

The asymmetry produced in the decays of N_1 can be written as

$$\epsilon_1 \approx -\frac{3m_t^2}{32\pi v^2}\frac{r_{ds}^3}{1-2r_{ds}^2+2r_{ds}^4}\sin\psi\sin(\phi_3'-\phi_2') \approx 3\cdot 10^{-3}\ \sin(\phi_3'-\phi_2') ,$$

where $\psi \equiv (\phi+\phi_1'-\phi_2'/2-\phi_3'/2)$. In the last equality we have chosen $r_{ds}=2$ and $\sin\psi = 1$, which are the most favorable values for obtaining a large η_B (note that, even though ϵ_1 is maximized at $r_{ds} \simeq 1$, in the limit $r_{ds} \to 1$ the parameter $\tilde{m}_1$ becomes very large, which signals a very strong washout of the asymmetry). Also in this case the fact that the CP parities of N_2 and N_3 are almost opposite leads to a strong cancellation:

$$\sin(\phi_3'-\phi_2') \sim \frac{m_u}{m_t} \approx 10^{-5} .$$

Thus we obtain

$$\eta_B \approx 0.01\cdot\epsilon_1\cdot\kappa_1 \lesssim 5\cdot 10^{-13}\left(\frac{m_u}{1\text{MeV}}\right)\left(\frac{m_t}{100\text{GeV}}\right) .$$

Increasing $m_u \cdot m_t$ (and also m_c^2 in order to keep r_{ds} fixed) would increase η_B.

However, it is unlikely that this would lead to a successful leptogenesis. Indeed, since all three RH neutrino masses are of the same order in this special case ($r_{ds} \sim 1$), the heavier neutrinos N_2 and N_3 are still abundant at the temperature $T \sim M_1$ at which the decays of N_1 take place. Therefore the strong washout effects due to the processes involving N_2 and N_3, which are characterized by very large $\tilde{m}_{2,3} \simeq 500$ eV, are expected to efficiently wash out the asymmetry ϵ_1 even though the parameter $\tilde{m}_1$ is relatively small. Therefore we do not expect this special case to lead to a successful baryogenesis through leptogenesis. A more accurate study of the case of three quasi-degenerate RH neutrinos would require solving numerically a coupled set of Boltzmann equations describing the evolution of the number densities of all RH neutrinos and $B - L$. We consider such a study, which is beyond the scope of the present analysis, to be very desirable.

4.6 Stability of the result

In the previous section we have computed the baryon asymmetry produced through the decays of RH neutrinos, in the framework of type-I seesaw mechanism with hierarchical Dirac masses and small left-handed Dirac-type mixing. We have found that the unique possibility to obtain successful thermal leptogenesis is the special case I.

Now we want to make some checks on the stability of this result. First we will analyze the effect of radiative corrections, in particular for the unique structure of M_R which leads to successful leptogenesis. Then we will relax the hypothesis of small left-handed Dirac-type mixing. Finally we will comment on the possibility of non-thermal leptogenesis.

1) Radiative corrections.

Let us discuss the renormalization group equation (RGE) evolution of the seesaw mass matrices.

We know from chapter 3 that the structure of the effective mass matrix M is stable under the Standard Model (or MSSM) radiative corrections [107, 108, 109, 202]. The corrections to its matrix elements can be written as

$$\Delta M_{\alpha\beta} \sim (\epsilon_\alpha + \epsilon_\beta) M_{\alpha\beta} \ ,$$

where ϵ_α ($\lesssim 10^{-2}$) describes the effect of the Yukawa coupling of the charged lepton l_α. Therefore both M_{ee} and $d_{12} \equiv (M_{ee}M_{\mu\mu} - M_{e\mu}^2)$ receive small corrections proportional to themselves: if M_{ee} and/or d_{12} are very small at the electroweak scale, they remain very small also at the seesaw scale (the mass scale of RH neutrinos), and so the level crossing conditions do not change.

Between the GUT and the seesaw scales one has to consider the evolution of the neutrino Yukawa couplings and of Majorana mass matrix of RH neutrinos rather than

the evolution of the effective matrix M [120, 121, 122, 233]. We assume that at the GUT scale the Yukawa couplings of neutrinos h are related with those of quarks or charged leptons. The evolution of h with decreasing mass scale will not modify the hierarchy $m_u \ll m_c \ll m_t$, and its effects can be absorbed into a redefinition of our indicative values of $m_{u,c,t}$.

The RGE effects on M_R are due to the neutrino Yukawa couplings; they can, in principle, be important in the cases of strongly degenerate RH neutrinos. Consider the stability of the structure of M_R in the special case that leads to a successful leptogenesis. Recall that in this case the (12)-sector of RH neutrinos is characterized by $M_{1,2} \approx 10^8$ GeV, $(M_2 - M_1)/M_1 \lesssim 10^{-5}$ and $\Delta \approx \pi/2$, where Δ is defined in Eq. (4.73). The largest correction to the (12)-block of M_R between $M_{\rm GUT}$ and $M_{1,2}$ is the correction to the 22-element:

$$\frac{(\Delta M_R)_{22}}{(M_R)_{22}} \sim \frac{m_c^2}{16\pi^2 v^2} \log\left(\frac{M_{\rm GUT}}{10^8\ {\rm GeV}}\right) \approx 6 \cdot 10^{-7} \left(\frac{m_c}{0.4\ {\rm GeV}}\right)^2 .$$

Therefore, the radiative corrections cannot generate a relative splitting between M_1 and M_2 exceeding 10^{-5}. Moreover, at one loop level, the phases of $(M_R)_{ij}$ have no RGE evolution and so the relation $\Delta \approx \pi/2$ is not modified.

2) Large left-handed Dirac-type mixing.

Let us abandon the hypothesis $U_L \approx \mathbb{1}$. If the matrix U_L is arbitrary, the direct connection between the low energy data and the structure of M_R is lost. This additional freedom relaxes the phenomenological constraints on RH neutrinos. In fact, now the unique low energy requirement on the seesaw mechanism is to reproduce the light neutrino masses, given by the eigenvalues of $\hat{M}$ (Eq. (4.11)); the correct leptonic mixing matrix U_{PMNS} can always be obtained through the proper choice of U_L. As an example, let us consider the case of non-degenerate RH masses and take the following RH mixing matrix:

$$U_R = \begin{pmatrix} \frac{1}{\sqrt{2}} & \frac{1}{\sqrt{2}} & 0 \\ -\frac{1}{\sqrt{2}} & \frac{1}{\sqrt{2}} & 0 \\ 0 & 0 & 1 \end{pmatrix} \cdot K \ .$$

The maximal mixing of the two lighter RH neutrinos will maximize the lepton asymmetry. The eigenvalues of the matrix

$$\hat{M} = -m_D^{diag} W m_D^{diag}$$

(see Eq. (4.10)) are given, approximately, by $m_c^2/(4M_2)$, $m_c^2/(2M_1)$, m_t^2/M_3. Taking $M_1 \approx 10^{10}$ GeV$\cdot(m_c/0.4\ {\rm GeV})^2$, M_2 a few times larger and $M_3 \approx 2 \cdot 10^{14}$ GeV $\cdot(m_t/100\ {\rm GeV})^2$, one can reproduce the solar and atmospheric mass squared differences. Since $\hat{M}$ is approximately diagonal, the solar and atmospheric mixing angles are generated by U_L, which should have an almost bimaximal form.

It is easy to calculate the washout mass parameter and the asymmetry produced in the decays of N_1:

$$\tilde{m}_1 = \frac{m_c^2}{2M_1} \approx \sqrt{\Delta m^2_{sol}}\ , \qquad \epsilon_1 \approx \frac{3m_c^2}{32\pi v^2}\sin(\phi_2 - \phi_1)\frac{M_1}{M_2}\ .$$

Assuming $\phi_2 - \phi_1 \sim \pi/2$ (note that the CP parities of N_1 and N_2 are not constrained in this case), we get

$$\eta_B \approx 3 \cdot 10^{-11}\frac{M_1}{M_2}\left(\frac{m_c}{0.4\ \text{GeV}}\right)^2\ .$$

Thus, for a moderate hierarchy between M_1 and M_2, a value of m_c around a few GeV can lead to a successful leptogenesis. This example shows that, relaxing the hypothesis $U_L \approx \mathbb{1}$, it is easier to realize baryogenesis via leptogenesis. In particular, the degeneracy of the masses of RH neutrinos M_i is no longer necessary, but the hierarchy of M_i should not be as large as it is in the generic case.

3) Non-thermal leptogenesis.

Let us comment on the possibility of non-thermal production of the heavy RH neutrinos (see, e.g., [248, 249, 250, 251]), that in principle can lead to a successful leptogenesis for values of the parameters M_1 and $\tilde{m}_1$ for which thermal leptogenesis does not work.

In fact, it is interesting that also non-thermal leptogenesis is strongly constrained in our framework. Consider the generic case (section 4.2). Since M_1 is relatively light ($\lesssim 10^7$ GeV), ϵ_1 is very small. Moreover, as $\tilde{m}_1$ is relatively large ($\gtrsim \sqrt{\Delta m^2_{sol}}$), thermal effects washout (at least partially) the asymmetry generated in the decays of non-thermally produced RH neutrinos [252]. As a consequence, even in the non-thermal case, the asymmetry generated by N_1 turns out to be insufficient and, to enhance it, one has to resort again to the special case I (sections 4.3.1, 4.5.2).

It is known, however (see, e.g., [253]), that also the asymmetries generated by N_2 and/or N_3 can survive if (1) they are produced non-thermally at reheating and (2) N_1 is not in thermal equilibrium at the reheating temperature T_{RH}. In fact, the asymmetries $\epsilon_{2,3}$ can be large (they are of the order of $m^2_{c,t}/(16\pi v^2)$ in the generic case and even larger in the special case II: $\epsilon_{2,3} \sim m_c/m_t$). However, partial thermalization of $N_{2,3}$ and subsequent washout can occur after reheating. Moreover, to avoid later cancellation of $\epsilon_{2,3}$, N_1 should not enter into thermal equilibrium at any temperature $T \lesssim T_{RH}$.

In this case an accurate computation of the final asymmetry would require to solve the complete set Boltzmann equations describing the evolution of the number densities of all three RH neutrinos and of $B - L$.

Chapter 5

Conclusions

5.1 Understanding the neutrino mass matrix structure

The motivation of our study is to understand how far one can go in the construction of the theory of neutrino mass using the bottom-up approach, that is, starting from experimental results. Neutrino mass matrix in flavor basis unifies the information contained in masses and mixing angles measured in experiments and therefore can give deeper insight into the underlying physics.

We have elaborated a method which allows one to study the dependences of the individual matrix elements and of the structure of the mass matrix as a whole on the unknown yet parameters. In particular, we have performed for the first time a systematic and comprehensive study of the dependence of the matrix elements on the CP violating phases.

We have introduced the $\rho - \sigma$ plots which show contours of constant mass in the plane of the Majorana phases ρ and σ. Each point in the $\rho - \sigma$ plots represents a certain neutrino mass matrix, so that it is easy to scan all possible matrix structures. Vice versa one can check if a given mass matrix satisfies the data for at least a pair of values of ρ and σ. The $\rho - \sigma$ plots shows the ranges in which the elements can change and their extremal values (minimal and maximal), the correlations between different matrix elements, the consequences of the measurement of m_{ee} on the matrix structure.

Let us summarize the main properties of the possible mass matrices.

1) The structure of the mass matrix changes significantly with the mass scale and the mass ordering.

For strong normal hierarchy ($m_1 \to 0$), the mass matrix has a structure with dominant $\mu\tau$-block and small e-row elements. The ratio of masses of these two groups can be as small as 0.1. The dominant structure becomes less profound for relatively large Δm^2_{sol} and s_{13} and for significant deviation from maximal 2-3 mixing.

For partially degenerate spectrum, the gap between the $\mu\tau$-block elements and e-row elements disappears and all elements can be of the same order. Various equalities

between the elements and orderings can be realized depending on the CP violating phases.

In the case of degenerate mass spectrum, the mass matrix can have a hierarchical structure with some elements (in particular, from the $\mu\tau$-block) being much smaller than other elements. The hierarchical structures appear for specific ranges of the Majorana phases.

In the case of inverted ordering, the largest matrix element is m_{ee} for almost all the choices of the phases. For strong inverted hierarchy ($m_3 \to 0$) there is dominance of the e-row elements or, at least, of the ee-element. The matrix structure mainly depends on the relative phase between ν_1 and ν_2. Both structures with very small elements or with all elements of the same order are allowed.

2) The Majorana phases ρ and σ and the Dirac phase δ have different impact on the structure of the mass matrix. This impact depends on the values of oscillation parameters and on the type of mass spectrum.

(a) The Dirac phase δ is associated with the small parameter s_{13}. The influence of this phase on the $\mu\tau$-block elements is relatively weak for any type of spectrum. In contrast, the elements of e-row can be substantially influenced by δ, especially in the case of normal hierarchical spectrum, since s_{13}-terms are enhanced by $\sqrt{\Delta m^2_{atm}/\Delta m^2_{sol}}$. In the $\rho - \sigma$ plot, for fixed pattern of the $\mu\tau$-block elements, the phase δ produces a shift of the patterns of e-row elements along the axis σ. Improvements of the upper bound on s_{13} in future experiments will further suppress the influence of the Dirac phase on the structure of the mass matrix.

(b) The phase ρ is associated with the mass eigenvalue m_1. So, it has very small effect on the mass matrix in the case of normal hierarchy. The influence of ρ increases with m_1 and it is stronger if the solar mixing angle is larger. Therefore more stringent upper limits on θ_{12} will allow one to further restrict the effect of ρ on the structure of the mass matrix. The dependence of $\mu\tau$-block elements on ρ is quite weak in the case of normal ordering while it is stronger in the case of inverted ordering. The e-row elements $m_{e\mu}$ and $m_{e\tau}$ have minima at $\rho \approx 0, \pi$ and they are maximal at $\rho \approx \pi/2$. The ee-element depends on ρ in the opposite way. There is a chance to measure/restrict ρ in the $\beta\beta_{0\nu}$-decay searches, provided that the absolute mass scale will be determined (further restricted) in the direct kinematic measurements or using cosmological data.

(c) The phase σ is associated with the third mass eigenstate m_3 and, consequently, the σ-dependence is stronger for $\mu\tau$-block elements, is suppressed by s_{13} for $m_{e\mu}$ and $m_{e\tau}$ and by s^2_{13} for m_{ee}. In spite of this, in the case of normal hierarchy the variations of $m_{e\mu}$ and $m_{e\tau}$ with σ can be strong. In contrast, the dependence of $\mu\tau$-block elements on σ is stronger if the spectrum is not hierarchical. In the case of quasi degenerate spectrum, variations of the $\mu\tau$-block elements with σ can be maximal, so that, at different values of the phase, a given element can be zero or the largest one.

There are correlations among the dependences of the matrix elements on phases.

In general, patterns of $m_{\mu\mu}$ and $m_{\tau\tau}$ are complementary to the pattern of $m_{\mu\tau}$. The patterns for $m_{e\mu}$ and $m_{e\tau}$ are shifted by $\Delta\sigma = \pi/2$ with respect to each other, *etc.*.

3) The following results from forthcoming experiments will have crucial impact on the structure of the neutrino mass matrix:

- stronger bound on (or determination of) the deviation from maximal 2-3 mixing;
- more stringent upper limit on θ_{12};
- improvement of the bound on (or determination of) s_{13};
- determination of the ordering (normal or inverted) of neutrino masses;
- improvement of the bound on (or determination of) m_{ee};
- kinematic or cosmological measurements of the neutrino mass.

Is it possible to determine uniquely the mass matrix, at least in principle? If all the above results were achieved, we will know eight out of the nine parameters which define the mass matrix. The determination of σ looks practically impossible, unless methods of direct measurement or independent reconstruction of at least one another matrix element (apart from m_{ee}) will be found.

The $\rho - \sigma$ plots show clearly the uncertainty in the structure of the mass matrix due to the unknown value of σ. For inverted hierarchy the matrix does not depend on σ and therefore can be completely characterized. For normal hierarchy the dependence on σ is quite small and the dominant $\mu\tau$-block structure can be established. For non-hierarchical spectra the ambiguity due to the choice of σ is strong. In particular the structure of the $\mu\tau$-block cannot be determined.

4) The matrix may have hierarchical form with various dominant structures and small or zero elements. The dominant structures can be identified considering the limit $s_{13} \to 0$. In contrast, the s_{13}-order terms can be important or even give main contribution to the sub-dominant elements of the mass matrix. The phase δ does not influence the dominant structure.

In the case of hierarchical mass spectrum the dominant structure is formed by the $\mu\tau$-block and any element of the e-row can be zero, but not $m_{e\mu}$ and $m_{e\tau}$ at the same time.

For the other mass spectra, the dominant structures of the mass matrix are determined, essentially, by four parameters: $r \equiv m_3/m_2$, θ_{23}, $x = x(\rho, \theta_{12})$ and σ. In contrast, the values of s_{13}, δ and Δm^2_{sol} are related to small details of the matrix structure. In the degenerate case, also Δm^2_{atm} is very weakly imprinted in the structure of the mass matrix.

Any element but m_{ee} can be zero. The elements $m_{e\mu}$ and $m_{e\tau}$ can be very small for any type of the mass spectrum. In addition, one or two elements of the $\mu\tau$-block can be very small.

The unique hierarchical structure which is present in the whole range $0 \leq r \lesssim 3$ is that with $m_{e\mu}$ and $m_{e\tau}$ much smaller than the other matrix elements. This means that this structure is stable under modifications of the neutrino mass scale (in fact also

under inversion of the mass ordering).

In the case of quasi-degenerate mass spectrum one arrives at two rather stable structures:
(i) the matrix which equals approximately the unit matrix with small off-diagonal terms;
(ii) the matrix which has a dominant structure formed by $m_{ee} \approx m_{\mu\tau}$, while all other elements are small.
Apart from these known hierarchical matrices we have found several new structures with non-trivial values of CP violating phases. In particular, for non-maximal 2-3 mixing only the element $m_{\mu\mu}$ or $m_{\tau\tau}$ can be small. Typically, CP violating phases which differ substantially from from 0 , $\pi/2$ or π lead to non-hierarchical matrices.

Various equalities between matrix elements are possible. In particular, equalities of the e-row elements or/and $\mu\tau$-block elements, or diagonal elements or/and off-diagonal elements can be achieved. The "democratic" mass matrix of moduli is possible in flavor basis, but only for quasi-degenerate spectrum. Some equalities of elements (in contrast to zeros) can be realized for non-trivial phases only.

If s_{13} stays at the present upper bound (~ 0.2), $\mathcal{O}(s_{13})$ corrections can modify significantly the matrix structure, because they shift in opposite directions the elements $m_{e\mu}$ and $m_{e\tau}$, $m_{\mu\mu}$ and $m_{\tau\tau}$.

5) We have found that the matrix may have certain flavor ordering (alignment), that is masses increasing with change of the flavor from e to τ or vice versa, for normal or inverted mass spectrum respectively. The ordering of masses with flavor cannot be as steep as for quarks or charged leptons: it can be described in terms of a rather large expansion (ordering) parameter: $\lambda \approx 0.5 \div 0.8$. At the same time we find that the data can be reproduced by matrices with flavor "disorder", when no correlation between the size of the mass terms and the flavor is observed.

Typical separations among the elements in the structures of the neutrino mass matrix are characterized by a factor $0.2 \div 0.3$. We have found that in some cases it is possible to parameterize the matrix by powers of a single parameter λ (whose origin can be in the breaking of some flavor symmetry at high energy). The value $\lambda \approx 0.2 \div 0.3$ is consistent with the Cabibbo angle and also it can be related to the ratios of charge lepton masses.

We have discussed the relation between flavor basis and symmetry basis. Under the natural assumption of small (CKM-like) charged lepton mixing, we have shown that some features of the mass matrix in flavor basis can be explained as deviations from some symmetric limit (for example, deviations from bimaximal mixing).

5.2 Toward the origin of neutrino masses

There are some strong indications that neutrinos bring us information on the physics at very high energy, around the Grand Unification scale:

- The Standard Model allows for a neutrino mass term only at the non-renormalizable level, that is through an operator suppressed by the energy scale at which SM is no longer the correct effective theory.

- The neutrinos are the only known fermions with right-handed components (if any exists) that are singlets under the SM gauge group.

Dealing with very different scales, the first issue is to keep radiative corrections under control. The structure of the neutrino mass matrix at the electroweak scale m_Z changes with RGE running to the high energy scale m_0. We have analyzed the features of the running between the two scales.

The SM (MSSM) radiative corrections do not modify the matrix structure. In flavor basis, the value of each matrix element at m_Z is proportional to the one at m_0. Moreover, the corrections to this value cannot be larger than few percents. Therefore, both the dominant structure of the mass matrix and the small matrix elements are not modified significantly between m_0 and m_Z. Zero elements remain zero.

At the same time SM and MSSM corrections can change significantly the observables: corrections can enhance or suppress mixing, modify strongly Δm^2 or even generate mass split. Substantial change of observables occurs for the quasi-degenerate spectrum, with common scale of neutrino mass $m_i \gtrsim 0.1$ eV.

We have also studied the radiative effects induced by new particles and interactions at a scale m_X, with $m_Z < m_X < m_0$. These non-standard (flavor changing) corrections lead to coupled RGE's of different matrix elements. As a consequence, small tree-level elements get corrections proportional to the large matrix elements. We have considered non-standard corrections induced by new scalar bosons, new fermions and new gauge bosons.

In all cases, the dominant structure of the mass matrix remains the same between m_Z and m_0. Therefore, if the matrix structure at m_0 is determined by some symmetry, this symmetric structure can be identified from the experimental data at m_Z. However, the values of small elements can be strongly modified. We show that small elements of hierarchical matrices can be zero at the scale m_0 and receive non-zero contributions from radiative corrections. At the high mass scale, only the dominant block elements can be non-zero.

In the case of exactly degenerate neutrino masses, small ($\sim (0.1 \div 1)\%$) corrections to zero elements can generate large mixing angles and mass squared differences in the range required by phenomenology, both for solar and atmospheric neutrinos. We have shown, in particular, that the unit matrix can be the exact form of the neutrino mass matrix at m_0.

In the case of inverted hierarchy, the structure with zero $e\mu$ and $e\tau$ elements at m_0 can lead to correct predictions for low energy solar parameters, if 1% non-standard corrections are present.

In the case of normal hierarchical neutrino masses, we have studied the matrix with dominant $\mu\tau$-block. Solar mass squared difference and mixing angle can get large renormalization effects. To generate a mass difference in the LMA region, one needs 10% radiative corrections.

At the scale m_0, new physics appear. We have considered the type-I seesaw as the mechanism which generates the effective Majorana mass matrix. In this case m_0 should be identified with the lightest right-handed neutrino mass. To make connection between low energy neutrino data and the right-handed neutrino sector, we have assumed neutrino Yukawa couplings analogue to quark or charged lepton ones. This is equivalent to assume hierarchical eigenvalues of the Dirac mass matrix m_D and small Dirac-type left-handed mixing ($U_L \approx \mathbb{1}$). The masses and mixing angles of heavy right-handed neutrinos have been reconstructed. We have analyzed the possibility of explaining both the low energy neutrino data and the observed baryon asymmetry of the Universe in this framework.

Our main conclusions on seesaw and thermal leptogenesis are the following:

1) In the generic case (all elements of M of the same order), the mass matrix of RH neutrinos has a strong (nearly quadratic in m_D) hierarchy of eigenvalues and small mixing. The lightest RH neutrino has a mass $M_1 < 10^6$ GeV, well below the absolute lower bound coming from the condition of a successful leptogenesis. As a result, the predicted lepton asymmetry is smaller than 10^{-14} and the scenario of baryogenesis via leptogenesis does not work.

2) The special cases correspond to the level crossing points, when either two or all three masses of RH neutrinos are nearly equal. We have found two level crossing conditions: (1) $M_{ee} \to 0$ (the $N_1 - N_2$ crossing) and (2) $d_{12} \equiv (M_{ee}M_{\mu\mu} - M_{e\mu}^2) \to 0$ ($N_2 - N_3$ crossing), where m_{ee} and d_{12} should be evaluated in the basis where the Yukawa couplings of neutrinos are diagonal. In the crossing points the mixing of the corresponding neutrino states is maximal and their CP parities are nearly opposite.

3) For $U_L \simeq \mathbb{1}$ the leptogenesis can be successful only in the special case with small element M_{ee}, which corresponds to the $N_1 - N_2$ crossing. It is characterized by $M_1 \approx M_2 \approx 10^8$ GeV, $M_3 \approx 10^{14}$ GeV and $(M_2 - M_1)/M_2 \lesssim 10^{-5}$. N_1 and N_2 are strongly mixed and their mixing with N_3 is very small. The CP-violating phase $\Delta_{e\mu}$ should be very close to π. Notice that this unique case with a successful leptogenesis is defined very precisely. It has a number of characteristic features which can give important hints for model building.

4) For $U_L = \mathbb{1}$, the successful scenario is realized for the normal mass hierarchy of light neutrinos and predicts a very small effective Majorana mass probed in the neutrinoless 2β-decay: $m_{ee} \lesssim 10^{-4}$ eV. However, for $U_L \approx U_{CKM}$, this case can be realized also for other mass spectra and m_{ee} as large as ~ 0.1 eV.

5) We find that low-energy neutrino data allow also the other special cases, with $2-3$ crossing or both $1-2$ and $2-3$ crossings of the masses of RH neutrinos. These cases, however, do not lead to a successful baryogenesis through leptogenesis.

6) The level crossing conditions $m_{ee} \to 0$ and $d_{12} \to 0$ are stable under RGE running. The RGE effects on M_R can, in principle, be important in the cases of strongly degenerate RH neutrinos. We have verified the stability of the structure of M_R in the special case that leads to a successful leptogenesis. The radiative corrections cannot generate a relative splitting between M_1 and M_2 exceeding 10^{-5}. Moreover, at one loop level, the phases of $(M_R)_{ij}$ have no RGE evolution and so the relation $\Delta_{e\mu} \approx \pi$ is not modified.

7) If the matrix U_L is considered arbitrary, the direct connection between the low energy data and the structure of M_R is lost. It turns out that in this case it is easier to realize baryogenesis via leptogenesis. In particular, the degeneracy of the masses of RH neutrinos M_i is no longer necessary, but the hierarchy of M_i should not be as large as it is in the generic case.

The seesaw mechanism can account for both the low-energy neutrino data and a successful thermal leptogenesis, but a very specific structure of the mass matrices is required. Although this structure may look as an extreme fine tuning when viewed from the low-energy (effective theory) side, it does not appear unnatural from the point of view of the fundamental physics responsible for the seesaw mechanism: indeed, it just requires an approximate degeneracy and nearly maximal mixing of the two lightest RH neutrinos, which may well be a consequence of some flavor symmetry operating in the RH sector.

Can the unique successful special case that we found be ruled out? Since it requires a suppression of m_{ee}, it will be excluded in case of a positive signal of $0\nu2\beta$-decay with m_{ee} close to the heaviest of the light neutrino masses (which could be measured in direct neutrino mass search experiments). In that case one will be left with the following alternatives:

- the quark-lepton symmetry is strongly violated: there is no strong hierarchy of the eigenvalues of m_D and/or the Dirac-type left-handed mixing is large;
- type-I seesaw is not the sole source of neutrino mass; the simplest alternative could be type-II seesaw in which there is an additional contribution from an $SU(2)_L$-triplet Higgs; another possibility is that the seesaw is not the true mechanism of neutrino mass generation;
- a mechanism other than the decay of thermally produced RH neutrinos contributes to leptogenesis or the baryon asymmetry of the Universe is generated through a different mechanism, which has nothing to do with the leptogenesis scenario.

Each of these alternatives scenarios deserves further investigation, in the pathway toward the origin of neutrino masses. At the same time it would be interesting to construct a specific model for the special structure of RH neutrino sector which is favored by our analysis.

Bibliography

[1] W. Pauli, in *Neutrino physics* (K. Winter, ed.), p. 1. Cambridge University Press, 1991.

[2] E. Fermi, *Trends to a theory of beta radiation. (in italian)*, *Nuovo Cim.* **11** (1934) 1–19.

[3] G. Gamow and E. Teller, *Selection rules for the beta disintegration*, *Phys. Rev.* **49** (1936) 895–899.

[4] F. Perrin, *Comptes Rendues* **197** (1933) 1625.

[5] F. Reines and C. L. Cowan, *Detection of the free neutrino*, *Phys. Rev.* **92** (1953) 830–831.

[6] R. Davis and D. S. Harmer, *An attempt to observe the 37 cl (, e-) 37 ar reaction induced by reactor antineutrinos*, *Bull. Am. Phys. Soc.* **4** (1959) 217.

[7] C. S. Wu, E. Ambler, R. W. Hayward, D. D. Hoppes, and R. P. Hudson, *Experimental test of parity conservation in beta decay*, *Phys. Rev.* **105** (1957) 1413–1414.

[8] L. D. Landau, *On the conservation laws for weak interactions*, *Nucl. Phys.* **3** (1957) 127–131.

[9] A. Salam, *On parity conservation and neutrino mass*, *Nuovo Cim.* **5** (1957) 299–301.

[10] T. D. Lee and C.-N. Yang, *Parity nonconservation and a two component theory of the neutrino*, *Phys. Rev.* **105** (1957) 1671–1675.

[11] M. Goldhaber, L. Grodzins, and A. W. Sunyar, *Helicity of neutrinos*, *Phys. Rev.* **109** (1958) 1015–1017.

[12] B. Pontecorvo, *Mesonium and antimesonium*, *Sov. Phys. JETP* **6** (1957) 429.

[13] B. Pontecorvo, *Inverse beta processes and nonconservation of lepton charge*, *Sov. Phys. JETP* **7** (1958) 172–173.

[14] B. Pontecorvo, *Universal fermi interaction and astrophysics*, *Zh. Eksp. Teor. Fiz.* **36** (1959) 1615.

[15] B. Pontecorvo, *Electron and muon neutrinos*, *Sov. Phys. JETP* **10** (1960) 1236–1240.

[16] G. Danby *et. al.*, *Observation of high-energy neutrino reactions and the existence of two kinds of neutrinos*, *Phys. Rev. Lett.* **9** (1962) 36–44.

[17] Z. Maki, M. Nakagawa, and S. Sakata, *Remarks on the unified model of elementary particles*, *Prog. Theor. Phys.* **28** (1962) 870.

[18] S. M. Bilenky and B. Pontecorvo, *Lepton mixing and neutrino oscillations*, *Phys. Rept.* **41** (1978) 225–261.

[19] B. Pontecorvo, *Neutrino experiments and the question of leptonic-charge conservation*, *Sov. Phys. JETP* **26** (1968) 984–988.

[20] V. N. Gribov and B. Pontecorvo, *Neutrino astronomy and lepton charge*, *Phys. Lett.* **B28** (1969) 493.

[21] B. T. Cleveland *et. al.*, *Measurement of the solar electron neutrino flux with the homestake chlorine detector*, *Astrophys. J.* **496** (1998) 505–526.

[22] **Kamiokande** Collaboration, Y. Fukuda *et. al.*, *Solar neutrino data covering solar cycle 22*, *Phys. Rev. Lett.* **77** (1996) 1683–1686.

[23] **Super-Kamiokande** Collaboration, S. Fukuda *et. al.*, *Constraints on neutrino oscillations using 1258 days of super-kamiokande solar neutrino data*, *Phys. Rev. Lett.* **86** (2001) 5656–5660, [hep-ex/0103033].

[24] **Super-Kamiokande** Collaboration, S. Fukuda *et. al.*, *Determination of solar neutrino oscillation parameters using 1496 days of super-kamiokande-i data*, *Phys. Lett.* **B539** (2002) 179–187, [hep-ex/0205075].

[25] **GALLEX** Collaboration, W. Hampel *et. al.*, *Gallex solar neutrino observations: Results for gallex iv*, *Phys. Lett.* **B447** (1999) 127–133.

[26] **GNO** Collaboration, M. Altmann *et. al.*, *Gno solar neutrino observations: Results for gno i*, *Phys. Lett.* **B490** (2000) 16–26, [hep-ex/0006034].

[27] **SAGE** Collaboration, J. N. Abdurashitov *et. al.*, *Measurement of the solar neutrino capture rate by the russian-american gallium solar neutrino experiment during one half of the 22-year cycle of solar activity*, *J. Exp. Theor. Phys.* **95** (2002) 181–193, [astro-ph/0204245].

[28] **SNO** Collaboration, Q. R. Ahmad *et. al.*, *Measurement of the charged current interactions produced by b-8 solar neutrinos at the sudbury neutrino observatory*, *Phys. Rev. Lett.* **87** (2001) 071301, [nucl-ex/0106015].

[29] **SNO** Collaboration, Q. R. Ahmad *et. al.*, *Direct evidence for neutrino flavor transformation from neutral-current interactions in the sudbury neutrino observatory*, *Phys. Rev. Lett.* **89** (2002) 011301, [nucl-ex/0204008].

[30] **SNO** Collaboration, Q. R. Ahmad *et. al.*, *Measurement of day and night neutrino energy spectra at sno and constraints on neutrino mixing parameters*, *Phys. Rev. Lett.* **89** (2002) 011302, [nucl-ex/0204009].

[31] L. Wolfenstein, *Neutrino oscillations in matter*, *Phys. Rev.* **D17** (1978) 2369.

[32] S. P. Mikheev and A. Y. Smirnov, *Resonance enhancement of oscillations in matter and solar neutrino spectroscopy*, *Sov. J. Nucl. Phys.* **42** (1985) 913–917.

[33] S. P. Mikheev and A. Y. Smirnov, *Resonant amplification of neutrino oscillations in matter and solar neutrino spectroscopy*, *Nuovo Cim.* **C9** (1986) 17–26.

[34] **KamLAND** Collaboration, K. Eguchi *et. al.*, *First results from kamland: Evidence for reactor anti- neutrino disappearance*, *Phys. Rev. Lett.* **90** (2003) 021802, [hep-ex/0212021].

[35] V. Barger and D. Marfatia, *Kamland and solar neutrino data eliminate the low solution*, *Phys. Lett.* **B555** (2003) 144–146, [hep-ph/0212126].

[36] G. L. Fogli *et. al.*, *Solar neutrino oscillation parameters after first kamland results*, *Phys. Rev.* **D67** (2003) 073002, [hep-ph/0212127].

[37] M. Maltoni, T. Schwetz, and J. W. F. Valle, *Combining first kamland results with solar neutrino data*, *Phys. Rev.* **D67** (2003) 093003, [hep-ph/0212129].

[38] P. Creminelli, G. Signorelli, and A. Strumia, *Frequentist analyses of solar neutrino data*, *JHEP* **05** (2001) 052, [hep-ph/0102234 v4].

[39] A. Bandyopadhyay, S. Choubey, R. Gandhi, S. Goswami, and D. P. Roy, *The solar neutrino problem after the first results from kamland*, *Phys. Lett.* **B559** (2003) 121–130, [hep-ph/0212146].

[40] J. N. Bahcall, M. C. Gonzalez-Garcia, and C. Pena-Garay, *Solar neutrinos before and after kamland*, *JHEP* **02** (2003) 009, [hep-ph/0212147].

[41] H. Nunokawa, W. J. C. Teves, and R. Zukanovich Funchal, *Determining the oscillation parameters by solar neutrinos and kamland*, *Phys. Lett.* **B562** (2003) 28–35, [hep-ph/0212202].

[42] P. Aliani, V. Antonelli, M. Picariello, and E. Torrente-Lujan, *Neutrino mass parameters from kamland, sno and other solar evidence*, hep-ph/0212212.

[43] P. C. de Holanda and A. Y. Smirnov, *Lma msw solution of the solar neutrino problem and first kamland results*, *JCAP* **0302** (2003) 001, [hep-ph/0212270].

[44] **KAMIOKANDE-II** Collaboration, K. S. Hirata *et. al.*, *Experimental study of the atmospheric neutrino flux*, *Phys. Lett.* **B205** (1988) 416.

[45] **Kamiokande** Collaboration, Y. Fukuda *et. al.*, *Atmospheric muon-neutrino / electron-neutrino ratio in the multigev energy range*, *Phys. Lett.* **B335** (1994) 237–245.

[46] R. Clark *et. al.*, *Atmospheric muon-neutrino fraction above 1-gev*, *Phys. Rev. Lett.* **79** (1997) 345–348.

[47] **Super-Kamiokande** Collaboration, Y. Fukuda *et. al.*, *Evidence for oscillation of atmospheric neutrinos*, *Phys. Rev. Lett.* **81** (1998) 1562–1567, [hep-ex/9807003].

[48] **Soudan-2** Collaboration, W. W. M. Allison *et. al.*, *The atmospheric neutrino flavor ratio from a 3.9 fiducial kiloton-year exposure of soudan 2*, *Phys. Lett.* **B449** (1999) 137–144, [hep-ex/9901024].

[49] **MACRO** Collaboration, M. Ambrosio *et. al.*, *Matter effects in upward-going muons and sterile neutrino oscillations*, *Phys. Lett.* **B517** (2001) 59–66, [hep-ex/0106049].

[50] **K2K** Collaboration, M. H. Ahn *et. al.*, *Indications of neutrino oscillation in a 250-km long- baseline experiment*, *Phys. Rev. Lett.* **90** (2003) 041801, [hep-ex/0212007].

[51] G. L. Fogli, E. Lisi, A. Marrone, and D. Montanino, *Status of atmospheric nu/mu –¿ nu/tau oscillations and decoherence after the first k2k spectral data*, *Phys. Rev.* **D67** (2003) 093006, [hep-ph/0303064].

[52] **CHOOZ** Collaboration, M. Apollonio *et. al.*, *Limits on neutrino oscillations from the chooz experiment*, *Phys. Lett.* **B466** (1999) 415–430, [hep-ex/9907037].

[53] F. Boehm *et. al.*, *Final results from the palo verde neutrino oscillation experiment*, *Phys. Rev.* **D64** (2001) 112001, [hep-ex/0107009].

[54] H. V. Klapdor-Kleingrothaus *et. al.*, *Latest results from the heidelberg-moscow double-beta-decay experiment*, *Eur. Phys. J.* **A12** (2001) 147–154, [hep-ph/0103062].

[55] **IGEX** Collaboration, C. E. Aalseth *et. al.*, *The igex ge-76 neutrinoless double-beta decay experiment: Prospects for next generation experiments*, *Phys. Rev.* **D65** (2002) 092007, [hep-ex/0202026].

[56] W. Hu, D. J. Eisenstein, and M. Tegmark, *Weighing neutrinos with galaxy surveys*, *Phys. Rev. Lett.* **80** (1998) 5255–5258, [astro-ph/9712057].

[57] M. Fukugita, G.-C. Liu, and N. Sugiyama, *Limits on neutrino mass from cosmic structure formation*, *Phys. Rev. Lett.* **84** (2000) 1082–1085, [hep-ph/9908450].

[58] O. Elgaroy *et. al.*, *A new limit on the total neutrino mass from the 2df galaxy redshift survey*, *Phys. Rev. Lett.* **89** (2002) 061301, [astro-ph/0204152].

[59] K. Kainulainen and K. A. Olive, *Astrophysical and cosmological constraints on neutrino masses*, hep-ph/0206163.

[60] D. N. Spergel *et. al.*, *First year wilkinson microwave anisotropy probe (wmap) observations: Determination of cosmological parameters*, astro-ph/0302209.

[61] S. Hannestad, *Neutrino masses and the number of neutrino species from wmap and 2dfgrs*, astro-ph/0303076.

[62] S. W. Allen, R. W. Schmidt, and S. L. Bridle, *A preference for a non-zero neutrino mass from cosmological data*, astro-ph/0306386.

[63] E. Majorana, *Theory of the symmetry of electrons and positrons*, *Nuovo Cim.* **14** (1937) 171–184.

[64] G. Racah, *On the symmetry of particle and antiparticle*, *Nuovo Cim.* **14** (1937) 322–328. In *Klapdor-Kleingrothaus, H.V.: Sixty years of double beta decay* 110-116.

[65] B. Kayser, *Neutrino mass, mixing, and flavor change*, hep-ph/0211134.

[66] J. H. Christenson, J. W. Cronin, V. L. Fitch, and R. Turlay, *Evidence for the 2 pi decay of the k(2)0 meson*, *Phys. Rev. Lett.* **13** (1964) 138–140.

[67] S. M. Bilenky, J. Hosek, and S. T. Petcov, *On oscillations of neutrinos with dirac and majorana masses*, *Phys. Lett.* **B94** (1980) 495.

[68] J. Schechter and J. W. F. Valle, *Neutrino oscillation thought experiment*, *Phys. Rev.* **D23** (1981) 1666.

[69] C. D. Froggatt and H. B. Nielsen, *Hierarchy of quark masses, cabibbo angles and cp violation*, *Nucl. Phys.* **B147** (1979) 277.

[70] E. Papageorgiu, *Yukawa textures from an extra u(1) symmetry?*, *Z. Phys.* **C64** (1994) 509–514, [hep-ph/9405256].

[71] P. Binetruy, S. Lavignac, and P. Ramond, *Yukawa textures with an anomalous horizontal abelian symmetry*, *Nucl. Phys.* **B477** (1996) 353–377, [hep-ph/9601243].

[72] J. K. Elwood, N. Irges, and P. Ramond, *Family symmetry and neutrino mixing*, *Phys. Rev. Lett.* **81** (1998) 5064–5067, [hep-ph/9807228].

[73] G. Altarelli and F. Feruglio, *A simple grand unification view of neutrino mixing and fermion mass matrices*, *Phys. Lett.* **B451** (1999) 388–396, [hep-ph/9812475].

[74] S. Lola and G. G. Ross, *Neutrino masses from u(1) symmetries and the super-kamiokande data*, *Nucl. Phys.* **B553** (1999) 81–107, [hep-ph/9902283].

[75] S. F. King, *Large mixing angle msw and atmospheric neutrinos from single right-handed neutrino dominance and u(1) family symmetry*, *Nucl. Phys.* **B576** (2000) 85–105, [hep-ph/9912492].

[76] K. Choi, E. J. Chun, K. Hwang, and W. Y. Song, *Bi-maximal neutrino mixing and small u(e3) from abelian flavor symmetry*, *Phys. Rev.* **D64** (2001) 113013, [hep-ph/0107083].

[77] D. B. Kaplan and M. Schmaltz, *Flavor unification and discrete nonabelian symmetries*, *Phys. Rev.* **D49** (1994) 3741–3750, [hep-ph/9311281].

[78] M. Fukugita, M. Tanimoto, and T. Yanagida, *Atmospheric neutrino oscillation and a phenomenological lepton mass matrix*, *Phys. Rev.* **D57** (1998) 4429–4432, [hep-ph/9709388].

[79] Z. Berezhiani and A. Rossi, *Grand unified textures for neutrino and quark mixings*, *JHEP* **03** (1999) 002, [hep-ph/9811447].

[80] P. H. Frampton and A. Rasin, *Nonabelian discrete symmetries, fermion mass textures and large neutrino mixing*, *Phys. Lett.* **B478** (2000) 424–433, [hep-ph/9910522].

[81] H. Fritzsch and Z.-z. Xing, *Mass and flavor mixing schemes of quarks and leptons*, *Prog. Part. Nucl. Phys.* **45** (2000) 1–81, [hep-ph/9912358].

[82] S. M. Barr and I. Dorsner, *A general classification of three neutrino models and u(e3)*, *Nucl. Phys.* **B585** (2000) 79–104, [hep-ph/0003058].

[83] R. Barbieri, L. J. Hall, D. R. Smith, A. Strumia, and N. Weiner, *Oscillations of solar and atmospheric neutrinos*, *JHEP* **12** (1998) 017, [hep-ph/9807235].

[84] R. Barbieri, L. J. Hall, and A. Strumia, *Textures for atmospheric and solar neutrino oscillations*, *Phys. Lett.* **B445** (1999) 407–411, [hep-ph/9808333].

[85] F. Vissani, *Large mixing, family structure, and dominant block in the neutrino mass matrix*, *JHEP* **11** (1998) 025, [hep-ph/9810435].

[86] A. Abada and M. Losada, *Constraints on a general 3-generation neutrino mass matrix from neutrino data: Application to the mssm with r-parity violation*, *Nucl. Phys.* **B585** (2000) 45–78, [hep-ph/9908352].

[87] E. K. Akhmedov, *Small entries of neutrino mass matrices*, *Phys. Lett.* **B467** (1999) 95–105, [hep-ph/9909217].

[88] F. Vissani, *Expected properties of massive neutrinos for mass matrices with a dominant block and random coefficients order unity*, *Phys. Lett.* **B508** (2001) 79–84, [hep-ph/0102236].

[89] F. Vissani, *A statistical approach to leptonic mixings and neutrino masses*, hep-ph/0111373.

[90] T. Hambye, *Neutrino mass matrix solutions and neutrinoless double beta decay*, *Eur. Phys. J. direct* **C4** (2002) 13, [hep-ph/0201307].

[91] H. V. Klapdor-Kleingrothaus and U. Sarkar, *Neutrino mixing schemes and neutrinoless double beta decay*, *Phys. Lett.* **B532** (2002) 71–76, [hep-ph/0202006].

[92] J. Sato and T. Yanagida, *Low-energy predictions of lopsided family charges*, *Phys. Lett.* **B493** (2000) 356–365, [hep-ph/0009205].

[93] G. Altarelli and F. Feruglio, *Neutrino masses and mixings: A theoretical perspective*, *Phys. Rept.* **320** (1999) 295–318.

[94] S. T. Petcov, *On pseudodirac neutrinos, neutrino oscillations and neutrinoless double beta decay*, *Phys. Lett.* **B110** (1982) 245–249.

[95] F. Feruglio, A. Strumia, and F. Vissani, *Neutrino oscillations and signals in beta and 0nu 2beta experiments*, *Nucl. Phys.* **B637** (2002) 345–377, [hep-ph/0201291].

[96] H. Fritzsch and Z.-Z. Xing, *Lepton mass hierarchy and neutrino oscillations*, *Phys. Lett.* **B372** (1996) 265–270, [hep-ph/9509389].

[97] G. C. Branco, M. N. Rebelo, and J. I. Silva-Marcos, *Large neutrino mixing with universal strength of yukawa couplings*, *Phys. Rev.* **D62** (2000) 073004, [hep-ph/9906368].

[98] E. K. Akhmedov, G. C. Branco, F. R. Joaquim, and J. I. Silva-Marcos, *Neutrino masses and mixing with seesaw mechanism and universal breaking of extended democracy*, *Phys. Lett.* **B498** (2001) 237–250, [hep-ph/0008010].

[99] K. Fukuura, T. Miura, E. Takasugi, and M. Yoshimura, *Maximal cp violation, large mixings of neutrinos and democratic-type neutrino mass matrix*, *Phys. Rev.* **D61** (2000) 073002, [hep-ph/9909415].

[100] L. J. Hall, H. Murayama, and N. Weiner, *Neutrino mass anarchy*, *Phys. Rev. Lett.* **84** (2000) 2572–2575, [hep-ph/9911341].

[101] N. Haba and H. Murayama, *Anarchy and hierarchy*, *Phys. Rev.* **D63** (2001) 053010, [hep-ph/0009174].

[102] A. de Gouvea and H. Murayama, *Statistical test of anarchy*, hep-ph/0301050.

[103] G. Altarelli, F. Feruglio, and I. Masina, *Models of neutrino masses: Anarchy versus hierarchy*, *JHEP* **01** (2003) 035, [hep-ph/0210342].

[104] J. R. Espinosa, *Anarchy in the neutrino sector?*, hep-ph/0306019.

[105] S. Weinberg, *Baryon and lepton nonconserving processes*, *Phys. Rev. Lett.* **43** (1979) 1566–1570.

[106] S. Weinberg, *Varieties of baryon and lepton nonconservation*, *Phys. Rev.* **D22** (1980) 1694.

[107] P. H. Chankowski and Z. Pluciennik, *Renormalization group equations for seesaw neutrino masses*, *Phys. Lett.* **B316** (1993) 312–317, [hep-ph/9306333].

[108] K. S. Babu, C. N. Leung, and J. Pantaleone, *Renormalization of the neutrino mass operator*, *Phys. Lett.* **B319** (1993) 191–198, [hep-ph/9309223].

[109] S. Antusch, M. Drees, J. Kersten, M. Lindner, and M. Ratz, *Neutrino mass operator renormalization revisited*, *Phys. Lett.* **B519** (2001) 238–242, [hep-ph/0108005].

[110] J. A. Casas, J. R. Espinosa, A. Ibarra, and I. Navarro, *General rg equations for physical neutrino parameters and their phenomenological implications*, *Nucl. Phys.* **B573** (2000) 652–684, [hep-ph/9910420].

[111] E. J. Chun and S. Pokorski, *Slepton flavour mixing and neutrino masses*, *Phys. Rev.* **D62** (2000) 053001, [hep-ph/9912210].

[112] P. H. Chankowski, A. Ioannisian, S. Pokorski, and J. W. F. Valle, *Neutrino unification*, *Phys. Rev. Lett.* **86** (2001) 3488–3491, [hep-ph/0011150].

[113] P. H. Chankowski and P. Wasowicz, *Low energy threshold corrections to neutrino masses and mixing angles*, *Eur. Phys. J.* **C23** (2002) 249–258, [hep-ph/0110237].

[114] J. A. Casas, J. R. Espinosa, and I. Navarro, *New supersymmetric source of neutrino masses and mixings*, *Phys. Rev. Lett.* **89** (2002) 161801, [hep-ph/0206276].

[115] J. A. Casas, J. R. Espinosa, and I. Navarro, *Large mixing angles for neutrinos from infrared fixed points*, hep-ph/0306243.

[116] M. Gell-Mann, P. Ramond, and R. Slansky, *Complex spinors and unified theories*, . Print-80-0576 (CERN), in Supergravity, P. van Nieuwenhuizen and D.Z. Freedman ed., North Holland, Amsterdam 1979, p.315.

[117] T. Yanagida, *Horizontal gauge symmetry and masses of neutrinos*, . In proc. of the *Workshop on the Unified Theory and Baryon Number in the Universe*, O.Sawada and A.Sugamoto eds., KEK report 79-18, 1979, p.95, Tsukuba, Japan.

[118] S. L. Glashow, *The future of elementary particle physics*, . In *Cargese 1979, Proceedings, Quarks and Leptons*, 687-713 and Harvard Univ.Cambridge - HUTP-79-A059 (79,REC.DEC.) 40p.

[119] R. N. Mohapatra and G. Senjanovic, *Neutrino mass and spontaneous parity nonconservation*, *Phys. Rev. Lett.* **44** (1980) 912.

[120] N. Haba, N. Okamura, and M. Sugiura, *The renormalization group analysis of the large lepton flavor mixing and the neutrino mass*, *Prog. Theor. Phys.* **103** (2000) 367–377, [hep-ph/9810471].

[121] J. A. Casas, J. R. Espinosa, A. Ibarra, and I. Navarro, *Nearly degenerate neutrinos, supersymmetry and radiative corrections*, *Nucl. Phys.* **B569** (2000) 82–106, [hep-ph/9905381].

[122] S. Antusch, J. Kersten, M. Lindner, and M. Ratz, *Neutrino mass matrix running for non-degenerate see-saw scales*, *Phys. Lett.* **B538** (2002) 87–95, [hep-ph/0203233].

[123] S. T. Petcov and A. Y. Smirnov, *Neutrinoless double beta decay and the solar neutrino problem*, *Phys. Lett.* **B322** (1994) 109–118, [hep-ph/9311204].

[124] M. Fukugita and T. Yanagida, *Baryogenesis without grand unification*, *Phys. Lett.* **B174** (1986) 45.

[125] A. S. Joshipura, E. A. Paschos, and W. Rodejohann, *A simple connection between neutrino oscillation and leptogenesis*, *JHEP* **08** (2001) 029, [hep-ph/0105175].

[126] M. Hirsch and S. F. King, *Leptogenesis with single right-handed neutrino dominance*, *Phys. Rev.* **D64** (2001) 113005, [hep-ph/0107014].

[127] T. Hambye, *Leptogenesis at the tev scale*, *Nucl. Phys.* **B633** (2002) 171–192, [hep-ph/0111089].

[128] J. R. Ellis and M. Raidal, *Leptogenesis and the violation of lepton number and cp at low energies*, *Nucl. Phys.* **B643** (2002) 229–246, [hep-ph/0206174].

[129] J. R. Ellis, M. Raidal, and T. Yanagida, *Observable consequences of partially degenerate leptogenesis*, *Phys. Lett.* **B546** (2002) 228–236, [hep-ph/0206300].

[130] L. Boubekeur, *Leptogenesis at low scale*, hep-ph/0208003.

[131] G. C. Branco *et. al.*, *Minimal scenarios for leptogenesis and cp violation*, *Phys. Rev.* **D67** (2003) 073025, [hep-ph/0211001].

[132] F. Vissani and A. Y. Smirnov, *Neutrino masses and b - tau unification in the supersymmetric standard model*, *Phys. Lett.* **B341** (1994) 173–180, [hep-ph/9405399].

[133] A. Brignole, H. Murayama, and R. Rattazzi, *Upper bound on hot dark matter density from so(10) yukawa unification*, *Phys. Lett.* **B335** (1994) 345–354, [hep-ph/9406397].

[134] F. Borzumati and A. Masiero, *Large muon and electron number violations in supergravity theories*, *Phys. Rev. Lett.* **57** (1986) 961.

[135] S. Lavignac, I. Masina, and C. A. Savoy, *tau -¿ mu gamma and mu -¿ e gamma as probes of neutrino mass models*, *Phys. Lett.* **B520** (2001) 269–278, [hep-ph/0106245].

[136] A. Y. Smirnov, *Seesaw enhancement of lepton mixing*, *Phys. Rev.* **D48** (1993) 3264–3270, [hep-ph/9304205].

[137] M. Tanimoto, *Seesaw enhancement of neutrino mixing due to the right- handed phases*, *Phys. Lett.* **B345** (1995) 477–482, [hep-ph/9503318].

[138] G. Altarelli, F. Feruglio, and I. Masina, *Large neutrino mixing from small quark and lepton mixings*, *Phys. Lett.* **B472** (2000) 382–391, [hep-ph/9907532].

[139] T. K. Kuo, G.-H. Wu, and S. W. Mansour, *Mass hierarchies and the seesaw neutrino mixing*, *Phys. Rev.* **D61** (2000) 111301, [hep-ph/9912366].

[140] T. K. Kuo, S.-H. Chiu, and G.-H. Wu, *Neutrino mixing in the seesaw model*, *Eur. Phys. J.* **C21** (2001) 281–289, [hep-ph/0011058].

[141] M. Patgiri and N. N. Singh, *Right-handed majorana neutrino mass matrices for generating bimaximal mixings in degenerate and inverted models of neutrinos*, *Int. J. Mod. Phys.* **A18** (2003) 743–754, [hep-ph/0301254].

[142] K. S. Babu and S. M. Barr, *Large neutrino mixing angles in unified theories*, *Phys. Lett.* **B381** (1996) 202–208, [hep-ph/9511446].

[143] S. F. King, *Atmospheric and solar neutrinos with a heavy singlet*, *Phys. Lett.* **B439** (1998) 350–356, [hep-ph/9806440].

[144] S. F. King, *Large mixing angle msw and atmospheric neutrinos from single right-handed neutrino dominance and u(1) family symmetry*, *Nucl. Phys.* **B576** (2000) 85–105, [hep-ph/9912492].

[145] S. M. Barr and I. Dorsner, *A general classification of three neutrino models and u(e3)*, *Nucl. Phys.* **B585** (2000) 79–104, [hep-ph/0003058].

[146] M. S. Berger and B. Brahmachari, *Leptogenesis and yukawa textures*, *Phys. Rev.* **D60** (1999) 073009, [hep-ph/9903406].

[147] D. Falcone and F. Tramontano, *Leptogenesis and neutrino parameters*, *Phys. Rev.* **D63** (2001) 073007, [hep-ph/0011053].

[148] D. Falcone, *Lepton number and lepton flavor violations in seesaw models*, *Mod. Phys. Lett.* **A17** (2002) 2467, [hep-ph/0207308].

[149] E. Nezri and J. Orloff, *Neutrino oscillations vs. leptogenesis in so(10) models*, hep-ph/0004227.

[150] G. C. Branco, R. Gonzalez Felipe, F. R. Joaquim, and M. N. Rebelo, *Leptogenesis, cp violation and neutrino data: What can we learn?*, *Nucl. Phys.* **B640** (2002) 202–232, [hep-ph/0202030].

[151] D. Falcone, *Seesaw mechanism, baryon asymmetry and neutrinoless double beta decay*, *Phys. Rev.* **D66** (2002) 053001, [hep-ph/0204335].

[152] D. Falcone, *Inverting the seesaw formula*, hep-ph/0305229.

[153] M. Frigerio and A. Y. Smirnov, *Structure of neutrino mass matrix and cp violation*, *Nucl. Phys.* **B640** (2002) 233–282, [hep-ph/0202247].

[154] M. Frigerio and A. Y. Smirnov, *Neutrino mass matrix: Inverted hierarchy and cp violation*, *Phys. Rev.* **D67** (2003) 013007, [hep-ph/0207366].

[155] L. Wolfenstein, *Cp properties of majorana neutrinos and double beta decay*, *Phys. Lett.* **B107** (1981) 77.

[156] S. M. Bilenky, N. P. Nedelcheva, and S. T. Petcov, *Some implications of the cp invariance for mixing of majorana neutrinos*, *Nucl. Phys.* **B247** (1984) 61.

[157] P. H. Frampton, S. L. Glashow, and D. Marfatia, *Zeroes of the neutrino mass matrix*, *Phys. Lett.* **B536** (2002) 79–82, [hep-ph/0201008].

[158] S. Lavignac, I. Masina, and C. A. Savoy, *Large solar angle and seesaw mechanism: A bottom-up perspective*, *Nucl. Phys.* **B633** (2002) 139–170, [hep-ph/0202086].

[159] Z.-z. Xing, *Texture zeros and majorana phases of the neutrino mass matrix*, *Phys. Lett.* **B530** (2002) 159–166, [hep-ph/0201151].

[160] P. H. Frampton, M. C. Oh, and T. Yoshikawa, *Majorana mass zeroes from triplet vev without majoron problem*, *Phys. Rev.* **D66** (2002) 033007, [hep-ph/0204273].

[161] A. Kageyama, S. Kaneko, N. Shimoyama, and M. Tanimoto, *See-saw realization of the texture zeros in the neutrino mass matrix*, *Phys. Lett.* **B538** (2002) 96–106, [hep-ph/0204291].

[162] **Super-Kamiokande** Collaboration, T. Nakaya, *Atmospheric and long baseline neutrino*, *eConf* **C020620** (2002) SAAT01, [hep-ex/0209036].

[163] G. L. Fogli *et. al.*, *Addendum to: Solar neutrino oscillation parameters after first kamland results*, hep-ph/0308055.

[164] J. Bonn *et. al.*, *The mainz neutrino mass experiment*, *Nucl. Phys. Proc. Suppl.* **91** (2001) 273–279.

[165] V. M. Lobashev *et. al.*, *Direct search for neutrino mass and anomaly in the tritium beta-spectrum: Status of 'troitsk neutrino mass' experiment*, *Nucl. Phys. Proc. Suppl.* **91** (2001) 280–286.

[166] A. Y. Smirnov, D. N. Spergel, and J. N. Bahcall, *Is large lepton mixing excluded?*, *Phys. Rev.* **D49** (1994) 1389–1397, [hep-ph/9305204].

[167] B. Jegerlehner, F. Neubig, and G. Raffelt, *Neutrino oscillations and the supernova 1987a signal*, *Phys. Rev.* **D54** (1996) 1194–1203, [astro-ph/9601111].

[168] H. Minakata and H. Nunokawa, *Inverted hierarchy of neutrino masses disfavored by supernova 1987a*, *Phys. Lett.* **B504** (2001) 301–308, [hep-ph/0010240].

[169] C. Lunardini and A. Y. Smirnov, *Neutrinos from sn1987a, earth matter effects and the lma solution of the solar neutrino problem*, *Phys. Rev.* **D63** (2001) 073009, [hep-ph/0009356].

[170] C. Lunardini and A. Y. Smirnov, *Supernova neutrinos: Earth matter effects and neutrino mass spectrum*, *Nucl. Phys.* **B616** (2001) 307–348, [hep-ph/0106149].

[171] V. Barger, D. Marfatia, and B. P. Wood, *Supernova 1987a did not test the neutrino mass hierarchy*, *Phys. Lett.* **B532** (2002) 19–28, [hep-ph/0202158].

[172] K. Takahashi and K. Sato, *Effects of neutrino oscillation on supernova neutrino: Inverted mass hierarchy*, *Prog. Theor. Phys.* **109** (2003) 919–931, [hep-ph/0205070].

[173] R. Buras, H.-T. Janka, M. T. Keil, G. G. Raffelt, and M. Rampp, *Electron-neutrino pair annihilation: A new source for muon and tau neutrinos in supernovae*, *Astrophys. J.* **587** (2003) 320–326, [astro-ph/0205006].

[174] **Particle Data Group** Collaboration, K. Hagiwara *et. al.*, *Review of particle physics*, *Phys. Rev.* **D66** (2002) 010001.

[175] M. Lindner, *The physics potential of future long baseline neutrino oscillation experiments*, hep-ph/0210377.

[176] M. Apollonio *et. al.*, *Oscillation physics with a neutrino factory*, hep-ph/0210192.

[177] H. V. Klapdor-Kleingrothaus, A. Dietz, H. L. Harney, and I. V. Krivosheina, *Evidence for neutrinoless double beta decay*, *Mod. Phys. Lett.* **A16** (2001) 2409–2420, [hep-ph/0201231].

[178] C. E. Aalseth *et. al.*, *Comment on 'evidence for neutrinoless double beta decay'*, *Mod. Phys. Lett.* **A17** (2002) 1475–1478, [hep-ex/0202018].

[179] H. V. Klapdor-Kleingrothaus, *Reply to a comment of article 'evidence for neutrinoless double beta decay'*, hep-ph/0205228.

[180] H. L. Harney, *Reply to the comment on 'evidence for neutrinoless double beta decay'. (mod. phys. lett. a16(2001) 2409)*, hep-ph/0205293.

[181] F. Vissani, *Signal of neutrinoless double beta decay, neutrino spectrum and oscillation scenarios*, *JHEP* **06** (1999) 022, [hep-ph/9906525].

[182] H. Nishiura, K. Matsuda, and T. Fukuyama, *Constraints of mixing angles from lepton number violating processes*, *Mod. Phys. Lett.* **A14** (1999) 433–446, [hep-ph/9809556].

[183] W. Rodejohann, *Neutrino oscillation experiments and limits on lepton number and lepton flavor violating processes*, *Phys. Rev.* **D62** (2000) 013011, [hep-ph/0003149].

[184] K. Zuber, *Effective majorana neutrino masses*, hep-ph/0008080.

[185] W. Rodejohann, *Phenomenological aspects of light and heavy majorana neutrinos*, *J. Phys.* **G28** (2002) 1477–1498.

[186] H. V. Klapdor-Kleingrothaus, H. Pas, and A. Y. Smirnov, *Neutrino mass spectrum and neutrinoless double beta decay*, *Phys. Rev.* **D63** (2001) 073005, [hep-ph/0003219].

[187] F. Vissani, *A study of the scenario with nearly degenerate majorana neutrinos*, hep-ph/9708483.

[188] H. Minakata and O. Yasuda, *Constraining almost degenerate three-flavor neutrinos*, *Phys. Rev.* **D56** (1997) 1692–1697, [hep-ph/9609276].

[189] W. Rodejohann, *On cancellations in neutrinoless double beta decay*, *Nucl. Phys.* **B597** (2001) 110–126, [hep-ph/0008044].

[190] D. O. Caldwell and R. N. Mohapatra, *An inverted neutrino mass hierarchy for hot dark matter and the solar neutrino deficit*, *Phys. Lett.* **B354** (1995) 371–375, [hep-ph/9503316].

[191] S. F. King and N. N. Singh, *Inverted hierarchy models of neutrino masses*, *Nucl. Phys.* **B596** (2001) 81–98, [hep-ph/0007243].

[192] K. S. Babu and S. M. Barr, *Bimaximal neutrino mixings from lopsided mass matrices*, *Phys. Lett.* **B525** (2002) 289–296, [hep-ph/0111215].

[193] H.-J. He, D. A. Dicus, and J. N. Ng, *Minimal schemes for large neutrino mixings with inverted hierarchy*, *Phys. Lett.* **B536** (2002) 83–93, [hep-ph/0203237].

[194] H. S. Goh, R. N. Mohapatra, and S. P. Ng, *Testing neutrino mass matrices with approximate l(e) - l(mu) - l(tau) symmetry*, *Phys. Lett.* **B542** (2002) 116–122, [hep-ph/0205131].

[195] **KATRIN** Collaboration, A. Osipowicz *et. al.*, *Katrin: A next generation tritium beta decay experiment with sub-ev sensitivity for the electron neutrino mass*, hep-ex/0109033.

[196] S. Hannestad, *Cosmological limit on the neutrino mass*, *Phys. Rev.* **D66** (2002) 125011, [astro-ph/0205223].

[197] S. Hannestad, *Can cosmology detect hierarchical neutrino masses?*, *Phys. Rev.* **D67** (2003) 085017, [astro-ph/0211106].

[198] A. Zee, *A theory of lepton number violation, neutrino majorana mass, and oscillation*, *Phys. Lett.* **B93** (1980) 389.

[199] M. Leurer, Y. Nir, and N. Seiberg, *Mass matrix models: The sequel*, *Nucl. Phys.* **B420** (1994) 468–504, [hep-ph/9310320].

[200] C. Giunti and M. Tanimoto, *Deviation of neutrino mixing from bi-maximal*, *Phys. Rev.* **D66** (2002) 053013, [hep-ph/0207096].

[201] C. Giunti and M. Tanimoto, *Cp violation in bilarge lepton mixing*, *Phys. Rev.* **D66** (2002) 113006, [hep-ph/0209169].

[202] M. Frigerio and A. Y. Smirnov, *Radiative corrections to neutrino mass matrix in the standard model and beyond*, *JHEP* **02** (2003) 004, [hep-ph/0212263].

[203] E. Ma, *Pathways to naturally small neutrino masses*, *Phys. Rev. Lett.* **81** (1998) 1171–1174, [hep-ph/9805219].

[204] R. N. Mohapatra and G. Senjanovic, *Neutrino masses and mixings in gauge models with spontaneous parity violation*, *Phys. Rev.* **D23** (1981) 165.

[205] J. Schechter and J. W. F. Valle, *Neutrino masses in su(2) x u(1) theories*, *Phys. Rev.* **D22** (1980) 2227.

[206] C. Wetterich, *Neutrino masses and the scale of b-l violation*, *Nucl. Phys.* **B187** (1981) 343.

[207] G. B. Gelmini and M. Roncadelli, *Left-handed neutrino mass scale and spontaneously broken lepton number*, *Phys. Lett.* **B99** (1981) 411.

[208] E. Ma and U. Sarkar, *Neutrino masses and leptogenesis with heavy higgs triplets*, *Phys. Rev. Lett.* **80** (1998) 5716–5719, [hep-ph/9802445].

[209] S. Antusch, J. Kersten, M. Lindner, and M. Ratz, *The lma solution from bimaximal lepton mixing at the gut scale by renormalization group running*, *Phys. Lett.* **B544** (2002) 1–10, [hep-ph/0206078].

[210] S. Antusch and M. Ratz, *Radiative generation of the lma solution from small solar neutrino mixing at the gut scale*, *JHEP* **11** (2002) 010, [hep-ph/0208136].

[211] P. H. Chankowski and S. Pokorski, *Quantum corrections to neutrino masses and mixing angles*, *Int. J. Mod. Phys.* **A17** (2002) 575–614, [hep-ph/0110249].

[212] J. R. Ellis and S. Lola, *Can neutrinos be degenerate in mass?*, *Phys. Lett.* **B458** (1999) 310–321, [hep-ph/9904279].

[213] A. S. Dighe and A. S. Joshipura, *No-go for exactly degenerate neutrinos at high scale?*, hep-ph/0010079.

[214] A. S. Joshipura, S. D. Rindani, and N. N. Singh, *Predictive framework with a pair of degenerate neutrinos at a high scale*, *Nucl. Phys.* **B660** (2003) 362–372, [hep-ph/0211378].

[215] A. S. Joshipura and S. D. Rindani, *Radiatively generated nu/e oscillations: General analysis, textures and models*, *Phys. Rev.* **D67** (2003) 073009, [hep-ph/0211404].

[216] M. B. Green and J. H. Schwarz, *Anomaly cancellation in supersymmetric d=10 gauge theory and superstring theory*, *Phys. Lett.* **B149** (1984) 117–122.

[217] M. Tanimoto, *Renormalization effect on large neutrino flavor mixing in the minimal supersymmetric standard model*, *Phys. Lett.* **B360** (1995) 41–46, [hep-ph/9508247].

[218] J. A. Casas, J. R. Espinosa, A. Ibarra, and I. Navarro, *Naturalness of nearly degenerate neutrinos*, *Nucl. Phys.* **B556** (1999) 3–22, [hep-ph/9904395].

[219] N. Haba and N. Okamura, *Stability of the lepton-flavor mixing matrix against quantum corrections*, *Eur. Phys. J.* **C14** (2000) 347–365, [hep-ph/9906481].

[220] K. R. S. Balaji, A. S. Dighe, R. N. Mohapatra, and M. K. Parida, *Generation of large flavor mixing from radiative corrections*, *Phys. Rev. Lett.* **84** (2000) 5034–5037, [hep-ph/0001310].

[221] N. Haba, Y. Matsui, and N. Okamura, *The effects of majorana phases in three-generation neutrinos*, *Eur. Phys. J.* **C17** (2000) 513–520, [hep-ph/0005075].

[222] W. Grimus and L. Lavoura, *A neutrino mass matrix with seesaw mechanism and two-loop mass splitting*, *Phys. Rev.* **D62** (2000) 093012, [hep-ph/0007011].

[223] A. S. Joshipura, *Radiative origin of solar scale and u(e3)*, *Phys. Lett.* **B543** (2002) 276–282, [hep-ph/0205038].

[224] S.-h. Chang and T. K. Kuo, *Renormalization invariants of the neutrino mass matrix*, *Phys. Rev.* **D66** (2002) 111302, [hep-ph/0205147].

[225] T. Miura, T. Shindou, and E. Takasugi, *Exploring the neutrino mass matrix at m(r) scale*, *Phys. Rev.* **D66** (2002) 093002, [hep-ph/0206207].

[226] G. Bhattacharyya, A. Raychaudhuri, and A. Sil, *Can radiative magnification of mixing angles occur for two zero neutrino mass matrix textures?*, *Phys. Rev.* **D67** (2003) 073004, [hep-ph/0211074].

[227] S. M. Bilenky, C. Giunti, J. A. Grifols, and E. Masso, *Absolute values of neutrino masses: Status and prospects*, *Phys. Rept.* **379** (2003) 69–148, [hep-ph/0211462].

[228] K. S. Babu, E. Ma, and J. W. F. Valle, *Underlying a(4) symmetry for the neutrino mass matrix and the quark mixing matrix*, *Phys. Lett.* **B552** (2003) 207–213, [hep-ph/0206292].

[229] E. Ma, *Plato's fire and the neutrino mass matrix*, *Mod. Phys. Lett.* **A17** (2002) 2361–2370, [hep-ph/0211393].

[230] E. K. Akhmedov, M. Frigerio, and A. Y. Smirnov, *Probing the seesaw mechanism with neutrino data and leptogenesis*, hep-ph/0305322.

[231] H. Fusaoka and Y. Koide, *Updated estimate of running quark masses*, *Phys. Rev.* **D57** (1998) 3986–4001, [hep-ph/9712201].

[232] H. V. Klapdor-Kleingrothaus, *Genius: A new underground observatory for non-accelerator particle physics*, *Nucl. Phys. Proc. Suppl.* **110** (2002) 364–368, [hep-ph/0206249].

[233] R. Gonzalez Felipe and F. R. Joaquim, *Is right-handed neutrino degeneracy compatible with the solar and atmospheric neutrino data?*, *JHEP* **09** (2001) 015, [hep-ph/0106226].

[234] S. L. Glashow, *Neutrinos with seesaw masses and suppressed interactions*, hep-ph/0301250.

[235] V. A. Kuzmin, V. A. Rubakov, and M. E. Shaposhnikov, *On the anomalous electroweak baryon number nonconservation in the early universe*, *Phys. Lett.* **B155** (1985) 36.

[236] M. A. Luty, *Baryogenesis via leptogenesis*, *Phys. Rev.* **D45** (1992) 455–465.

[237] M. Flanz, E. A. Paschos, and U. Sarkar, *Baryogenesis from a lepton asymmetric universe*, *Phys. Lett.* **B345** (1995) 248–252, [hep-ph/9411366].

[238] M. Plumacher, *Baryogenesis and lepton number violation*, *Z. Phys.* **C74** (1997) 549–559, [hep-ph/9604229].

[239] L. Covi, E. Roulet, and F. Vissani, *Cp violating decays in leptogenesis scenarios*, *Phys. Lett.* **B384** (1996) 169–174, [hep-ph/9605319].

[240] W. Buchmuller and M. Plumacher, *Cp asymmetry in majorana neutrino decays*, *Phys. Lett.* **B431** (1998) 354–362, [hep-ph/9710460].

[241] A. Pilaftsis, *Heavy majorana neutrinos and baryogenesis*, *Int. J. Mod. Phys.* **A14** (1999) 1811–1858, [hep-ph/9812256].

[242] W. Buchmuller, P. Di Bari, and M. Plumacher, *Cosmic microwave background, matter-antimatter asymmetry and neutrino masses*, *Nucl. Phys.* **B643** (2002) 367–390, [hep-ph/0205349].

[243] J. A. Harvey and M. S. Turner, *Cosmological baryon and lepton number in the presence of electroweak fermion number violation*, *Phys. Rev.* **D42** (1990) 3344–3349.

[244] E. W. Kolb and M. S. Turner, . The Early universe, Addison-Wesley (1990)

[245] H. B. Nielsen and Y. Takanishi, *Baryogenesis via lepton number violation in anti-gut model*, *Phys. Lett.* **B507** (2001) 241–251, [hep-ph/0101307].

[246] S. Davidson and A. Ibarra, *A lower bound on the right-handed neutrino mass from leptogenesis*, *Phys. Lett.* **B535** (2002) 25–32, [hep-ph/0202239].

[247] W. Buchmuller, P. Di Bari, and M. Plumacher, *The neutrino mass window for baryogenesis*, hep-ph/0302092.

[248] H. Murayama and T. Yanagida, *Leptogenesis in supersymmetric standard model with right- handed neutrino*, *Phys. Lett.* **B322** (1994) 349–354, [hep-ph/9310297].

[249] G. F. Giudice, M. Peloso, A. Riotto, and I. Tkachev, *Production of massive fermions at preheating and leptogenesis*, *JHEP* **08** (1999) 014, [hep-ph/9905242].

[250] M. Fujii, K. Hamaguchi, and T. Yanagida, *Leptogenesis with almost degenerate majorana neutrinos*, *Phys. Rev.* **D65** (2002) 115012, [hep-ph/0202210].

[251] L. Boubekeur, S. Davidson, M. Peloso, and L. Sorbo, *Leptogenesis and rescattering in supersymmetric models*, *Phys. Rev.* **D67** (2003) 043515, [hep-ph/0209256].

[252] J. Ellis, M. Raidal, and T. Yanagida, *Sneutrino inflation in the light of wmap: Reheating, leptogenesis and flavour-violating lepton decays*, hep-ph/0303242.

[253] T. Asaka, H. B. Nielsen, and Y. Takanishi, *Non-thermal leptogenesis from the heavier majorana neutrinos*, *Nucl. Phys.* **B647** (2002) 252–274, [hep-ph/0207023].